


Fall 11-20-2017

Development of biomimetic membrane assemblies on microspheres for high-throughput and multiplexable studies

Nadiezda P. Fernandez Oropeza
University of New Mexico

Follow this and additional works at: https://digitalrepository.unm.edu/bme_etds

 Part of the [Biomedical Devices and Instrumentation Commons](#), and the [Other Biomedical Engineering and Bioengineering Commons](#)

Recommended Citation

Fernandez Oropeza, Nadiezda P. "Development of biomimetic membrane assemblies on microspheres for high-throughput and multiplexable studies." (2017). https://digitalrepository.unm.edu/bme_etds/17

This Dissertation is brought to you for free and open access by the Engineering ETDs at UNM Digital Repository. It has been accepted for inclusion in Biomedical Engineering ETDs by an authorized administrator of UNM Digital Repository. For more information, please contact disc@unm.edu.

Nadiezda P. Fernandez Oropeza

Candidate

Biomedical Engineerng

Department

This dissertation is approved, and it is acceptable in quality and form for publication:
Approved by the Dissertation Committee:

Andrew P. Shreve, PhD. , Chairperson

Steven W. Graves, PhD.

Gabriel A. Montaña, Ph.D.

Deborah G. Evans, PhD.

**DEVELOPMENT OF BIOMIMETIC MEMBRANE
ASSEMBLIES
ON MICROSPHERES FOR HIGH-THROUGHPUT AND
MULTIPLEXABLE STUDIES**

by

NADIEZDA P. FERNANDEZ OROPEZA

B.S. Physics, West Texas A&M University, 2008
M.S. Physics, Univeristy of New Mexico, 2011

DISSERTATION

Submitted in Partial Fulfillment of the
Requirements for the Degree of

**Doctor of Philosophy
Engineering**

The University of New Mexico
Albuquerque, New Mexico

December 2017

Dedication

To my parent Luis Fernandez Villanueva and Nancy Oropeza de Fernandez for all their sacrifice, support and unconditional love. None of this would have been possible without you.

To my sister Annette Fernandez Oropeza for all her love, encouragement and inspiration.

To my husband Dr. Aram Gragossian for his unwavering love and support.

For all my family and friends who helped me throughout this challenging process with all your support and encouragement.

ACKNOWLEDGEMENTS

First and foremost, I would like to thank my advisor Dr. Andrew P. Shreve for his guidance, endless support and encouragement. His input and advice over these past 5 years inspired me, and helped me develop as a scientist and researcher, for which I am ever grateful. I would also like to thank Dr. Steven W. Graves for all the collaboration, advice and direction. Additionally, I also would like to thank Dr. Gabriel A. Montaña for helping me get access to his lab at the Center for Integrated Nanotechnologies, but most importantly for all his support and guidance. Finally, I thank Dr. Deborah G. Evans for kindly accepting being part of my committee in such short notice.

I must also thank Dr. Nesia A. Zurek for her sharing so much knowledge with me, for her time, feedback, and direction. In addition, I want to thank Mirella Galvan de la Cruz for all her help and support.

There are many fellow students at the Center for Biomedical Engineering at UNM with whom I had the privilege to work. I am grateful for such a wonderful collaborative and encouraging environment. Specially, I would like to thank Matthew Rush for all his help, time and support.

Last but not least, I would like to thank the Biomedical Engineering administrative personnel, who made this process much easier.

**DEVELOPMENT OF BIOMIMETIC MEMBRANE ASSEMBLIES
ON MICROPARTICLES FOR
HIGH-THROUGHPUT AND MULTIPLEXABLE STUDIES**

by

Nadiezda P. Fernandez Oropeza

B.S. Physics, West Texas A&M University, 2008

M.S. Physics, University of New Mexico, 2011

Ph.D. Biomedical Engineering, University of New Mexico, 2017

ABSTRACT

Membranes and membrane-associated components are the target of approximately 60% of the current drugs, of synthetic materials, such as polymers, which are used for drug delivery purposes and of other biomolecules, such as endotoxins, which gain entry into the cell by disrupting the membrane. Therefore, the development of biomimetic membrane assemblies allows the study of different biological processes in which cell membranes play an important role, and the characterization and screening of drug delivery tools and other membrane-bound components.

Since its development, membrane assemblies on planar silica surfaces have been the method of choice to study membrane-associated and membrane-bound components. However, the screening process of planar-substrate supported membranes has some

limitations, as they rely on non-high-throughput or multiplexable technologies, like microscopy or Surface Plasmon Resonance (SPR). This results in time consuming studies, high cost, and high variability from sample to sample. Another biomimetic assembly commonly used are giant unilamellar vesicles (GUVs), which has proven to be valuable, as it better mimics the size and shape of cell membranes. Nevertheless, their assembly is time consuming and presents polydispersity.

The need of a biomimetic platform amenable to high-throughput screening process inspired the development of silica microsphere-supported membranes, as an alternative to planar-supported membranes and GUVs. Microsphere-supported membranes can be screened using flow cytometry, which is a laser-based high-throughput technology that measures several thousand particles and their physical characteristics in a few seconds. Moreover, flow cytometry has the advantage of being highly sensitive, accurate, reproducible, and it uses small sample volumes, making the screening process faster and more affordable.

To that end, we built and characterized multiplexable biomimetic membranes on silica microspheres for flow-based screening applications. Furthermore, we demonstrated that this new biomimetic construct could potentially constitute a more effective way of performing target based screening assays for membrane-bound components. We used microsphere-supported biomimetic membranes to screen: 1) membrane-protein interactions, 2) membrane disruption assays, and 3) polymer membrane interactions. Future areas for application of these methods are in areas such as, drug screening, antimicrobial peptide screening, and protease assay development.

TABLE OF CONTENTS

LIST OF FIGURES	xi
Chapter 1. Introduction	1
1.1 Present studies	1
1.2 Cell membrane function, chemical composition, and physical properties	2
1.3 Membrane as targets in development drugs and medical devices.....	5
1.3.1 Protein-membrane interactions	5
1.3.2 Membrane disruption assays	7
1.3.3 1.3.3 Polymer-membrane interactions and block copolymers as an alternative to lipids in membrane formation	8
1.4 Screening processes of model membranes.....	10
1.4.1 Planar silica supported membrane bilayers (SSMB).....	10
1.4.2 Patterned planar-SSMBs	11
1.4.3 Giant unilamellar vesicles (GUVs)	12
1.4.3 Silica microsphere SMBs	13
1.5 Characterization processes of model membranes.....	14
1.5.1 Microscopy	14
1.5.2 Surface Plasmon Resonance.....	15
1.5.3 Ellipsometry.....	16
1.6 Flow cytometry.....	16
1.7 Goals and overview of the present work.....	20
1.8 References.....	26
Chapter 2. Materials and methods	42
2.1 Materials	42
2.1.1 Buffers	42
2.1.2 Microspheres	43
2.1.3 Lipids	44
2.1.4 Extruder	48
2.1.5 Proteins	49
2.1.6 Membrane disrupting agents	50
2.1.7 Polymers	52
2.1.8 Instruments	53
2.1.7 Data analysis	55

2.2 Methods	56
2.2.1 Lipid bilayers on silica microspheres protocol	56
2.2.1.1 Vesicle preparation	56
2.2.1.2 Extrusion	57
2.2.1.3 Lipid coating on beads	58
2.2.1.4 BSA-blocking	59
2.2.1.5 Rinsing	59
2.2.2 Protein-Membrane interaction assays	60
2.2.3 Membrane disruption assays	62
2.2.4 Block copolymer as an alternative to lipids	65
2.2.5 Flow cytometry data collection	68
2.3 References	69
Chapter 3. Multiplexed Lipid Bilayers on Silica Microspheres for Analytical Screening Applications	74
3.1 Abstract	75
3.2 Introduction	75
3.3 Materials and methods.....	79
3.3.1 Liposome preparation	79
3.3.2 Protein binding assays	80
3.3.3 Flow cytometry	81
3.4 Results and Discussions.....	82
3.4.1 Fluorescently Indexed Silica Microsphere Supported Lipid Bilayers.....	82
3.4.2 Flow cytometric characterization	82
3.4.3 Multiplexed Protein Binding Assays	84
3.4.4 Binding Specificity in Multiplexed Protein Binding Assays	91
3.5 Conclusion	93
3.6 Acknowledgements	94
3.7 References	95
Chapter 4. Membrane disruption assays on silica microsphere supported lipid bilayer membranes	99
4.1 Abstract	99
4.2 Introduction	99
4.3 Materials and methods.....	101

4.3.1 Materials	101
4.3.2 Formation of lipid membranes on silica microspheres	102
4.3.3 Membrane disruption assays	102
4.3.4 Backfilling of LPS induced holes on membrane with secondary fluorescently tagged lipid vesicles	103
4.3.5 Microscopy	104
4.3.6 Flow cytometry	104
4.4 Results and Discussions.....	105
4.4.1 Formation of lipid membranes on silica microspheres	105
4.4.2 Membrane disruption assays	105
4.4.2.1 Membrane disruption with LDAO	105
4.4.2.2 Membrane disruption with LPS	108
4.4.3 Backfilling of LPS induced holes on membrane with secondary fluorescently tagged lipid vesicles	111
4.5 Summary and Conclusions	114
4.6 Acknowledgements	115
4.7 References	116
Chapter 5. Microsphere-supported polymer membrane as an alternative to lipid membranes for screening applications	118
5.1 Abstract	118
5.2 Introduction	118
5.3 Materials and methods.....	120
5.3.1 Materials	120
5.3.2 Copolymer micelle formation	121
5.3.3 Formation of polymer membranes on silica microspheres	121
5.3.4 Multiplex set formation	122
5.3.5 Differential binding assays	122
5.3.6 Microscopy	123
5.3.7 Flow cytometry	123
5.4 Results and Discussions.....	124
5.4.1 Formation of polymer membranes on silica microspheres	124
5.4.2 Multiplex set formation	127
5.4.3 Differential binding assays	128

5.5 Summary and Conclusions	132
5.6 Acknowledgements	133
5.7 References	134
Chapter 6. Summary and Conclusions	137
Appendix I. Additional work	139
Appendix I 1 Introduction	139
Appendix I 2 Additional work – Detection of membrane disruption assays on microsphere-supported membranes	142
Appendix I 2.1 Disruption of fluorescent membranes with Triton X-100 and SDS.	142
Appendix I 2.2 Lipid protection assay	145
Appendix I 2.2.1 Preliminary results	155
Appendix I 2.2.1 Evaluation of BSA-FITC and fluorescein passivation of non- porous silica microspheres	149
Appendix I 2.2.1 Evaluation of BSA-passivated carboxylated-polystyrene coated with fluorescently-tagged lipids	152
Appendix I 2.3 Surface modification of polystyrene microspheres	154
Appendix I 3 Additional work – Polymer interaction with membranes supported on microspheres	161
Appendix I 3.1 Chitosan vs. different membrane compositions	161
Appendix I 3.2 Poly-L-lysine vs. different membrane compositions	169
Appendix I 4 References	174
Appendix I 5 Extra Figures	177
Appendix II	180
Appendix II 3. Supplemental Information for chapter 3	181
Appendix II 4. Supplemental Information for chapter 4	188
Appendix II 5. Supplemental Information for chapter 5	193

LIST OF FIGURES

Figure 2.1. Parts and Assembly of extruder	49
Figure 2.2. Lipid plaque formation with different lipid compositions	56
Figure 2.3. Lipid plaques with different lipid compositions resuspended in buffer	57
Figure 2.4. Liposome solution before and after extrusion	58
Figure 2.5. Schematic of the assembly of biomimetic membranes on non-porous silica microspheres	60
Figure 2.6. Block copolymer micelles solutions	66
Figure 3.1. Schematic of supported lipid bilayers on non-porous silica microspheres ..	83
Figure 3.2. Binding of cholera B subunit to GM1 on microspheres-supported membranes	85
Figure 3.3. Fractional binding of cholera B subunit to GM1 on microspheres-supported membranes	88
Figure 3.4. Fractional binding of streptavidin to biotin on microspheres-supported membranes	90
Figure 3.5. Binding Specificity in Multiplexed Protein Binding Assays	92
Figure 4.1. Flow cytometric data of microsphere-supported membranes treated with LDAO	106
Figure 4.2. Confocal image of microsphere-supported membranes treated with LDAO	108
Figure 4.3. Flow cytometric data of microsphere-supported membranes treated with LPS	109
Figure 4.4. Confocal image of microsphere-supported membranes treated with LPS	110
Figure 4.5. Confocal images of backfilling of LPS-induced holes on microsphere-supported membranes	112
Figure 4.6. Flow cytometric data of backfilling of LPS-induced holes on microsphere-supported membranes	113
Figure 5.1. Schematic of formation of block copolymer membranes on non-porous silica microspheres	125
Figure 5.2. Confocal microscopy images and flow cytometric detection of the different populations of block copolymer membranes supported on silica beads	126

Figure 5.3. Multiplex sample formation of microsphere-supported block copolymer membranes and flow cytometric analysis	128
Figure 5.4. Binding of cholera B subunit to GM1 on microspheres-supported block copolymer membranes	129
Figure 5.5. Fractional binding of cholera B subunit to GM1 on microspheres-supported block copolymer membranes	131
Figure AI-1. Flow cytometric data of microsphere-supported membranes treated with SDS and Triton X-100	143
Figure AI-2. Schematic of the lipid protection assay on membrane supported on microspheres	146
Figure AI-3. Stern-Volmer plots resulting from lipid membrane protection assays ...	147
Figure AI-4. BSA-FITC and fluorescein passivation of silica microspheres	149
Figure AI-5. Fluorescently-tagged liposome deposition on BSA-passivated silica and carboxylated-polystyrene microspheres	152
Figure AI-6. UV-modified polystyrene surfaces	155
Figure AI-7. Flow cytometric data of UV-modified polystyrene microspheres	156
Figure AI-8. O ₂ plasma-modified polystyrene surfaces	157
Figure AI-9. Flow cytometric data of O ₂ plasma-modified polystyrene beads	158
Figure AI-10. Fluorescently-tagged liposome deposition on O ₂ plasma-treated polystyrene microspheres	159
Figure AI-11. Screening of preferential binding of chitosan-FITC to different membrane compositions and charges	165
Figure AI-12. Disruption effects of chitosan on differently-charged fluorescently-tagged membranes	167
Figure AI-13. Screening of preferential binding of PLL-FITC to different membrane compositions and charges	171
Figure AI-14. Disruption effects of PLL on differently-charged fluorescently tagged membranes	173
Figure AI-Extra-1. Plain polystyrene beads after O ₂ plasma treatment	177
Figure AI-Extra-2. FITC-labeling of chitosan	178
Figure AI-Extra-3. Absorbance of chitosan-FITC and FITC in PBS	179

Figure A3.1. Time stability of individual and multiplex sets	181
Figure A3.2. Cholera toxin B subunit-Alexa 647 interactions with the NBD	182
Figure A3.3. Compensation details for biotin-streptavidin assays	183
Figure A3.4. Binding of streptavidin-PE/Cy5 to biotin in microspheres-supported membranes	184
Figure A3.5. Streptavidin-PE/Cy5 interactions with the NBD	185
Figure A3.6. Compensation details for cross-reactivity assays	186
Figure A3.7. Cross-reactivity median fluorescence intensities	187
Figure A4.1. Planar supported membranes after LDAO treatment	188
Figure A4.2. LDAO effect on different membrane compositions	189
Figure A4.3. Determination of LPS critical micelle concentration	190
Figure A4.4. Planar supported membranes after LPS treatment	191
Figure A4.2. LPS effect on different membrane compositions	192
Movie A5.1. Preview image of the FRAP experiment of block copolymer membranes supported on silica beads	193
Figure A5.1. Fluorescence intensity data of the FRAP experiment of block copolymer membranes supported on silica beads	194
Figure A5.2. Time stability of block copolymer membranes supported on silica microspheres	195
Figure A5.3. Compensation used in block copolymer experiments	196
Figure A5.4. Compensation matrix used in block copolymer experiments	197

Chapter 1.

Introduction

1.1 Present Studies

Developing biomimetic membrane assemblies for drug screening purposes is important for the discovery of new drugs that target membrane bound components or bacterial membranes, and for understanding how novel medical therapies, such as drug delivery tools, interact with membranes. Currently 40-60% of drugs target membrane bound components.¹ For example, about 95% of psychotropic drugs target membrane proteins, many novel cancer drugs use membrane proteins for entry into the cell, and novel classes of anti-bacterial agents such as anti-microbial peptides (AMPs) specifically target bacterial membranes. Other biological components, such as endotoxins and exotoxins, interact with mammalian cells by first disrupting the cell membrane. Moreover, membranes are also the target of some synthetic materials, such as polymers, as they are used for various biomedical purposes such as drug delivery.

The development of membrane assemblies on planar silica surfaces has provided an important route to study membrane-associated and membrane-bound components. Such systems are widely studied and characterized and demonstrate the feasibility of building supported bilayers on silica surfaces and the integration of membrane-bound proteins. An alternative platform, giant unilamellar vesicles, has also proven to be valuable for the study of the interaction of membranes with other biomolecules. However, membrane assemblies on planar silica or the use of giant unilamellar vesicles have many limitations for high-throughput and multiplexable studies, which limit their applicability in drug screening.

To that end, we propose the development of multiplexable biomimetic membrane bilayers on silica microspheres for flow-based screening applications. Our development of multiplexed biomimetic membranes on silica microspheres will provide a beneficial platform to allow high-throughput screening of biomolecules that target membrane bound components. The new biomimetic constructs that we will develop have the promise of enabling application of high-throughput multiplexed flow cytometry techniques to study membrane proteins, membrane disruption assays, and assess polymer membrane interactions. Future areas for application of these methods are in areas such as protease assay development, drug screening and antimicrobial peptide screening.

1.2 Cell membrane function, chemical composition, and physical properties.

All cells have a ~5-10 nm thick outer membrane,² also known as the plasma membrane or cytoplasmic membrane, which is a thin biological semi-permeable membrane that surrounds, protects and separates the cytoplasm from the outside environment by regulating what substances diffuse across the membrane and into the cell. Also, cell's membrane helps support and maintain the shape of the cell.³⁻⁵

The cell membrane's major components are lipids in the form of phospholipids, cholesterol and glycolipids,^{6,7} out of which phospholipids constitute approximately half of mammalian cell membranes.^{8,9}

Phospholipids are composed of a phosphate hydrophilic head and two hydrophobic hydrocarbon tails. They are insoluble in water and due to their amphiphilic nature, they spontaneously arrange into a bilayer form in which the hydrophilic head faces towards the aqueous cytosol and the extracellular fluid, while the hydrophobic tail areas face away.¹⁰

Some of the most common glycerophospholipids include phosphatidylcholine and phosphatidylethanolamine, which in spite of their similar structure, have different properties and tend to be in different leaflets of the membrane bilayer of the cell. Besides phosphatidylethanolamine, the inner cytoplasmic leaflet of the membrane also contains anionic phospholipids such as phosphatidylserine and phosphatidylinositol.⁶ Finally, the fifth most abundant phospholipid on cell membranes is sphingomyelin, which predominantly locates in the membrane's outer leaflet.⁸

Cholesterol is also a membrane component in animal cells, but absent in bacterial and mitochondrial membranes. At high temperatures, it serves the function of preventing phospholipids from being too closely packed, resulting in a stiffer (less fluid) membrane^{3,8,10} at low temperatures, it keeps the membrane fluid and it prevents its freezing.⁸ Cholesterol, along with sphingolipids, plays an important role in the process of lipid raft formation.¹¹ Animal cells have been estimated to contain 25 mol% to 50 mol% of cholesterol in their membranes,¹² but these percentages change in aging cells.¹³ In addition, there is an upper limit concentration for the cholesterol present in the membrane. The cholesterol solubility limit in phosphatidylcholine bilayers is 66 mol% and in phosphatidylethanolamine bilayers is 51 mol%.^{12,14}

Finally, glycolipids are structures composed of a carbohydrate attached to a lipid moiety by a glycosidic bond,¹⁵ which are located in the membrane's outer leaflet and constitute only 2% of the membrane's lipids.⁸ They play an important role in cell communication, recognition and adhesion,¹⁶ and in determining human blood type.¹⁷

In addition to lipids, the cell membranes also contain membrane proteins that account for almost half the mass of most cellular membranes.¹⁸ Membrane proteins are classified as integral membrane proteins and peripheral membrane proteins.

Integral membrane proteins account for up to one-third of the lipid bilayer membrane's mass,¹⁹ and they play crucial roles in cell transportation,²⁰ cell adhesion,²¹ and acting as receptors and channels.²² They also comprise the majority of drug targets.²³ Integral membrane proteins can be partially (integral monotopic proteins), or completely (transmembrane proteins) embedded in the lipid membrane. These proteins are usually hard to remove from the membrane, and the disruption of the lipid is necessary for their extraction. The solubilization of the membrane and subsequent extraction of the proteins is done using harsh solvents, like detergents.^{8,24}

Peripheral membrane proteins are temporarily bound to the lipid head groups²⁵ or to the integral membrane proteins. They can be dissociated from the membrane without perturbing the membrane structure. The dissociation process can be achieved by treatment with surfactants, solutions with high salt content or solutions with very high or low pH.⁸ Peripheral membrane proteins play very important roles for the proper function of the cell,^{18,26} playing a role in processes like signaling,²⁵ and transportation.²⁷

A very important characteristic of cell membranes is fluidity, which depends on the membrane's composition, pressure, ionic strength, pH, and temperature. The fluidity of the membrane allows two different types of diffusion to take place: lateral (with proteins and lipids moving sidewise within the membrane), or transverse (with molecules going from one membrane leaflet to the other). At physiological temperatures, cell membranes usually

exist in a fluid form where the hydrocarbon chains are disordered; at cooler temperatures, the membranes exist in a more ordered gel-like state where the hydrocarbon chains are fully extended and closely packed.²⁸ At characteristic temperatures, all lipids, depending on the charge, hydrocarbon length and head group, can undergo a phase transition (from gel to liquid phase or vice versa). Change in the membrane's fluidity can have effects on its permeability,^{29,30} freezing point,³¹ and viscosity.³²

1.3 Membrane as targets in development of drugs and medical devices.

Cell membranes have been widely studied since they serve many important functions in different biological processes. They mainly provide a semi-permeable barrier between the environment and the cytoplasm of the cell as well as barriers between the cytoplasm and organelles, but they also play an important role in other biological processes such as ion conductivity, cell adhesion, transfer of molecules across membranes, and cell signaling.^{10,33} In addition, prior to reaching and interacting with the cytoplasm, toxins and viruses must interact with cell membranes.^{34,35} These functions lead to membrane-associated components being the most druggable targets,³⁶⁻³⁸ and also account for membranes and membrane components being very important in the development of medical devices.³⁹ Some of the most studied membrane-interacting biomolecules are membrane proteins, membrane disruption agents and polymers. In this section, we explore the importance of the interaction of these types of molecules with cell membranes.

1.3.1 Membrane-protein interactions

Membrane-protein interactions regulate several important processes such as transport across membranes, enzymatic activity, and cell-cell recognition, making membrane

proteins of great interest for target-based drug screening. Developing new assays for target based screening against membrane proteins is important because membrane proteins constitute around 60% of today's approved drug targets.^{40,41}

There are various examples of studies related to membrane-protein interactions: drug interactions with membrane and embedded membrane proteins,⁴² cell signaling and membrane trafficking,⁴³ biophysical studies of membrane-protein interactions,^{44,45} cell adhesion to model-membranes containing transmembrane proteins studied on patterned solid supported membranes,⁴⁶ protein-induced membrane deformations studied in giant unilamellar vesicles (GUVs),⁴⁷ and many more.

Studies on membrane components are often done on model membranes supported on planar silica surfaces,^{48,49} arrays of patterned membrane structures,⁵⁰ or giant unilamellar vesicles (GUVs).⁵¹ Model membranes provide a good tool for studying individual lipid bilayers and some associated proteins, they also present some limitations. First, use of membranes on planar surfaces becomes time consuming especially if multiple samples need to be tested, and variability may occur from sample to sample.⁵² Second, membranes supported on planar silica rely on relatively low-throughput detection methods such as microscopy and surface plasmon resonance (SPR).⁵³⁻⁵⁶ Third, even though supported lipid bilayer arrays are currently used to help increase throughput, they are limited by the size of the array and the time-consuming process of fabrication.⁵⁷⁻⁵⁹ Finally, GUVs show some structural stability and size polydispersity.^{60,61} In summary, studying membrane-protein interactions on membranes supported on planar silica, arrays of patterned membrane structures or GUVs do not provide a cost effective, quick, and high-throughput method necessary for drug screening.⁶²

Hence, another model membrane structure was developed: lipid membrane supported on silica microspheres, which present the membrane in a manner appropriate for use with high-throughput and multiplexable technologies like flow cytometry.⁶³

1.3.2 Membrane disruption assays

The process of membrane disruption is of great interest as diverse biomolecules can rupture, form holes or simply disturb the cell lipid membrane. Some of the best-known disrupting bioparticles are: detergents and surfactants,^{64,65} antimicrobial peptides (AMPs),⁶⁶ metal nanoparticles,⁶⁷ toxins,^{68,69} conjugated polyelectrolytes (CPEs),⁷⁰ and some drugs.⁷¹ Membrane disruption assays are used to perform mechanistic studies, guide extraction and isolation of membrane-proteins, and to test the effect of possible disrupting agents. Most of the disruption agents, like AMPs, show lipid selectivity between bacterial and mammalian cell membranes.⁷² This selectivity is of extreme importance in the screening process of new microbe-targeted drugs, as it is expected for the drug to induce disruption in bacterial membranes and to have no disruption effect on mammalian cell membranes.

Most membrane disruption assays are performed on actual cells,^{73,74} where target identification is very difficult due to confounding factors such as membrane complexity and a wide variety of different components including lipids, proteins, and carbohydrates. Other membrane disruption assays are performed on planar-solid-supported membranes,^{75,76} which has some limitations; they rely on low-throughput screening processes, which makes the measurement slower. Even if these assays are performed on

systems that use arrays of patterned planar supported lipid bilayers, the preparation process is still time consuming.⁶⁹

To the best of our knowledge, there are limited studies showing microsphere-supported lipid bilayers as a platform to perform membrane disruption assays.⁷⁷ Therefore, studying, exploring and expanding the use of this platform provides an interesting and useful alternative method for the development of membrane disruption assays, one that could enable the testing of different membrane compositions such as membranes containing cholesterol or negatively charged lipids in a high-throughput or multiplexable manner.

1.3.3 Polymer-membrane interactions and block copolymers as an alternative to lipids in membrane formation.

The interaction of polymers with lipid membranes and cell membranes is of key importance for the development of novel medical devices, drug delivery mechanisms, and the discovery of antimicrobials and antimicrobial surfaces.⁷⁸ Polymers are used for various biomedical purposes such as drug delivery, as biosensors, and for surgical sutures and implants.⁷⁹ Biodegradable polymers in particular are widely studied as scaffolds for tissue engineering,⁸⁰ they are used as drug encapsulants,⁸¹ in chemotherapeutics,⁸² in vaccines,⁸³ as substrates or support to lipid membranes,^{84,85} and as drug delivery tools.⁸⁶ The incorporation of polymers into lipid membranes can alter the physiochemical properties of the membrane, acting as membrane sealants,⁸⁷ as protecting agents against lipid peroxidation,⁸⁸ and also as membrane disrupters.⁸⁹ In many of these applications the interaction of polymers with membranes plays an important role. In general, the interaction of polymers and cell membranes depends on the cell type, membrane composition and the

biochemical properties of the polymer. The study of interactions between polymers and membranes and the development and testing of most biodegradable and cationic polymers is done on whole cells, on planar silica supported lipid membranes, or on liposomes. Although very effective, the aforementioned study platforms are very time consuming as they rely on methods such as microscopy and SPR. Flow cytometry offers a good alternative, as it is a faster option, analyzes a large number of parameter simultaneously, is a standard technique in many laboratories, and rapidly produces detailed data.

There is one particular group of polymers known as the amphiphilic block copolymers that have proven to have possible biological,⁹⁰ and medical applications.⁹¹ For instance, structures like polymersomes or amphiphilic block copolymer vesicles have been studied as potential drug carriers,^{92,93} and are a synthetic alternative to lipid vesicles, both containing a bilayer membrane structure.^{94,95} One major advantage offered by block copolymers is that block copolymer membrane properties, like permeability and lateral diffusivity, can be systematically tuned by varying the block copolymer molecular weight^{96,97} and composition.^{91,98} In addition, there are many reported techniques for the preparation of amphiphilic block copolymers, which result in diverse nanostructures.⁹⁹ Polymersomes also are compatible with a wider variety of analysis technologies, including flow cytometry.¹⁰⁰

To the best of our knowledge, block copolymer membranes supported on microspheres have not been studied. Their development and use would provide an alternative platform to study synthetic membranes as cell membrane mimics, and the interaction of such membranes with other biomolecules. Furthermore, such platforms could be expanded into a multiplex set and would allow the use of high-throughput flow cytometry technologies.

1.4 Screening processes of model membranes

Biological membranes are complex structures, and biophysical interactions between membranes and other components, such as drugs and drug delivery systems,⁴² are very challenging to investigate. Model lipid membranes have been developed as an alternative, where a simplified artificial membrane can be tailored to have a certain composition, geometry and structure that mimics a natural membrane.^{101–104}

1.4.1 Planar silica supported membrane bilayers (SSMB)

Solid supported lipid bilayers are model lipid membranes that are deposited on solid substrates, where there is a layer of trapped water, only a few Ångstrom-thick, between the bilayer and the solid support.⁵² The most widely used substrate materials are silica, mica and borosilicate glass.⁴⁴ SSMB can be formed by applying one of three major techniques. The first and simplest method is the adsorption and fusion of lipid vesicles, which is a spontaneous process where the lipid vesicles first adhering to and then rupture on top of the glass surface, forming the bilayer.⁵⁶ The second is the Langmuir–Blodgett (LB) technique, which uses a special barrier to assemble a monolayer of amphiphilic molecules on a water surface, which is then transferred to a substrate. This step is followed by the horizontal deposition of a second monolayer on top of the first monolayer.^{105,106} The third method is a combination of the last two, where the first step is to form a monolayer using the LB technique and the second step is the deposition of vesicles on top of the monolayer to form the upper leaflet and/or multi layers.

SSMB have been widely used in multiple studies and for different purposes including characterization of membrane processes,¹⁰⁷ membrane interaction with small

biomolecules,¹⁰⁸ drug permeability,^{101,109} immunology studies,¹¹⁰ and other biological applications.^{111–113}

SSMB have major advantages. They are easy to ensemble and very stable, and they are highly mobile, maintaining the fluidity observed in natural cell membranes and any biomolecule linked to it.¹¹⁰ Nevertheless, SSMB also face some challenges. Incorporation of transmembrane proteins is difficult in standard SSMBs, as the proteins come into direct contact with the substrate and lose their function.¹⁰³ To mitigate this problem, some groups built and successfully used polymer-cushioned bilayers supported on solid substrates.^{114,115} SSMBs on planar surfaces can only be used with detection or characterization methods such as microscopy or surface plasmon resonance. These are low to, at best medium throughput, making any analytical study expensive and time consuming.

1.4.2 Patterned planar-SSMBs

As an alternative to regular SSMBs, patterned planar-SSMBs for analytical studies, and lipid bilayer arrays were developed. This is achieved by micro¹¹⁶ or nano-patterning¹¹⁷ of the substrate by using metals or plastic before the lipid bilayer formation.¹¹⁸ These partitions allow scientists to tailor, organize and/or limit the bilayer formation,¹¹⁹ its lateral diffusion,^{50,120} and its composition.¹²¹ A typical method to pattern the substrates is the exposure of different regions of the surface to resisting materials (metal or plastic) using photolithography or ebeam lithography, before membrane formation. Also, so-called stamping methods or post-deposition masked UV exposure can create patterned membranes.¹²²

Patterned planar-SSMBs have been used in diverse studies such as characterization of the immune synapse,¹²³ study of intracellular signaling,⁵⁰ screening of interactions between drugs or proteins with membranes,¹²⁴ and cell-based biosensor technology,^{125,126} among others. The main advantage of patterned planar-SSMBs is the fact that the compartmentalization allows screening of different compositions, phases, and domains against various biocomponents simultaneously.¹²⁷ However, they are limited by the size of the array, the time-consuming process of fabrication,⁵⁷⁻⁵⁹ and the cost of preparation and analysis.¹¹⁸

1.4.3 Giant unilamellar vesicles (GUVs)

GUVs are vesicles in the range of 1 to 100 μm in diameter.¹²⁸ These structures are well suited for membrane-related studies as they mimic the curvature and size of cell membranes,¹²⁹ which makes them easily visible with an optical microscope.¹³⁰ GUVs have been used in various membrane-related studies,⁵¹ including membrane-protein interactions,¹³¹ gene transcription,¹³² immunoassays,¹³³ and biosensors.¹³⁴

There are many techniques to form GUVs. The most common ones are: the solvent evaporation method, the gentle hydration method and the electro-formation method.¹³⁵ New, innovative and improved methods for preparation are also being published frequently as there has been a great effort to optimize the assembly and production of GUVs. To name a few, these include GUV formation by small vesicle fusion, from an initially planar bilayer,¹³⁴ or by gel-assisted formation.⁵¹ One advantage of GUVs, besides their size and curvature, is that they are independent of a solid substrate, presenting a more natural and cell-like structure. Nevertheless, studies using GUVs exhibit some important

disadvantages. They are typically heterogenous in size and their structure is fragile,^{63,136} plus the production process can be time consuming.¹³⁷ They are also not suitable for drug delivery studies.¹³⁴ Typically, analysis of GUVs also relies on low-throughput measuring techniques, such as microscopy, although a few flow cytometry studies have been published.¹³⁸

1.4.4 Silica microsphere SMBs

Silica microspheres are commercially available monodisperse beads with multiple biotechnology applications. These include biosensing,^{63,139} drug delivery,^{140,141} and as solid substrates to support lipid membrane structures.¹⁴² The lipid bilayer formation on the silica beads is achieved via lipid vesicle adsorption, a simple and time efficient process, or by chemical crosslinking.^{63,119} The quality of the membranes is similar to those created on planar surfaces.^{77,142–145} Silica microsphere-supported membranes are used in microscopy,⁸⁴ and flow-based assays.^{146,147}

There are many advantages to this platform. They present a more natural membrane environment relative to planar membranes since the curvature of the membrane mimics that of an actual mammalian or bacterial cell.¹⁴⁸ Also, compared to their planar counterparts they present a higher quantity of membrane surface area when dispersed in solution. In addition, they can be analyzed using high-throughput technologies like flow cytometry, where poorly coated or defective membranes can be gated out. Unfortunately, this platform also has some shortcomings. Most notably, silica is a dense material, so it is hard to keep silica microspheres in suspension. To address this limitation, currently there are ongoing efforts of modifying the surface chemistry of commercially available, naturally buoyant

polystyrene microspheres to make them able to present membrane components in their natural lipid environment. However, said efforts have not yet achieved positive results.¹⁴⁹

1.5 Characterization processes of model membranes

To study lipid bilayers many analytical techniques have been used; fluorescence microscopy,^{150,151} atomic force microscopy (AFM),^{152,153} spectroscopy,^{154,155} quartz-crystal microgravimetry (QCM),¹⁵⁶ surface plasmon resonance (SPR),^{157,158} and ellipsometry.^{159,160} Here we briefly review the most used characterization techniques.

1.5.1 Microscopy

The development of microscopy dates back to the 1600s and has radically influenced scientific fields such as biology, geology and histology.¹⁶¹ Briefly, there are three branches of microscopy: optical, electron, and scanning probe microscopy.¹⁶² Optical microscopy (also known as light microscopy) is the most widely used and it has two major subcategories: bright field and fluorescence.¹⁶³ Fluorescence microscopy, in particular, has many variants that allow the microscopes to better achieve different purposes, such as fluorophore detection by epifluorescence or increased optical resolution by confocal microscopy, among many others.¹⁶⁴ Electron microscopy uses a beam of accelerated electrons to create and enlarge the image of a sample.¹⁶⁵ Some electron microscopes have a magnification capability of 2 million times allowing scientists to observe much smaller objects.¹⁶⁶ There are 4 types of electron microscopes: Transmission Electron Microscope (TEM), Scanning Electron Microscope (SEM), Reflection Electron Microscope (REM), and Scanning Transmission Electron Microscope (STEM). These microscopes are very expensive and require high maintenance. Scanning probe microscopy (SPM) uses a

scanning process to move a nanostructured tip across the sample, allowing imaging of surfaces at a nanometer length scale. The scanning probe gathers the information and sends it to a computer where the software generates an image to represent the surface.¹⁶⁷

Microscopy has been the technology of choice to study planar supported lipid bilayers.¹³⁷ These studies provided information about the membrane's mechanical properties and morphology using atomic force microscopy (AFM) and AFM-based force spectroscopy (AFM-FS),¹⁶⁸ the membrane's phase using fluorescence recovery after photobleaching (FRAP), the spatial relationships between molecules and the membrane by means of contact-dependent fluorescence quenching and fluorescence resonance energy transfer (FRET),¹⁶⁹ and membrane interactions with membrane-bound components such as proteins,^{170,171} enzymes,¹⁷² DNA molecules,¹⁷³ and drugs.^{174,175} Furthermore, optical microscopy and AFM, along with spectroscopy, have been the major technologies used for the study of giant unilamellar vesicles (GUVs) as model membranes.^{137,176}

As significant as microscopy has been for the study of biological and model membranes, it still faces some limitations such as a slow measurement process and a limited number of detection parameters, which leads to low to medium throughput. Achieving high throughput using microscopy requires expensive and specialized imaging instrumentation.

1.5.2 Surface Plasmon Resonance

Surface plasmon resonance (SPR) is an optical detection technique that monitors the interaction between two label-free biomolecules. This is achieved by having one of the molecules (the ligand) immobilized onto a thin metal film (sensor) and the other molecule

(the analyte) is injected under continuous flow.¹⁷⁷ As the binding takes place there is a change in the local refractive index at the surface, which can be monitored in real time. Analysis of rates of said changes quantitatively describes the affinity.^{178,179} SPR has been used extensively to study the affinity and interaction of supported lipid bilayers (SSLBs) and proteins,^{54,180,181} but also with some other biomolecules such as antimicrobial peptides.¹⁸² One major advantage of SPR is that it is label free and does not require adding a fluorophore to the system. Nevertheless, SPR also has some major disadvantages. It is not being high throughput, has a limited sensor area, suffers from mass transport limitations, and most importantly, is very susceptible to complications from non-specific binding.^{183,184}

1.5.3 Ellipsometry

Ellipsometry is a very sensitive characterization technique that uses polarized light to measure film thickness and optical constants. Ellipsometry can detect film thicknesses ranging from a few angstroms to tens of microns, relying on optical models to fit the data.¹⁵⁹ One of the applications of ellipsometry is the characterization of model lipid membranes.^{185,186} Ellipsometry has several advantages such as being highly accurate, non-perturbative and label-free.¹⁸⁷ However, it also has some disadvantages, most notably that it is time consuming and not implemented in a high throughput manner. Also, the characterization becomes more difficult if the films are non-uniform.¹⁸⁸

1.6 Flow cytometry

Flow cytometry is a laser-based high-throughput technology that can individually measure several thousand cells or particles suspended in a stream of fluid every second,¹⁸⁹

and can also simultaneously analyze multiple physical characteristics and surface properties of each particle in “real time”.¹⁹⁰ This technology has many advantages. It is fast, reproducible, highly sensitive, accurate, and uses very small sample volumes.¹⁹⁰ In addition, several commercially available flow cytometers automatically can sample from 96 to 1536 well plates, making the screening process faster and more affordable.^{190,191}

Briefly, flow cytometry works by passing cells or particles (~ 1µm -15µm) suspended in a fluid through a laser beam.¹⁹² Then, the scattered light or fluorescence emitted by each particle individually is collected and measured.¹⁹³ In order to individually interrogates each cell or particle, the flow cytometry’s fluidics system spatially focuses the sample into a single-particle stream.¹⁹⁴ Each particle’s emitted light is directed through the flow cytometer’s optical system, measured by the detectors and converted into digital signals by the computer system. The following paragraphs provide a more detailed description of each of the components in a flow cytometer.

- Fluidics system

The flow cytometer’s fluidic system consists mainly of a flow chamber that can be fully closed for analyzing purposes only, or can be open air for analyzing and cell sorting.¹⁹⁵ Via a syringe pump system, the flow chamber injects the sample stream containing the cells or particles into a flowing stream enclosed by an outer flow of water or buffer called sheath fluid.¹⁹⁶ The combination of sample and sheath flow spatially focuses the particles to a narrow diameter stream, so that they are passed through the laser beam one at a time. This process is called hydrodynamic focusing, and it is used by most flow cytometers.¹⁹⁵ Some newer flow cytometers use an improved technology called acoustic focusing which uses

ultrasonic radiation pressure to pre-focus the samples before using hydrodynamic focusing.¹⁹⁷

- Light source

The most commonly used light sources are moderately low-power lasers, but arc lamps and LED are used as well.¹⁹⁴ To achieve optimal flow cytometric results, the light source ideally needs to have a tight focus, making lasers the best candidate as a light source.^{195,198,199} Most flow cytometers have at least one laser producing 10 to 25 mW of blue light at 488 nm, and modern flow cytometers also have other lasers such as He-Ne, He-Cd, and solid-state lasers.^{195,199}

- Optics

Once each sample particle passes through the interrogation point, the light scattered or emitted by the particle is collected. There is a detector right in front of the laser beam that collects the light scattered in the forward direction; this signal is known as the forward scattered channel (FSC). The FCS measurement correlates with the size of the particle. There is another detector at a 90° angle of the interrogation point called side scatter channel (SSC). The SSC measurement correlates with the granularity and internal structure of the particle. Moreover, fluorescent emission collected at different wavelengths can also be measured. As each fluorescently-labeled particle passes through the interrogation point, a fluorescent signal is generated and then it is directed through different mirrors and filters.

The major filters in flow cytometers are: Long pass (LP) filters allow the transmission of light above a specific wavelength. Short pass (SP) filters allow the transmission of light

below a specific wavelength. Band pass (BP) filters allow transmission of photons that have wavelengths within a range of wavelengths (also known as band width).^{194,200}

- Detectors and electronics

As each cell or particle passes through the interrogation point, photons are emitted and directed to a detector where it is translated into a voltage pulse.^{196,200} Typically, photomultiplier tubes (PMT) are used for detection. The electric current produced by a PTM when illuminated is translated into a voltage, so each particle's passage through the interrogation spot produces a voltage pulse. The signal can be amplified by increasing the gain.²⁰¹ However, not all signals detected are retained. Those due to debris, dust particles or other interferents are excluded by setting a threshold on the signal intensity, so only signal from the particles of interest is processed. Next, the voltage pulses are converted from analogue to digital format by the Analogue-to-Digital Converter (ADC). Finally, the data is stored in a flow cytometry standard (FCS) format and can be analyzed using software programs such as FlowJo, FCS Express, and FCSalyzer, among others.

Overall, flow cytometry offers many advantages compared to other detection methods. It is high throughput, with some cytometers being able to analyze up to 100,000 event/second,¹⁹⁰ it can analyze multiple parameters simultaneously, due to its high specificity it can distinguish discrete cell subsets and rare populations,¹⁸⁹ it is fast, reproducible, accurate, and it uses small sample volumes.²⁰⁰ In addition, some flow cytometers are equipped with well plate readers, making drug screening faster and more affordable.¹⁹⁰ Flow cytometry is a technology traditionally used for cell screening and cell

sorting, but all its aforementioned advantages make it a great candidate to optimize the analysis of model membranes against various biological components.

1.7 Goals and Overview of this Work

Cell membranes have been widely studied since they serve many important functions in different biological processes. They mainly provide a semi-permeable barrier between the environment and the cytoplasm of the cell as well as barriers between the cytoplasm and organelles, but they also play an important role in other biological processes such as ion conductivity, cell adhesion, and cell signaling.^{10,33}

The development of biomimetic membrane assemblies was crucial in the study of all the aforementioned processes. The most commonly used membrane assemblies are solid-substrate supported membrane constructs,¹⁵⁷ which served as good platforms to investigate membrane-associated and membrane-bound components.²⁰² As an alternative to planar-supported membrane, some groups have worked with giant unilamellar vesicles (GUVs), which better mimic the curvature and size of the cell membranes, and have been used in various membrane-related studies.⁵¹

While planar-substrate supported membranes and GUVs have proven to be very effective, studies done using both platforms rely on methods such as Surface Plasmon Resonance (SPR) or microscopy which have limitations for screening purposes. In particular, they are neither high-throughput nor multiplexable resulting in time consuming studies, high cost, and high variability from sample to sample⁵³⁻⁵⁶ **Therefore, there is a technology need for the development of biomimetic membrane assemblies that will enable high-throughput studies.**

Some scientists have worked on building membranes on silica microspheres,²⁰³ which can be studied using high-throughput technologies, such as flow cytometry. Flow cytometric studies have many advantages. They are fast, reproducible, highly sensitive, accurate, and use small sample volumes. In addition, several commercially available flow cytometers automatically can sample from well plates, making drug screening faster and more affordable.¹⁹⁰

Microsphere-supported membranes plus the advantages of flow cytometry would potentially constitute a more effective technology for performing target based screening assays for membrane bound components, studying the potential disruption effect of some biomolecules (drugs, antimicrobial peptides, etc.), or studying the interaction of the membrane and synthetic compounds such as polymers. **To that end, we propose the development of multiplexable biomimetic membrane assemblies on silica microspheres for flow-based screening applications.**

Our development of multiplexed biomimetic membranes on silica microspheres will provide a beneficial platform that, ultimately, could allow high-throughput screening of drugs that target membrane bound components. The new biomimetic constructs that we will develop have the promise of enabling application of high-throughput multiplexed flow cytometry techniques to study and assess: **1) membrane-protein interactions, 2) membrane disruption assays, and 3) polymer-membrane interactions.** Future areas for application of these methods are in areas such as protease assay development, drug screening and antimicrobial peptide screening. Chapters 3, 4 and 5 describe in detail work we did in assessing the topics (1-3) just listed.

The work detailed in **Chapter 3** had the specific **goal of developing and characterizing multiplexed silica microsphere supported biomimetic membranes for flow cytometry studies of membrane associated proteins**. The results of this part of the project was published as a research article in the *ACS – Journal of Analytical Chemistry*.

Briefly, we developed a multiplex system on silica microspheres by coating silica microparticles with lipid bilayer membranes that contain variable amounts of fluorescently tagged lipids. Each type of these labeled microspheres also contained varying concentrations of other membrane components or potentially other integral membrane components. These fluorescently-indexed silica microsphere supported lipid bilayer architectures were characterized by flow cytometry and confocal microscopy to assess the quality and uniformity of the supported membrane bilayer. The fluorescent nature of the lipids let us observe, distinguish, and gate upon the populations of microspheres with well-formed lipid membrane structures, resulting in more trustworthy and robust statistics in a high-speed detection format. To demonstrate this technology, we assessed the preferential binding of fluorescently tagged soluble proteins to different membrane-associated ligands present in the multiplex system.

In more detail, the characterization studies on the multiplexable silica microsphere platform show that we can generate stable membrane assemblies. We performed initial studies on the platform where fluorescently labeled Cholera toxin subunit B differentially binds to lipid membranes with increasing amounts of GM1, and where fluorescently labeled Streptavidin differentially binds to membranes with increasing biotin concentration. The success of this work demonstrates that this technology can enable multiplexed membrane-protein assays in flow-based methods.

This chapter kept the format of the original publication and the supporting information was added to the Appendix II 3 section.

Furthermore, the assembly of biomimetic lipid membranes supported on microspheres discussed on chapter 3 was successfully used as a platform to implement DNA nanotechnologies on a fluid lipid surface by members of Dr. Graves' group at CBME. The results of this work were published in the *ACS Journal of Applied Material & Interfaces*,²⁰⁴ and I am listed as a co-author.

The work detailed in **Chapter 4** had the specific **goal of developing technology to enable microsphere-based membrane disruption assays with flow cytometric detection**. This chapter presents the ongoing efforts of characterizing the effect of different membrane-disrupting agents (detergents, endotoxins, etc.) on microsphere supported membranes.

First, we used the fluorescently tagged lipid membranes supported on silica microspheres-assembly described in chapter 3, and some well-characterized surfactants (LDAO, SDS and Triton X-100) that are widely used to disrupt cell membranes and that have been also tested in planar-supported membrane assemblies. Then, relying on the flow cytometric data, we found the correlation between the loss of fluorescence of the microsphere-supported membranes, and the partial or complete disruption of the membrane caused by the surfactants. Our conclusions were supported and corroborated by the images obtained with confocal microscopy.

Second, we tested one of the most significant endotoxins, lipopolysaccharide (LPS), and its effect on silica microsphere-supported membrane bilayers. We compared our

observations with previously reported results by Dr. Montaña's group, at CINT,^{69,205} which were obtained relying on planar-supported lipid bilayers. Flow-based studies show that LPS-induced hole formation resulted in loss of fluorescence of the microsphere-supported membranes, and that we can backfill the holes with a secondary set of fluorescently-tagged lipid vesicles. These studies are intended to be a stepping stone on the way to a faster and more effective screening for membrane disrupting agents. Future studies will assess the LPS effect in the presence of varying factors: pH, buffer composition, and most importantly, against different lipid compositions. Supporting information for this study was added to the Appendix II 4 section.

The work detailed in **Chapter 5** had the specific **goal of developing and characterizing multiplexable block copolymer membrane assemblies supported on silica microspheres as an alternative to lipid membranes**. The results of this part of the project was written as a manuscript and is ready to be submitted to the *Journal ACS-Langmuir*.

Polymers are of great interest for biomedical applications due to their good biocompatibility, light weight, flexibility, wide variety and commercial availability. In particular, polymersomes or amphiphilic block copolymer vesicles present themselves as a synthetic alternative to lipid vesicles, as polymersomes' diffusivity and permeability can be modified by changing the molecular weight or the composition of the polymersome.

Briefly, we first prepared different sets of diblock copolymer micelles, each set was tagged with a different fluorescent lipid and a specific concentration of GM1. Then, relying on a polymer equivalent process of vesicle fusion, we used the diblock copolymer micelles

to form a polymer bilayer membrane supported on silica microspheres. Finally, as done in chapter 3, we tested the differential binding of Cholera toxin subunit B to polymer membranes with increasing concentrations of GM1. Finally, we tested the lateral mobility of the polymer membranes supported on the microspheres and assessed the effect of mobility on effective binding affinity. The success of this work demonstrates that polymer membranes can be used as an alternative to some lipid membranes and can also enable multiplexed membrane-protein assays in flow-based methods.

This chapter kept the format of the original manuscript and the supporting information was added to the Appendix II 5 section.

Chapter 6 summarizes the present work, draws overall conclusions, and discusses future directions of the project.

Appendix I. In addition to the work presented in chapter 4 and chapter 5, there is a different set of experiments that were inconclusive, others that presented some limitation and required re-designing, and others that are still in progress. This chapter aims to present some of the work that was done in the past years to achieve the objectives and goals of the present project.

Appendix II presents supplemental figures for chapters 3, 4, and 5.

1.8 References.

1. Santos R, Ursu O, Gaulton A, et al. A comprehensive map of molecular drug targets. *Nat Rev Drug Discov*. 2016;16(1):19-34. doi:10.1038/nrd.2016.230.
2. Steck TL. The organization of proteins in the human red blood cell membrane. A review. *J Cell Biol*. 1974;62(1):1-19.
3. van Meer G, Voelker DR, Feigenson GW. Membrane lipids: where they are and how they behave. *Nat Rev Mol Cell Biol*. 2008;9(2):112-124. doi:10.1038/nrm2330.
4. Edidin M. Timeline: Lipids on the frontier: a century of cell-membrane bilayers. *Nat Rev Mol Cell Biol*. 2003;4(5):414-418. doi:10.1038/nrm1102.
5. Seydel JK. Introduction. In: Michael Wiese, ed. *Drug-Membrane Interactions: Analysis, Drug Distribution, Modeling*. Wiley Online Library; 2003:1-33. doi:10.1002/3527600639.ch1.
6. Epand RM. Introduction to Membrane Lipids. In: Owen DM, ed. *Methods in Membrane Lipids*. 2nd ed. New York: Humana Press; 2015:1-6. doi:10.1007/978-1-4939-1752-5_1.
7. Yeagle PL. Lipid regulation of cell membrane structure and function. *FASEB J*. 1989;3(7):1833-1842.
8. Cooper GM. *The Cell : A Molecular Approach*. 2nd ed. Sunderland (MA): ASM Press; 2000. <https://www.ncbi.nlm.nih.gov/books/NBK9839/>.
9. van Meer G. Cellular lipidomics. *EMBO J*. 2005;24(18):3159-3165. doi:10.1038/sj.emboj.7600798.
10. Alberts B, Johnson A, Lewis J. The Lipid Bilayer. In: *Molecular Biology of the Cell*. New York: Garland Science; 2002. <https://www.ncbi.nlm.nih.gov/books/NBK26871/>.
11. Ferreira TM, Coreta-Gomes F, Ollila OHS, Moreno MJ, Vaz WLC, Topgaard D. Cholesterol and POPC segmental order parameters in lipid membranes: solid state ¹H– ¹³C NMR and MD simulation studies. *Phys Chem Chem Phys*. 2013;15(6):1976-1989. doi:10.1039/C2CP42738A.
12. Huang J, Buboltz JT, Feigenson GW. Maximum solubility of cholesterol in phosphatidylcholine and phosphatidylethanolamine bilayers. *Biochim Biophys Acta - Biomembr*. 1999;1417(1):89-100. doi:10.1016/S0005-2736(98)00260-0.
13. Zs-Nagy I. The role of membrane structure and function in cellular aging: a review. *Mech Ageing Dev*. 1979;9(3-4):237-246.
14. Krause MR, Regen SL. The Structural Role of Cholesterol in Cell Membranes:

- From Condensed Bilayers to Lipid Rafts. *Acc Chem Res.* 2014;47(12):3512-3521. doi:10.1021/ar500260t.
15. Ando T, Imamura A, Ishida H, Kiso M. Synthesis of Glycolipids. In: *Comprehensive Glycoscience.* Elsevier; 2007:797-813. doi:10.1016/B978-044451967-2/00022-2.
 16. Yu RK, Suzuki Y, Yanagisawa M. Membrane glycolipids in stem cells. *FEBS Lett.* 2010;584(9):1694-1699. doi:10.1016/j.febslet.2009.08.026.
 17. Ewald DR, Sumner SCJ. Blood type biochemistry and human disease. *Wiley Interdiscip Rev Syst Biol Med.* 2016;8(6):517-535. doi:10.1002/wsbm.1355.
 18. Lodish H, Berk A, Zipursky SL. Molecular Cell Biology. In: *Molecular Cell Biology.* 4th ed. New York: W. H. Freeman; 2000. <https://www.ncbi.nlm.nih.gov/books/NBK21570/>.
 19. Whitelegge JP. Integral Membrane Proteins and Bilayer Proteomics. *Anal Chem.* 2013;85(5):2558-2568. doi:10.1021/ac303064a.
 20. Dahl SG, Sylte I, Ravna AW. Structures and models of transporter proteins. *J Pharmacol Exp Ther.* 2004;309(3):853-860. doi:10.1124/jpet.103.059972.
 21. McCarthy JB, Basara ML, Palm SL, Sas DF, Furcht LT. The role of cell adhesion proteins--laminin and fibronectin--in the movement of malignant and metastatic cells. *Cancer Metastasis Rev.* 1985;4(2):125-152.
 22. Zhang X, Fu W, Palivan CG, Meier W. Natural channel protein inserts and functions in a completely artificial, solid-supported bilayer membrane. *Sci Rep.* 2013;3(1):2196. doi:10.1038/srep02196.
 23. Ulmschneider MB, Sansom MSP, Di Nola A. Properties of integral membrane protein structures: Derivation of an implicit membrane potential. *Proteins Struct Funct Bioinforma.* 2005;59(2):252-265. doi:10.1002/prot.20334.
 24. Smith SM. Strategies for the Purification of Membrane Proteins. In: *Methods in Molecular Biology (Clifton, N.J.).* Vol 681. ; 2011:485-496. doi:10.1007/978-1-60761-913-0_29.
 25. Kholodenko BN, Hancock JF, Kolch W. Signalling ballet in space and time. *Nat Rev Mol Cell Biol.* 2010;11(6):414-426. doi:10.1038/nrm2901.
 26. Whited AM, Johs A. The interactions of peripheral membrane proteins with biological membranes. *Chem Phys Lipids.* 2015;192:51-59. doi:10.1016/j.chemphyslip.2015.07.015.
 27. Morozova D, Guigas G, Weiss M. Dynamic Structure Formation of Peripheral Membrane Proteins. Tajkhorshid E, ed. *PLoS Comput Biol.* 2011;7(6):e1002067. doi:10.1371/journal.pcbi.1002067.

28. Matsuki H, Goto M, Tada K, Tamai N. Thermotropic and Barotropic Phase Behavior of Phosphatidylcholine Bilayers. *Int J Mol Sci.* 2013;14(2):2282-2302. doi:10.3390/ijms14022282.
29. Drori S, Eytan GD, Assaraf YG. Potentiation of anticancer-drug cytotoxicity by multidrug-resistance chemosensitizers involves alterations in membrane fluidity leading to increased membrane permeability. *Eur J Biochem.* 1995;228(3):1020-1029.
30. Yang NJ, Hinner MJ. Getting Across the Cell Membrane: An Overview for Small Molecules, Peptides, and Proteins. *Methods Mol Biol.* 2015;(1266):29-53. doi:10.1007/978-1-4939-2272-7_3.
31. Lee D-K, Kwon BS, Ramamoorthy A. Freezing point depression of water in phospholipid membranes: a solid-state NMR study. *Langmuir.* 2008;24(23):13598-13604. doi:10.1021/la8023698.
32. Nipper ME, Majd S, Mayer M, Lee JC-M, Theodorakis EA, Haidekker MA. Characterization of changes in the viscosity of lipid membranes with the molecular rotor FCVJ. *Biochim Biophys Acta - Biomembr.* 2008;1778(4):1148-1153. doi:10.1016/j.bbamem.2008.01.005.
33. Ludewig U, Frommer WB. *Genes and Proteins for Solute Transport and Sensing.* 1st ed.; 2002. doi:10.1199/tab.0092.
34. Lesieur C, Vécsey-Semjén B, Abrami L, Fivaz M, Gisou van der Goot F. Membrane insertion: The strategies of toxins (review). *Mol Membr Biol.* 14(2):45-64.
35. Villanueva RA, Rouillé Y, Dubuisson J. Interactions Between Virus Proteins and Host Cell Membranes During the Viral Life Cycle. In: *International Review of Cytology.* Vol 245. ; 2005:171-244. doi:10.1016/S0074-7696(05)45006-8.
36. Yin H, Flynn AD. Drugging Membrane Protein Interactions. *Annu Rev Biomed Eng.* 2016;18(1):51-76. doi:10.1146/annurev-bioeng-092115-025322.
37. Allen JA, Roth BL. Strategies to Discover Unexpected Targets for Drugs Active at G Protein–Coupled Receptors. *Annu Rev Pharmacol Toxicol.* 2011;51(1):117-144. doi:10.1146/annurev-pharmtox-010510-100553.
38. Overington JP, Al-Lazikani B, Hopkins AL. How many drug targets are there? *Nat Rev Drug Discov.* 2006;5(12):993-996. doi:10.1038/nrd2199.
39. Iwasaki Y, Ishihara K. Cell membrane-inspired phospholipid polymers for developing medical devices with excellent biointerfaces. *Sci Technol Adv Mater.* 2012;13(6):64101. doi:10.1088/1468-6996/13/6/064101.
40. Yıldırım MA, Goh K-I, Cusick ME, Barabási A-L, Vidal M. Drug–target network. *Nat Biotechnol.* 2007;25(9). doi:10.1038/nbt1338.

41. Escribá P V., González-Ros JM, Goñi FM, et al. Membranes: a meeting point for lipids, proteins and therapies. *J Cell Mol Med.* 2008;12(3):829-875. doi:10.1111/j.1582-4934.2008.00281.x.
42. Knobloch J, Suhendro DK, Zieleniecki JL, Shapter JG, Köper I. Membrane–drug interactions studied using model membrane systems. *Saudi J Biol Sci.* 2015;22(6):714-718. doi:10.1016/J.SJBS.2015.03.007.
43. Cho W, Stahelin R V. Membrane-Protein Interactions in Cell Signaling and Membrane Trafficking. *Annu Rev Biophys Biomol Struct.* 2005;34(1):119-151. doi:10.1146/annurev.biophys.33.110502.133337.
44. Andersson J, Köper I. Tethered and Polymer Supported Bilayer Lipid Membranes: Structure and Function. *Membranes (Basel).* 2016;6(2):30. doi:10.3390/membranes6020030.
45. Canale C, Jacono M, Diaspro A, Dante S. Force spectroscopy as a tool to investigate the properties of supported lipid membranes. *Microsc Res Tech.* 2010;73(10):965-972. doi:10.1002/jemt.20834.
46. Kam L, Boxer SG. Cell adhesion to protein-micropatterned-supported lipid bilayer membranes. *J Biomed Mater Res.* 2001;55(4):487-495.
47. Sens P, Johannes L, Bassereau P. Biophysical approaches to protein-induced membrane deformations in trafficking. *Curr Opin Cell Biol.* 2008;20(4):476-482. doi:10.1016/j.ceb.2008.04.004.
48. Jass J, Tjärnhage T, Puu G. From liposomes to supported, planar bilayer structures on hydrophilic and hydrophobic surfaces: an atomic force microscopy study. *Biophys J.* 2000;79(6):3153-3163. doi:10.1016/S0006-3495(00)76549-0.
49. Cremer PS, Boxer SG. Formation and Spreading of Lipid Bilayers on Planar Glass Supports. *J Phys Chem B.* 1999;103(13):2554–2559. doi:10.1021/jp983996x.
50. Nair PM, Salaita K, Petit RS, Groves JT. Using patterned supported lipid membranes to investigate the role of receptor organization in intercellular signaling. *Nat Protoc.* 2011;6(4):523-539. doi:10.1038/nprot.2011.302.
51. Weinberger A, Tsai F-C, Koenderink GH, et al. Gel-Assisted Formation of Giant Unilamellar Vesicles. *Biophys J.* 2013;105(1):154-164. doi:10.1016/j.bpj.2013.05.024.
52. Castellana ET, Cremer PS. Solid supported lipid bilayers: From biophysical studies to sensor design. *Surf Sci Rep.* 2006;61:429-444. doi:10.1016/j.surfrep.2006.06.001.
53. Wittenberg NJ, Im H, Xu X, et al. High-affinity binding of remyelinating natural autoantibodies to myelin-mimicking lipid bilayers revealed by nanohole surface plasmon resonance. *Anal Chem.* 2012;84(14):6031-6039. doi:10.1021/ac300819a.

54. Patching SG. Surface plasmon resonance spectroscopy for characterisation of membrane protein-ligand interactions and its potential for drug discovery. *Biochim Biophys Acta*. 2014;1838(1 Pt A):43-55. doi:10.1016/j.bbamem.2013.04.028.
55. Andrecka J, Spillane KM, Ortega-Arroyo J, Kukura P. Direct observation and control of supported lipid bilayer formation with interferometric scattering microscopy. *ACS Nano*. 2013;7(12):10662-10670. doi:10.1021/nn403367c.
56. Johnson JM, Ha T, Chu S, Boxer SG. Early steps of supported bilayer formation probed by single vesicle fluorescence assays. *Biophys J*. 2002;83(6):3371-3379. doi:10.1016/S0006-3495(02)75337-X.
57. Moran-Mirabal JM, Edel JB, Meyer GD, Throckmorton D, Singh AK, Craighead HG. Micrometer-sized supported lipid bilayer arrays for bacterial toxin binding studies through total internal reflection fluorescence microscopy. *Biophys J*. 2005;89(1):296-305. doi:10.1529/biophysj.104.054346.
58. Bally M, Bailey K, Sugihara K, Grieshaber D, Vörös J, Städler B. Liposome and lipid bilayer arrays towards biosensing applications. *Small*. 2010;6(22):2481-2497. doi:10.1002/sml.201000644.
59. Smith KA, Gale BK, Conboy JC. Micropatterned fluid lipid bilayer arrays created using a continuous flow microspotter. *Anal Chem*. 2008;80(21):7980-7987. doi:10.1021/ac800860u.
60. Nishimura K, Hosoi T, Sunami T, et al. Population Analysis of Structural Properties of Giant Liposomes by Flow Cytometry. *Langmuir*. 2009;25(18):10439-10443. doi:10.1021/la902237y.
61. Nishimura K, Matsuura T, Nishimura K, Sunami T, Suzuki H, Yomo T. Cell-free protein synthesis inside giant unilamellar vesicles analyzed by flow cytometry. *Langmuir*. 2012;28(22):8426-8432. doi:10.1021/la3001703.
62. Pereira DA, Williams JA. Origin and evolution of high throughput screening. *Br J Pharmacol*. 2007;152(1):53-61. doi:10.1038/sj.bjp.0707373.
63. Chemburu S, Fenton K, Lopez GP, Zeineldin R. Biomimetic Silica Microspheres in Biosensing. *Molecules*. 2010;15(3):1932-1957. doi:10.3390/molecules15031932.
64. Helenius A, Simons K. Solubilization of membranes by detergents. *Biochim Biophys Acta*. 1975;415(1):29-79.
65. Wang X-L, Ramusovic S, Nguyen T, Lu Z-R. Novel Polymerizable Surfactants with pH-Sensitive Amphiphilicity and Cell Membrane Disruption for Efficient siRNA Delivery. *Bioconjug Chem*. 2007;18(6):2169-2177. doi:10.1021/bc700285q.
66. Lee J, Lee DG. Antimicrobial Peptides (AMPs) with Dual Mechanisms: Membrane Disruption and Apoptosis. *J Microbiol Biotechnol*. 2015;25(6):759-

764.

67. Hajipour MJ, Fromm KM, Ashkarran AA, et al. Antibacterial properties of nanoparticles. *Trends Biotechnol.* 2012;30(10):499-511. doi:10.1016/J.TIBTECH.2012.06.004.
68. Czajkowsky DM, Iwamoto H, Cover TL, Shao Z. The vacuolating toxin from *Helicobacter pylori* forms hexameric pores in lipid bilayers at low pH. *Proc Natl Acad Sci U S A.* 1999;96(5):2001-2006.
69. Adams PG, Swingle KL, Paxton WF, et al. Exploiting lipopolysaccharide-induced deformation of lipid bilayers to modify membrane composition and generate two-dimensional geometric membrane array patterns. *Sci Rep.* 2015;5(1):10331. doi:10.1038/srep10331.
70. Wang Y, Jett SD, Crum J, Schanze KS, Chi EY, Whitten DG. Understanding the dark and light-enhanced bactericidal action of cationic conjugated polyelectrolytes and oligomers. *Langmuir.* 2013;29(2):781-792. doi:10.1021/la3044889.
71. Kitagawa N, Oda M, Totoki T. Possible mechanism of irreversible nerve injury caused by local anesthetics: detergent properties of local anesthetics and membrane disruption. *Anesthesiology.* 2004;100(4):962-967.
72. Maturana P, Martinez M, Noguera ME, et al. Lipid selectivity in novel antimicrobial peptides: Implication on antimicrobial and hemolytic activity. *Colloids Surfaces B Biointerfaces.* 2017;153:152-159. doi:10.1016/j.colsurfb.2017.02.003.
73. Kafsack BFC, Pena JDO, Coppens I, Ravindran S, Boothroyd JC, Carruthers VB. Rapid membrane disruption by a perforin-like protein facilitates parasite exit from host cells. *Science.* 2009;323(5913):530-533. doi:10.1126/science.1165740.
74. Prentice P, Cuschieri A, Dholakia K, Prausnitz M, Campbell P. Membrane disruption by optically controlled microbubble cavitation. 2005. doi:10.1038/nphys148.
75. Lok K, Lam H, Ishitsuka Y, et al. Mechanism of Supported Membrane Disruption by Antimicrobial Peptide Protegrin-1. *J Phys Chem B.* 2006;110(42):21282-21286. doi:10.1021/jp0630065.
76. Eid M, Rippa S, Castano S, et al. Exploring the Membrane Mechanism of the Bioactive Peptaibol Ampullosporin A Using Lipid Monolayers and Supported Biomimetic Membranes. *J Biophys.* 2010;2010:12. doi:10.1155/2010/179641.
77. Piyasena ME, Zeineldin R, Fenton K, Buranda T, Lopez GP. Biosensors based on release of compounds upon disruption of lipid bilayers supported on porous microspheres. *Biointerphases.* 2008;3(2):38. doi:10.1116/1.2918743.
78. Kahveci Z, Martínez-Tomé M, Esquembre R, Mallavia R, Mateo C. Selective Interaction of a Cationic Polyfluorene with Model Lipid Membranes: Anionic

- versus Zwitterionic Lipids. *Materials (Basel)*. 2014;7(3):2120-2140. doi:10.3390/ma7032120.
79. Langer R, Tirrell DA. Designing materials for biology and medicine. *Nature*. 2004;428(6982):487-492. doi:10.1038/nature02388.
 80. Armentano I, Dottori M, Fortunati E, Mattioli S, Kenny JM. Biodegradable polymer matrix nanocomposites for tissue engineering: A review. *Polym Degrad Stab*. 2010;95:2126-2146. doi:10.1016/j.polymdegradstab.2010.06.007.
 81. Wang XP, Chen TN, Yang ZX. Modeling and simulation of drug delivery from a new type of biodegradable polymer micro-device. *Sensors Actuators, A Phys*. 2007;133(2 SPEC. ISS.):363-367. doi:10.1016/j.sna.2006.06.016.
 82. Sutradhar KB, Amin ML. Nanotechnology in Cancer Drug Delivery and Selective Targeting. *ISRN Nanotechnol*. 2014;12. doi:10.1155/2014/939378.
 83. Men Y, Gander B, Merklet HP, Corradin G. Induction of sustained and elevated immune responses to weakly immunogenic synthetic malarial peptides by encapsulation in biodegradable polymer microspheres. *Vaccine*. 1996;14(15):1442-1450.
 84. Fried ES, Luchan J, Gilchrist ML. Biodegradable, Tethered Lipid Bilayer–Microsphere Systems with Membrane-Integrated α -Helical Peptide Anchors. *Langmuir*. 2016;32(14):3470-3475. doi:10.1021/acs.langmuir.6b00008.
 85. McCabe IP, Forstner MB. Polymer Supported Lipid Bilayers. *Open J Biophys*. 2013;3(1):59-69. doi:10.4236/ojbiphy.2013.31A008.
 86. Adams ML, Lavasanifar A, Kwon GS. MINIREVIEW Amphiphilic Block Copolymers for Drug Delivery. *Pharm Assoc J Pharm Sci*. 2003;92:1343-1355.
 87. Cho Y, Borgens R Ben. Polymer and nano-technology applications for repair and reconstruction of the central nervous system. *Exp Neurol*. 2012;233(1):126-144. doi:10.1016/j.expneurol.2011.09.028.
 88. Jelinek R, Kolusheva S, Mann E, Aviram M. Chromatic polymer assays for the analysis of lipid and lipoprotein peroxidation. *Lipid Technol*. 2015;27(4):86-89. doi:10.1002/lite.201500010.
 89. Murthy N, Robichaud JR, Tirrell DA, Stayton PS, Hoffman AS. The design and synthesis of polymers for eukaryotic membrane disruption. *J Control Release*. 1999;61(1-2):137-143. doi:10.1016/S0168-3659(99)00114-5.
 90. Blanzas A, Armes SP, Ryan AJ. Self-Assembled Block Copolymer Aggregates: From Micelles to Vesicles and their Biological Applications. *Macromol Rapid Commun*. 2009;30(4-5):267-277. doi:10.1002/marc.200800713.
 91. Discher DE, Ortiz V, Srinivas G, et al. Emerging applications of polymersomes in delivery: From molecular dynamics to shrinkage of tumors. *Prog Polym Sci*.

- 2007;32(8-9):838-857. doi:10.1016/j.progpolymsci.2007.05.011.
92. Liao J, Wang C, Wang Y, Luo F, Qian Z. Recent advances in formation, properties, and applications of polymersomes. *Curr Pharm Des.* 2012;18(23):3432-3441.
 93. Anajafi T, Mallik S. Polymersome-based drug-delivery strategies for cancer therapeutics. *Ther Deliv.* 2015;6(4):521-534. doi:10.4155/tde.14.125.
 94. Brinkhuis RP, Rutjes FPJT, van Hest JCM. Polymeric vesicles in biomedical applications. *Polym Chem.* 2011;2(7):1449. doi:10.1039/c1py00061f.
 95. Goertz MP, Marks LE, Montañó GA. Biomimetic Monolayer and Bilayer Membranes Made From Amphiphilic Block Copolymer Micelles. *ACS Nano.* 2012;6(2):1532-1540. doi:10.1021/nn204491q.
 96. Bermudez H, Brannan AK, Hammer DA, Bates FS, Discher DE. Molecular Weight Dependence of Polymersome Membrane Structure, Elasticity, and Stability. *Macromolecules.* 2002;35(21):8203–8208. doi:10.1021/MA020669L.
 97. Discher DE, Eisenberg A. Polymer Vesicles. *Science (80-).* 2002;297(5583):967-973. doi:10.1126/science.1074972.
 98. Lee JC-M, Santore M, Bates FS, Discher DE. From Membranes to Melts, Rouse to Reptation: Diffusion in Polymersome versus Lipid Bilayers. *Macromolecules.* 2001;35(2):323–326. doi:10.1021/MA0112063.
 99. Karayianni M, Pispas S. *Self-Assembly of Amphiphilic Block Copolymers in Selective Solvents.* Springer, Cham; 2016. doi:10.1007/978-3-319-26788-3_2.
 100. Nallani M, Woestenenk R, de Hoog H-PM, et al. Sorting Catalytically Active Polymersome Nanoreactors by Flow Cytometry. *Small.* 2009;5(10):1138–1143. doi:10.1002/sml.200801204.
 101. Peetla C, Stine A, Labhasetwar V. Biophysical interactions with model lipid membranes: applications in drug discovery and drug delivery. *Mol Pharm.* 2009;6(5):1264-1276. doi:10.1021/mp9000662.
 102. Dowhan W. Molecular Basis For Membrane Phospholipid Diversity: Why Are There So Many Lipids? *Annu Rev Biochem.* 1997;66(1):199-232. doi:10.1146/annurev.biochem.66.1.199.
 103. Chan Y-HM, Boxer SG. Model membrane systems and their applications. *Curr Opin Chem Biol.* 2007;11(6):581-587. doi:10.1016/j.cbpa.2007.09.020.
 104. Siontorou CG, Nikoleli G-P, Nikolelis DP, Karapetis SK. Artificial Lipid Membranes: Past, Present, and Future. *Membranes (Basel).* 2017;7(3):38. doi:10.3390/membranes7030038.
 105. Modlińska A, Bauman D. The Langmuir-Blodgett technique as a tool for

- homeotropic alignment of fluorinated liquid crystals mixed with arachidic acid. *Int J Mol Sci*. 2011;12(8):4923-4945. doi:10.3390/ijms12084923.
106. Komitov L, Stebler B, Gabrielli G, Puggelli M, Sparavigna A, Strigazzi A. Amphiphilic Langmuir-Blodgett Films as a New Tool for Inducing Alignment Transition in Nematics. *Mol Cryst Liq Cryst Sci Technol Sect A Mol Cryst Liq Cryst*. 1994;243(1):107-124. doi:10.1080/10587259408037764.
 107. Richter RP, Bérat R, Brisson AR. Formation of Solid-Supported Lipid Bilayers: An Integrated View. doi:10.1021/la052687c.
 108. Lind TK, Wacklin H, Schiller J, et al. Formation and Characterization of Supported Lipid Bilayers Composed of Hydrogenated and Deuterated Escherichia coli Lipids. Atzberger PJ, ed. *PLoS One*. 2015;10(12):e0144671. doi:10.1371/journal.pone.0144671.
 109. Omote H, Al-Shawi MK. Interaction of transported drugs with the lipid bilayer and P-glycoprotein through a solvation exchange mechanism. *Biophys J*. 2006;90(11):4046-4059. doi:10.1529/biophysj.105.077743.
 110. Groves JT, Dustin ML. Supported planar bilayers in studies on immune cell adhesion and communication. *J Immunol Methods*. 2003;278(1-2):19-32.
 111. Knoll W, Park H, Sinner E-K, Yao D, Yu F. Supramolecular interfacial architectures for optical biosensing with surface plasmons. *Surf Sci*. 2004;570(1-2):30-42. doi:10.1016/J.SUSC.2004.06.192.
 112. Kam L, Boxer SG. Spatially Selective Manipulation of Supported Lipid Bilayers by Laminar Flow: Steps Toward Biomembrane Microfluidics. *Langmuir*. 2003;19(5):1624–1631. doi:10.1021/LA0263413.
 113. Larsson C, Rodahl M, Höök F. Characterization of DNA Immobilization and Subsequent Hybridization on a 2D Arrangement of Streptavidin on a Biotin-Modified Lipid Bilayer Supported on SiO₂. *Anal Chem*. 2003;75(19):5080–5087. doi:10.1021/AC034269N.
 114. Diaz AJ, Albertorio F, Daniel S, Cremer PS. Double cushions preserve transmembrane protein mobility in supported bilayer systems. *Langmuir*. 2008;24(13):6820-6826. doi:10.1021/la800018d.
 115. Mashghi S, van Oijen AM. A versatile approach to the generation of fluid supported lipid bilayers and its applications. *Biotechnol Bioeng*. 2014;111(10):2076-2081. doi:10.1002/bit.25273.
 116. Groves JT, Ulman N, Boxer SG. Micropatterning fluid lipid bilayers on solid supports. *Science*. 1997;275(5300):651-653.
 117. Reimhult E, Baumann M, Kaufmann S, Kumar K, Spycher P. Advances in nanopatterned and nanostructured supported lipid membranes and their applications. *Biotechnol Genet Eng Rev*. 2010;27:185-216.

118. Kam LC. Capturing the nanoscale complexity of cellular membranes in supported lipid bilayers. *J Struct Biol.* 2009;168(1):3-10. doi:10.1016/j.jsb.2009.05.006.
119. Crites TJ, Maddox M, Padhan K, Muller J, Eigsti C, Varma R. Supported Lipid Bilayer Technology for the Study of Cellular Interfaces. *Curr Protoc cell Biol.* 2015;68:24.5.1-31. doi:10.1002/0471143030.cb2405s68.
120. Ratto T V, Longo ML. Obstructed diffusion in phase-separated supported lipid bilayers: a combined atomic force microscopy and fluorescence recovery after photobleaching approach. *Biophys J.* 2002;83(6):3380-3392. doi:10.1016/S0006-3495(02)75338-1.
121. Johnson JM, Ha T, Chu S, Boxer SG. Early Steps of Supported Bilayer Formation Probed by Single Vesicle Fluorescence Assays. *Biophys J.* 2002;83(6):3371-3379. doi:10.1016/S0006-3495(02)75337-X.
122. Ryu Y-S, Wittenberg NJ, Suh J-H, et al. Continuity of Monolayer-Bilayer Junctions for Localization of Lipid Raft Microdomains in Model Membranes. *Sci Rep.* 2016;6(1). doi:10.1038/srep26823.
123. Choudhuri K, Llodrá J, Roth EW, et al. Polarized release of T-cell-receptor-enriched microvesicles at the immunological synapse. *Nature.* 2014;507(7490):118-123. doi:10.1038/nature12951.
124. Majd S, Mayer M. Hydrogel Stamping of Arrays of Supported Lipid Bilayers with Various Lipid Compositions for the Screening of Drug-Membrane and Protein-Membrane Interactions. *Angew Chemie Int Ed.* 2005;44(41):6697-6700. doi:10.1002/anie.200502189.
125. Im H, Wittenberg NJ, Lesuffleur A, Lindquist NC, Oh S-H. Membrane protein biosensing with plasmonic nanopore arrays and pore-spanning lipid membranes. *Chem Sci.* 2010;1(6):688-696. doi:10.1039/C0SC00365D.
126. Groves JT, Mahal LK, Bertozzi CR. Control of Cell Adhesion and Growth with Micropatterned Supported Lipid Membranes. *Langmuir.* 2001;17(17):5129–5133. doi:10.1021/LA010481F.
127. Wu M, Holowka D, Craighead HG, Baird B. Visualization of plasma membrane compartmentalization with patterned lipid bilayers. *Proc Natl Acad Sci U S A.* 2004;101(38):13798-13803. doi:10.1073/pnas.0403835101.
128. Bhatia T, Husen P, Brewer J, et al. Preparing giant unilamellar vesicles (GUVs) of complex lipid mixtures on demand: Mixing small unilamellar vesicles of compositionally heterogeneous mixtures. *Biochim Biophys Acta - Biomembr.* 2015;1848(12):3175-3180. doi:10.1016/j.bbamem.2015.09.020.
129. Lira RB, Dimova R, Riske KA. Giant Unilamellar Vesicles Formed by Hybrid Films of Agarose and Lipids Display Altered Mechanical Properties. *Biophys J.* 2014;107(7):1609-1619. doi:10.1016/j.bpj.2014.08.009.

130. Fenz SF, Sengupta K. Giant vesicles as cell models. *Integr Biol.* 2012;4(9):982. doi:10.1039/c2ib00188h.
131. Sunami T, Sato K, Matsuura T, Tsukada K, Urabe I, Yomo T. Femtoliter compartment in liposomes for in vitro selection of proteins. *Anal Biochem.* 2006;357(1):128-136. doi:10.1016/j.ab.2006.06.040.
132. Noireaux V, Libchaber A. A vesicle bioreactor as a step toward an artificial cell assembly. *Proc Natl Acad Sci U S A.* 2004;101(51):17669-17674. doi:10.1073/pnas.0408236101.
133. Kalyankar ND, Sharma MK, Vaidya S V., et al. Arraying of Intact Liposomes into Chemically Functionalized Microwells. *Langmuir.* 2006;22(12):5403-5411. doi:10.1021/la0602719.
134. Walde P, Cosentino K, Engel H, Stano P. Giant vesicles: preparations and applications. *Chembiochem.* 2010;11(7):848-865. doi:10.1002/cbic.201000010.
135. Bagatolli LA, Parasassi T, Gratton E. Giant phospholipid vesicles: comparison among the whole lipid sample characteristics using different preparation methods: a two photon fluorescence microscopy study. *Chem Phys Lipids.* 2000;105(2):135-147.
136. Silva-López EI, Edens LE, Barden AO, Keller DJ, Brozik JA. Conditions for liposome adsorption and bilayer formation on BSA passivated solid supports. *Chem Phys Lipids.* 2014;183:91-99. doi:10.1016/j.chemphyslip.2014.06.002.
137. Bagatolli LA. Membranes and Fluorescence Microscopy. In: *Reviews in Fluorescence 2007.* Springer, New York, NY; 2009:33-51. doi:10.1007/978-0-387-88722-7_2.
138. Jalmar O, García-Sáez AJ, Berland L, Gonzalez F, Petit PX. Giant unilamellar vesicles (GUVs) as a new tool for analysis of caspase-8/Bid-FL complex binding to cardiolipin and its functional activity. *Cell Death Dis.* 2010;1(12):e103. doi:10.1038/cddis.2010.81.
139. Demir A, Serpengüzel A. Silica microspheres for biomolecular detection applications. *IEE Proc - Nanobiotechnology.* 2005;152(3):105. doi:10.1049/ip-nbt:20045010.
140. Yang P, Gai S, Lin J. Functionalized mesoporous silica materials for controlled drug delivery. *Chem Soc Rev.* 2012;41(9):3679. doi:10.1039/c2cs15308d.
141. Ashley CE, Carnes EC, Phillips GK, et al. The targeted delivery of multicomponent cargos to cancer cells by nanoporous particle-supported lipid bilayers. *Nat Mater.* 2011;10(5):389. doi:10.1038/nmat2992.
142. Buranda T, Huang J, Ramarao G V., et al. Biomimetic Molecular Assemblies on Glass and Mesoporous Silica Microbeads for Biotechnology. *Langmuir.* 2003;19(5):1654-1663. doi:10.1021/la026405+.

143. Zeineldin R, Piyasena ME, Sklar LA, Whitten D, Lopez GP. Detection of membrane biointeractions based on fluorescence superquenching. *Langmuir*. 2008;24(8):4125-4131. doi:10.1021/la703575r.
144. Conway JW, Madwar C, Edwardson TG, et al. Dynamic behavior of DNA cages anchored on spherically supported lipid bilayers. *J Am Chem Soc*. 2014;136(37):12987-12997. doi:10.1021/ja506095n.
145. Gopalakrishnan G, Rouiller I, Colman DR, Lennox RB. Supported bilayers formed from different phospholipids on spherical silica substrates. *Langmuir*. 2009;25(10):5455-5458. doi:10.1021/la9006982.
146. Adem SM. Development and characterization of stabilized, polymerized phospholipid bilayers on silica particles for specific immobilization of His-tagged proteins. *J Chem Sci*. 2015;127(4):729-735. doi:10.1007/s12039-015-0829-7.
147. Lauer SA, Nolan JP. Development and characterization of Ni-NTA-bearing microspheres. *Cytometry*. 2002;48(3):136-145. doi:10.1002/cyto.10124.
148. McMahon HT, Gallop JL. Membrane curvature and mechanisms of dynamic cell membrane remodelling. *Nature*. 2005;438(7068):590-596. doi:10.1038/nature04396.
149. Hua D, Yang Y, Zhang X, Zhu P, Fei J, Li J. Biotinylated lipid membrane patterns supported by proteins for the recognition of streptavidin polystyrene microspheres. *J Nanosci Nanotechnol*. 2010;10(10):6318-6323.
150. Crane JM, Tamm LK. Fluorescence Microscopy to Study Domains in Supported Lipid Bilayers. In: *Methods in Molecular Biology (Clifton, N.J.)*. Vol 400. ; 2007:481-488. doi:10.1007/978-1-59745-519-0_32.
151. Galush WJ, Nye JA, Groves JT. Quantitative fluorescence microscopy using supported lipid bilayer standards. *Biophys J*. 2008;95(5):2512-2519. doi:10.1529/biophysj.108.131540.
152. Mingeot-Leclercq M-P, Deleu M, Brasseur R, Dufrêne YF. Atomic force microscopy of supported lipid bilayers. *Nat Protoc*. 2008;3(10):1654-1659. doi:10.1038/nprot.2008.149.
153. El Kirat K, Morandat S, Dufrêne YF. Nanoscale analysis of supported lipid bilayers using atomic force microscopy. *Biochim Biophys Acta - Biomembr*. 2010;1798(4):750-765. doi:10.1016/j.bbamem.2009.07.026.
154. Hull MC, Cambrea LR, Hovis JS. Infrared Spectroscopy of Fluid Lipid Bilayers. *Anal Chem*. 2005;77(18):6096-6099. doi:10.1021/ac050990c.
155. Grélard A, Loudet C, Diller A, Dufourc EJ. NMR Spectroscopy of Lipid Bilayers. In: *Methods in Molecular Biology (Clifton, N.J.)*. Vol 654. ; 2010:341-359. doi:10.1007/978-1-60761-762-4_18.

156. Zwang TJ, Fletcher WR, Lane TJ, Johal MS. Quantification of the Layer of Hydration of a Supported Lipid Bilayer. *Langmuir*. 2010;26(7):4598-4601. doi:10.1021/la100275v.
157. Tawa K, Morigaki K. Substrate-supported phospholipid membranes studied by surface plasmon resonance and surface plasmon fluorescence spectroscopy. *Biophys J*. 2005;89(4):2750-2758. doi:10.1529/biophysj.105.065482.
158. Salamon Z, Wang Y, Tollin G, Macleod HA. Assembly and molecular organization of self-assembled lipid bilayers on solid substrates monitored by surface plasmon resonance spectroscopy. *Biochim Biophys Acta*. 1994;1195(2):267-275. doi:10.1016/0005-2736(94)90266-6.
159. Howland MC, Szmodis AW, Sanii B, Parikh AN. Characterization of physical properties of supported phospholipid membranes using imaging ellipsometry at optical wavelengths. *Biophys J*. 2007;92(4):1306-1317. doi:10.1529/biophysj.106.097071.
160. Beneš M, Billy D, Benda A, Speijer H, Hof M, Hermens WT. Surface-Dependent Transitions during Self-Assembly of Phospholipid Membranes on Mica, Silica, and Glass. *Langmuir*. 2004;20(23):10129–10137. doi:10.1021/LA048811U.
161. Webb AJ. Early microscopy: history of fine needle aspiration (FNA) with particular reference to goitres. *Cytopathology*. 2001;12(1):1-6. doi:10.1046/j.1365-2303.2001.00276.x.
162. Van Meerbeek B, Vargas M, Inoue S, et al. Microscopy investigations. Techniques, results, limitations. *Am J Dent*. 2000;13(Spec No):3D-18D.
163. Thorn K. A quick guide to light microscopy in cell biology. *Mol Biol Cell*. 2016;27(2):219-222. doi:10.1091/mbc.E15-02-0088.
164. Webb RH. Confocal optical microscopy. *Reports Prog Phys*. 1996;59(3):427-471. doi:10.1088/0034-4885/59/3/003.
165. Reichelt R. Scanning Electron Microscopy. In: *Science of Microscopy*. New York, NY: Springer New York; 2007:133-272. doi:10.1007/978-0-387-49762-4_3.
166. Goldstein JI, Newbury DE, Echlin P, et al. *Scanning Electron Microscopy and X-Ray Microanalysis*. Boston, MA: Springer US; 1992. doi:10.1007/978-1-4613-0491-3.
167. Salapaka S, Salapaka M. Scanning Probe Microscopy. *IEEE Control Syst Mag*. 2008;28(2):65-83. doi:10.1109/MCS.2007.914688.
168. Gumí-Audenis B, Costa L, Carlá F, Comin F, Sanz F, Giannotti MI. Structure and Nanomechanics of Model Membranes by Atomic Force Microscopy and Spectroscopy: Insights into the Role of Cholesterol and Sphingolipids. *Membranes (Basel)*. 2016;6(4):58. doi:10.3390/membranes6040058.

169. Silvius JR, Nabi IR. Fluorescence-quenching and resonance energy transfer studies of lipid microdomains in model and biological membranes (Review). *Mol Membr Biol*. 2006;23(1):5-16. doi:10.1080/09687860500473002.
170. Casuso I, Sens P, Rico F, Scheuring S. Experimental evidence for membrane-mediated protein-protein interaction. *Biophys J*. 2010;99(7):L47-L49. doi:10.1016/j.bpj.2010.07.028.
171. Zhao H, Lappalainen P. A simple guide to biochemical approaches for analyzing protein-lipid interactions. *Mol Biol Cell*. 2012;23(15):2823-2830. doi:10.1091/mbc.E11-07-0645.
172. Campanella ME, Chu H, Low PS. Assembly and regulation of a glycolytic enzyme complex on the human erythrocyte membrane. *Proc Natl Acad Sci*. 2005;102(7):2402-2407. doi:10.1073/pnas.0409741102.
173. Leonenko ZV, Cramb DT. Dynamics in Model Membranes and DNA-Membrane Complexes Using Temperature Controlled Atomic Force Microscopy. In: *Scanning Probe Microscopy: Characterization, Nanofabrication and Device Application of Functional Materials*. Dordrecht: Kluwer Academic Publishers; 2005:475-483. doi:10.1007/1-4020-3019-3_29.
174. Berquand A, Mingeot-Leclercq M-P, Dufrêne YF. Real-time imaging of drug-membrane interactions by atomic force microscopy. *Biochim Biophys Acta*. 2004;1664(2):198-205. doi:10.1016/j.bbamem.2004.05.010.
175. Li M, Liu L, Xi N, Wang Y. Nanoscale monitoring of drug actions on cell membrane using atomic force microscopy. *Acta Pharmacol Sin*. 2015;36(7):769-782. doi:10.1038/aps.2015.28.
176. Dimova R, Aranda S, Bezlyepkina N, Nikolov V, Riske KA, Lipowsky R. A practical guide to giant vesicles. Probing the membrane nanoregime via optical microscopy. *J Phys Condens Matter*. 2006;18(28):S1151-S1176. doi:10.1088/0953-8984/18/28/S04.
177. Drescher DG, Drescher MJ, Ramakrishnan NA. Surface Plasmon Resonance (SPR) Analysis of Binding Interactions of Proteins in Inner-Ear Sensory Epithelia. In: *Methods in Molecular Biology (Clifton, N.J.)*. Vol 493. ; 2009:323-343. doi:10.1007/978-1-59745-523-7_20.
178. Vaseashta A (Ashok), Braman E, Susmann P. *Technological Innovations in Sensing and Detection of Chemical, Biological, Radiological, Nuclear Threats and Ecological Terrorism*. Springer; 2012.
179. Stahelin R V. Surface plasmon resonance: a useful technique for cell biologists to characterize biomolecular interactions. *Mol Biol Cell*. 2013;24(7):883-886. doi:10.1091/mbc.E12-10-0713.
180. Hodnik V, Anderluh G. Surface Plasmon Resonance for Measuring Interactions of

- Proteins with Lipid Membranes. In: *Methods in Molecular Biology (Clifton, N.J.)*. Vol 974. ; 2013:23-36. doi:10.1007/978-1-62703-275-9_2.
181. Liu Y, Cheng Q. Detection of Membrane-Binding Proteins by Surface Plasmon Resonance with an All-Aqueous Amplification Scheme. *Anal Chem*. 2012;84(7):3179-3186. doi:10.1021/ac203142n.
 182. Hall K, Aguilar M-I. Surface Plasmon Resonance Spectroscopy for Studying the Membrane Binding of Antimicrobial Peptides. In: *Methods in Molecular Biology (Clifton, N.J.)*. Vol 627. ; 2010:213-223. doi:10.1007/978-1-60761-670-2_14.
 183. Ahmed FE, Wiley JE, Weidner DA, Bonnerup C, Mota H. Surface plasmon resonance (SPR) spectrometry as a tool to analyze nucleic acid-protein interactions in crude cellular extracts. *Cancer Genomics Proteomics*. 2010;7(6):303-309.
 184. Helmerhorst E, Chandler DJ, Nussio M, Mamotte CD. Real-time and Label-free Bio-sensing of Molecular Interactions by Surface Plasmon Resonance: A Laboratory Medicine Perspective. *Clin Biochem Rev*. 2012;33(4):161-173.
 185. Masina R, Zhu XD, Parikh AN, Bruch R, Landry JP. Biophotonics studies on lipid membranes using oblique incidence reflectivity difference (OI-RD) ellipsometry. In: Cartwright AN, Nicolau D V., eds. *Nanobiophotonics and Biomedical Applications III*. Vol 6095. International Society for Optics and Photonics; 2006:60950T. doi:10.1117/12.657478.
 186. Marquês JMT. Supported lipid bilayers with micro/nanodomains in the study of membrane lipid organization and interactions. 2015. <http://repositorio.ul.pt/handle/10451/22728>.
 187. Trewby W, Livesey D, Voitchovsky K. Buffering agents modify the hydration landscape at charged interfaces. *Soft Matter*. 2016;12(9):2642-2651. doi:10.1039/C5SM02445E.
 188. Pascu R, Dinescu M. Spectroscopic Ellipsometry. *Rom Reports Phys*. 2012;64(1):135-142.
 189. Jahan-Tigh RR, Ryan C, Obermoser G, Schwarzenberger K. Flow Cytometry. *J Invest Dermatol*. 2012;132(10):1-6. doi:10.1038/jid.2012.282.
 190. Edwards BS, Sklar LA. Flow Cytometry: Impact on Early Drug Discovery. *J Biomol Screen*. 2015;20(6):689-707. doi:10.1177/1087057115578273.
 191. Morgan E, Varro R, Sepulveda H, et al. Cytometric bead array: a multiplexed assay platform with applications in various areas of biology. *Clin Immunol*. 2004;110(3):252-266. doi:10.1016/j.clim.2003.11.017.
 192. Piyasena ME, Graves SW. The intersection of flow cytometry with microfluidics and microfabrication. *Lab Chip*. 2014;14(6):1044-1059. doi:10.1039/C3LC51152A.

193. Givan AL. *Flow Cytometry: First Principles*. New York, USA: John Wiley & Sons, Inc.; 2001. doi:10.1002/0471223948.
194. Bio-Rad Laboratories. *Flow Cytometry Basics Guide*. <https://www.bio-rad-antibodies.com/static/2017/flow/flow-cytometry-basics-guide.pdf>.
195. Ormerod MG. *The Flow Cytometer*. DeNovo Software
<http://flowbook.denovosoftware.com/chapter-2-flow-cytometer>.
196. Macey MG. Principles of Flow Cytometry. In: *Flow Cytometry Principles and Applications*. Totowa, New Jersey: Humana Press; 2007:1-16.
197. Pereira M de L, Oliveira H, Fonseca H, MAC, Costa FG, Santos C. The Role of Cytometry for Male Fertility Assessment in Toxicology. In: *Flow Cytometry - Select Topics*. InTech; 2016. doi:10.5772/62965.
198. Shapiro HM. *Practical Flow Cytometry*. 4th ed. Wiley-Liss; 2003.
199. Shapiro HM. Lasers for Flow Cytometry. In: *Current Protocols in Cytometry*. 4th ed. Hoboken, NJ, USA: John Wiley & Sons, Inc.; 2004.
doi:10.1002/0471142956.cy0109s27.
200. Becton Dickinson and Company. *Introduction to Flow Cytometry: A Learning Guide*. San Jose, CA; 2002.
201. Baumgarth N, Roederer M. A practical approach to multicolor flow cytometry for immunophenotyping. *J Immunol Methods*. 2000;243(1-2):77-97.
doi:10.1016/S0022-1759(00)00229-5.
202. Purruicker O, Hillebrandt H, Adlkofer K, Tanaka M. Deposition of highly resistive lipid bilayer on silicon–silicon dioxide electrode and incorporation of gramicidin studied by ac impedance spectroscopy. *Electrochim Acta*. 2001;47:791-798.
203. Mornet S, Lambert O, Duguet E, Brisson A. The Formation of Supported Lipid Bilayers on Silica Nanoparticles Revealed by Cryoelectron Microscopy. *Nano Lett*. 2005;5(2):281–285. doi:10.1021/nl048153y.
204. Fabry-Wood A, Fetrow ME, Brown CW, et al. A Microsphere-Supported Lipid Bilayer Platform for DNA Reactions on a Fluid Surface. *ACS Appl Mater Interfaces*. 2017;9(35):30185–30195. doi:10.1021/acsami.7b11046.
205. Adams PG, Lamoureux L, Swingle KL, Mukundan H, Montañó GA. Lipopolysaccharide-Induced Dynamic Lipid Membrane Reorganization: Tubules, Perforations, and Stacks. *Biophys J*. 2014;106(11):2395-2407.
doi:10.1016/j.bpj.2014.04.016.

Chapter 2.

Materials and Methods

This chapter intends to explore, in great detail, the materials, methods and protocols used in the experiments described in chapters 3-5, an Appendix I.

2.1 Materials

2.1.1 Buffers

When working with cells or cell-like structures a buffer is needed to provide an environment of appropriate pH and ionic composition for biological compounds. For the experiments detailed in Chapters 3-5, we used Phosphate buffered saline (PBS) and 4-(2-hydroxyethyl)-1-piperazineethanesulfonic acid (HEPES buffer).

- **PBS**

PBS is a commonly used buffer solution to maintain pH and osmotic balance. Usually, PBS contains deionized water, disodium hydrogen phosphate (Na_2HPO_4), sodium chloride (NaCl) and, in some formulations, potassium dihydrogen phosphate (KH_2PO_4) and potassium chloride (KCl). The pH of PBS is set to be close to physiological pH (~7.4), its osmolarity is kept close to that in the human body, and it is non-toxic.¹ We purchased Phosphate buffered saline (PBS) in powder form from Sigma Aldrich (P3813). After its dilution in deionized Millipore water, the final concentration is 0.01 M PBS (NaCl 0.138 M; KCl 0.0027 M); pH 7.4, at 25 °C.

- **HEPES**

HEPES is a biological dipolar ionic buffering solution widely used in cell culture, as it maintains a physiological pH despite the presence of carbon dioxide.² HEPES can be prepared in combination with different salts and it has a useful pH range of 6.8 - 8.2. However, it can be toxic to some cell types at concentrations greater than 40 mM.³ We purchased HEPES in powder form from Sigma Aldrich (Product code: H3375). After its dilution in deionized Millipore water, and the addition of NaCl and CaCl₂, the final concentrations are: 10 mM HEPES, 10 mM NaCl, and 2.5 mM CaCl₂; pH 7.35 (titrated with NaOH). The solution was stored at 25 °C. We purchased CaCl₂ •2(H₂O) from Millipore Sigma (Calbiochem) (Product code: 208290); NaCl from Suprapur (Product code: 1064060050); and NaOH from Sigma Aldrich (Product code: S8045).

2.1.2 Microspheres

In this work we explore and discuss the use of microspheres as a substrate for membranes, as well as the advantages and potentials of similar platforms. Briefly, unlike planar-supported lipid bilayers, microsphere-supported lipid bilayers and their interaction with different components can be studied using medium to high-throughput screening processes. Most of the previous work done on microsphere-supported lipid bilayers was done using porous microspheres,⁴ and although the pores can be used to be loaded, the non-porous microspheres offer a more uniform support, similar to planar silica.

Non-porous silica microspheres are produced in cGMP facilities, through different processes, among which the most common is the Stöber method, in which silicates and solvents like water, alcohol and ammonia are agitated, resulting in silica particles of different sizes.⁵ On the other hand, polystyrene microspheres are generated by suspension,

emulsion, precipitation and dispersion polymerizations.⁶ Polystyrene microspheres can be functionalized by including certain groups to the microsphere surface, the most common groups being amine and carboxyl groups.

For the experiments detailed in here, we used Spherotech's microparticles, which are kept in a buffer consisting of deionized water with 0.02% sodium azide. We purchased and used the following products:

- 3.14 μm diameter (SIP-30-10) and 7.9 μm diameter (SIP-60-10) non-porous silica microspheres, with a density of 1.96 g/ml. They maintain their shape and size when exposed to aqueous or non-aqueous environments and can withstand temperatures of up to 1000°C.
- 5.28 μm diameter (CP-50-10) non-porous carboxylated-polystyrene microspheres with a density of 1.05 g/ml and a refractive index of 1.59. These beads are highly uniform and monodisperse and are stable only in aqueous solvents and typically contain ~ 50 $\mu\text{eq/g}$ of carboxyl groups on their surface.

2.1.3 Lipids

Since phospholipids are the major component of cell membranes, we use different commercially available lipids to build membrane structures. Lipids are usually extracted from cells, tissues or fluids. Then, they are separated from any other type of molecules, such as proteins or amino acids, and finally are preserved. All the lipids used in the experiments reported in chapters 3-5 were purchased in lyophilized form from Avanti Polar Lipids. Following, there is the list of all the lipids we used:

- POPC (16:0-18:1 PC) (1-palmitoyl-2-oleoyl-sn-glycero-3-phosphocholine), is one of the most common lipids used in model lipids for mammalian cell-mimicking experiments⁷ since phosphatidylcholines are the major component of biological membranes. Phosphatidylcholines are widely commercially available, as they can be easily chemically extracted from soybeans, egg yolk and others.⁸ The POPC we purchased is neutrally charged, it has a pKa ~ 1.0, and its phase transition temperature is -2°C. We used POPC in the work described in chapter 3. Avanti Polar Lipids product code: 850457.
- Biotin-DOPE (18:1 Biotinyl-PE) (1,2-dioleoyl-sn-glycero-3-phosphoethanolamine-N-(biotinyl)). Phosphoethanolamine (PE) is the most abundant phospholipid in bacterial membranes and the second most abundant in mammalian and plant cell membranes.⁹ PE can be found in high quantities in the human nervous system and it plays an important role in different biological processes such as cell division,¹⁰ membrane fusion,¹¹ and protein modification,¹² among others. Biotin is a B-complex vitamin that plays an important role in processes such as fatty acid and amino acid production, cell growth and the stabilization of blood sugar levels.¹³ Biotin's small size (MW = 244.31 Da) and its high affinity for avidin, streptavidin and NeutrAvidin make biotin a widely used label for protein detection.¹⁴ Moreover, the biotin-streptavidin binding is resistant to changes in pH and extreme heat.¹⁴ The Biotin-DOPE we purchased is neutrally charged, it has two pKa values: 5.61 and 10.39, and its phase transition temperature is -8.1°C. We used Biotin-DOPE in the work described in chapter 3. Avanti Polar Lipids product code: 870282.

- NBD-DOPE (18:1 NBD-PE) (1,2-dioleoyl- sn-glycero- 3-phosphoethanolamine-N- (7-nitro- 2-1,3- benzoxadiazol-4- yl) was the lipid we used for fluorescent tagging in chapters 3, 4, 5 and Appendix I. NBD (7-nitro- 2-1,3- benzoxadiazol-4- yl) is a widely used fluorophore in biochemical and cell biological assays due to its stability at varying pH and its neutral charge.¹⁵ NBD has an excitation maximum of 460nm and an emission maximum of 535 nm. In this product, the NBD label is attached to the head groups of PE. Avanti Polar Lipids product code: 810145.
- GM1 (monosialotetrahexosylganglioside) is a member of the Gangliosides family, which are amphiphilic molecules located in the outer leaflet of the plasma membrane.^{16,17} GM1 plays important roles in processes such as cell adhesion, cell-cell recognition and neuroprotection.^{18,19} There is special interest in GM1 as it acts as the binding site for Cholera toxin and E. coli heat-labile enterotoxin.^{20,21} We used GM1 in the work described in chapters 3 and 5. The GM1 we purchase was extracted from ovine brain. Avanti Polar Lipids product code: 860065.
- DOPC (18:1 (Δ^9 -Cis) PC) (1,2-dioleoyl-sn-glycero-3-phosphocholine) is a naturally occurring phospholipid. DOPC is the cis- counterpart of POPC, and it has been reported that the Ld phase of DOPC is less ordered than that of POPC.²² We used DOPC in the work described in chapters 4, 5 and Appendix I. The DOPC we purchased is neutrally charged, and its phase transition temperature is -17°C. Avanti Polar Lipids product code: 850375.
- Lissamine Rhodamine B– DOPE (18:1 Liss Rhod PE) (1,2-dioleoyl-sn-glycero-3-phosphoethanolamine-N-(lissamine rhodamine B sulfonyl) (ammonium salt)) was one of the lipids used for fluorescent tagging in Appendix I. This fluorophore is stable at

varying pH values,²³ and it is neutrally charged. Lissamine Rhodamine B has an excitation maximum of 560 nm and an emission maximum of 583 nm. In this product, the Lissamine Rhodamine B label is attached to the head groups of PE. We used Lissamine Rhodamine B– DOPE in the work described in chapter 4. Avanti Polar Lipids product code: 810150.

- Cholesterol (ovine wool, >98%) is one of the most important components in animal cells, as it constitutes about 1/3 of their membranes and regulates membrane fluidity and permeability. We used Cholesterol in the work described in Appendix I. Avanti Polar Lipids product code: 700000.
- DPPG (16:0 PG) (1,2-dipalmitoyl-sn-glycero-3-phospho-(1'-rac-glycerol) (sodium salt)) is an anionic lipid molecule present in alveolar cells in humans.²⁴ Its phase transition temperature is 41°C. We used DPPG in the work described in Appendix I. Avanti Polar Lipids product code: 840455.
- DOTAP (18:1 TAP) (1,2-dioleoyl-3-trimethylammonium-propane) is a cationic lipid molecule that has been shown to be effective DNA and RNA transfection.²⁵ Its phase transition temperature is <5°C. We used DOTAP in the work described in Appendix I. Avanti Polar Lipids product code: 890890.
- (Texas Red-DHPE) (Texas Red 1,2-Dihexadecanoyl-sn-Glycero-3-Phosphoethanolamine, Triethylammonium Salt) was used in the work described in chapter 5. Texas Red has an excitation maximum of 595 nm and an emission maximum of 615 nm. In this product, the Texas Red label is placed in the head groups of PE. ThermoFisher Scientific Lipid product code: T1395MP.

Lipids are dissolved in non-polar solvents. One of the most common solvents is chloroform (CHCl_3), which is a colorless and volatile substance used also as a reagent in industry. We purchased the chloroform from EMD Millipore (product code CX1055), that contains 1%-5% of ethanol as a stabilizer.

2.1.4 Extruder

Extrusion is one of the most common methods to break multilamellar vesicles (MLVs) into monodisperse unilamellar vesicles with the aid of filters and moderate pressure applied by syringes.²⁶

We purchased a Mini-Extruder set with a holder/ heating block, which included:

- Extruder
 - Extruder outer casing
 - Retaining nut
 - Teflon bearing
 - 2 internal membrane supports
 - 2 O-rings
- 2 syringes (1 ml volume)
- Polycarbonated membranes (0.1 μm pore sizes)
- Filter supports,
- Holder/heating block.

Avanti Polar Lipids product code: 610000. See Figure 2.1 to observe the assembly process.

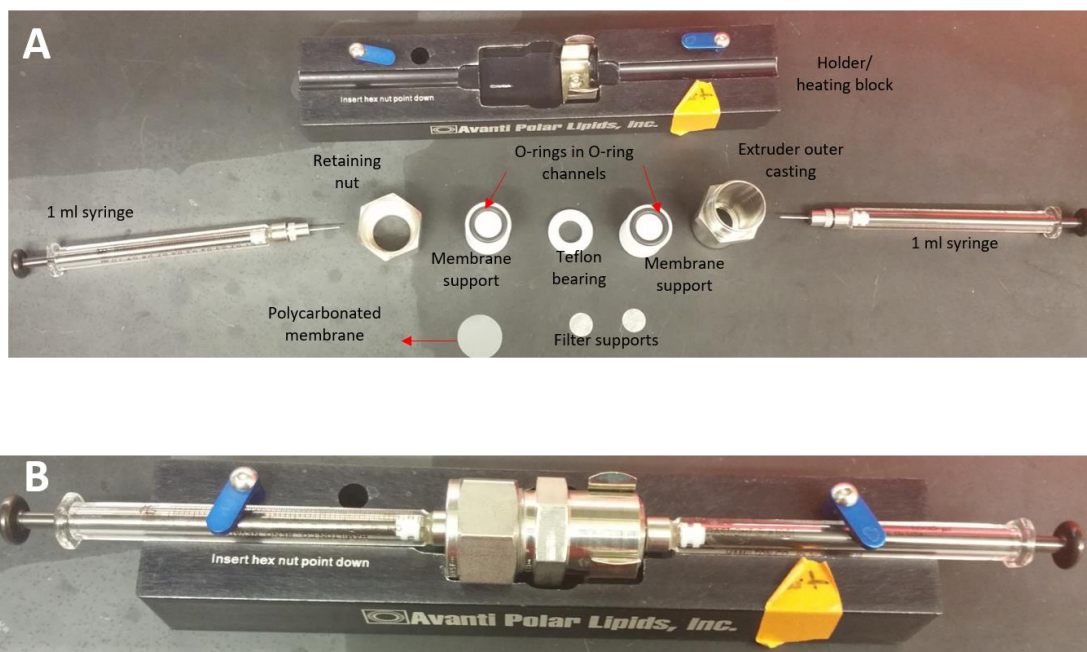


Figure 2.1. A) Parts of the mini extruder. B) Assembly of the extruder.

2.1.5 Proteins

- Cholera is a toxin produced by *Vibrio cholerae* and it has two types of subunits; the A subunit carries the toxic part, and the pentameric B subunit binds to the high-affinity GM₁ receptors, usually located in the intestinal epithelial cell membranes.^{27,28} We purchased cholera toxin B subunit (recombinant)-Alexa Fluor 647 (CTxB-Alexa 647) from ThermoFisher in powder form. Alexa Fluor 647 has an excitation maximum of 650 nm and an emission maximum of 668 nm. We diluted the CTxB-Alexa 647 in PBS, and it was stored at 2°C until use. ThermoFisher product code: C34778.
- Streptavidin is a protein that binds to biotin with high affinity due to a very strong non-covalent interaction. Compared to similar proteins, like avidin, streptavidin has lower non-specific binding.²⁹ We purchased streptavidin-PE/Cy5 (SAv-Cy5) diluted in phosphate-buffered solution, pH 7.2, (containing 0.09% sodium azide) from Biolegend.

PE/Cy5 has an excitation maximum of 488 nm and an emission maximum of 670 nm. We stored the solution at 2°C until use. Biolegend product code: 405205.

- BSA (Bovine serum albumin) is a globular protein isolated from cows, and it is widely used in various biochemical applications. BSA is used as a blocking agent, meaning that BSA binds to nonspecific binding sites, and prevents the analyte from doing the same.³⁰ BSA has a negative net charge at physiological pH.³¹ We used BSA as a blocking agent in the assays described in chapters 3, 4, 5 and Appendix I. We purchased BSA from Sigma Aldrich (Product code: A3294) in powder form, protease free and at pH 7.
- BSA-FITC (Albumin bovine–fluorescein isothiocyanate conjugate) has the same properties of regular BSA. The fluorescent tag FITC has an excitation maximum of 495 nm and an emission maximum of 520 nm. We purchased the BSA-FITC from Sigma Aldrich (Product code: A9771) in powder form. We used BSA-FITC in part of the work described in Appendix I.
- Although propidium iodide (PI) is not a protein, we included it in this list as it was used alongside the BSA-FITC. PI is a fluorescent stain that is not permeant to intact cell membranes and such is used to detect apoptotic cells.³² We purchased PI from Sigma Aldrich (Product code: P4170). PI has an excitation maximum of 533 nm and an emission maximum of 617 nm. We used the PI for some of the experiments described in Appendix I.

2.1.6 Membrane disruption agents

- LDAO (N,N-Dimethyldodecylamine N-oxide) is a zwitterionic detergent commonly used to gently disrupt the cell's phospholipid bilayer, and to then extract the

- undisrupted membrane proteins that were embedded in the membrane.³³ We purchased the LDAO in powder form from Avanti Polar Lipids. We diluted in PBS, pH 7.34, and we stored it at -20°C until use. LDAO has a critical micelle concentration (c.m.c.) of ~1-2mM. Avanti Polar Lipids product code: 850545.
- LPS (Lipopolysaccharides) are macromolecules located on the outer membrane of Gram-negative bacteria. They have a toxic effect on healthy mammalian cells, as they induce a strong immune response.³⁴ LPS are comprised of three parts: 1) The lipid A, which is the hydrophobic moiety of LPS and it carries the toxic properties; 2) the core polysaccharide chain, which usually contains phosphates or amino acids; and 3) the O antigen, which is a repeating oligosaccharide chain, unique to each bacterial serotype.³⁵ The reported c.m.c of LPS is ~ 15-25 µg/mL.³⁶ The LPS we used in chapter 4 was kindly provided by Dr. Montano's group at CINT, and it was originally purchased from Sigma Aldrich in a lyophilized form. LPS was purified by phenol extraction from Escherichia coli O111:B4. Sigma Aldrich product code: L2630.
 - SDS (Sodium dodecyl sulfate) is a common anionic detergent used for cell lysing for DNA or protein extraction.³⁷ SDS has a c.m.c. of ~ 8-8.5mM.³⁸ SDS is also present in many household cleaning and hygiene products. We purchased SDS from Bio Rad at 10% (w/v). Bio Rad product code: 1610416.
 - Triton X-100 ($C_{14}H_{22}O(C_2H_4O)_n$; n= 9-10) is nonionic surfactant commonly used for cell lysing for protein extraction. At high concentration or long exposure can be toxic for the cells.³⁹ Triton X-100 has a c.m.c. ~ 0.22 -0.24 mM.⁴⁰ We purchased Triton X-100 from OmniPur via Sigma Aldrich with a pH of 6.0-8.0. OmniPur product code: 9410.

2.1.7 Polymers

- pEO-b-pBD (Poly[butadiene(1,4 addition or 1,2 addition)-b-ethylene oxide]) is an amphiphilic block copolymer that can be directly synthesized using diverse methods, and it is soluble in THF, chloroform, and toluene. We used this diblock copolymer in the work described in chapter 5. pEO-b-pBD (1.2-b-1.3) was kindly provided by Dr. Montaña's group at CINT, and it was originally purchased from Polymer Source (Product code: P6723-BdEO).
- Chitosan is an extensively studied cationic polymer with non-toxicity, antibacterial activity, antioxidant activity, and high biocompatibility.⁴¹ Chitosan is used in different areas such as cosmetics and foods,^{42,43} but most importantly it has a variety of pharmaceutical and biomedical applications.⁴⁴ Moreover, chitosan has the advantage of being widely commercially available at a low cost. We used chitosan in part of the work described in Appendix I. We purchased low molecular weight chitosan from Sigma Aldrich (Product code: 448869)
- PLL (Poly-L-lysine) is a cationic synthetic polymer used to enhance the interaction and attachment of cell membranes to solid culture surfaces.⁴⁵ PLL has also applications as a food preservative.⁴⁶ We used PLL in part of the work described in Appendix I. We purchased poly-L-lysine hydrobromide with a molecular weight 4,000-15,000 by viscosity from Sigma Aldrich (Product code: P6516).
- PLL-FITC (Poly-L-lysine hydrobromide-FITC Labeled) was used in part of the work described in Appendix I, for detection purposes. We purchased PLL-FITC from Sigma Aldrich (Product code: P3543). The PLL-FITC has a molecular weight of 15,000-30,000 by viscosity, and an extent of labeling of 0.003-0.01 mole FITC per mole lysine

monomer. FITC has an excitation maximum of 490 nm and an emission maximum of 525 nm.

- FITC (Fluorescein isothiocyanate) is a widely used fluorescein-derivative fluorochrome. FITC has an excitation maximum of 490 nm and an emission maximum of 525 nm at neutral pH. FITC emission levels are pH sensitive (FITC fluorescence intensity increases with increasing pH).⁴⁷ We used FITC in the fluorescent tagging of chitosan in the work described on Appendix I. We purchased FITC from Sigma Aldrich (Product code: F7250).
- THF (tetrahydrofuran) is a popular organic solvent and is commonly used in polymer science. We used THF as a polymer solvent in the work described in chapter 5. THF anhydrous was kindly provided by Dr. Montaña's group at CINT, and it was originally purchased from Sigma Aldrich (Product code: 401757).

2.1.8 Instruments

Flow cytometers. The main goal of this work was the development of multiplexable biomimetic membrane assemblies on silica microspheres for flow-based screening applications. Therefore, flow cytometry was our technology of choice for the analysis of the proposed studies. We used the following two flow cytometers:

- **BD Accuri C6** is a highly sensitive flow cytometer that relies on low-pressure pumping and hydrodynamic focusing to be able to screen as many as 10,000 events per second. Its collection sip supports any tubes 75x12 mm or smaller, but it can also support the BD CSampler that can hold 48- and 96-well plates, or 24-tube rack. Finally, this flow cytometer can use laboratory-grade water as sheath fluid.⁴⁸ The BD Accuri C6 is equipped with two lasers with independent optical paths; a blue laser (488 nm) and a

red laser (640 nm) and with 4 detection channels; three from the blue laser -- FL-1 (533 nm center with 30 nm bandpass (BP)); FL-2 (585 nm center with 40 nm BP); FL-3 (670 nm long-pass (LP)); and one from the red laser -- FL-4 (675 nm center wavelength/25 nm BP). Moreover, some other filters are available for purchase.⁴⁸

We used the BD Accuri C6 for the work described in chapter 3 and part of Appendix I.

- The **Attune NxT** flow cytometer by ThermoFisher Scientific relies on acoustic-assisted hydrodynamic focusing, which significantly reduces the chance of clogging. This technology's effectiveness allows rapid detection of rare events and minimal data variation regardless of sample rate. The Attune NxT has sample flow rates ranging from 12.5–1,000 $\mu\text{L}/\text{min}$, hence it can screen up to 35,000 events per second.⁴⁹ The Attune NxT is equipped with four lasers with independent optical paths: violet (405 nm); blue (488 nm); yellow (561 nm); and red (637 nm); and a fifth laser is available for purchase: green (532 nm). It can detect up to 14 colors, as it has many detection channels⁴⁹ (See Appendix I, Figure AI-9 (Table)).

We used the Attune NxT for the work described in chapters 4, 5 and part of Appendix I.

Confocal microscope. We used laser-scanning confocal microscopy (LSCM) to obtain complementary visual support to the flow cytometric data obtained in chapters 3, 4, 5 and Appendix I. The images and FRAP experiments were done using **FV-1000** inverted optical microscope (**Olympus, Tokyo, Japan**).

UV cleaner. We used the UVO-Cleaner by Jelight Company, Inc. Model No 144AX. in our first attempt to modify the surface of polystyrene beads (detailed in Appendix I).

Ozone cleaner. We used a Harrick Plasma Cleaner PDC-32G in our second attempt to modify the surface of polystyrene beads (detailed in Appendix I).

2.1.9 Data Analysis

To analyze all the data, we generated in the work described in chapters 3-5 and Appendix I, we used the following software:

FlowJo software was used to the flow cytometric data (gating, compensation, statistics, etc.).

MatLab and **Excel** were used for the numerical and statistical analysis. **MatLab** and **Igor** were used to generate the plots.

In addition to all the materials listed above, we used basic laboratory equipment such as micro-centrifuge vials, pipettes, glass vials, shaker, micro-centrifuge, syringes, syringe pumps, quartz cuvettes, etc.

2.2 Methods

2.2.1 *Lipid bilayers on silica microspheres protocol.*

2.2.1.1 Vesicle preparation

All the lipids were purchased in lyophilized form and they were dissolved and resuspended in chloroform. The lipid solutions were stored in glass vials, sealed and wrapped with parafilm and at -20 °C in the dark until use.

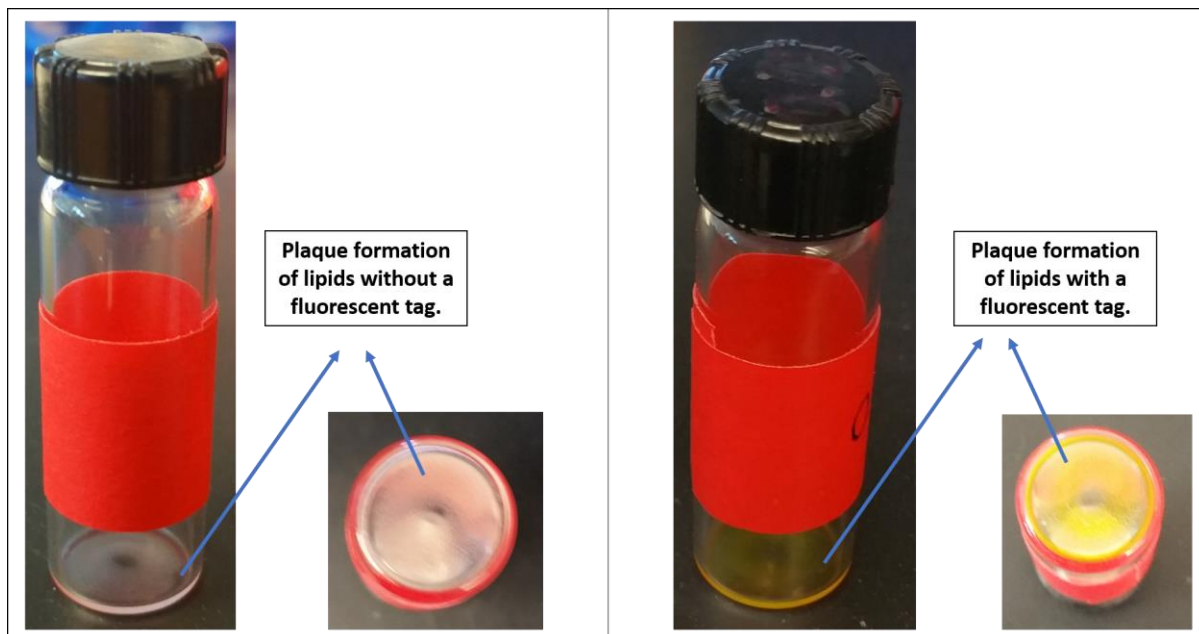


Figure 2.2. Lipid plaque formation with different lipid compositions.

In chapters 3-5 and Appendix I we prepared lipid vesicles with different compositions by mixing the right amount of stock lipids with glass syringes in different glass vials. The various mixtures of lipids were left under vacuum overnight to let the chloroform evaporate and to form lipid plaques at the bottom of the vials (see Figure 2.2).

Then, the lipid plaques were rehydrated and resuspended in buffer at a final concentration of 1mM. For all the liquid-phase lipids we worked with, the resuspension

process only required vortexing the rehydrated lipid plaques, which forms multilamellar

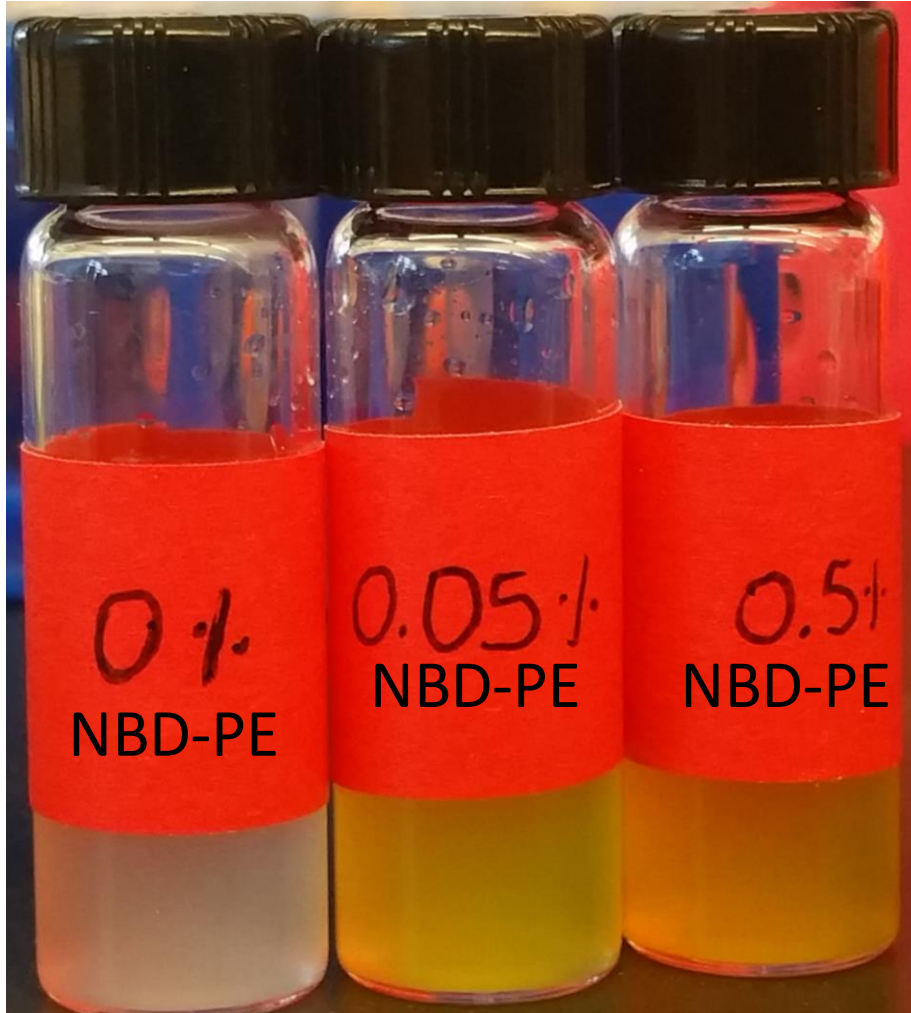


Figure 2.3. Lipid plaques with different lipid compositions resuspended in buffer.

vesicle (MLVs) solutions. As a visual example, Figure 2.3 show the picture of the resuspended lipids used in the experiments described in chapter 3.

2.2.1.2 Extrusion

We formed large unilamellar vesicles (LUVs) by extruding the MLVs solution. Briefly, we first wet the filter supports and 0.1 μm polycarbonate (PC) membranes with DI water and assemble the mini-extruder part as shown in Figure 2.1. Then, we passed the rehydrated

and resuspended lipids through the PC membrane 11 or 13 times. Finally, Figure 2.4 shows the tubes with the lipids before and after extrusion; the solution before extrusion is cloudy due to the presence of the MLVs and/or other large lipid particles, and after extrusion the solution gets clearer, as it contains the LUVs which are approximately 100 nm in size. Comparing both solutions is a good visual confirmation that the extrusion process was successful.

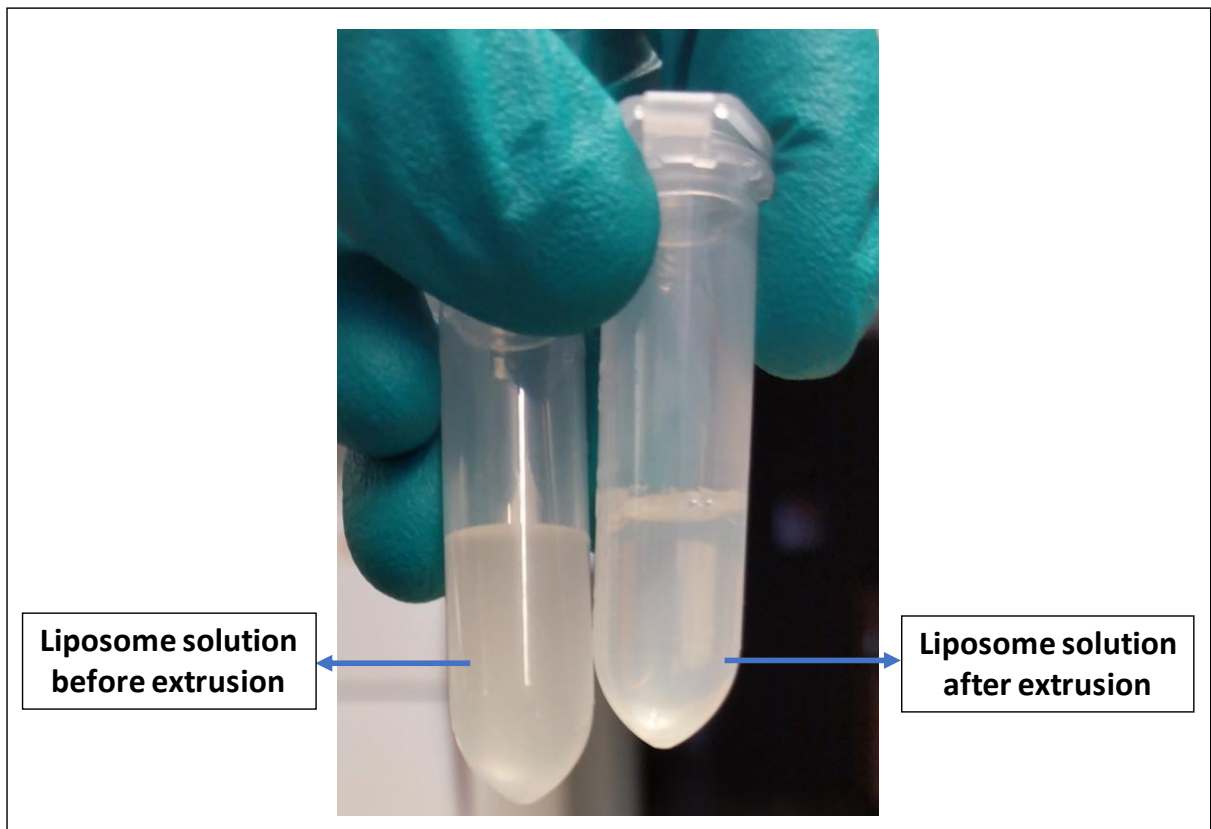


Figure 2.4. Liposome solution before and after extrusion

2.2.1.3 Lipid coating on beads

Although all the purchased silica microspheres come suspended in a clean aqueous solution, we made sure to keep the microsphere's surface clean and debris-free. We accomplished that by first suspending them in a basic solution (4% NH_4OH), centrifuging

and rinsing three times, then suspending them in an acidic solution (4% HCl), centrifuging and rinsing five times.

We used siliconized polypropylene Eppendorf tubes that we passivated before use by filling them with a 0.1 mg/mL BSA solution and placing them on a shaker for 45 min.

We formed lipid bilayers on the silica microspheres by incubating the suspension with 1mM LUVs solutions resulting from the extrusion process with the clean silica microspheres to a final concentration of 10^5 - 10^6 beads/ml. The incubation process consisted of placing the tubes with the LUVs and the microspheres on a shaker and vortexing them on high speed at room temperature for 10 min and on low speed for 45 min at 37 °C. These conditions promote the spontaneous fusion of the vesicles to the microspheres' surface to form the bilayers.

2.2.1.4 BSA-blocking

After incubating the beads with lipids, we added BSA to each sample to a final concentration of 0.5 mg/mL and we let them vortex on low speed for 45 minutes at room temperature. This was done to passivate the parts of the microspheres' surface that may have not been properly coated with the lipids. The presence of the BSA minimizes the nonspecific binding of the membrane-bound component to the silica bead.

2.2.1.5 Rinsing

All the samples were washed and rinsed three times to remove the unbound liposomes and extra BSA in solution. This was done by centrifuging the samples for 45 seconds at 10 000 rpm, removing the supernatant (leaving enough supernatant to keep the lipid-coated

beads hydrated ~ 50 μ L) and resuspending the samples in fresh buffer to bring them back up to volume.

Figure 2.5 shows the different steps of the lipid bilayers on silica microspheres

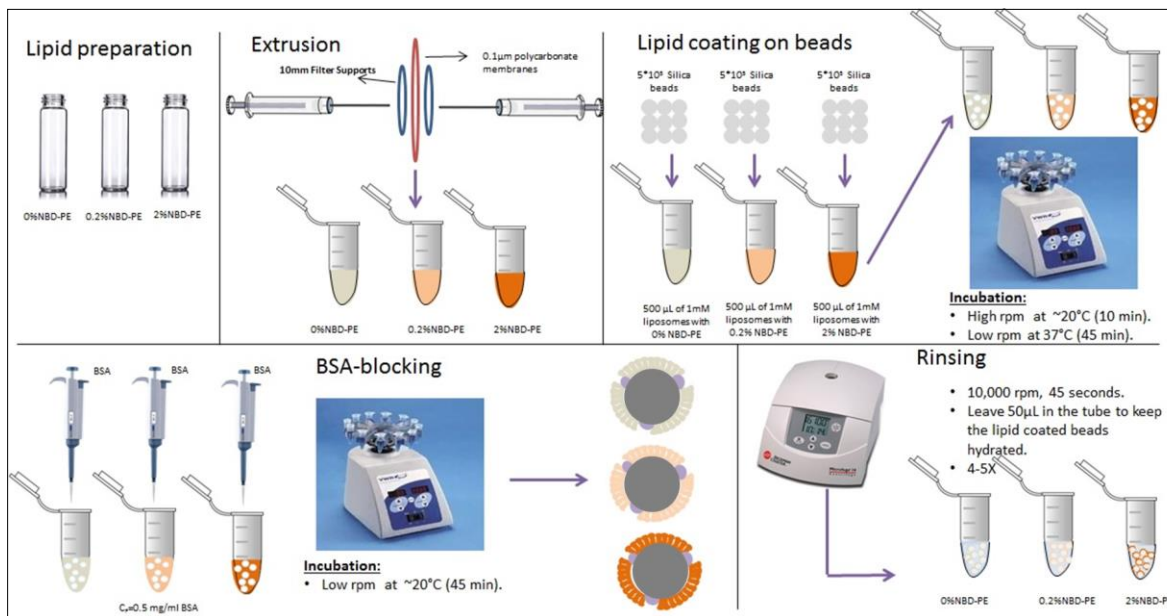


Figure 2.5. Schematic of the assembly of biomimetic membranes on non-porous silica microspheres.

protocol.

2.2.2 Protein-Membrane interaction assay

This section includes a more in-depth description of the methods used in the work described on chapter 3.

- **Multiplex set formation**

After the lipid bilayer formation on silica microspheres (3 μ m – diameter) is complete, we form a multiplex set by adding equal volumes of the different membrane compositions and fluorescent-tags to a single BSA-passivated Eppendorf tube.

- CTxB-Alexa 647 and GM1 binding.

We prepared the stock solution of CTxB-Alexa 647 by diluting the powdered toxin in PBS to a final concentration of 175nM, and we also prepared dilutions with a 75nM concentration. We stored the stock and dilution solutions at 2°C until use.

The membrane compositions on bilayers on the microspheres for this experiment consisted of POPC membranes containing specific amounts of GM1 (0–0.5 mol %) and NBD (0-2 mol%).

We used the 75nM CTxB-Alexa 647 aliquots to test the preferential binding of CTxB-Alexa 647 to GM1-containing membranes on microspheres by adding the right volumes to the individual and multiplex samples. The tested concentrations of CTxB-Alexa 647 were: 0nM, 2nM, 10nM and 20nM.

- SA_v-Cy5 and biotin binding

We prepared the stock solution of SA_v-Cy5 by diluting the powdered toxin in PBS to a final concentration of 421nM, and we also prepared dilutions with a 4.21nM concentration. We stored the stock and dilution solutions stored at 2°C until use.

The membrane compositions on bilayers on the microspheres for this experiment consisted of POPC membranes containing specific amounts of biotin-DOPE (0–0.5 mol %) and NBD (0-2 mol%).

We used the 4.21nM SA_v-Cy5 aliquots to test the preferential binding of SA_v-Cy5 to biotin-containing membranes on microspheres by adding the right volumes to the

individual and multiplex samples. The tested concentrations of SAV-Cy5 were: 0nM, 0.25nM, 0.5nM and 2.5nM.

- Cross reactivity assay

In this case, the multiplex set contained one sample with GM1 (0.5% mol), another one with biotin-DOPE (0.5% mol), and a final one with neither (100% POPC); all with different concentrations of NBD-DOPE.

We used the same aliquots described in the last two sub-sections to test the specific binding of CTxB-Alexa 647 to GM1 and SAV-Cy5 to biotin. The tested concentrations were: 20 nM CTxB-Alexa 647 and 2.5 nM SAV-Cy5.

2.2.3 *Membrane disruption assays.*

This section includes a more in-depth description of the methods used in the work described on chapter 4.

- Membrane composition of bilayers supported on microspheres.

The formation of lipid bilayers on silica microspheres was done following the same protocol as describe before. For all these assays testing the effects of SDS and Triton-X100 we used the 3 μm -diameter microspheres, and for the assays testing the effect of LDAO and LPS we used the 7.9 μm -diameter microspheres. The membrane compositions used were: 1) 99.5%mol DOPC+0.5%mol NBD-DOPE, or 2) 99.9%mol DOPC+0.1%mol Liss-Rhod-DOPE. The samples' final concentration of microspheres coated with lipid bilayers was $\sim 10^5$ beads/ml.

- Membrane-disrupting agents

We tested the membrane disrupting effects of **SDS** on microsphere-supported membranes with the following composition: 99.5%mol DOPC+0.5%mol NBD-DOPE. The stock solution of SDS was 10% w/v (346.77mM) and we prepared a dilution of 1% w/v (34.67mM); both were kept well-sealed and at room temperature. The tested SDS concentrations were: 0 mM, 0.08 mM, 0.8mM and 8mM.

We tested the membrane disrupting effects of **Triton X-100** on microsphere-supported membranes with the following composition: 99.5%mol DOPC+0.5%mol NBD-DOPE. The stock solution of Triton X-100 (~1.7M) and we prepared a dilution in DI water (1.7mM); both were kept well-sealed and at room temperature. The tested Triton X-100 concentrations were: 0mM, 0.0024mM, 0.024mM and 0.24mM.

We tested the membrane disrupting effects of **LDAO** on microsphere-supported membranes with the following composition: 99.5%mol DOPC+0.5%mol NBD-DOPE. The stock solution of LDAO was 20mM which was kept well-sealed, in the dark at -20 °C until use. and at room temperature. The tested LDAO concentrations were: 0 mM, 0.5mM, 0.75mM, 1mM, 1.25mM and 1.5mM.

We tested the membrane disrupting effects of **LPS** on microsphere-supported membranes with the following compositions: 1) 99.5%mol DOPC+0.5%mol NBD-DOPE, or 2) 99.9%mol DOPC+0.1%mol Liss-Rhod-DOPE. The stock solution of LPS was 2.5 mg/ml which was kept well-sealed at -20 °C until use. and at room temperature. The tested LPS concentrations were: 0 µg/ml, 50 µg/ml, 150 µg/ml, 250 µg/ml, 350 µg/ml, and 500 µg/ml.

- Membrane disruption with LDAO

We tested the membrane disruption effect of LDAO on planar-supported membranes and on microsphere-supported membranes, both with a membrane composition of 99.5%mol DOPC+0.5%mol NBD-DOPE. On both instances, we added the different concentrations of LDAO and let incubate (without shaking or rotating) with the membranes for 20, 40 and 60 min. We imaged both sets with a confocal microscope, and we collected the flow cytometric data of the microsphere-supported membranes set.

- Membrane disruption with LPS

First, we calculated the c.m.c of the LPS solution stock we used in chapter 4 by preparing a series of dilutions and measuring the derived count rate of each dilution in a Dynamic Light Scattering (DLS) machine, provided by CINT.

We tested the membrane disruption effect of LPS on planar-supported membranes and on microsphere-supported membranes, both with a membrane composition of 99.5%mol DOPC+0.5%mol NBD-DOPE. On both instances, we added the different concentrations of LPS and let incubate (without shaking or rotating) with the membranes for 20, 40 and 60 min. We imaged both sets with a confocal microscope, and we collected the flow cytometric data of the microsphere-supported membranes set.

Finally, we assembled membrane bilayers (99.9%mol DOPC+0.1%mol Liss-Rhod-DOPE) on planar silica and on silica microspheres, we induced hole formation on the membranes by exposure to LPS and we backfilled the holes with lipid vesicles with a different florescent tag (99.5%mol DOPC+0.5%mol NBD-DOPE) for detection purposes.

We imaged the results on both platforms and we collected the flow cytometric data on the silica microsphere set.

2.2.4 Block copolymer as an alternative to lipids.

This section includes a more in-depth description of the methods used in the work described on chapter 5.

- Block copolymer-lipid micelle formation

The formation of block copolymer micelles is achieved by self-assembly in aqueous medium.⁵⁰ For the work described on chapter 5, we prepared assemblies that included mostly amphiphilic block copolymers (pEO-b-pBD) and small amounts of phospholipids to add fluorescent tags and binding ligands.

Using glass syringes, we first dissolved the desired amount of copolymer and the lipids in tetrahydrofuran (THF) in a glass vial to a final volume of 750 μ l. Then, using 14.5 mm-diameter plastic syringes, we exchanged the solvent to molecular biology grade water by gradual injection (2 ml/hr rate) to a final volume of 2.5 ml, while the THF is removed by rotary evaporation. The process took place at room temperature and in the dark.

After the solvent exchange process was finalized, the samples were kept in the glass vials, were covered with tightly sealed parafilm and were stored at 4 °C until use. (See Figure 2.6.)

- Polymer membrane formation on microspheres

The polymer membrane formation on silica microspheres was done following the same

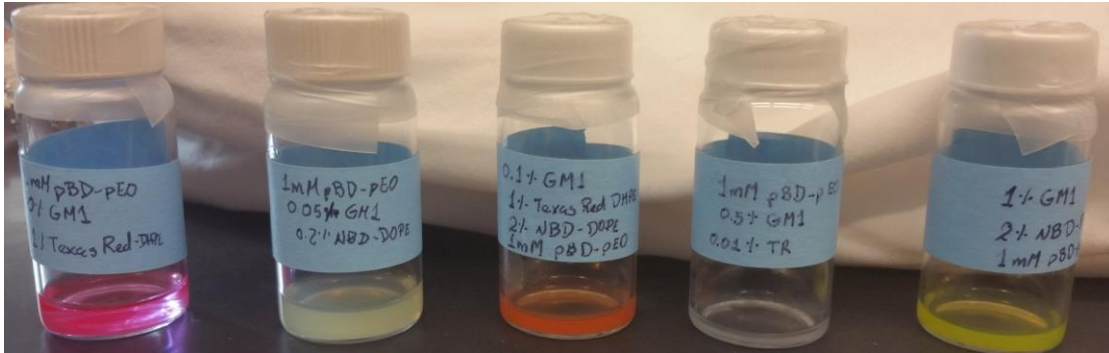


Figure 2.6. Block copolymer micelles solutions

protocol for lipid coating on silica beads, as described in Section 2.2.1, with some minor differences. Briefly, in BSA-passivated Eppendorf tubes, we incubated the 1mM polymer micelle solutions with clean silica microspheres (7.9 μm -diameter) to a final concentration of 10^5 - 10^6 beads/ml. The incubation process consisted on placing the tubes with the copolymer micelles and the microspheres on a shaker and vortexing them on medium speed 1 hour at 37 °C. These conditions promote the spontaneous fusion of the polymer micelles to the microspheres' surface forming the bilayers. Then, we added BSA, for blocking purposes, to each sample to a final concentration of 0.5 mg/mL and we let them vortex on low speed for 20 minutes at room temperature. Finally, all the samples were washed and rinsed three times to remove the unbound micelles and extra BSA in solution. This was done by centrifuging the samples for 45 seconds at 10 000 rpm, removing the supernatant and resuspending the samples in fresh buffer to bring them back up to volume.

- Multiplex formation

After the polymer bilayer formation on silica microspheres (7.9 μm – diameter) process is complete, we form a multiplex set by adding equal volumes of the different membrane compositions to a single BSA-passivated Eppendorf tube.

- Time stability test

The flow cytometric data of all the individual samples and the multiplex set were recorded at times 0, 0.5, 1, 2, 4, 8, and 24 hours. The results show that both individual and multiplex sets are stable for at least 4 hours.

- Fluorescence recovery after photobleaching (FRAP)

The fluidity and lateral mobility of the polymer membranes on silica microspheres was tested by photobleaching a specific area on the membrane supported on one of the silica beads, and the fluorescence level of said area was tracked for 30 minutes. The immobility of the polymer-lipid membranes was determined by the lack of recovery of the fluorescence of the photobleached area. The FRAP experiment was done using the beads coated with polymer membranes with the following composition: 1mM pBD-pEO, 0% GM1, 1%mol Texas Red-DHPE.

- Preferential binding of CTxB-Alexa to GM1 on polymer membrane on silica beads

For the work described in chapter 5, we assembled and tested five different compositions of polymer membranes supported on microspheres: **1)** 1mM pBD-b-pEO, 0% GM1, 1%mol Texas Red-DHPE; **2)** 1mM pBD-b-pEO, 0.05% GM1, 0.2%mol NBD-DOPE; **3)** 1mM pBD-b-pEO, 0.1% GM1, 2%mol NBD-DOPE, 1%mol Texas Red-DHPE;

4) 1mM pBD-b-pEO, 0.5% GM1, 0.01% Texas Red-DHPE; and 5) 1mM pBD-b-pEO, 1% GM1, 2%mol NBD-DOPE.

Similar to lipid membranes on microspheres, we used 75nM CTxB-Alexa 647 aliquots to test the preferential binding of CTxB-Alexa 647 to GM1-containing polymer membranes on silica microspheres by adding the right volumes to the individual and multiplex samples. The tested concentrations of CTxB-Alexa 647 were: 0nM, 5nM, 10nM, 50nM and 100nM.

2.2.5 Flow cytometry data collection

The flow cytometers we work with were cleaned and calibrated before and after use.

In all the work described in chapter 3-5 and Appendix I, the flow cytometric data is presented in contour plots with a 10% probability contour and dotted outlying event.

The microsphere population was detected and gated using the forward scatter versus side scatter plot. Then, the gated microsphere population was observed in bivariate plots where the axes show the fluorescence intensity in two different fluorescence detection channels or in the side scatter channel and a fluorescence detection channel. Said channels are the ones able to detect the emission of the fluorophores present in the membranes at a given assay. From the bivariate plots, we gated the event once more to only include the microspheres with complete membrane coating, and exclude defective or incomplete membrane coverage and outlier events. If two or more fluorophores are present, compensation is run as necessary.

Gating, compensation and statistical data collection were done using FlowJoV10 software.

2.3 References

1. Medicago AB. *Smart Buffers*.
http://www.medicago.se/sites/default/files/pdf/productsheets/PBS_Buffer_v._01.pdf.
2. Baicu SC, Taylor MJ. Acid-base buffering in organ preservation solutions as a function of temperature: new parameters for comparing buffer capacity and efficiency. *Cryobiology*. 2002;45(1):33-48.
3. Will MA, Clark NA, Swain JE. Biological pH buffers in IVF: help or hindrance to success. *J Assist Reprod Genet*. 2011;28(8):711-724. doi:10.1007/s10815-011-9582-0.
4. Piyasena ME, Zeineldin R, Fenton K, Buranda T, Lopez GP. Biosensors based on release of compounds upon disruption of lipid bilayers supported on porous microspheres. *Biointerphases*. 2008;3(2):38. doi:10.1116/1.2918743.
5. Liberman A, Mendez N, Trogler WC, Kummel AC. Synthesis and surface functionalization of silica nanoparticles for nanomedicine. *Surf Sci Rep*. 2014;69(2-3):132-158. doi:10.1016/j.surfrep.2014.07.001.
6. Cho Y-S, Shin CH, Han S. Dispersion Polymerization of Polystyrene Particles Using Alcohol as Reaction Medium. *Nanoscale Res Lett*. 2016;11(1):46. doi:10.1186/s11671-016-1261-8.
7. Ridgway ND. Phospholipid Synthesis in Mammalian Cells. In: *Biochemistry of Lipids, Lipoproteins and Membranes*. Elsevier; 2016:209-236. doi:10.1016/B978-0-444-63438-2.00007-9.
8. Ide T, Murata M. Depressions by dietary phospholipids of soybean and egg yolk origins of hepatic triacylglycerol and fatty acid synthesis in fasted-refed rats. *Ann Nutr Metab*. 1994;38(6):340-348.
9. Vance JE, Tasseva G. Formation and function of phosphatidylserine and phosphatidylethanolamine in mammalian cells. *Biochim Biophys Acta - Mol Cell Biol Lipids*. 2013;1831(3):543-554. doi:10.1016/j.bbalip.2012.08.016.
10. Emoto K, Kobayashi T, Yamaji A, et al. Redistribution of phosphatidylethanolamine at the cleavage furrow of dividing cells during cytokinesis. *Proc Natl Acad Sci U S A*. 1996;93(23):12867-12872.
11. Pécheur E-I, Martin I, Maier O, Bakowsky U, Ruysschaert J-M, Hoekstra D. Phospholipid species act as modulators in p97/p47-mediated fusion of Golgi membranes. *Biochemistry*. 2002;41(31):9813-9823.
12. Menon AK, Stevens VL. Phosphatidylethanolamine is the donor of the ethanolamine residue linking a glycosylphosphatidylinositol anchor to protein. *J Biol Chem*. 1992;267(22):15277-15280.

13. Xiang X, Liu Y, Zhang X, Zhang W, Wang Z. Effects of biotin on blood glucose regulation in type 2 diabetes rat model. *J Hyg Res.* 2015;44(2):185-189, 195.
14. Bratthauer GL. The Avidin–Biotin Complex (ABC) Method and Other Avidin–Biotin Binding Methods. In: *Methods in Molecular Biology (Clifton, N.J.)*. Vol 588. ; 2010:257-270. doi:10.1007/978-1-59745-324-0_26.
15. Haldar S, Chattopadhyay A. Application of NBD-Labeled Lipids in Membrane and Cell Biology. In: Springer, Berlin, Heidelberg; 2012:37-50. doi:10.1007/4243_2012_43.
16. Basu I, Mukhopadhyay C. Insights into Binding of Cholera Toxin to GM1 Containing Membrane. *Langmuir.* 2014;30(50):15244-15252. doi:10.1021/la5036618.
17. McFarland MA, Marshall AG, Hendrickson CL, Nilsson CL, Fredman P, Månsson J-E. Structural characterization of the GM1 ganglioside by infrared multiphoton dissociation, electron capture dissociation, and electron detachment dissociation electrospray ionization FT-ICR MS/MS. *J Am Soc Mass Spectrom.* 2005;16(5):752-762. doi:10.1016/j.jasms.2005.02.001.
18. Karlsson KA. Animal Glycosphingolipids as Membrane Attachment Sites for Bacteria. *Annu Rev Biochem.* 1989;58(1):309-350. doi:10.1146/annurev.bi.58.070189.001521.
19. Posse de Chaves E, Sipione S. Sphingolipids and gangliosides of the nervous system in membrane function and dysfunction. *FEBS Lett.* 2010;584(9):1748-1759. doi:10.1016/j.febslet.2009.12.010.
20. Heyningen S Van. Cholera toxin: interaction of subunits with ganglioside GM1. *Science.* 1974;183(4125):656-657.
21. Mudrak B, Kuehn MJ. Heat-labile enterotoxin: beyond G(m1) binding. *Toxins (Basel).* 2010;2(6):1445-1470. doi:10.3390/toxins2061445.
22. Kaiser H-J, Lingwood D, Levental I, et al. Order of lipid phases in model and plasma membranes. *Proc Natl Acad Sci U S A.* 2009;106(39):16645-16650. doi:10.1073/pnas.0908987106.
23. Smith SN, Steer RP. The photophysics of Lissamine rhodamine-B sulphonyl chloride in aqueous solution: implications for fluorescent protein–dye conjugates. *J Photochem Photobiol A Chem.* 2001;139(2-3):151-156. doi:10.1016/S1010-6030(01)00372-0.
24. Veldhuizen R, Nag K, Orgeig S, Possmayer F. The role of lipids in pulmonary surfactant. *Biochim Biophys Acta - Mol Basis Dis.* 1998;1408(2-3):90-108. doi:10.1016/S0925-4439(98)00061-1.
25. Campbell RB, Balasubramanian S V, Straubinger RM. Phospholipid-cationic lipid interactions: influences on membrane and vesicle properties. *Biochim Biophys*

- Acta*. 2001;1512(1):27-39.
26. Lapinski MM, Castro-Forero A, Greiner AJ, Ofoli RY, Blanchard GJ. Comparison of Liposomes Formed by Sonication and Extrusion: Rotational and Translational Diffusion of an Embedded Chromophore. *Langmuir*. 2007;23(23):11677–11683. doi:10.1021/LA7020963.
 27. Bharati K, Ganguly NK. Cholera toxin: a paradigm of a multifunctional protein. *Indian J Med Res*. 2011;133:179-187.
 28. Lauer S, Goldstein B, Nolan RL, Nolan JP. Analysis of Cholera Toxin–Ganglioside Interactions by Flow Cytometry. *Biochemistry*. 2002;41(6):1742-1751. doi:10.1021/bi0112816.
 29. Weber PC, Ohlendorf DH, Wendoloski JJ, Salemme FR. Structural origins of high-affinity biotin binding to streptavidin. *Science*. 1989;243(4887):85-88.
 30. Xiao Y, Isaacs SN. Enzyme-linked immunosorbent assay (ELISA) and blocking with bovine serum albumin (BSA)--not all BSAs are alike. *J Immunol Methods*. 2012;384(1-2):148-151. doi:10.1016/j.jim.2012.06.009.
 31. Barbosa LRS, Ortore MG, Spinozzi F, Mariani P, Bernstorff S, Itri R. The importance of protein-protein interactions on the pH-induced conformational changes of bovine serum albumin: a small-angle X-ray scattering study. *Biophys J*. 2010;98(1):147-157. doi:10.1016/j.bpj.2009.09.056.
 32. Riccardi C, Nicoletti I. Analysis of apoptosis by propidium iodide staining and flow cytometry. *Nat Protoc*. 2006;1(3):1458-1461. doi:10.1038/nprot.2006.238.
 33. Arachea BT, Sun Z, Potente N, Malik R, Isailovic D, Viola RE. Detergent selection for enhanced extraction of membrane proteins. *Protein Expr Purif*. 2012;86(1):12-20. doi:10.1016/j.pep.2012.08.016.
 34. Rosenfeld Y, Shai Y. Lipopolysaccharide (Endotoxin)-host defense antibacterial peptides interactions: Role in bacterial resistance and prevention of sepsis. *Biochim Biophys Acta - Biomembr*. 2006;1758(9):1513-1522. doi:10.1016/j.bbamem.2006.05.017.
 35. Qiao S, Luo Q, Zhao Y, Zhang XC, Huang Y. Structural basis for lipopolysaccharide insertion in the bacterial outer membrane. *Nature*. 2014;511(7507):108-111. doi:10.1038/nature13484.
 36. Aurell CA, Wistrom AO. Critical Aggregation Concentrations of Gram-Negative Bacterial Lipopolysaccharides (LPS). *Biochem Biophys Res Commun*. 1998;253(1):119-123. doi:10.1006/bbrc.1998.9773.
 37. Beyaz A, Oh WS, Reddy VP. Ionic liquids as modulators of the critical micelle concentration of sodium dodecyl sulfate. *Colloids Surfaces B Biointerfaces*. 2004;35(2):119-124. doi:10.1016/J.COLSURFB.2004.02.014.

38. Moroi Y, Motomura K, Maruura R. The critical micelle concentration of sodium dodecyl sulfate-bivalent metal dodecyl sulfate mixtures in aqueous solutions. *J Colloid Interface Sci.* 1974;46(1):111-117. doi:10.1016/0021-9797(74)90030-7.
39. Koley D, Bard AJ. Triton X-100 concentration effects on membrane permeability of a single HeLa cell by scanning electrochemical microscopy (SECM). *Proc Natl Acad Sci.* 2010;107(39):16783-16787. doi:10.1073/pnas.1011614107.
40. Hait SK, Moulik SP. Determination of critical micelle concentration (CMC) of nonionic surfactants by donor-acceptor interaction with Iodine and correlation of CMC with hydrophile-lipophile balance and other parameters of the surfactants. *J Surfactants Deterg.* 2001;4(3):303-309. doi:10.1007/s11743-001-0184-2.
41. Richardson S. Potential of low molecular mass chitosan as a DNA delivery system: biocompatibility, body distribution and ability to complex and protect DNA. *Int J Pharm.* 1999;178(2):231-243. doi:10.1016/S0378-5173(98)00378-0.
42. Hirano S, Hirochi K, Hayashi K, Mikami T, Tachibana H. Cosmetic and Pharmaceutical Uses of Chitin and Chitosan. In: *Cosmetic and Pharmaceutical Applications of Polymers*. Boston, MA: Springer US; 1991:95-104. doi:10.1007/978-1-4615-3858-5_10.
43. No HK, Meyers SP, Prinyawiwatkul W, Xu Z. Applications of Chitosan for Improvement of Quality and Shelf Life of Foods: A Review. *J Food Sci.* 2007;72(5):R87-R100. doi:10.1111/j.1750-3841.2007.00383.x.
44. Rinaudo M. Chitin and chitosan: Properties and applications. *Prog Polym Sci.* 2006;31(7):603-632. doi:10.1016/j.progpolymsci.2006.06.001.
45. Mazia D, Schatten G, Sale W. Adhesion of cells to surfaces coated with polylysine. Applications to electron microscopy. *J Cell Biol.* 1975;66(1):198-200. doi:10.1083/JCB.66.1.198.
46. Chheda AH, Vernekar MR. Enhancement of ϵ -poly-L-lysine (ϵ -PL) production by a novel producer *Bacillus cereus* using metabolic precursors and glucose feeding. *3 Biotech.* 2015;5(5):839-846. doi:10.1007/s13205-015-0291-8.
47. Schulz A, Hornig S, Liebert T, Birckner E, Heinze T, Mohr GJ. Evaluation of fluorescent polysaccharide nanoparticles for pH-sensing. *Org Biomol Chem.* 2009;7(9):1884. doi:10.1039/b900260j.
48. Becton Dickinson and Company. *BD Accuri C6 Flow Cytometer Technical Specifications*. <http://static.bdbiosciences.com/documents/BD-Accuri-C6-Plus-Technical-Specs.pdf>.
49. Invitrogen. *Attune NxT Flow Cytometer Specification Sheet*. <https://tools.thermofisher.com/content/sfs/brochures/attune-nxt-flow-cytometer-spec-sheet.pdf>.
50. Gaucher G, Dufresne M-H, Sant VP, Kang N, Maysinger D, Leroux J-C. Block

copolymer micelles: preparation, characterization and application in drug delivery.
J Control Release. 2005;109(1-3):169-188. doi:10.1016/j.jconrel.2005.09.034.

Chapter 3.
Multiplexed Lipid Bilayers on Silica Microspheres for Analytical Screening Applications

Nadiezda Fernandez Oropeza^[1], Nesia A. Zurek^{[1]*}, Mirella Galvan-De La Cruz^[1], Aurora Fabry-Wood^[1], Jennifer M. Fetzer^[1], Steven W. Graves^{[1,2]*}, and Andrew P. Shreve^{[1,2]*}.

¹Center for Biomedical Engineering, and ²Department of Chemical and Biological Engineering, University of New Mexico, Albuquerque, New Mexico 87131, United States

Reprinted and adapted with permission from *Anal. Chem.*, 2017, 89 (12), pp 6440–6447.
DOI: 10.1021/acs.analchem.7b00296. Copyright © 2017 American Chemical Society

3.1 Abstract

Most druggable targets are membrane components, including membrane proteins and soluble proteins that interact with ligands or receptors embedded in membranes. Current target-based screening and intermolecular interaction assays generally do not include the lipid membrane environment in presenting these targets, possibly altering their native structure and leading to misleading or incorrect results. To address this issue, an ideal assay involving membrane components would (1) mimic the natural membrane environment, (2) be amenable to high-throughput implementation, and (3) be easily multiplexed. In a step toward developing such an ideal target-based analytical assay for membrane components, we present fluorescently indexed multiplexed biomimetic membrane assays amenable to high-throughput flow cytometric detection. We build fluorescently multiplexed biomimetic membrane assays by using varying amounts of a fluorescently labeled lipid, NBD-DOPE [1,2-dioleoyl-sn-glycero-3-phosphoethanolamine-N-(7-nitro-2-1,3-benzoxadiazol-4-yl)], incorporated into a phospholipid membrane bilayer supported on 3 μm silica microspheres. Using flow cytometry, we demonstrate this multiplexed approach by measuring specific affinity of two well-characterized systems, the fluorescently labeled soluble proteins cholera toxin B subunit-Alexa 647 and streptavidin-PE/Cy5, to membranes containing different amounts of ligand targets of these proteins, GM1 and biotin-DOPE, respectively. This work will enable future efforts in developing highly efficient biomimetic assays for interaction analysis and drug screening involving membrane components.

3.2 Introduction

Molecular interactions involving receptors or ligands in cell membranes are essential for cell signaling, transport across membranes, cell–cell recognition, and virus or toxin interactions with cells. As a result, most druggable targets are membrane-associated components, which are of great interest for target-based interaction assays or drug screening.^{1–3} Flow cytometry is an attractive method for high-throughput or multiplexed target-based assays and can quickly investigate interactions or conduct large-scale screens of potential drug candidates.^{4–10} For example, flow cytometers with automatic sampling methods can rapidly screen high-density microwell plates, where each well contains potentially active compounds and microspheres that present targets.⁷ An important element of optimized flow-based assays is the use of multiplexed microspheres so that each sample contains indexed beads that present different targets, as well as positive or negative controls.^{4–10} Such multiplexing increases the efficiency of assays by minimizing the cost of the reagents, assay time, and sample-to-sample variability.^{7–10} Commercially available sets of polymer microspheres provide high multiplexing capacity (e.g., up to ~500× through combinations of intensity levels and spectral windows) and are widely used for assays involving different types of soluble protein or nucleic acid targets presented through attachment to the particle.^{7,11} However, commercially available multiplexed microspheres, which are constructed from polystyrene, are unable to present membrane components in their natural lipid environment.

In general, for interaction analysis involving membrane components, the relevant biological molecules must be presented in either natural or biomimetic membranes, since the structure of membrane components depends on the presence of a lipid bilayer.^{1,2,12} A natural membrane environment is also important for functional reasons, including accurate

assessment of apparent affinities in multivalent protein–ligand interactions. For example, the natural interaction of cholera toxin with its GM1 ligand is multivalent, and the effective affinity is influenced by the lateral mobility of ligands in the membrane.¹³

Substrate-supported membrane bilayers (SMBs), typically formed on silica or modified gold surfaces, are widely used for presentation of membrane components in interaction assays.^{14–18} These are the basis of biosensor platforms with transduction of binding events through microscopy, surface plasmon resonance, ellipsometry, second-harmonic generation or quartz crystal microbalance response.^{13,19–25} Unfortunately, while planar SMBs mimic many aspects of natural cellular membranes, including incorporation of membrane proteins, they are difficult to integrate with highly multiplexed methods. Some work has developed patterned SMBs that contain different regions of membrane composition,^{26–30} possibly allowing for multiple target presentation, but even for low-throughput applications their use for assays requires complex surface patterning and fluidic engineering.^{29–31}

Motivated by these considerations, there is interest in producing a lipid bilayer membrane architecture that will enable multiplexed and high-throughput flow cytometry. Liposomes are one possibility, as membrane components can be readily integrated with them, and they can, in principle, be labeled for multiplexed indexing.³² However, typical liposomes of sizes ~200 nm or smaller are challenging to analyze using flow cytometry, and for assays, analytical limitations also arise from the mismatch between the size of the analyte particle and the interrogation volume.^{33,34} Giant unilamellar vesicles (GUVs), several micrometers or larger in size, are another alternative amenable to incorporation of membrane components.^{35,36} Further investigation of GUVs in this context is warranted, but

to date, GUVs have only rarely been used as a platform for flow cytometry, in part because of complications arising from structural and size heterogeneities.^{37,38}

An ideal platform for multiplexed flow-based studies of membrane components would incorporate the best features of vesicles and particle-based multiplexing methods. Our work presents an initial step toward that goal, relying upon SMBs formed on silica microspheres. Monodisperse silica microspheres are commercially available and are easily detected and analyzed using flow cytometry. SMBs on silica microspheres are used for flow-based assays and are similar to SMBs on planar silica in membrane quality.³⁹⁻⁴³ However, to date, no studies have demonstrated multiplexing methods for SMBs on silica microspheres, and there are no readily available sources of standardized multiplexed silica particles optimized for use in flow cytometry.

As a proof-of-principle demonstration of multiplexing methods for membrane components in flow cytometry, we present measurements that rely upon use of different amounts of fluorescently tagged lipids incorporated into SMBs on silica microspheres to index the particles. Each type of indexed particle presents a lipid membrane of different composition. For the experiments reported here, each membrane contains different amounts of lipid-based small-molecule ligands that bind to the fluorescently labeled proteins cholera toxin (B subunit) and streptavidin. These two systems have been widely studied and offer well-characterized test cases to validate the multiplexing technology we are developing.^{13,22,24,25,44,45} This work demonstrates technology for multiplexed membrane-based assays in flow cytometry and represents an initial step toward building more efficient analysis methods for membrane-associated components.

3.3 Materials and Methods

3.3.1 Liposome Preparation.

Liposomes were prepared as previously reported.⁴⁶ Briefly, powdered 1-palmitoyl-2-oleoylsn-glycero-3-phosphocholine (POPC), 1,2-dioleoyl-sn-glycero-3-phosphoethanolamine-N-(biotinyl) (biotin-DOPE), 1,2-dioleoyl-sn-glycero-3-phosphoethanolamine-N-(7-nitro-2-1,3-benzoxadiazol-4-yl) (NBD-DOPE), and ganglioside GM1 purchased from Avanti Lipids were dissolved in chloroform (EMD Millipore) and stored in glass vials at $-20\text{ }^{\circ}\text{C}$ until use. Using glass syringes, stock lipids were mixed in different glass vials in various final mixtures. The mixtures of chloroform-dissolved lipids were dried overnight under vacuum to form lipid plaques. The lipid plaques were then rehydrated to a final concentration of 1 mM in phosphate-buffered saline (PBS, Sigma) at pH 7.4. Large unilamellar vesicles (LUVs) were formed by extrusion using the Mini-Extruder, filter supports, and $0.1\text{ }\mu\text{m}$ polycarbonate (PC) membranes (Avanti Polar Lipids) by passing rehydrated lipids through the PC membranes 13 times.

Microsphere Supported Bilayer Formation. All Eppendorf tubes were passivated with 0.1 mg/mL bovine serum albumin (BSA) for 45 min prior to use. The $3\text{ }\mu\text{m}$ nonporous silica microspheres purchased from SpheroTech were cleaned by first suspending them in a basic solution (4% NH_4OH), followed by slow centrifugation and rinsing with Millipore water three times. Next, the beads were suspended in an acidic solution (4% HCl), followed by slow centrifugation and rinsing with Millipore water five times.⁴³ Cleaned beads were suspended in PBS. The silica beads were coated with a lipid bilayer as previously described, with some modifications.⁴³ Briefly, the silica beads ($1.5\text{ }\mu\text{L}$ of suspended beads) were added to the LUVs (1 mM lipid concentration) to a final concentration $\sim 10^6$ beads/mL

in 0.5 mL final volume. The mixture of LUVs and microspheres was vortexed on high speed at room temperature for 10 min and on low speed for 45 min at 37 °C. Under these conditions, liposomes fuse to the surface, forming a uniform supported lipid bilayer.⁴⁷ As a precaution to minimize nonspecific binding, BSA was then added to samples at a concentration of 0.5 mg/mL and the samples were vortexed on low speed at room temperature for 45 min. Beads were then washed 4–5 times to remove unbound liposomes by cycles of centrifugation at 10 000 rpm for 45 s, followed by removing the supernatant, always leaving at least 50 µL in the tube to keep the lipid-coated beads hydrated. Beads were resuspended in fresh PBS to bring the samples back up to volume. A multiplexed set was formed by mixing beads coated with different membrane compositions in a BSA-passivated tube. Following rinsing, resuspension, and addition of analyte solution (see below), the final bead concentration for analysis was $\sim 10^5$ beads/mL.

3.3.2 Protein Binding Assays.

Cholera toxin B subunit (recombinant)-Alexa Fluor 647 (CTxB-Alexa 647) purchased from ThermoFisher at a concentration of 175 nM was diluted to a stock concentration of 75 nM in PBS and stored in aliquots at -20 °C until use. Streptavidin-PE/Cy5 (SAv-Cy5) diluted in PBS purchased from Biolegend at a concentration of 421 nM was diluted in PBS to a stock concentration of 4.21 nM and stored in aliquots at -20 °C until use. Concentrations of GM1, CTxB-Alexa 647, biotin-DOPE, and SAv-Cy5 were chosen based on previous literature.^{13,44,45} POPC membrane bilayers containing specific amounts of GM1 (0–0.5 mol %) or biotin-DOPE (0–0.5 mol %), and as appropriate, NBD-DOPE (0–2.0 mol %) as a fluorescent indexing label, were prepared on silica microspheres as single

samples or, by mixing the single samples, as multiplexed sets. From microsphere size, concentration and the membrane compositions, the maximum concentration of protein binding sites is estimated to be of order 10^{-11} M. Different amounts of CTxB-Alexa 647 (0–20 nM) and/or SA_v-Cy5 (0–2.5 nM) were added in solution to both single samples and multiplexed samples and incubated for 10 min before analysis. A multiplexed cross-reactivity assay was also performed on silica microspheres coated with the following lipid compositions: (1) 100 mol % POPC; (2) 0.5 mol % GM1, 0.2 mol % NBD-DOPE, and 99.3 mol % POPC; (3) 0.5 mol % biotin-DOPE, 2 mol % NBD-DOPE, and 97.5 mol % POPC. Different proteins (2.5 nM SA_v-Cy5, 20 nM CTxB-Alexa Fluor 647, or the combination of 2.5 nM SA_v-Cy5 and 20 nM CTxB-Alexa) were added in solution to the multiplexed beads and incubated for 10 min before analysis.

3.3.3 Flow cytometry.

Flow cytometric studies were done as previously described using an Accuri C6 flow cytometer, with minor modifications to the protocol.⁴⁸ This instrument has two lasers with independent optical paths (488 and 640 nm) and four fluorescence detectors (three from the 488 nm excitation line—FL-1, 533 nm center wavelength/30 nm bandpass; FL-2, 585 nm center wavelength/40 nm bandpass; FL-3, 670 nm long-pass emission; one from the 640 nm excitation line—FL-4, 675 nm center wavelength/25 nm bandpass emission). For convenience, we sometimes describe filters using the center wavelength and bandpass, so for example, FL-1 corresponds to 533/30. For each event, data were collected for forward scatter (FSC) and side scatter (SSC) (from the 488 nm laser) and all four fluorescence channels. The Accuri C6 was calibrated with eight-peak rainbow beads (Spherotech, Inc.),

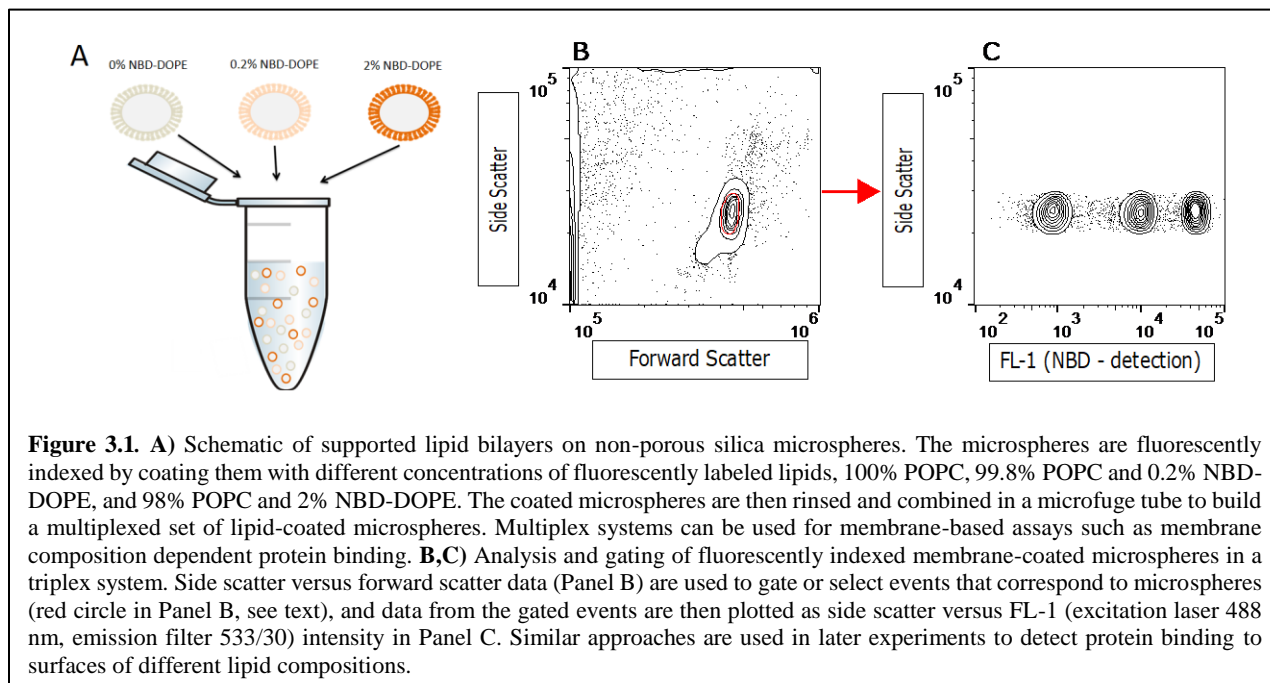
and fluorescence data were quite stable over time, as gauged by coefficient of variation (CV) values. The instrument was back-flushed between sample types, and the system was cleaned and decontaminated after each use. Collected data were analyzed, gated, and compensated as necessary using FlowJoV10 software. Bivariate flow cytometry data are presented as 10% contour levels of the probability density of events, with additional points representing (outlying) events that occur outside the lowest 10% probability contour. Red lines indicate gates that show populations selected for quantitative analysis. Median fluorescence intensity measurements were obtained using FlowJoV10, and data were analyzed and plotted using Microsoft Excel, Matlab, or Igor Pro software.

3.4 Results and Discussion

3.4.1 Fluorescently Indexed Silica Microsphere Supported Lipid Bilayers.

Multiplexed flow cytometry allows researchers to include several different samples, including controls, in each sample well prior to screening.⁴⁻¹⁰ This approach decreases sample-to-sample variation and lowers reagent cost. In this proof-of-principle study, we use fluorescently tagged lipids to provide different fluorescent intensity levels to index 3 μm silica microspheres. To test this approach, we coat silica microspheres in lipid mixtures containing 100% POPC, 99.8% POPC + 0.2% NBD-DOPE, or 98% POPC + 2% NBD-DOPE. Next, we rinse the microspheres and combine the three samples into a single tube to build a fluorescently indexed multiplex set (Figure 3.1A).

3.4.2 Flow Cytometric Characterization.



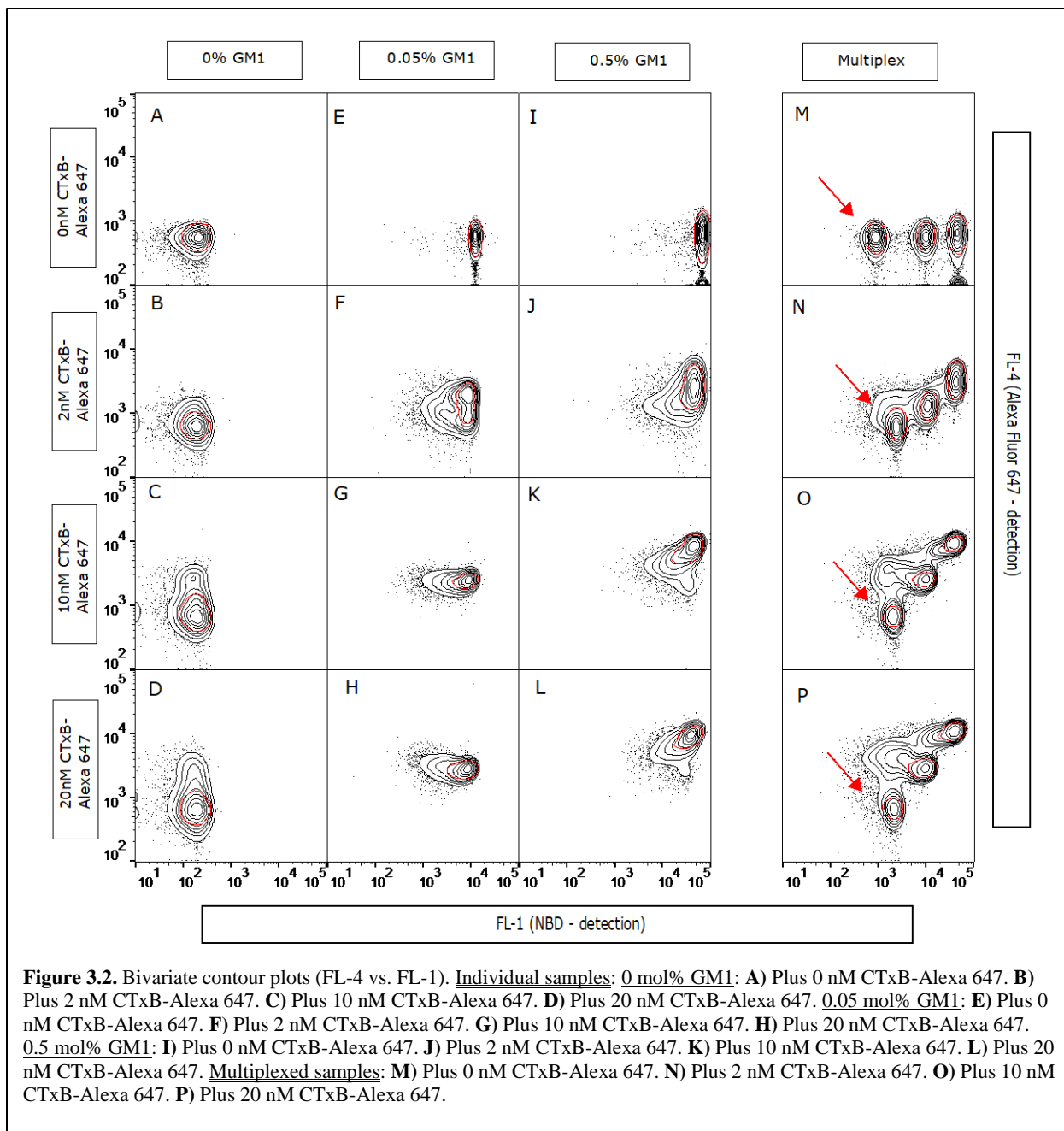
We analyze fluorescently indexed microspheres by flow cytometry (Figure 3.1, parts B and C). The population of events is gated using side scatter (Figure 3.1B, y-axis) versus forward scatter (Figure 3.1B, x-axis) and the automated gating function in FlowJoV10 (Figure 3.1B, red line). Signals from the events selected in Figure 3.1B are plotted on a bivariate plot of side scatter (Figure 3.1C, y-axis) versus green fluorescence (FL-1) (Figure 3.1C, x-axis), and the three different microsphere populations in the multiplexed system are clearly identifiable. When the fluorescence of the multiplexed silica microspheres is tracked over time, the signal intensities are stable over sufficiently long times for typical assay measurements (in our case, assay times up to 30 min were used), and the stability of the fluorescence intensities is comparable to that of the individual samples used to generate the multiplexed samples (Appendix II 3, Figure A3.1). These data show that we produce fluorescently indexed silica microspheres bearing lipid bilayers by varying the amounts of NBD-DOPE lipids in each single sample and that a multiplexed sample is made when these microspheres are combined.

3.4.3 Multiplexed Protein Binding Assays.

Fluorescently indexed microspheres coated with different concentrations of GM1 in POPC membrane bilayers show differential binding of CTxB-Alexa 647, a protein with a multivalent association with the glycolipid GM1 ligand.¹³ Silica microspheres are coated with increasing concentrations of GM1 and NBD-DOPE (100% POPC, 99.75 POPC + 0.05% GM1 + 0.2% NBDDOPE, or 97.5% POPC + 0.5% GM1 + 2% NBD-DOPE), building a fluorescently multiplexed bead set to test the affinity of CTxB-Alexa 647 to GM1-containing membranes. Next, different concentrations of CTxB-Alexa 647 ranging from 0 to 20 nM are added to both the individual samples and the multiplexed sample and analyzed after a 10-min incubation. The event population is first gated using a forward scatter versus side scatter plot, as in Figure 3.1B, which selects a population of microspheres. Then, data from the selected events are shown on a bivariate plot of FL-4 channel intensity (excitation, 640 nm; emission, 675/25 nm; CTxB-Alexa 647 detection channel; Figure 3.2, y-axis) versus FL-1 channel intensity (excitation, 488 nm; emission, 533/30 nm; NBD-DOPE multiplexing channel; Figure 3.2, x-axis). From this plot, gates are further refined to include only well-coated microspheres, excluding other debris or particles with poorly formed membranes (Figure 3.2, red gates). When no CTxB-Alexa 647 is added to either the individual or multiplexed samples (0 nM CTxB-Alexa 647), the FL-4 fluorescence intensity does not change (Figure 3.2, parts A, E, I, and M), consistent with no CTxB-Alexa 647 binding.

Results from the addition of increasing concentrations of CTxB-Alexa 647 to samples with no GM1 (Figure 3.2A–D) indicate little nonspecific binding of CTxB-Alexa 647 for the main population of microspheres. However, a small subpopulation of events does show

an increase in FL-4 signal, as would be observed for nonspecific interactions of CTxB-



Alexa 647 with microspheres containing no GM1. A likely origin of this subpopulation is apparent by inspection of the bivariate FL-4 versus FL-1 plots for the cases where DOPE-NBD is present (0.2% or 2.0% GM1 columns, Figure 3.2, parts E–H and I–L, respectively). In these cases, a broadening of the population distribution toward lower FL-1 intensity coinciding with FL-4 intensity above background level is consistent with nonspecific

binding of CTxB-Alexa 647 to a subpopulation of microspheres that have nonuniform or incomplete lipid coating. This result is also consistent with the observation (data not shown) that some concentration-dependent nonspecific binding of CTxB-Alexa 647 to bare silica microspheres occurs. Gating of the bivariate data to retain only the main populations of microspheres, those with well-formed lipid membranes, removes much of this complicating nonspecific interaction effect, illustrating a powerful aspect of multivariate flow cytometry analysis of interactions of proteins and membranes. An increase of fluorescence in FL-4 in single-composition beads with higher concentrations of GM1 indicates that CTxB-Alexa 647 interacts specifically with GM1 (Figure 3.2E–L). Separate control experiments confirm the absence of concentration-dependent CTxB-Alexa 647 binding to NBD-DOPE on particles with well-formed membranes when no GM1 is present (Appendix II 3, Figure A3.2).

In the multiplexed set with three fluorescently indexed bead populations in a single tube, higher fluorescence in the multiplexing channel (FL-1; NBD-DOPE) is matched to increasing GM1 content in the membrane (Figure 3.2M–P). Specifically, when increasing concentrations of CTxB-Alexa 647 are added to multiplexed samples, the FL-4 signal increases for beads with membranes that contain more GM1 (Figure 3.2M–P), consistent with binding of CTxB-Alexa 647 to GM1. The bead population with no GM1 in its membranes maintains low binding of CTxB-Alexa 647 (Figure 3.2M–P, red arrows). Overall, these data indicate the specific binding of CTxB-Alexa 647 to GM1 in a multiplex format.

The median FL-4 signal of the main bead populations (e.g., Figure 3.2M–P, red gates) is used to measure the amount of CTxB-Alexa 647 bound to microspheres. A multiplexed

data set thus consists of the median FL-4 signal of each microsphere population as a function of CTxB-Alexa 647 concentration. Each microsphere population corresponds to a different GM1 concentration, so a full multiplexed data set provides the amount of CTxB-Alexa 647 bound to microspheres as a function of both CTxB-Alexa 647 concentration (different panels of Figure 3.2M–P) and GM1 concentration (different populations within each panel). For each GM1 concentration, the median FL-4 signal, S , as a function of CTxB-Alexa 647 concentration, $[CTxB]$, is fit to a first-order Hill equation including background, B :

$$S = B + (M - B) \left(\frac{K_{eff}[CTxB]}{1 + K_{eff}[CTxB]} \right) \quad (3.1)$$

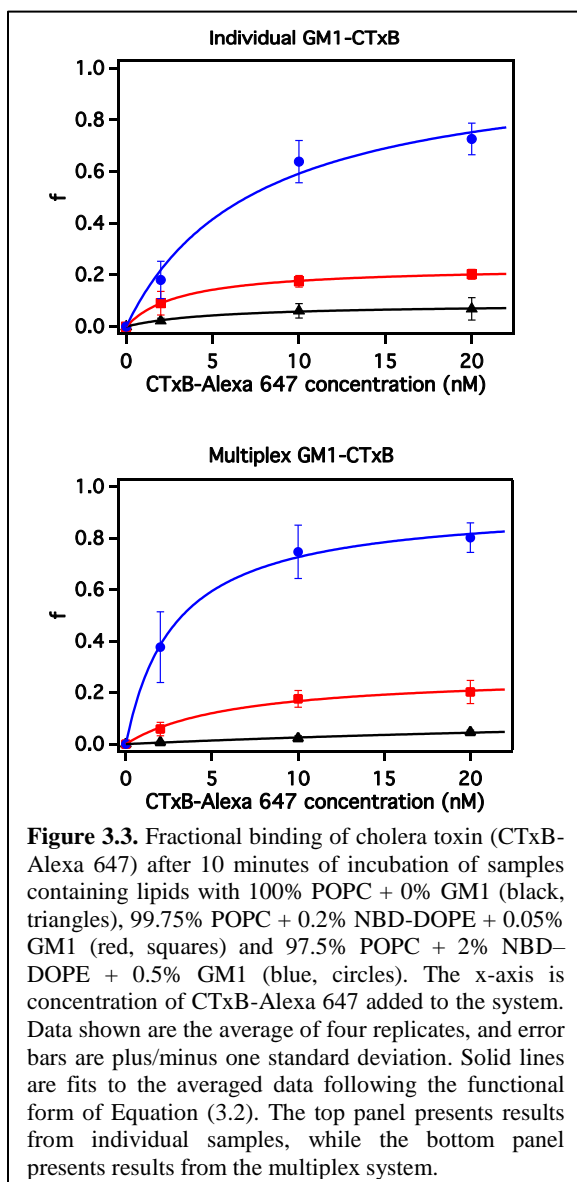
In eq. 3.1, K_{eff} is an effective association constant and M is the maximum signal predicted by the model. For each data set from a population of microspheres, this fit yields values of B , M , and K_{eff} for the GM1 concentration of those microspheres. Then, using the value of M obtained for the maximum GM1 concentration of 0.5 mol %, designated $M_{0.5}$, a normalized fractional signal for each data set is generated as

$$f = \frac{S - B}{M_{0.5} - B} = \frac{K_{eff}[CTxB]}{1 + K_{eff}[CTxB]} \quad (3.2)$$

where f is the fraction of the maximum amount of CTxB-Alexa 647 binding that occurs for GM1 membrane concentration of 0.5 mol %. This normalization process generates a family of curves for each complete multiplexed and individual data set. Four complete replica experiments are analyzed, and the f values are averaged and plotted to produce binding

data (Figure 3.3).

Two major results are found. First, the multiplexed approach agrees well with the



results of individual samples. In fact, fitting of the four data sets in Figure 3.3 that correspond to nonzero values of GM1 concentration (red and blue curves of the upper and lower panels) provides values of K_{eff} with 95% confidence intervals that all overlap. More detailed analysis is unwarranted, given the small number of degrees of freedom in the nonlinear regression models. Averaging the two values of K_{eff} obtained from the multiplex fits yields a value of $K_{eff} = 0.25 \pm 0.12$ nM^{-1} , corresponding to an effective or apparent affinity of $1/K_{eff} = 4.0 \pm 1.9$ nM , where the reported uncertainties are 95% confidence intervals. Second, the multiplex results found here are also in agreement

with previously published work. A detailed study by Lauer et al. presented a complete analysis of the multivalent interaction of cholera toxin with GM1, describing both single-site binding interactions and enhancement of apparent affinity through surface avidity.¹³ These authors report an effective affinity of approximately 5 nM , which agrees with our

result. They also report the single-site affinity of GM1 for cholera toxin to be several hundred times weaker. Their model demonstrates that observation of nanomolar effective affinity is consistent with multivalent cholera–GM1 interaction arising from the presentation of GM1 in a laterally fluid membrane. Our results thus confirm that the important lateral fluidity function of natural membranes is maintained in the multiplex assay.

To further validate the multiplexed detection approach, we also present protein binding assays using biotin-DOPE lipids and streptavidin-PE/Cy5 (abbreviated as SAv-Cy5). Silica microspheres coated with lipid mixtures containing varying concentrations of biotinylated-DOPE and NBD-DOPE (100% POPC, 99.75% POPC + 0.05% biotin-DOPE + 0.2% NBDDOPE, or 97.5% POPC + 0.5% biotin-DOPE + 2.0% NBDDOPE) are combined into a multiplexed set. Different concentrations of SAv-Cy5 from 0 to 2.5 nM are added to the multiplex, incubated for 10 min, and flow cytometry data are collected. For the fluorophores used in this study, there is some spectral overlap in the FL-1 (NBD-DOPE detection) and FL-3 (SAv-Cy5 detection) channels. Therefore, flow cytometric data compensation methods are applied (Appendix II 3, Figure A3.3).⁴⁹ Following compensation, bead populations are plotted on bivariate plots of FL-3 versus FL-1 intensities, gates are drawn around the main bead populations, and median fluorescence intensities in FL-3 are obtained using FlowJoV10 (Appendix II 3, Figure A3.4, red gates). Analysis of the median fluorescence FL-3 signal intensity is performed using a similar procedure to that outlined above for four replicate experiments.

Figure 3.4 presents results for both multiplexed and individual samples. In both cases, the median FL-3 signal increases slightly at high concentrations of SAv-Cy5 even when

no biotin-DOPE is present, indicating some nonspecific binding of SAV-Cy5 to the beads

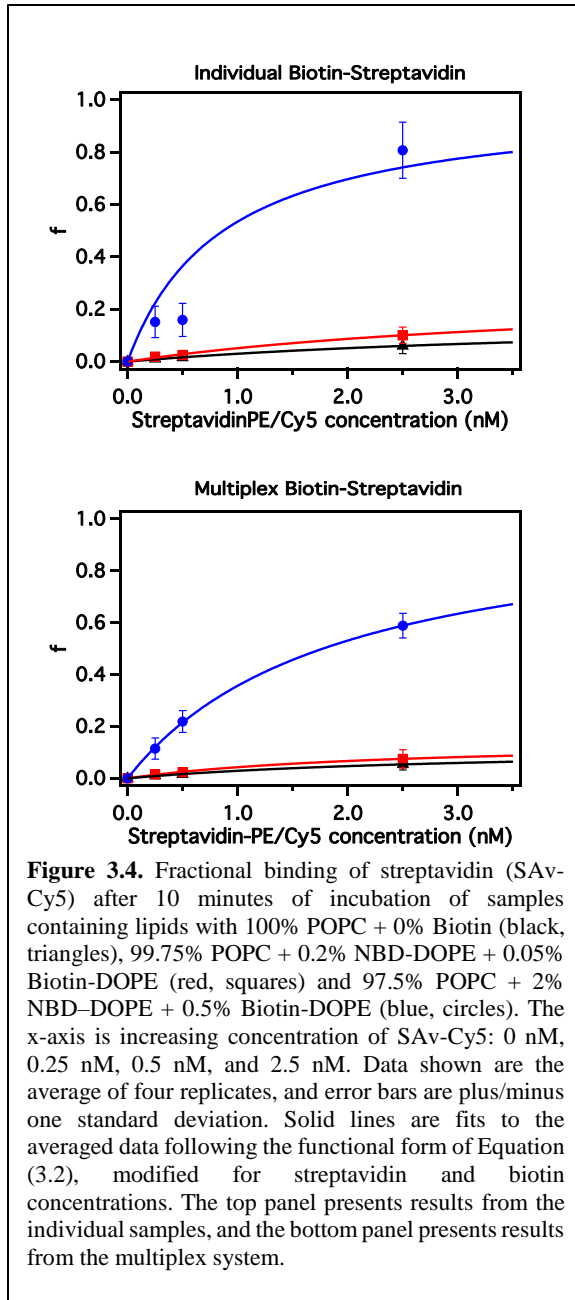


(Figure 3.4, lowest curves). However, separate control experiments confirm the absence of any additional specific interaction of SAV-Cy5 with the multiplexing label NBD-DOPE when no biotin-DOPE is present (Appendix II 3, Figure A3.5). In this example, the appreciable nonspecific binding of SAV-Cy5 to beads with no biotin-DOPE and the increased specific binding to beads containing biotin-DOPE in the multiplexed set demonstrates the power of multiplexed analysis. The multiplexed sample contains all three biotin compositions and a single SAV-Cy5 concentration, thus reducing sample-to-sample variability in quantitative determination of specific and nonspecific responses. As for the case of

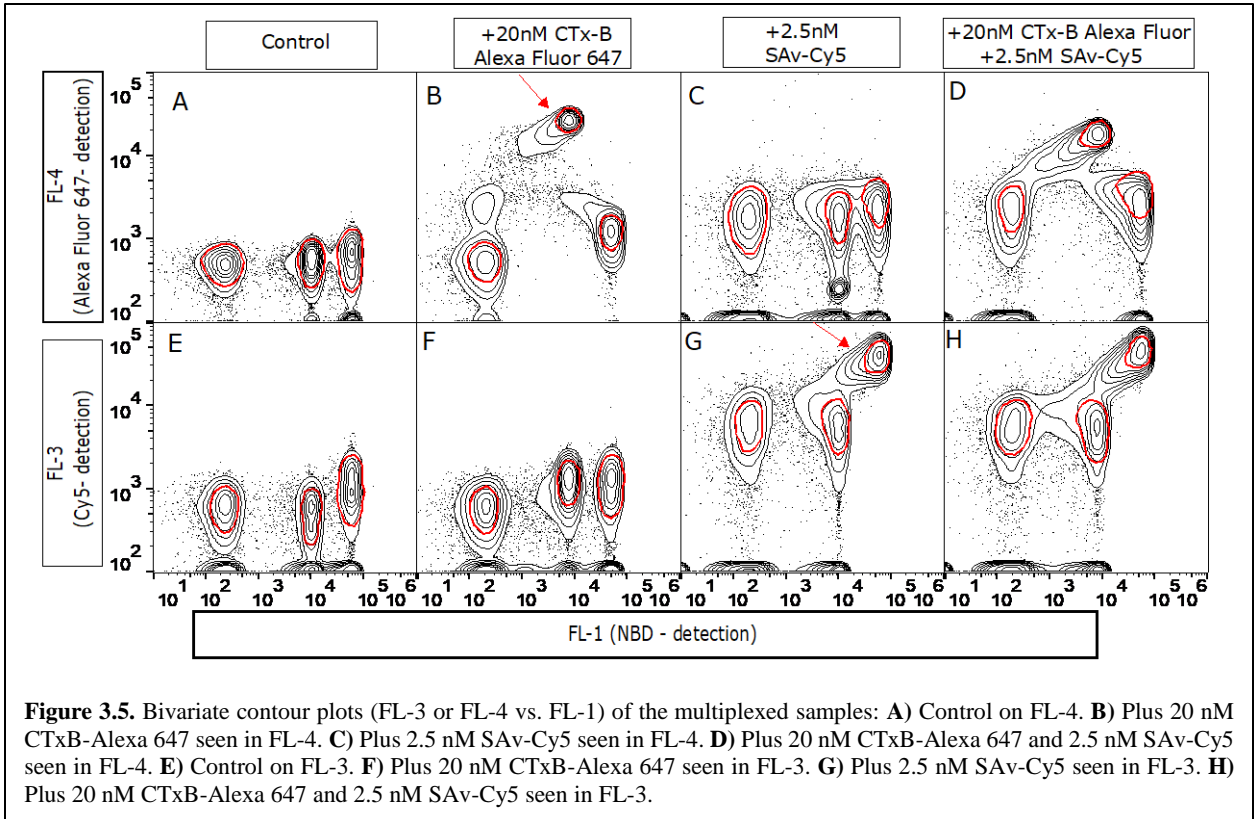
CTxB-Alexa 647 interaction with GM1, similar quantitative behavior in the individual and multiplex samples confirms that fluorescently indexed membrane-coated silica microspheres provide a reliable alternative to individual bead-based measurements.

A similar analysis to that described above was carried out for the concentration-dependent binding data presented in Figure 3.4. The 95% confidence intervals of all the effective affinities again overlap, and when averaged, the resulting effective affinity of the two multiplexed results is $1/K_{eff} = 2.1 \pm 1.6$ nM (reported uncertainty is the 95% confidence interval). The apparent affinity of streptavidin association with biotin- presenting surfaces has been treated in detail by several investigators.^{44,45} Again, our goal is to demonstrate that the multiplexed approach provides an accurate assessment of the effective affinity for the chosen experimental conditions. To that end, our results are similar to previous reports of an apparent affinity of ~ 2.3 nM by Nguyen et al. or, for biotin covalently attached to surfaces, of ~ 6 nM by Seto et al.,^{44,45} providing additional evidence that the multiplexed approach produces accurate assessments of effective interactions involving membrane components.

3.4.4 Binding Specificity in Multiplexed Protein Binding Assays.

For realistic multiplexed applications, each sample should contain beads with different membrane components, and not just different concentrations of a single component. To verify that we can use silica microspheres with different membrane components in a single well, we coat the particles with membranes of 100% POPC (negative control), 0.5% GM1 and 0.2% NBD-DOPE (to bind CTxB-Alexa 647), or 0.5% biotin-DOPE and 2% NBD-DOPE (to bind SAv-Cy5). The three fluorescently indexed membrane-coated silica microspheres are mixed into a single tube, and 20 nM CTxB-Alexa 647 and 2.5 nM SAv-Cy5 are added to assess the binding specificity of each protein to membrane components. Flow cytometry data is collected and analyzed as before, with compensation applied to account for partial overlap of the FL-3 channel with both FL-1 and FL-4 signals (Appendix

II 3, Figure A3.6). The bead population of each multiplexed sample is gated as in Figure



3.1B and plotted on bivariate plots of FL-4 (Figure 3.5A–D) or FL-3 (Figure 3.5E–H) versus FL-1. In samples where neither protein is added, FL-3 and FL-4 signals are low (Figure 3.5, parts A and E). In the presence of 20 nM CTxB-Alexa 647, fluorescence is low on all bead populations in the FL-3 channel (Figure 3.5F) but increases in the FL-4 channel on the bead population containing 0.5% GM1 (Figure 3.5B). These results show specific binding of CTxB-Alexa 647 to GM1. When 2.5 nM SAV-Cy5 is added, the fluorescence intensity in the FL-3 channel increases on the bead population containing 0.5% biotin-DOPE (Figure 3.5G). Fluorescence also increases slightly on the other bead populations in the FL-3 channel (Figure 3.5G), showing nonspecific binding of SAV-Cy5 to other lipid compositions as discussed previously. There is also a small increase in FL-4 fluorescence in the sample containing SAV-Cy5 (Figure 3.5C), attributed to Cy5 fluorescence spillover into the FL-4 channel. When both 20 nM CTxB-Alexa 647 and 2.5

nM SA_v-Cy5 are added, FL-4 fluorescence increases substantially on the bead population containing GM1, slightly on the population containing biotin-DOPE (indicating nonspecific binding), and not on the population containing 100% POPC (Figure 3.5D), indicating the absence of any additional nonspecific binding beyond that observed in Figure 3.5C. Additionally, fluorescence in the FL-3 channel increases similarly to the sample containing only SA_v-Cy5, indicating specific binding of the SA_v-Cy5 to biotin-DOPE (Figure 3.5H). The median intensities in FL-4 and FL-3 corresponding to the gated data from Figure 3.5, averaged over four replicate experiments, are shown in Appendix II 3, Figure A3.7.

3.5 Conclusion

Our results demonstrate the use of multiplexed microsphere-based assays for differential binding assays that involve membrane components. These methods are similar to those required for screening applications. While we have presented a small multiplex, expansion to large multiplexed sets ($n \sim 100$ or larger) should be possible using strategies similar to those implemented for polymer-based indexed microspheres.⁷ To achieve that long-term goal in a commercially viable implementation, one of two materials development paths can be followed. Since supported membrane bilayers on silica microspheres are readily produced, one approach is to develop reliable labeling strategies to index silica microspheres without altering the surface chemistry needed for stable membrane assembly. An alternative approach is to develop well-characterized model membranes on commercially available highly multiplexed polymer microspheres. To conclude, our results show that fluorescently indexed membranes on silica microspheres enable multiplexed differential binding assays using flow cytometry. For two test cases,

the multiplexed methods we present yield results in good agreement with prior studies. Overall, this study provides an initial step to building multiplexed high-throughput flow cytometry assays involving membrane-associated components. Continued development of this multiplexed lipid membrane platform will occur through investigation of methods to generate larger multiplexed sets of targets and controls and in applications of this technology to flow-cytometry-based interaction analysis or screening studies.

3.6 Acknowledgements

A.P.S., S.W.G., and J.M.F. were supported by NIH R21 EB016339. N.A.Z. was supported for a portion of this work for training opportunities through the New Mexico Cancer Nanotechnology Training Center CA-R25153825. A.F.-W. and S.W.G. were also supported in part by NSF 1318833, NSF 1518861, and NIH R21 AI115105. M.G.-D. was funded by UNM-IMSD/NIH GM060201. Some data were generated in the UNM Shared Flow Cytometry and High Throughput Screening Resource Center supported by the University of New Mexico Health Sciences Center and the University of New Mexico Cancer Center with current funding from NCI 2P30 CA118100-11 “UNM Cancer Center Support Grant”.

3.7 References

1. Yin H, Flynn AD. Drugging Membrane Protein Interactions. *Annu Rev Biomed Eng.* 2016;18(1):51-76. doi:10.1146/annurev-bioeng-092115-025322.
2. Allen JA, Roth BL. Strategies to Discover Unexpected Targets for Drugs Active at G Protein–Coupled Receptors. *Annu Rev Pharmacol Toxicol.* 2011;51(1):117-144. doi:10.1146/annurev-pharmtox-010510-100553.
3. Overington JP, Al-Lazikani B, Hopkins AL. How many drug targets are there? *Nat Rev Drug Discov.* 2006;5(12):993-996. doi:10.1038/nrd2199.
4. Vignali DA. Multiplexed particle-based flow cytometric assays. *J Immunol Methods.* 2000;243(1-2):243-255.
5. Kellar KL, Iannone MA. Multiplexed microsphere-based flow cytometric assays. *Exp Hematol.* 2002;30(11):1227-1237.
6. Kellar KL, Douglass JP. Multiplexed microsphere-based flow cytometric immunoassays for human cytokines. *J Immunol Methods.* 2003;279(1-2):277-285.
7. Edwards BS, Sklar LA. Flow Cytometry: Impact on Early Drug Discovery. *J Biomol Screen.* 2015;20(6):689-707. doi:10.1177/1087057115578273.
8. Saunders MJ, Edwards BS, Zhu J, Sklar LA, Graves SW. Microsphere-based flow cytometry protease assays for use in protease activity detection and high-throughput screening. *Curr Protoc Cytom.* 2010;Chapter 13:Unit 13.12.1-17. doi:10.1002/0471142956.cy1312s54.
9. Simons PC, Young SM, Carter MB, et al. Simultaneous in vitro molecular screening of protein-peptide interactions by flow cytometry, using six Bcl-2 family proteins as examples. *Nat Protoc.* 2011;6(7):943-952. doi:10.1038/nprot.2011.339.
10. Edwards BS, Zhu J, Chen J, et al. Cluster cytometry for high-capacity bioanalysis. *Cytometry A.* 2012;81(5):419-429. doi:10.1002/cyto.a.22039.
11. Yu C, Mannan AM, Yvone GM, et al. High-throughput identification of genotype-specific cancer vulnerabilities in mixtures of barcoded tumor cell lines. *Nat Biotechnol.* 2016;34(4):419-423. doi:10.1038/nbt.3460.
12. Tiefenauer L, Demarche S. Challenges in the Development of Functional Assays of Membrane Proteins. *Materials (Basel).* 2012;5(12):2205-2242. doi:10.3390/ma5112205.
13. Lauer S, Goldstein B, Nolan RL, Nolan JP. Analysis of Cholera Toxin–Ganglioside Interactions by Flow Cytometry. *Biochemistry.* 2002;41(6):1742-1751. doi:10.1021/bi0112816.
14. Sackmann E. Supported membranes: scientific and practical applications. *Science.* 1996;271(5245):43-48.

15. Heyse S, Ernst OP, Dienes Z, Hofmann KP, Vogel H. Incorporation of Rhodopsin in Laterally Structured Supported Membranes: Observation of Transducin Activation with Spatially and Time-Resolved Surface Plasmon Resonance. *Biochemistry*. 1998;37(2):507–522. doi:10.1021/BI971564R.
16. Plant AL. Self-assembled phospholipid/alkanethiol biomimetic bilayers on gold. *Langmuir*. 1993;9(11):2764-2767. doi:10.1021/la00035a004.
17. Wagner ML, Tamm LK. Tethered polymer-supported planar lipid bilayers for reconstitution of integral membrane proteins: silane-polyethyleneglycol-lipid as a cushion and covalent linker. *Biophys J*. 2000;79(3):1400-1414. doi:10.1016/S0006-3495(00)76392-2.
18. Diaz AJ, Albertorio F, Daniel S, Cremer PS. Double cushions preserve transmembrane protein mobility in supported bilayer systems. *Langmuir*. 2008;24(13):6820-6826. doi:10.1021/la800018d.
19. Plant AL. Supported Hybrid Bilayer Membranes as Rugged Cell Membrane Mimics. *Langmuir*. 1999;15(15):5128–5135. doi:10.1021/LA981662T.
20. Song X, Swanson BI. Rapid assay for avidin and biotin based on fluorescence quenching. *Anal Chim Acta*. 2001;442(1):79-87. doi:10.1016/S0003-2670(01)01128-X.
21. Shreve AP, Howland MC, Sapuri-Butti AR, Allen TW, Parikh AN. Evidence for Leaflet-Dependent Redistribution of Charged Molecules in Fluid Supported Phospholipid Bilayers. *Langmuir*. 2008;24(23):13250-13253. doi:10.1021/la802909c.
22. Jung H, Robison AD, Cremer PS. Multivalent ligand–receptor binding on supported lipid bilayers. *J Struct Biol*. 2009;168(1):90-94. doi:10.1016/j.jsb.2009.05.010.
23. Nguyen TT, Conboy JC. High-Throughput Screening of Drug–Lipid Membrane Interactions via Counter-Propagating Second Harmonic Generation Imaging. *Anal Chem*. 2011;83(15):5979-5988. doi:10.1021/ac2009614.
24. Worstell NC, Krishnan P, Weatherston JD, Wu H-J. Binding Cooperativity Matters: A GM1-Like Ganglioside-Cholera Toxin B Subunit Binding Study Using a Nanocube-Based Lipid Bilayer Array. Nabi IR, ed. *PLoS One*. 2016;11(4):e0153265. doi:10.1371/journal.pone.0153265.
25. Tran RJ, Sly KL, Conboy JC. Applications of Surface Second Harmonic Generation in Biological Sensing. *Annu Rev Anal Chem*. 2017;10(1):387-414. doi:10.1146/annurev-anchem-071015-041453.
26. Nair PM, Salaita K, Petit RS, Groves JT. Using patterned supported lipid membranes to investigate the role of receptor organization in intercellular signaling. *Nat Protoc*. 2011;6(4):523-539. doi:10.1038/nprot.2011.302.

27. Oliver AE, Kendall EL, Howland MC, Sanii B, Shreve AP, Parikh AN. Protecting, patterning, and scaffolding supported lipid membranes using carbohydrate glasses. *Lab Chip*. 2008;8(6):892-897. doi:10.1039/b800370j.
28. Yang T-HC, Yee CK, Amweg ML, et al. Optical detection of ion-channel-induced proton transport in supported phospholipid bilayers. *Nano Lett*. 2007;7(8):2446-2451. doi:10.1021/nl071184j.
29. Smith KA, Gale BK, Conboy JC. Micropatterned Fluid Lipid Bilayer Arrays Created Using a Continuous Flow Microspotter. *Anal Chem*. 2008;80(21):7980-7987. doi:10.1021/ac800860u.
30. Chao L, Daniel S. Measuring the Partitioning Kinetics of Membrane Biomolecules Using Patterned Two-Phase Coexistent Lipid Bilayers. *J Am Chem Soc*. 2011;133(39):15635-15643. doi:10.1021/ja205274g.
31. Costello DA, Millet JK, Hsia C-Y, Whittaker GR, Daniel S. Single particle assay of coronavirus membrane fusion with proteinaceous receptor-embedded supported bilayers. *Biomaterials*. 2013;34(32):7895-7904. doi:10.1016/j.biomaterials.2013.06.034.
32. Beloglazova NV, Goryacheva OA, Speranskaya ES, et al. Silica-coated liposomes loaded with quantum dots as labels for multiplex fluorescent immunoassay. *Talanta*. 2015;134:120-125. doi:10.1016/j.talanta.2014.10.044.
33. Friedrich R, Block S, Alizadehheidari M, et al. A nano flow cytometer for single lipid vesicle analysis. *Lab Chip*. 2017;17(5):830-841. doi:10.1039/c6lc01302c.
34. Piyasena ME, Graves SW. The intersection of flow cytometry with microfluidics and microfabrication. *Lab Chip*. 2014;14(6):1044-1059. doi:10.1039/C3LC51152A.
35. Czogalla A, Grzybek M, Jones W, Coskun Ü. Validity and applicability of membrane model systems for studying interactions of peripheral membrane proteins with lipids. *Biochim Biophys Acta - Mol Cell Biol Lipids*. 2014;1841(8):1049-1059. doi:10.1016/j.bbalip.2013.12.012.
36. Jørgensen IL, Kemmer GC, Pomorski TG. Membrane protein reconstitution into giant unilamellar vesicles: a review on current techniques. *Eur Biophys J*. 2017;46(2):103-119. doi:10.1007/s00249-016-1155-9.
37. Nishimura K, Hosoi T, Sunami T, et al. Population Analysis of Structural Properties of Giant Liposomes by Flow Cytometry. *Langmuir*. 2009;25(18):10439-10443. doi:10.1021/la902237y.
38. Nishimura K, Matsuura T, Nishimura K, Sunami T, Suzuki H, Yomo T. Cell-free protein synthesis inside giant unilamellar vesicles analyzed by flow cytometry. *Langmuir*. 2012;28(22):8426-8432. doi:10.1021/la3001703.
39. Zeineldin R, Piyasena ME, Sklar LA, Whitten D, Lopez GP. Detection of

- membrane biointeractions based on fluorescence superquenching. *Langmuir*. 2008;24(8):4125-4131. doi:10.1021/la703575r.
40. Conway JW, Madwar C, Edwardson TG, et al. Dynamic behavior of DNA cages anchored on spherically supported lipid bilayers. *J Am Chem Soc*. 2014;136(37):12987-12997. doi:10.1021/ja506095n.
 41. Gopalakrishnan G, Rouiller I, Colman DR, Lennox RB. Supported bilayers formed from different phospholipids on spherical silica substrates. *Langmuir*. 2009;25(10):5455-5458. doi:10.1021/la9006982.
 42. Piyasena ME, Zeineldin R, Fenton K, Buranda T, Lopez GP. Biosensors based on release of compounds upon disruption of lipid bilayers supported on porous microspheres. *Biointerphases*. 2008;3(2):38. doi:10.1116/1.2918743.
 43. Buranda T, Huang J, Ramarao G V., et al. Biomimetic Molecular Assemblies on Glass and Mesoporous Silica Microbeads for Biotechnology. *Langmuir*. 2003;19(5):1654-1663. doi:10.1021/la026405+.
 44. Nguyen TT, Sly KL, Conboy JC. Comparison of the Energetics of Avidin, Streptavidin, NeutrAvidin, and Anti-Biotin Antibody Binding to Biotinylated Lipid Bilayer Examined by Second-Harmonic Generation. *Anal Chem*. 2012;84(1):201-208. doi:10.1021/ac202375n.
 45. Seto H, Yamashita C, Kamba S, et al. Biotinylation of Silicon and Nickel Surfaces and Detection of Streptavidin as Biosensor. *Langmuir*. 2013;29(30):9457-9463. doi:10.1021/la401068n.
 46. Werner JH, Montaña GA, Garcia AL, et al. Formation and dynamics of supported phospholipid membranes on a periodic nanotextured substrate. *Langmuir*. 2009;25(5):2986-2993. doi:10.1021/la802249f.
 47. Silva-López EI, Edens LE, Barden AO, Keller DJ, Brozik JA. Conditions for liposome adsorption and bilayer formation on BSA passivated solid supports. *Chem Phys Lipids*. 2014;183:91-99. doi:10.1016/j.chemphyslip.2014.06.002.
 48. Corbitt TS, Zhou Z, Tang Y, Graves SW, Whitten DG. Rapid evaluation of the antibacterial activity of arylene-ethynylene compounds. *ACS Appl Mater Interfaces*. 2011;3(8):2938-2943. doi:10.1021/am200277c.
 49. Herzenberg LA, Tung J, Moore WA, Herzenberg LA, Parks DR. Interpreting flow cytometry data: a guide for the perplexed. *Nat Immunol*. 2006;7(7):681-685. doi:10.1038/ni0706-681.

Chapter 4.

Membrane disruption assays on silica microsphere supported lipid bilayer membranes

4.1 Abstract

We report a set of membrane disruption assays performed on NBD-DOPE [1,2-dioleoyl-sn-glycero-3-phosphoethanolamine-N-(7-nitro-2-1,3-benzoxadiazol-4-yl)] or Lissamine Rhodamine B [1,2-dioleoyl-sn-glycero-3-phosphoethanolamine-N-(lissamine rhodamine B sulfonyl) fluorescently-tagged 1,2-dioleoyl-sn-glycero-3-phosphocholine (DOPC) lipid biomimetic membranes supported on 8 μm non-porous silica microspheres. The membranes were presented to different concentrations of the surfactant (LDAO) and the endotoxin (LPS), which through perturbation or disruption caused significant loss of fluorescence in the membranes. All the samples were screened and analyzed using flow cytometry and corroborated using confocal fluorescence microscopy. These studies provide a proof-of-principle demonstration for a flow-based membrane disruption assay that can be readily multiplexed to investigate multiple lipid compositions.

4.2 Introduction

Cell membranes serve many biological functions: they serve as a barrier that protects the contents of the cell¹, they serve as support for membrane proteins², they control the permeation of substances in and out of the cell³, and they are crucial in cell signaling processes.⁴ Hence, cell membranes constitute important targets for drug screening processes, and for mechanistic studies of antimicrobial peptides, nanoparticles, surfactants or toxins, among other important biomolecules. An important step of these studies consists of testing the potential membrane disruption effect of the screened drug or surfactant. This is done via membrane disruption assays, which may be carried out on actual cells.^{5,6}

However, in such studies, target identification is very difficult due to confounding factors such as membrane complexity and the wide variety of different components that are present, including lipids, proteins, and carbohydrates. Studies can also be performed on planar-solid-supported membranes,^{7,8} but this platform is limited to low to medium throughput screening processes. The current study aims to demonstrate that the interaction between surfactants or toxins and biomimetic membranes presented on alternative platforms that would allow multiplexed or high-throughput screening is feasible.

In the present work, we initially investigated the surfactant lauryldimethylamine oxide (LDAO) as it is a very common zwitterionic surfactant⁹ found in house cleaning and personal hygiene products^{10,11}. LDAO is widely used to solubilize integral proteins from their native membranes¹², as it is a non-denaturing agent. Since the disruption effects of LDAO on membranes is well studied and characterized, the present work analyzes the effects of LDAO on silica microsphere-supported lipid membranes as a control experiment and as a proof-of-principle.

For the subsequent studies we chose lipopolysaccharides (LPS), which are heat stable and highly potent mammalian amphiphilic endotoxins¹³, and also are a characteristic component of the outer membrane of Gram-negative bacteria¹⁴, and *Escherichia coli*¹⁵. The LPS structure has been shown to be altered by the presence of monovalent and divalent cations, becoming more aggregated and less mobile in the presence of the latter¹⁶⁻¹⁸. Furthermore, it has been reported that the treatment of fluid-phase planar-supported lipid bilayers with LPS induces hole formation on the membrane, which depends on the incubation time and LPS concentration.¹⁹ Moreover, Adams et al. demonstrated that the ability of LPS to form pores on fluid lipid membranes can be used to generate microscale

2-D array patterns of domains with pores that can be backfilled with other membrane components²⁰.

Hence, the present work aims to explore the possibility of running similar studies to those presented by Adams et al. and to test and characterize the interaction of LPS with lipid membranes supported on non-porous silica microspheres using flow cytometry as the screening process.

4.3 Materials and Methods

4.3.1 Materials

The lipids 1,2-dioleoyl- sn-glycero- 3-phosphoethanolamine-N- (7-nitro- 2-1,3-benzoxadiazol-4- yl (NBD-DOPE), 1,2-dioleoyl-sn-glycero-3-phosphocholine (DOPC), 1,2-dioleoyl-sn-glycero-3-phosphoethanolamine-N-(lissamine rhodamine B sulfonyl (Lissamine Rhodamine B– DOPE), 1,2-distearoyl-sn-glycero-3-phosphocholine (DSPC), and 1,2-distearoyl-sn-glycero-3-phosphoethanolamine-N-(7-nitro-2-1,3-benzoxadiazol-4- yl (NBD-DSPE) were purchased from Avanti Polar Lipids in lyophilized form. As solvent for lipids, we used chloroform that contains 1%-5% of ethanol as a stabilizer, purchased from EMD Millipore. N,N-dimethyldodecylamine N-oxide (LDAO) was purchased in powder form from Avanti Polar Lipids. Lipopolysaccharides (LPS) purified by phenol extraction from *Escherichia coli* O111:B4 was purchased from Sigma Aldrich. The non-porous silica microspheres (7.9 μm) suspended in deionized water with 0.02% sodium azide were purchased from Spherotech. Finally, all the experiments were performed using phosphate-buffered saline (PBS) as the main buffer, and bovine serum albumin (BSA) as a blocking and passivating agent; both were purchased from Sigma Aldrich.

4.3.2 Formation of lipid membranes on silica microspheres.

The assembly of fluid lipid bilayers on silica microspheres were done following previously reported protocols.²¹ Briefly, all the lyophilized lipids were dissolved in chloroform and stored in glass vials at $-20\text{ }^{\circ}\text{C}$ until use. In separate glass vials, different volumes of the stock lipids were mixed to achieve the desired final concentrations, and they were left under vacuum overnight to let the chloroform evaporate. Next, the lipid plaques were then rehydrated in PBS to a final concentration of 1 mM to later form $0.1\text{ }\mu\text{m}$ large unilamellar vesicles (LUVs) by extrusion. The liposomes solution (1 mM lipid concentration) are then incubated with $\sim 10^6$ beads/mL of non-porous silica microspheres by vortexing them together first at room temperature on high speed for 10 minutes, and then at $37\text{ }^{\circ}\text{C}$ on low speed for 45 minutes. Afterwards, the samples were passivated with BSA by incubation with 0.5 mg/mL BSA for 45 minutes at room temperature and low speed. Finally, the samples were washed and rinsed 3 times to remove extra BSA and liposomes in solution by centrifugation at 10,000 rpm for 45 s, followed by removing the supernatant and resuspending the beads in fresh PBS.

4.3.3 Membrane disruption assays.

The samples consisted of silica microsphere-supported lipid membranes, which were built with lipid fluorescent tags (either NBD-DOPE or Lissamine Rhodamine-DOPE) in them. The samples were split into equal-amount aliquots to reduce sample to sample experimental variation. The disruption effect of the surfactants was tested by incubating sample aliquots with increasing amounts of the membrane disrupting agent, LPS or LDAO. The incubation took place at room temperature and protected from light. The samples that

were exposed to increasing concentrations of LDAO (0.5 -1.5 mM) or LPS (50 – 500 µg/ml) and the controls were measured with the flow cytometer after 20, 40 and 60 minutes of incubation to evaluate the loss of fluorescence as an indication of membrane disruption. Moreover, the sample that was exposed to the highest concentration of LDAO and the control were imaged with a confocal microscope to provide visual proof of the damage on the membrane caused by the surfactant.

4.3.4 Backfilling of LPS-induced membrane holes with lipid vesicles with a secondary lipid fluorescent tag.

First, liquid-phase liposomes (99.5% DOPC + 0.5 mol% NBD-DOPE) were prepared as described above, and gel-phase liposomes (99.5 mol% DSPC + 0.5 mol% NBD-DSPE) were prepared by forming plaques under vacuum and resuspending them in PBS to later go under three cycles of freeze-thaw and intermittent probe sonication for 10 minutes at >60 °C, as a previously reported method describes.²⁰ The gel-phase liposomes were kept at ~60 °C until use.

Second, samples containing silica-supported lipid membranes with a composition of 99.9 mol% DOPC + 0.1 mol% Lissamine Rhodamine B-PE were incubated with LPS (0, 5, 50 or 500 µg/ml) for ~50 minutes. Next, the fluorescence levels of all the samples was measured using flow cytometry. Then, the samples were incubated with either liquid-phased liposomes (1 mM lipid concentration) or the gel-phase liposomes (1 mM lipid concentration) for ~ 7minutes. Afterwards, the fluorescence intensity of the samples in the channels detecting Lissamine Rhodamine and NBD channel was measured by flow cytometry. Finally, the sample that was first incubated with 500 µg/ml and later backfilled

with the gel-phased vesicles was imaged with a confocal microscope to provide visual proof of the backfilling process.

4.3.5 Microscopy.

Confocal fluorescence microscopy imaging was performed using a Fluoview FV-1000 confocal laser scanning microscope (Olympus, Tokyo, Japan). The images were acquired with a 40X objective (NA = 0.95) and a 6.0 zoom. The samples containing Lissamine Rhodamine were imaged by exciting them by a 559 nm LD559 laser and collecting the emitted light with a bandpass (BP) filter (570-605 nm). The samples containing NBD were imaged by exciting them by a 488 nm Multi Argon laser and collecting the emitted light with a bandpass (BP) filter (505-525 nm).

4.3.6 Flow cytometry.

All the flow cytometric data was collected using an Attune® NxT acoustic focusing flow cytometer by Thermo Fisher Scientific. The Attune® NxT has four lasers (405, 488, 561, and 638 nm) with independent optical paths, and 14 different detection channels. The channels used in the work presented here are: BL-1: 488 nm laser excitation, and emission 530 nm center/30 nm bandpass (BP), and YL-1: 561 nm laser excitation, and emission 585 nm center/16 nm BP. The flow cytometer went under regular maintenance, cleaning and calibration before and after use.

For each sample, a total of 10,000 events were collected, out of which about 7,000 corresponded to the main population (fluorescently-tagged lipid membrane supported on silica microspheres). All the collected data was saved as Flow Cytometry Standard (FCS) files and was further analyzed using FlowJoV10 software. The gating was generated by the

auto-gating tool and the software provided statistical information of the gated events. Further numerical analysis and graph plotting was done using Microsoft Excel.

4.4 Results and Discussion

4.4.1 Formation of lipid membranes on silica microspheres.

The silica microsphere-supported membranes used in the present work had the following compositions: 99.8 mol% DOPC + 0.2 mol% NBD-DOPE; 99 mol% DOPC+1% Liss. Rhod-PE; and 99.9 mol% DOPC + 0.1 mol% Liss. Rhod. B-PE.

4.4.2 Membrane disruption assays.

Fluorescence microscopy images show a uniform and complete membrane coverage on the microspheres (Figures 4.2A and 4.4A). Hence, the loss of fluorescence quantified by flow cytometric screening was analyzed as a measurement of membrane disruption. The correlation between membrane disruption and loss of fluorescence was qualitatively corroborated with fluorescence microscopy imaging.

4.4.2.1 Membrane disruption with LDAO

The sample used to test the disrupting effects of LDAO, as proof of concept, consisted of biomimetic lipid membranes supported on silica microspheres with a composition of 99.8%mol DOPC + 0.2%mol NBD-DOPE. After the splitting of the main sample into smaller aliquots, the lipid-coated bead concentration in solution was $\sim 10^5$ beads/ml. One aliquot served as a control and the rest were incubated with increasing concentrations of LDAO (0.5, 0.75, 1, 1.25, 1.5 mM). These values were chosen to be around the c.m.c value (the reported LDAO c.m.c. is ~ 1 mM).²² The samples were incubated with LDAO for 20,

40 and 60 minutes before being analyzed in the flow cytometer. First, the bead population

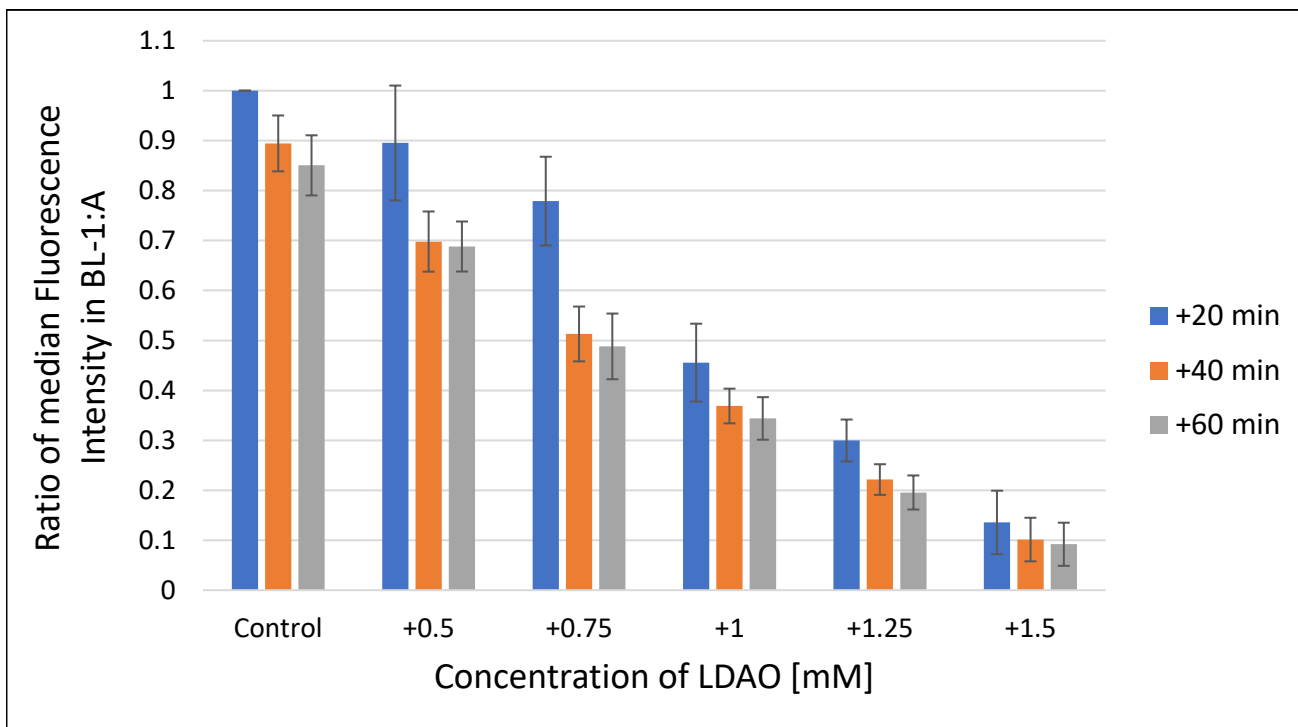


Figure 4.1. Flow cytometry acquired median fluorescence intensity in BL-1 channel (NBD-detection channel) of DOPC+0.2%mol NBD-DOPE membrane supported on silica beads in the presence of increasing concentrations of LDAO (0.5, 0.75, 1, 1.25, 1.5 mM) and increasing incubation times (20, 40, and 60 minutes). Data shown are normalized to the 20-minute control (no LDAO) sample, and are the average of three replicates, and error bars are plus/minus one standard deviation.

was gated from the side scatter versus forward scatter plot, and the gated population was then observed in the side scatter versus BL-1 (NBD detection channel) where the gating was further refined by selecting only the well-coated beads. Finally, the median fluorescence intensity was recorded for all the samples. The experiment was repeated three different times. The median fluorescence intensity (in the BL-1 channel) resulting from the three replicates were averaged and normalized and are presented in Figure 4.1. The error bars represent plus/minus one standard deviation.

Overall, Figure 4.1 shows a clear decrease in BL-1 fluorescence of the membrane-coated microspheres in the presence of increasing concentrations of LDAO, and with increasing incubation times. The control samples (first block of columns to the left) shows

that there is a small natural decrease in fluorescence of the samples in time, possibly reflecting some membrane instability, but that loss of fluorescence does not account for more than ~ 10-15% after 60 minutes of initial assembly. After 20 minutes of incubation (blue bars) there is a decrease in fluorescence ranging from ~10% (in presence of 0.5 mM LDAO) to ~85% (in presence of 1.5 mM LDAO). After 40 minutes of incubation (orange bars), there is an even higher decrease of in fluorescence ranging from ~20% (in presence of 0.5 mM LDAO) to ~90% (in presence of 1.5 mM LDAO). Finally, after 60 minutes of incubation (gray bars) the fluorescence values of the samples are very similar to those observed at a 40-minute incubation process, indicating that the action of LDAO has stabilized in the 30 to 60-minute time frame.

The fluorescently-tagged lipid membranes on silica microspheres were imaged with the confocal fluorescent microscope before (Figure 4.2A) and after a 30-minute incubation with 1.5 mM of LDAO (Figure 4.2B). These images provide a visual proof of what the data of Figure 4.1 shows; at concentrations 1.25 and 1.5 mM there is, practically, a complete disruption of the membrane. Finally, for further comparison, we tested the disrupting effect of high concentration LDAO (1.5 mM) in planar-supported lipid bilayers with the same composition of their microsphere-supported counterparts. Appendix II 4, Figure A4.1 shows fluorescence microscopy images of the planar-supported membrane as control (Appendix II 4, Figure A4.1), and plus LDAO after 25, 30 and 45 minutes of

incubation (Appendix II 4, Figure A4 B-D). These images show the same qualitative loss of fluorescence observed in the silica bead-supported membranes.

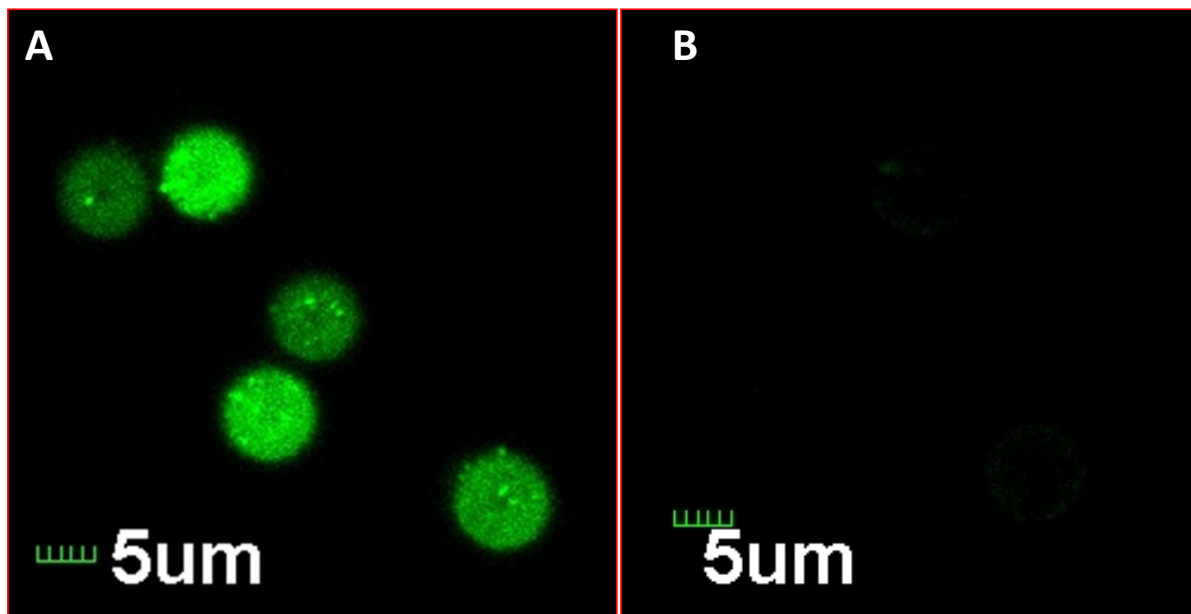


Figure 4.2. Confocal microscopy images of DOPC+0.2%mol NBD-DOPE membranes on silica microspheres. **A)** In absence of LDAO. **B)** After a 30-minute incubation with 1.5 mM of LDAO. The images were acquired with a 40X objective (NA = 0.95) and a 6.0 zoom.

Finally, silica microsphere-supported lipid membranes with different composition were incubated with increasing concentrations of LDAO and increasing incubation times. The fluorescence loss was similar to those presented in Figure 4.1; however, there was no clear difference in the disruptive effect of LDAO with respect to the different membrane composition (Appendix II 4, Figure A4.2).

4.4.2.2 Membrane disruption with LPS

First, the c.m.c. of the LPS used in the work presented here was measured by calculating the derived count rate versus LPS concentration using Dynamic Light Scattering. Appendix II 4, Figure A4.3 shows that the c.m.c. of LPS is 10-20 µg/ml.

As mentioned in the introduction, LPS reportedly induces hole formation on lipid membranes supported on planar surfaces.¹⁹ Hence, this work explores the effect of LPS on microsphere-supported lipid membranes. The sample used to test the disrupting effects of LPS consisted of biomimetic lipid membranes supported on silica microspheres with a

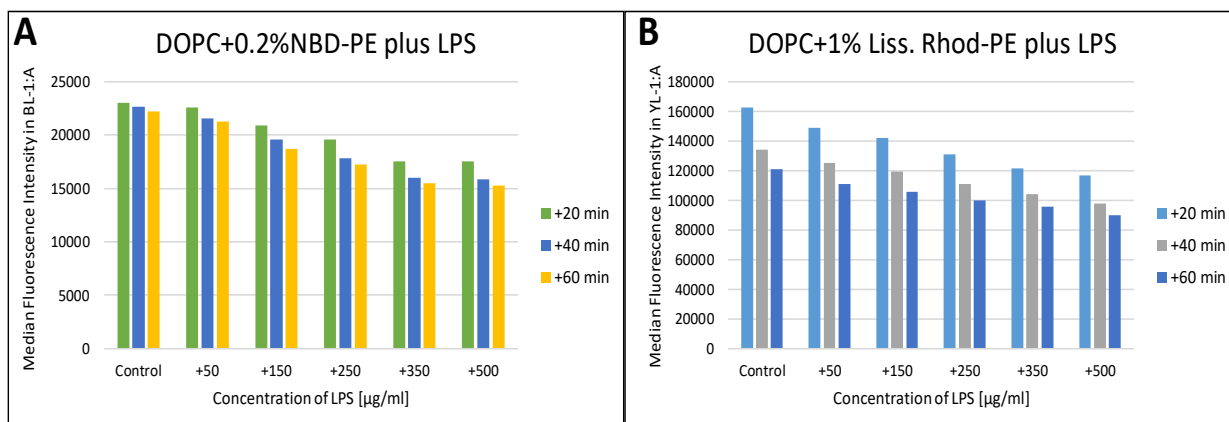


Figure 4.3. Flow cytometry acquired median fluorescence intensity of membrane supported on silica beads in the presence of increasing concentrations of LPS (50, 150, 250, 350, 500 µg/ml) and increasing incubation times (20, 40, and 60 minutes). **A**) Median fluorescence intensity in BL-1 (NBD-detection channel); membrane composition: DOPC+0.2%mol NBD-DOPE membranes. **B**) Median fluorescence intensity in YL-1 (Lissamine Rhodamine B detection channel); membrane composition: DOPC+1%mol Lissamine Rhodamine B-DOPE membranes.

composition of 99.8 mol% DOPC + 0.2 mol% NBD-DOPE (set 1) and 99 mol% DOPC + 1 mol% Liss. Rhod.-DOPE (set 2). Both sets were split into smaller aliquots with a lipid-coated bead concentration in solution of $\sim 10^5$ beads/ml. One aliquot served as a control and the rest were incubated with increasing concentrations of LPS (50, 150, 250, 350, 500 µg/ml). These values were chosen to be above the c.m.c value. The samples were incubated with LPS for 20, 40 and 60 minutes before being analyzed in the flow cytometer. The flow cytometric gating and analysis was done as described above. Briefly, samples were first gated from the side scatter versus forward scatter plot to later be further refined in the side scatter versus BL-1 (NBD detection channel) for set 1, or in in the side scatter versus YL-1 (Liss. Rhod. detection channel) for set 2. Figure 4.3A shows the median fluorescence intensity in the BL-1 channel (set 1) of the NBD-containing samples after incubation with

increasing amount of LPS and incubation times. Figure 4.3B shows the median fluorescence intensity in the YL-1 channel (set 1) of the Liss-Rhod.-containing samples after incubation with increasing amount of LPS and incubation times.

Both, Figures 4.3A and 4.3B show a clear decrease of fluorescence (in BL-1 and YL-1 respectively) of the membrane-coated microspheres in the presence of increasing concentrations of LPS, and increasing incubation times. In both cases, after 20 minutes of incubation (green bars for NBD and light blue ones for Liss. Rhod.) the decrease of fluorescence goes from ~5% (in the presence of 50 $\mu\text{g/ml}$) to ~ 25% (in the presence of 500 $\mu\text{g/ml}$). After 40 minutes (blue bars for NBD and gray ones for Liss. Rhod.) and 60 minutes (yellow bars for NBD and dark blue ones for Liss. Rhod.) of incubation the fluorescence loss was around the same; it goes from 25% (in the presence of 50 $\mu\text{g/ml}$) to ~ 40% (in the presence of 500 $\mu\text{g/ml}$).

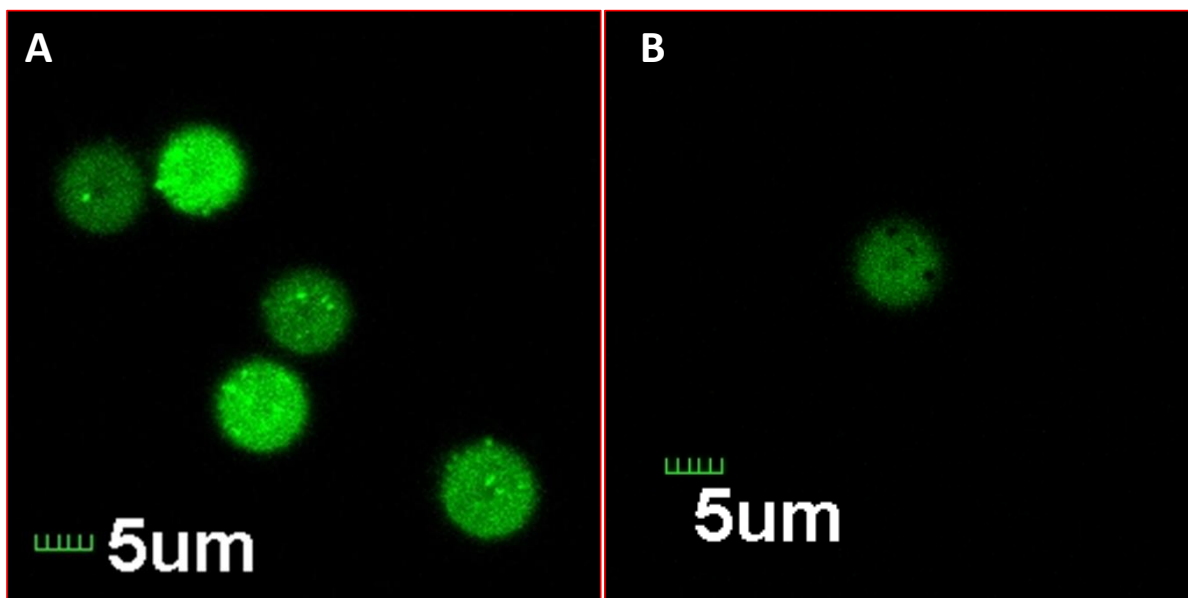


Figure 4.4. Confocal microscopy images of DOPC+0.2%mol NBD-DOPE membranes on silica microspheres. **A)** In absence of LPS. **B)** After a 30-minute incubation with 500 $\mu\text{g/ml}$ of LPS. The images were acquired with a 40X objective (NA = 0.95) and a 6.0 zoom.

The fluorescently-tagged lipid membranes on silica microspheres were imaged with the confocal fluorescent microscope before (Figure 4.4A) and after the addition of 500 $\mu\text{g/ml}$ of LPS (Figure 4.4B). The images show the LPS-induced holes of $\sim 1 \mu\text{m}$ in diameter on the membrane, which is consistent with the behavior observed of LPS effect on planar supported-lipid membranes (Appendix II 4, Figure A4.4).

The loss of fluorescence shown in Figure 4.3 is much less compared to that observed with LDAO. This is consistent with the fact that LDAO nearly fully disrupts and pulls the membrane, but LPS induces the formation of sporadic holes throughout the surface of the membrane, leaving much of the bilayer intact.

Finally, silica microsphere-supported lipid membranes with different composition were incubated with increasing concentrations of LPS and increasing incubation times. The fluorescence loss was similar to those presented in Figure 4.3; however, there was no clear difference in the disruptive effect of LPS with respect to the different membrane composition (Appendix II 4, Figure A4.5).

4.4.3 Backfilling of LPS-induced membrane holes with lipid vesicles with a secondary lipid fluorescent tag.

Adams et. al., showed that LPS-generated membrane holes could be backfilled with secondary lipids in either gel-phase or liquid-phase. Here, we test if a similar process could take place in membranes supported on microspheres, and more importantly if the changes in the composition due to the backfilling were detectable and measurable in flow cytometry.

Figure 4.5 shows the fluorescence microscopy image of 99.9% mol DOPC + 0.1% mol Lissamine Rhodamine B-PE membranes supported on silica beads. Figure 4.5A is the control set; Figure 4.5B shows the membranes after a 30-minute LPS treatment (500 $\mu\text{g}/\text{ml}$); and Figure 4.5C shows the LPS treated membranes after being backfilled with gel-phased liposomes (99.5% DSPC + 0.5% mol NBD-DSPE). The images visually corroborate the hole formation after treatment with LPS and the ability of a set of liposomes, with a secondary fluorescent dye, to backfill those holes.

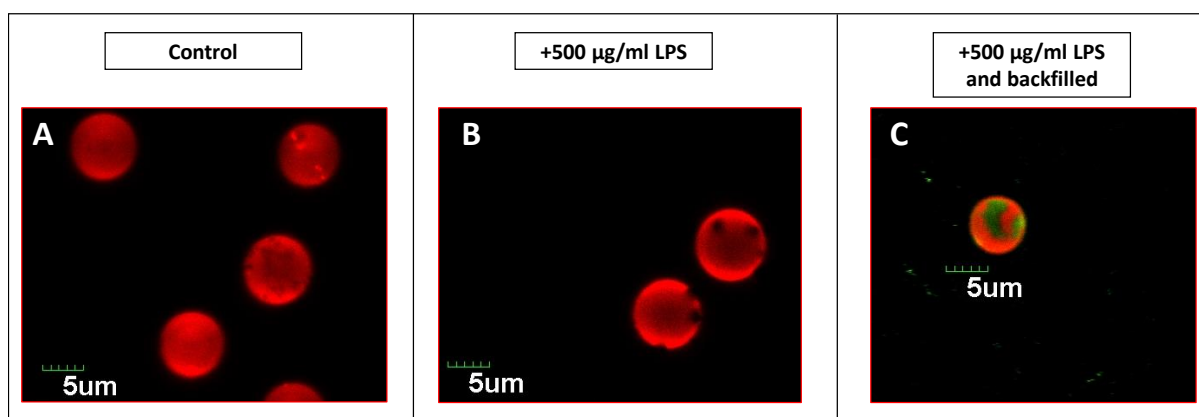


Figure 4.5. Confocal microscopy images of DOPC+1% mol Lissamine Rhodamine B-DOPE membranes supported on silica microspheres. **A)** Control set. **B)** After treatment with 500 $\mu\text{g}/\text{ml}$ for 50 minutes; **C)** Samples in (B) where the LPS-induced holes were backfilled with 99.5% DSPC + 0.5% mol NBD-DSPE liposomes.

Figure 4.6A shows the flow cytometric obtained median fluorescence intensity in YL-1 channel (Lissamine Rhodamine detection channel) in the absence (blue bars) and presence of LPS; 5 $\mu\text{g}/\text{ml}$ (orange bars), 50 $\mu\text{g}/\text{ml}$ (grey bars), and 500 $\mu\text{g}/\text{ml}$ (yellow bars). Starting from the left, the first block of columns shows the samples before the backfilling process. The second block of columns show the samples that were backfilled with gel-phase liposomes and the third block of columns show the samples that were backfilled with liquid-phase liposomes. The loss of fluorescence intensity observed before and after backfilling remain the similar and consistent with that of Figure 4.3.

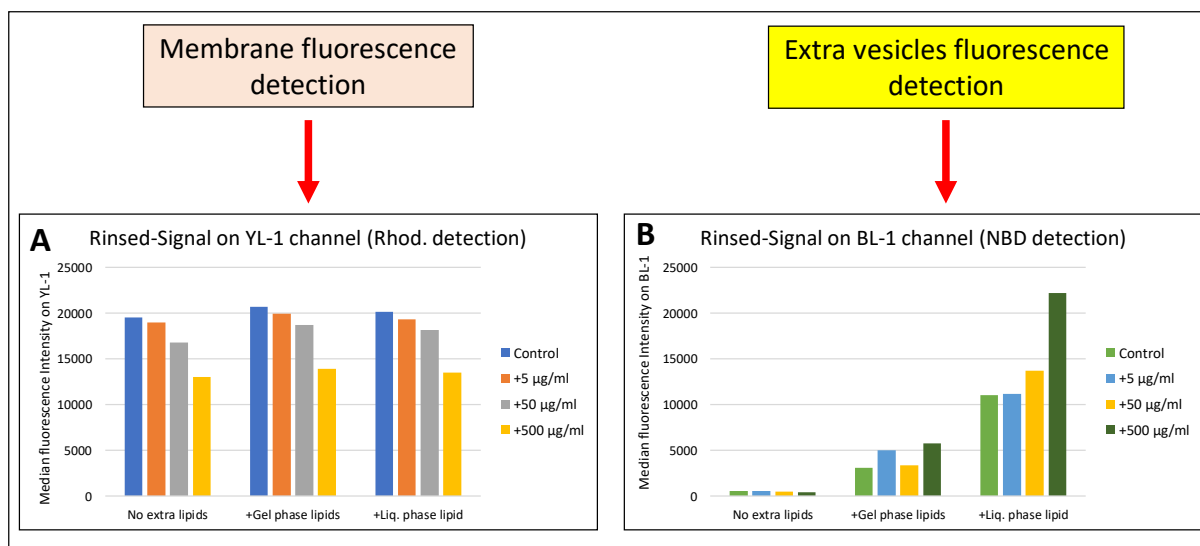


Figure 4.7. Flow cytometric data of DOPC+0.1%mol Lissamine Rhodamine B-DOPE membranes supported on microspheres, treated with increasing concentrations of LPS and backfilled with gel-phase (99.5% DSPC + 0.5%mol NBD-DSPE) or liquid-phase (99.5% DOPC + 0.5%mol NBD-DOPE) liposomes. **A)** Median fluorescence intensity in YL-1 channel (Lissamine Rhodamine detection channel) showing the fluorescence of the membrane; control set (blue bars); treated with 5 µg/ml of LPS (orange bars); treated with 50 µg/ml of LPS (grey bars), and treated with 500 µg/ml of LPS (yellow bars). **B)** Median fluorescence intensity in BL-1 channel (NBD detection channel) showing the integration of the gel-phase or liquid-phase liposomes; control set (light green bars); treated with 5 µg/ml of LPS (light blue bars); treated with 50 µg/ml of LPS (yellow bars), and treated with 500 µg/ml of LPS (dark green bars).

Figure 4.6B shows the flow cytometric obtained median fluorescence intensity in BL-1 channel (NBD detection channel) of the same samples as in Figure 4.6A. Briefly, plus 0 µg/ml (light green), plus 5 µg/ml (light blue), plus 50 µg/ml (yellow), and plus 500 µg/ml (dark green). The first block of columns shows the samples before the backfilling process, and as expected they show no presence of NBD in the samples since they are the samples before the backfilling process. The second block of columns show the samples that were backfilled with gel-phase liposomes. There is a clear small increase of fluorescence intensity, indicating the presence of the gel-phase lipids in the membrane, although the fluorescence levels are not proportional to the concentration of LPS. This might be indicative of the fact that the gel-phase lipids backfill only some of the holes and do not diffuse across the membrane. Finally, the third block of columns show the samples that

were backfilled with liquid-phase liposomes. There is a large increase of fluorescence intensity, indicating the presence of the liquid-phase lipids in the membrane. The high NBD fluorescence levels indicate that there is a presence of the liquid-phase lipids and that they might be more efficient at backfilling, plus they are able to diffuse across the membrane. Moreover, the NBD fluorescence level is inversely proportional to the concentration of LPS used to treat the membranes.

4.5 Summary and Conclusions

Our results demonstrate the viability of membrane disruption assays using non-porous silica microspheres-supported biomimetic membranes and flow cytometry. The proof-of-principle assay results presented here are similar to those previously reported on planar membrane surfaces, but the assays here were carried out using flow cytometry. This result proves that membranes supported on microspheres have the potential to serve as platforms to study the membrane disruptive effect of drugs, antimicrobial peptides, polymers, or other biomolecules. Importantly, the multiplexable potential of this platform²¹ can allow for the simultaneous screening of different lipid compositions against potential disruption agents. In addition to the assays described in the present work, microsphere-supported membranes can be used in other types of membrane disruption assays, like lipid protection assays. Overall, this study presents an alternative method for the screening of biomimetic membranes against potential membrane disrupting agents by using flow cytometry, and demonstrates what may ultimately prove to be a rapid and multiplexable new platform for such studies.

4.6 Acknowledgements

The present work was done in collaboration with Matthew Rush (Center for Biomedical Engineering at The University of New Mexico and Los Alamos National Laboratories at the Center for Integrated Technologies CINT). Some of the protocols were provided by Kirstie L. Swingle.

4.7 References

1. van Meer G, Voelker DR, Feigenson GW. Membrane lipids: where they are and how they behave. *Nat Rev Mol Cell Biol.* 2008;9(2):112-124. doi:10.1038/nrm2330.
2. Lodish H, Berk A, Zipursky SL. Molecular Cell Biology. In: *Molecular Cell Biology*. 4th ed. New York: W. H. Freeman; 2000.
3. Alberts B, Johnson A, Lewis J, Raff M, Roberts K, Walter P. The Lipid Bilayer. 2002. <http://www.ncbi.nlm.nih.gov/books/NBK26871/>. Accessed January 11, 2016.
4. Grecco HE, Schmick M, Bastiaens PIH. Signaling from the living plasma membrane. *Cell.* 2011;144(6):897-909. doi:10.1016/j.cell.2011.01.029.
5. Kafsack BFC, Pena JDO, Coppens I, Ravindran S, Boothroyd JC, Carruthers VB. Rapid membrane disruption by a perforin-like protein facilitates parasite exit from host cells. *Science.* 2009;323(5913):530-533. doi:10.1126/science.1165740.
6. Prentice P, Cuschieri A, Dholakia K, Prausnitz M, Campbell P. Membrane disruption by optically controlled microbubble cavitation. 2005. doi:10.1038/nphys148.
7. Lok K, Lam H, Ishitsuka Y, et al. Mechanism of Supported Membrane Disruption by Antimicrobial Peptide Protegrin-1. *J Phys Chem B.* 2006;110(42):21282-21286. doi:10.1021/jp0630065.
8. Eid M, Rippa S, Castano S, et al. Exploring the Membrane Mechanism of the Bioactive Peptaibol Ampullosporin A Using Lipid Monolayers and Supported Biomimetic Membranes. *J Biophys.* 2010;2010:12. doi:10.1155/2010/179641.
9. Friedli FE. *Detergency of Specialty Surfactants*. New York: M. Dekker; 2001.
10. Travis BR, Mittal R, Huff SM, Huang L, Tang L. Cleaning solution. November 2013.
11. Novelle A, Crowther R, Murphy F. Compositions for treating and removing noxious materials malodors and microbes, and methods of use and preparation thereof. 2005.
12. Nazari M. Properties of surfactants that govern their functions and applications on lipid membranes. 2012.
13. Raetz CRH, Whitfield C. Lipopolysaccharide Endotoxins. *Annu Rev Biochem.* 2002;71(1):635-700. doi:10.1146/annurev.biochem.71.110601.135414.
14. Wang X, Quinn PJ. Endotoxins: Lipopolysaccharides of Gram-Negative Bacteria. In: *Sub-Cellular Biochemistry*. Vol 53. ; 2010:3-25. doi:10.1007/978-90-481-

9078-2_1.

15. Nikaido H, Vaara M. Molecular basis of bacterial outer membrane permeability. *Microbiol Rev.* 1985;49(1):1-32.
16. Coughlin RT, Tonsager S, McGroarty EJ. Quantitation of metal cations bound to membranes and extracted lipopolysaccharide of *Escherichia coli*. *Biochemistry.* 1983;22(8):2002-2007. doi:10.1021/bi00277a041.
17. Coughlin RT, Haug A, McGroarty EJ. Physical properties of defined lipopolysaccharide salts. *Biochemistry.* 1983;22(8):2007-2013.
18. Kučerka N, Papp-Szabo E, Nieh M-P, et al. Effect of Cations on the Structure of Bilayers Formed by Lipopolysaccharides Isolated from *Pseudomonas aeruginosa* PAO1. *J Phys Chem B.* 2008;112(27):8057-8062. doi:10.1021/jp8027963.
19. Adams PG, Lamoureux L, Swingle KL, Mukundan H, Montañó GA. Lipopolysaccharide-Induced Dynamic Lipid Membrane Reorganization: Tubules, Perforations, and Stacks. *Biophys J.* 2014;106(11):2395-2407. doi:10.1016/j.bpj.2014.04.016.
20. Adams PG, Swingle KL, Paxton WF, et al. Exploiting lipopolysaccharide-induced deformation of lipid bilayers to modify membrane composition and generate two-dimensional geometric membrane array patterns. *Sci Rep.* 2015;5(1):10331. doi:10.1038/srep10331.
21. Fernandez Oropeza N, Zurek NA, Galvan-De La Cruz M, et al. Multiplexed Lipid Bilayers on Silica Microspheres for Analytical Screening Applications. *Anal Chem.* 2017;89(12):6440–6447. doi:10.1021/acs.analchem.7b00296.
22. Thiyagarajan P, Tiede DM. Detergent micelle structure and micelle-micelle interactions determined by small-angle neutron scattering under solution conditions used for membrane protein crystallization. *J Phys Chem.* 1994;98(40):10343-10351. doi:10.1021/j100091a058.

Chapter 5.

Microsphere-supported polymer membrane as an alternative to lipid membranes for screening applications

5.1 Abstract

We report the assembly of fluorescently multiplexed block copolymer biomimetic membranes on 8 μm non-porous silica microspheres, where the amphiphilic diblock copolymer, poly(ethylene oxide)-block-poly(butadiene), serves as a synthetic alternative to lipids in the membranes. The membranes are fluorescently tagged with various amounts of NBD-DOPE [1,2-dioleoyl-sn-glycero-3-phosphoethanolamine-N-(7-nitro-2-1,3-benzoxadiazol-4-yl)] and/or Texas Red - DHPE [1,2-Dihexadecanoyl-sn-Glycero-3-Phosphoethanolamine, Triethylammonium Salt]. Using flow cytometry and the fluorescently multiplexed block copolymer biomimetic membranes on silica microspheres with increasing concentrations of GM1, we demonstrate the differential binding affinity of cholera toxin B subunit-Alexa 647 to the ligand target. Analysis of the multiplexed assay results yields an effective affinity of ~ 50 nM for binding of cholera toxin B subunit to its GM1 ligand in these synthetic membranes. These results demonstrate that synthetic block copolymer membranes on microspheres provide a stable and useful architecture for multiplexed flow cytometry study of membrane-associated components.

5.2 Introduction

Polymers are some of the most widely used biomaterials, as they have low cost and their synthesis offers great flexibility in physical properties and functionality.^{1,2} Polymers are used in general surgical implants,³ orthopedic implants,⁴ cardio-vascular intervention,⁵ dentistry, neurosurgery,⁶ as drug delivery tools and encapsulants,^{7,8} and as biosensors⁹. There is one particular group of polymers known as the amphiphilic block copolymers that

are composed of two domains, one hydrophilic and one hydrophobic. Amphiphilic block copolymers have proven to have possible biological¹⁰ and medical applications.¹¹ For instance, structures like polymersomes or amphiphilic block copolymer vesicles have been applied as potential drug carriers.^{12,13} Polymersomes, like liposomes, are capable of forming biomimetic membranes or films.^{14,15} Previous studies showed that biomimetic block copolymer membrane properties, like permeability and lateral diffusivity, can be tuned by varying the block copolymer molecular weight,^{16,17} composition,^{11,18} pH, or ion concentration.¹⁹ This flexibility makes them a great synthetic alternative to lipids in the development of biomimetic membranes.²⁰

The amphiphilic block copolymer poly(ethylene oxide)-block-poly(butadiene) (PEO-b-PBD) is well-studied,^{14,16} and the formation and characterization of short-chain length PEO-b-PBD copolymer membranes on planar silica supports was previously reported.¹⁴ Briefly, the amphiphilic nature of PEO-b-PBD favors the formation of biomimetic bilayer films on hydrophilic support surfaces. The lateral fluidity of PEO-b-PBD biomimetic bilayers is very limited, similar to that of lipid rafts.²¹ Moreover, PEO-b-PBD has proven to form hybrid vesicles with phospholipids, which keeps the versatility of polymersomes and the biocompatibility of liposomes.²²

In principle then, these synthetic polymer-based systems provide an alternative to pure lipid membranes for biological analysis applications. They are easy to prepare, readily available, provide options for control of the membrane fluidity and may be much more stable than lipid membrane systems. In prior work, multiplexed lipid bilayers supported on silica microspheres were developed as a platform for flow cytometry study of the interaction of lipid bilayers with membrane-bound components.²³ The ability to multiplex

provides many advantages in assays, including the potential for greater speed and reliability. However, multiplex lipid systems do have some disadvantages, most notably a lack of long-term stability due to apparent lipid exchange in a multiplexed solution.²⁴ Here, we investigate the use of synthetic polymers, to form multiplexed membrane-based architectures that can be used on silica microspheres in flow cytometry assays.

To that end, this work presents: 1) the technology to assemble hybrid block copolymer and phospholipid membranes on silica beads; 2) a proof-of-principle flow cytometric characterization of a preferential binding assay on the copolymer membranes supported on the silica microspheres; and 3) a comparison of these systems to lipid-based systems in terms of stability and performance.

5.3 Experimental (Materials and Methods)

5.3.1 Materials.

The poly(ethylene oxide)-block-poly(butadiene) (pEO-b-pBD) with a 1,300/1,200 Da ratio was purchased from Polymer Source™. The monosialotetrahexosylganglioside (GM1) and 1,2-dioleoyl- sn-glycero- 3-phosphoethanolamine-N- (7-nitro- 2-1,3- benzoxadiazol- 4- yl (NBD-DOPE) lipids were purchased from Avanti Polar Lipids in lyophilized form. The Texas Red 1,2-Dihexadecanoyl-sn-Glycero-3-Phosphoethanolamine, Triethylammonium Salt (Texas Red-DHPE) lipids and the cholera toxin B subunit (recombinant)-Alexa Fluor 647 (CTxB-Alexa 647) were purchased from Thermo Fisher Scientific in powder form. As solvents, we used chloroform that contains 1%-5% of ethanol as a stabilizer, purchased from EMD Millipore, and Tetrahydrofuran (THF) purchased from Sigma Aldrich. We used phosphate-buffered saline (PBS) as the main buffer, and

bovine serum albumin (BSA) as a blocking and passivating agent; both were purchased from Sigma Aldrich. Finally, the non-porous silica microspheres (7.9 μm) suspended in deionized water with 0.02% sodium azide were purchased from Spherotech.

5.3.2 Copolymer micelle formation.

The lipid stocks were prepared by dissolving and resuspending the lyophilized lipids; GM1 and NBD-DOPE (in chloroform), or Texas Red-DHPE (in THF). Then, the lipid stock solutions were stored in glass vials, sealed and wrapped with parafilm, at $-20\text{ }^{\circ}\text{C}$ in the dark until use. The powdered pEO-b-pBD was dissolved in THF to a final concentration of 20mM and it was stored in a glass vial, at $2\text{ }^{\circ}\text{C}$ until use.

In the work presented here, we prepared copolymer micelle assemblies that included the amphiphilic block copolymers (pEO-b-pBD) and small amounts of phospholipids to add fluorescent tags (NBD-DOPE and/or Texas Red-DHPE) and increasing concentrations of the binding ligands (GM₁). This was done by following previously reported protocols.²⁵ Briefly, in different glass vials, the desired amounts of copolymer and lipids were dissolved in THF. Then, the THF solvent was exchanged with molecular biology grade water by gradual injection (2 ml/hr rate) to a final volume of 2.5 ml and a final micelle concentration of 1mM, while the THF is removed by rotary evaporation. Then, once the THF was completely evaporated, the samples were covered, sealed with parafilm and stored in the dark at $4\text{ }^{\circ}\text{C}$ until use.

5.3.3 Formation of polymer membranes on silica microspheres.

Similar to the formation of lipid membranes on silica microspheres,²⁶ polymer membrane formation relies on the spontaneous fusion of the copolymer micelles to the surface of the non-porous silica microspheres.²⁷

The formation of polymer membranes on silica microspheres was done by mixing, in separate Eppendorf tubes, the different solutions of 1mM pEO-b-pBD micelles (with varying concentrations of GM1, NBD-DOPE and Texas Red-DHPE) with the silica microspheres suspended in PBS pH 7.35, at a concentration of 10^6 beads/ml. The samples' incubation process consisted on vortexing the tubes for 1 hour at medium speed and 37 °C. Afterwards, for blocking purpose, BSA was added to each sample to a final concentration of 0.5 mg/ml. Then, the samples were vortexed on low speed for 20 minutes at room temperature. Finally, all the samples were washed and rinsed three times to remove the unbound micelles and extra BSA in solution. This was done by centrifuging the samples for 45 seconds at 10,000 rpm, removing the supernatant and resuspending the polymer-coated microspheres with fresh PBS buffer, bringing the samples back up to volume.

5.3.4 Multiplex set formation.

Once the assembly of the polymer membranes with different compositions on the silica beads was completed, a multiplex set was formed by adding equal volumes of each set to a single Eppendorf tube.

5.3.5 Differential binding assays.

First, five different sets of 1mM pBD-b-pEO micelles were prepared, each tagged with a different concentration of a lipid fluorophore NBD-DOPE (0 – 2mol%) and/or Texas Red-DHPE (0 – 1mol%) and different concentrations of GM1 (0 – 1mol%). Then,

copolymer membranes were formed on silica microspheres using the individual sets of copolymer micelles previously prepared, and a combination of all the individual sets formed a multiplexed sample. Second, powdered CTxB-Alexa 647 was dissolved and suspended in PBS pH 7.35 to a final stock concentration of 17,5nM, and a dilution of concentration to 17.5nM was also prepared. Both CTxB-Alexa 647 solutions were stored at 4 °C until use. Third, both single samples and multiplexed samples were incubated with increasing amounts of CTxB-Alexa 647 (0–100nM) for 1 hour. Finally, the flow cytometric data was collected for each sample.

5.3.6 Microscopy.

Fluorescence microscopy image collection and the Fluorescence recovery after photobleaching (FRAP) experiments were performed using a Fluoview FV-1000 confocal laser scanning microscope (Olympus, Tokyo, Japan). The images were acquired with a 40X objective (NA = 0.95) and a 6.0 zoom. The samples containing NBD were imaged by exciting them by a 488 nm Multi Argon laser and collecting the emitted light with a bandpass (BP) filter (505-525 nm). The samples containing Texas Red were imaged by exciting them by a 559 nm LD559 laser and collecting the emitted light with a bandpass (BP) filter (655-755). The collected images had a resolution of 512 x 512 pixels. The FRAP experiment was performed on samples that contained Texas Red as a fluorescent tag; therefore, the preferential bleaching was achieved by using the LD559 laser. The FRAP analysis was done using ImageJ software.

5.3.7 Flow cytometry.

Flow cytometric data was collected using an Attune® NxT acoustic focusing flow cytometer by Thermo Fisher Scientific. This flow cytometer has four lasers (405, 488, 561, and 638 nm) with independent optical paths, and 14 different detection channels. Here listed are only the detection channels used in the present studies; BL-1: 488 nm laser excitation, and emission 530 nm center/30 nm bandpass (BP); YL-2: 561 nm laser excitation, and emission 620 nm center/15 nm BP; and RL-1: 638 nm laser excitation, and emission 670 nm center/14 nm BP. The flow cytometer underwent regular maintenance, cleaning and calibration before and after use.

For each sample, 10,000 events were collected, out of which about 80% or more corresponded to the main events (copolymer membrane-coated silica microspheres). For each sample, the data collected in all 14 detection channels, in the forward scatter channel, and the side scatter channel were saved as Flow Cytometry Standard (FSC) files. Then, the data analysis was done using FlowJoV10 software. The gating was generated by the auto-gating tool, the compensation matrix was modified manually, and the statistical values were automatically recomputed once a gate was created or modified. Further numerical analysis and graph plotting was done using Microsoft Excel and Matlab.

5.4 Results and Discussion

5.4.1 Formation of polymer membranes on silica microspheres.

Figure 5.1 shows a sketch depicting the formation of polymer membrane on silica microspheres. Briefly, the micelles were formed by suspending the block copolymer and

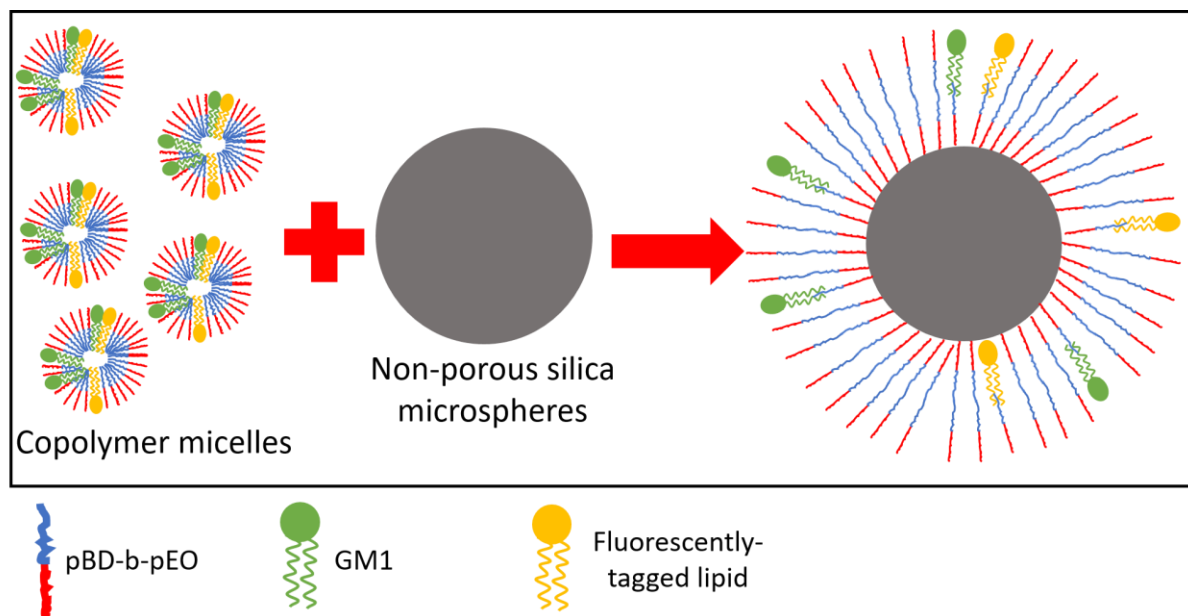


Figure 5.1. Schematic of formation of block copolymer membranes on non-porous silica microspheres.

lipids first in THF and after a solvent exchange, the micelles were suspended in molecular biology grade water. Then, the micelles were incubated with silica microspheres and due to spontaneous fusion, copolymer membranes are formed on the surface of the silica beads. Polymer membranes on silica microspheres constitute a biomimetic system that can be used in flow-based analysis, potentially including high throughput screening processes. In the present work, copolymer micelle assemblies containing pEO-b-pBD, GM1 and fluorescently-tagged phospholipids were assembled. More specifically, following the protocol in the materials and methods section, five different compositions of polymer membranes supported on silica microspheres were prepared: **1)** 1mM pBD-b-pEO, 0 mol% GM1, 1 mol% Texas Red-DHPE; **2)** 1mM pBD-b-pEO, 0.05 mol% GM1, 0.2 mol% NBD-DOPE; **3)** 1mM pBD-b-pEO, 0.1 mol% GM1, 2 mol% NBD-DOPE, 1 mol% Texas Red-DHPE; **4)** 1mM pBD-b-pEO, 0.5 mol% GM1, 0.01 mol% Texas Red-DHPE; and **5)** 1mM

pBD-b-pEO, 1 mol% GM1, 2 mol% NBD-DOPE. Figures 5.2(A-E) shows the fluorescence microscopy images of each individual sample. Uniform coverage of the silica

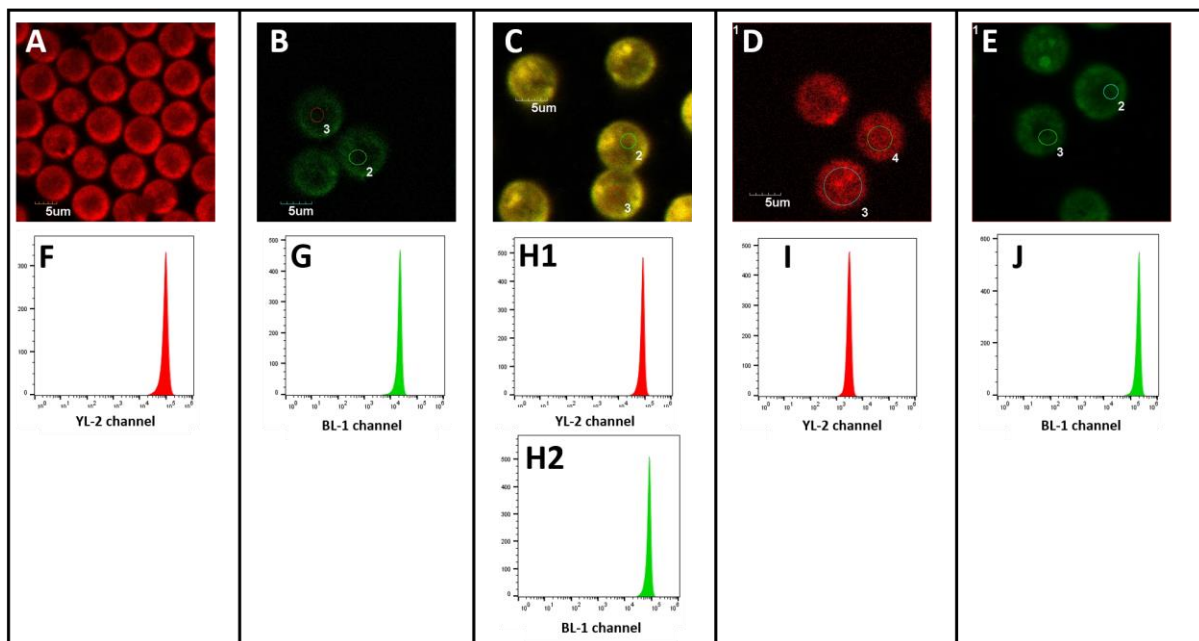


Figure 5.2. Block copolymer membrane composition present in his study. Confocal microscopy image of: **A)** 1mM pBD-pEO, 0% GM1, 1%mol Texas Red-DHPE. **B)** 1mM pBD-pEO, 0.05% GM1, 0.2%mol NBD-DOPE. **C)** 1mM pBD-pEO, 0.1% GM1, 2%mol NBD-DOPE, 1%mol Texas Red-DHPE. **D)** 1mM pBD-pEO, 0.5% GM1, 0.01% Texas Red-DHPE. **E)** 1mM pBD-pEO, 1% GM1, 2%mol NBD-DOPE. Flow cytometry fluorescence histograms of: **F)** YL-2 fluorescence of the population shown in A). **G)** BL-1 fluorescence of the population shown in B). **H1)** BL-1 and **H2)** YL-2 fluorescence of the population shown in C). **I)** YL-2 fluorescence of the population shown in D). **J)** BL-1 fluorescence of the population shown in E).

beads with copolymer membrane can be observed, similar to the uniform coverage offered by lipid bilayers.²⁴

The same samples were analyzed using the Attune® NxT acoustic focusing flow cytometer. Briefly, the microspheres populations were gated on the side scatter versus forward scatter plot. The gated population was then observed on a BL-1 (NBD detection) versus YL-2 (Texas Red detection) plot and gated again to select only the well-coated beads. The signal from that secondary gate can later be observed in any other detection channel. Figures 5.2(F-J) shows the flow cytometric data in the form of histograms

depicting the fluorescence intensity of each sample in the detection channel corresponding to their fluorescent tag.

The lateral fluidity of the copolymer membranes was tested in a FRAP experiment, where silica microspheres coated with a copolymer membrane (1mM pBD-b-pEO, 0% GM1, 1%mol Texas Red-DHPE). The sample was imaged with a fluorescent microscope, and a small spot on one of the copolymer membranes was bleached using the LD559 full laser intensity. (Appendix II 5, Movie A5.1). The bleached region did not display fluorescence recovery over a period of 30 minutes, which means that the pBD-b-pEO membrane bilayers have little lateral fluidity. (Appendix II 5, Figure A5.1). This is consistent with previously reported data on pBD-b-pEO films on planar supported silica.

5.4.2 Multiplex set formation.

The five different populations of copolymer membranes coated on beads were mixed in equal volumes to form a multiplexed set (Figure 5.3A), and split into aliquots. The flow cytometric analysis for multiplex samples was the same as for individual samples. The multiplexed samples seen in the BL-1 vs YL-2 bivariate plot (Figure 5.3B) shows the five different sub-populations, which are clearly distinguishable from one another and can be independently gated.

The time stability of the fluorescent signals of the individual and multiplexed samples were tracked over time (Appendix II 5, Figure A5.2). Both sets of samples showed to be

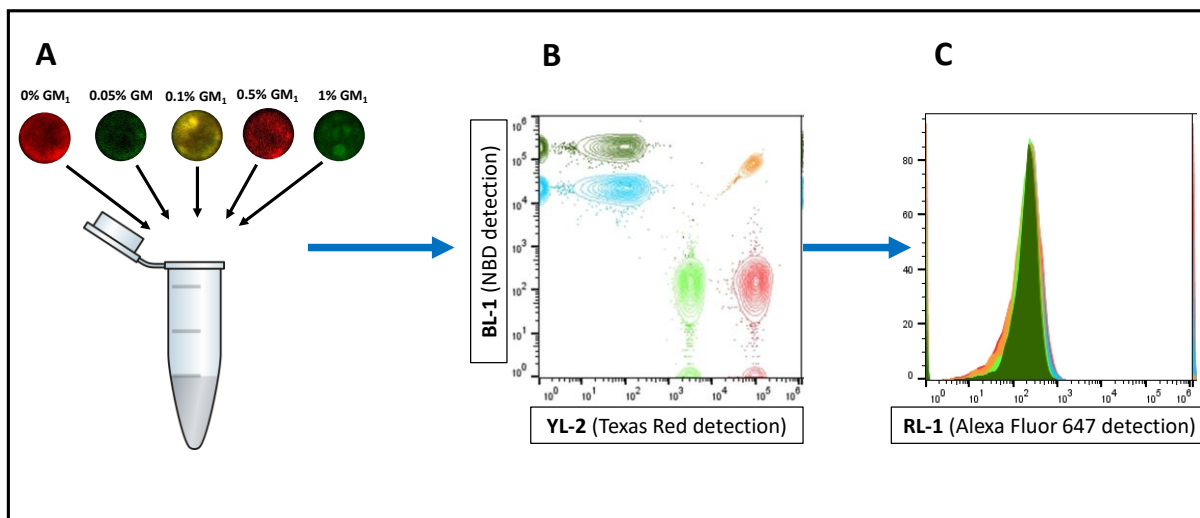


Figure 5.3. **A)** Schematic of the multiplex formation of supported block copolymer biomimetic membranes on non-porous silica microspheres. The five different populations of silica beads coated with different polymer and phospholipid membrane composition and fluorescence tags are mixed in equal amounts. **B)** Bivariate plot BL-1 (NBD detection) versus YL-2 (Texas Red detection) where all the five populations are distinguishable and therefore can be gated. **C)** Histograms on RL-1 (Alexa Fluor 647 detection) of the gated population in B).

stable over a period of 8 hours, where the populations show stable fluorescence levels, and distinguishable sub-populations in the multiplexed set. This stability is much greater than observed for similar multiplexed sets containing lipids, where substantial mixing occurs on a time scale of about one hour.²³

5.4.3 Differential binding of CTxB-Alexa to GM1.

The interaction between cholera toxin and GM1 has been characterized and studied extensively.^{28,29} As a proof-of-principle demonstration, we analyze the interaction between CTxB-Alexa 647 and GM1-containing copolymer membranes supported on silica microspheres. A similar study was reported on silica microsphere-supported lipid bilayers,²³ and the analysis was done on a similar way. Briefly, the individual and multiplexed sets (described in the last two sections) were incubated with increasing concentrations of CTxB-Alexa 647 (0, 5, 10, 50 and 100 nM) for 1 hour, immediately followed by the flow cytometric analysis of each sample.

The samples were first gated on the side scatter vs forward scatter to select the silica bead population. The fluorescent tags on the copolymer membranes (NBD and Texas Red) and the fluorescent tag on the cholera toxin (Alexa Fluor 647) have some spectral overlap, so compensation on the channels BL-1 (NBD detection), YL-2 (Texas Red detection), and RL-1 (Alexa Fluor 647 detection) was applied (Appendix II 5, Figure A5.3 and Figure A5.4). After compensation, the gated bead population was observed on a BL-1 (NBD detection) versus YL-2 (Texas Red detection) bivariate plot (Figure 5.3B), where each sample set was gated again to refine the selection of well-coated beads. Finally, the data from the selected events are shown in histograms of the fluorescence intensity in the RL-1 channel (Alexa Fluor 647 detection) (Figure 5.3C).

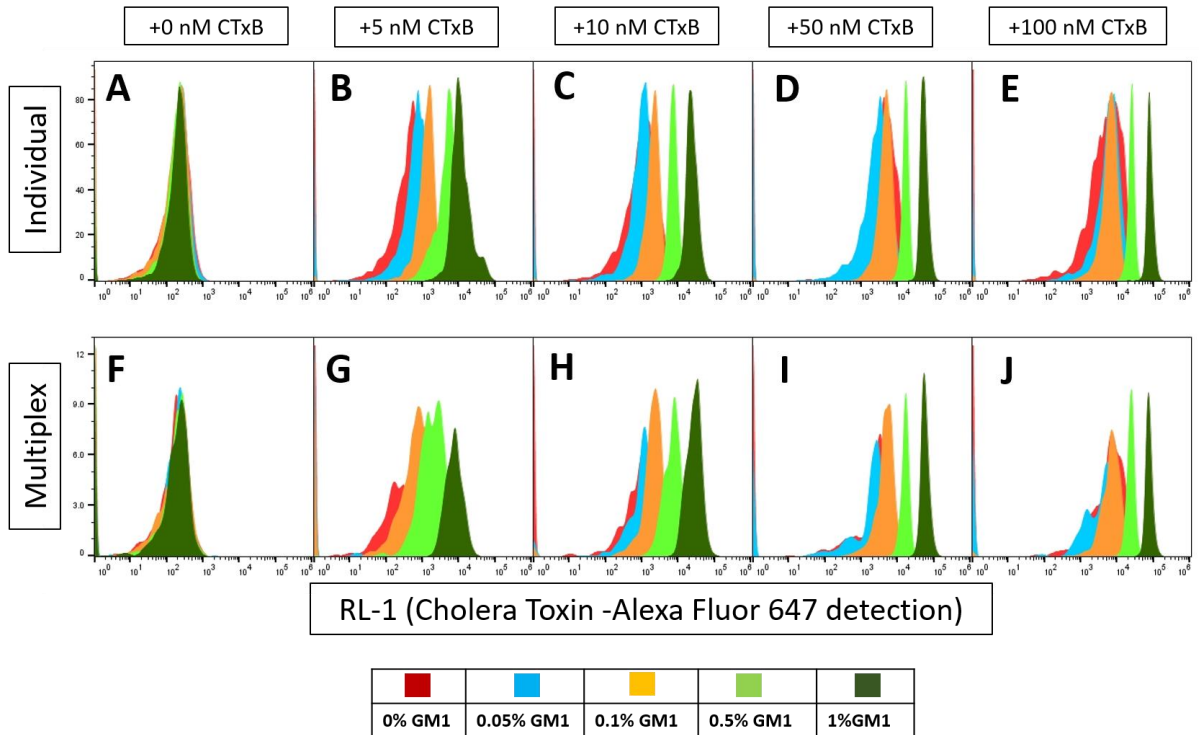


Figure 5.4. Histograms in RL-1 (cholera toxin-Alexa Fluor 647 detection) of the five sub-populations in the presence of increasing concentrations of cholera toxin-Alexa Fluor 647. **A)** Control for individual sets. **F)** Control for multiplex sets. **Plus 5 nM CTxB:** **B)** Individual set. **G)** Multiplex set. **Plus 10 nM CTxB:** **C)** Individual set. **H)** Multiplex set. **Plus 50 nM CTxB:** **D)** Individual set. **I)** Multiplex set. **Plus 100 nM CTxB:** **E)** Individual set. **J)** Multiplex set.

Figure 5.4 shows the histograms of the fluorescence intensity in the RL-1 channel (cholera toxin detection) of the individual (Figure 5.4A-E) and multiplexed (Figure 5.4F-J) samples after 1-hour incubation with increasing concentrations of CTxB-Alexa (0 – 100nM). On both individual and multiplex sets, the samples with no GM1 (red-labeled) have low fluorescence levels in RL-1 in the presence of 5nM and 10nM CTxB-Alexa, and in the presence of 50nM and 100nM CTxB-Alexa the RL-1 fluorescence has a very broad distribution, but still lower than samples with higher concentrations of GM1. This is indicative of low non-specific binding of CTxB-Alexa to pBD-b-pEO and the fluorescently tagged-phospholipids. For the remaining samples, 0.05 mol% GM1 (light blue-labeled), 0.1 mol% GM1 (orange-labeled), 0.5 mol% GM1 (light green-labeled), and 1 mol% GM1 (dark blue-labeled), there is a steady increase of fluorescence in RL-1 as the concentration of GM1 and concentration of CTxB-Alexa increased. This result is indicative of selective binding of CTxB to GM1.

The quantitative analysis was done as previously reported.²³ The data was fit to a first-order Hill equation, where the maximum signal (M) was predicted by model for the maximum GM₁ concentration of 1 mol%. Figure 5.5A (individual samples) and Figure 5.5B (multiplexed samples) show the normalized fractional signal for each data set with respect to M versus the total concentration of CTxB-Alexa in solution [$CTxB-Alexa$]. The experiment was repeated three times; the values in Figure 5.5 represent the averaged values, and the error bars are calculated based on standard deviation. A model fit was included for each set of GM₁ concentrations, which provided the calculation of effective association constant (K_{eff}) of each set.

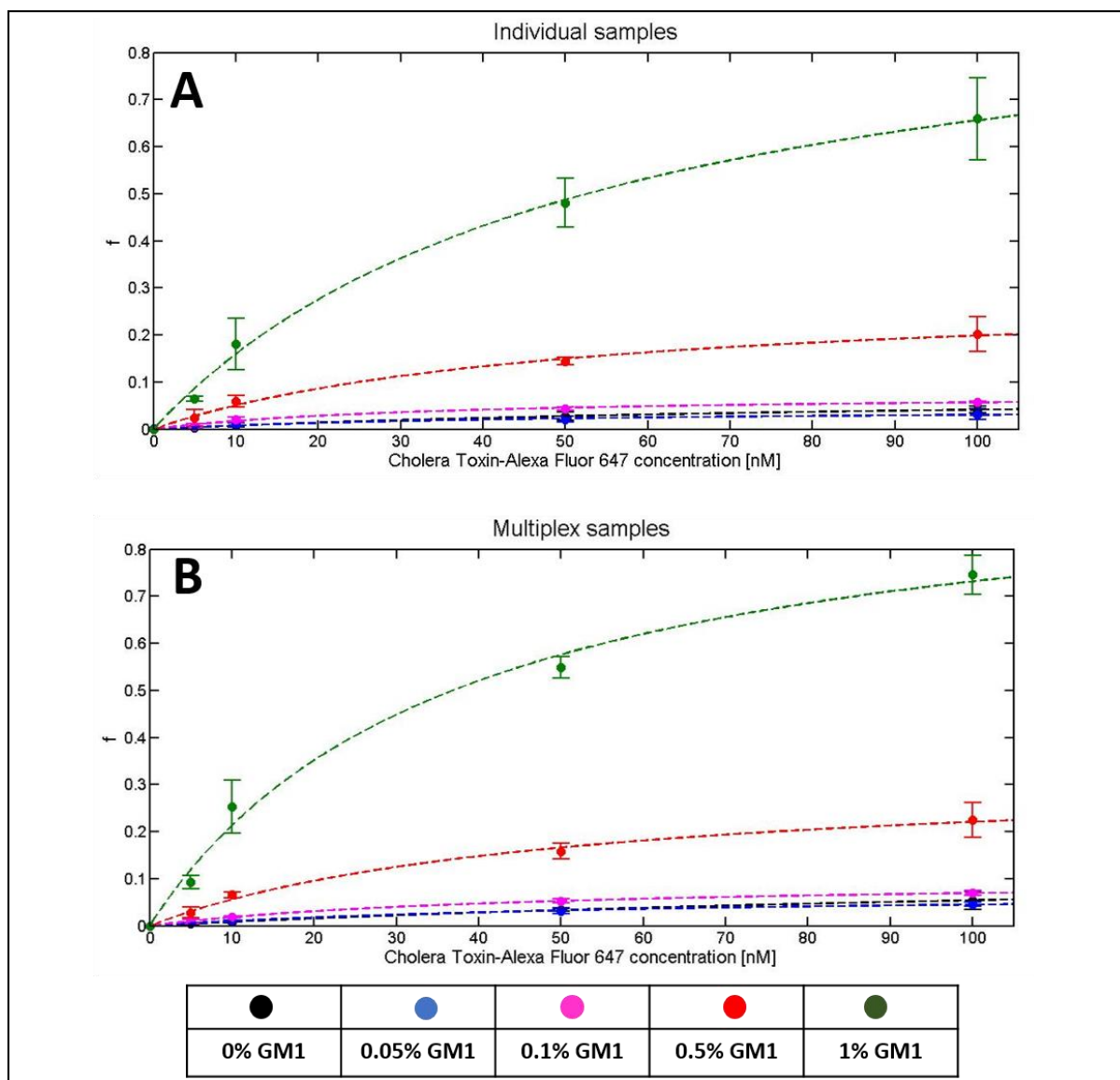


Figure 5.5. Fractional binding of cholera toxin (CTxB-Alexa 647) after 1 hour of incubation of samples containing block copolymer membranes containing 1mM pBD-pEO, 0% GM1, 1%mol Texas Red-DHPE (**black**); 1mM pBD-pEO, 0.05% GM1, 0.2%mol NBD-DOPE (**blue**); 1mM pBD-pEO, 0.1% GM1, 2%mol NBD-DOPE, 1%mol Texas Red-DHPE (**pink**); 1mM pBD-pEO, 0.5% GM1, 0.01% Texas Red-DHPE (**red**); and 1mM pBD-pEO, 1% GM1, 2%mol NBD-DOPE (**green**). The x-axis is concentration of CTxB-Alexa 647 added to the system. Data shown are the average of three replicates, and error bars are plus/minus one standard deviation. Solid lines are fits of the averaged data to Hill's equation. **A)** Individual samples. **B)** Multiplex samples.

The analysis of the individual samples resulted in an averaged $K_{eff} = 0.022 \pm 0.005 \text{ nM}^{-1}$ (uncertainties are 95% confidence), which corresponds to an effective or apparent affinity of $1/ K_{eff} = 46.02 \pm 8.6 \text{ nM}$. Similar results were obtained for the multiplexed set: $K_{eff} = 0.21 \pm 0.04 \text{ nM}^{-1}$ and $1/ K_{eff} = 48.16 \pm 10.4 \text{ nM}$. These values are ~ 10 -fold weaker than

those reported by Lauer, et al., and by our group²³ in fluid lipid membranes with multivalent binding (~ 5 nM); and ~ 80 -fold stronger than the one reported for single-site binding of the soluble pentasaccharide portion of GM1 (~ 4 μ M).²⁸ They are however, closer to single-site affinities estimated by Lauer et al. for GM1 presented in a membrane, where an approximate value of ~ 12.5 nM is obtained from models of multivalent binding. The apparent affinity values we determine here are thus consistent with a non-multivalent binding process of GM1 presented in a membrane with low lateral fluidity, which is consistent with the results obtained in the FRAP experiment.

5.5 Summary and Conclusions

Our results demonstrate the use of a multiplexed block copolymer biomimetic membrane supported on silica microspheres for a binding assay using flow cytometry and microscopy. While the use of pBD-b-pEO has proven to be a good synthetic alternative to lipid rafts, the use of different biodegradable block copolymers could expand this platform to ensemble more fluid membranes, monolayers, or more complex hybrid copolymer/phospholipids. The expansion of the number of sub-populations in the multiplex set could also be achieved by the use of copolymer giant polymer vesicles, as they have been explored as possible flow cytometry amenable system,³⁰ However, their self-assembly still results in polydisperse populations.³¹ A different alternative could be the use of different solid supports, such as commercially available indexed polymer microspheres. To conclude, our results show the viability of assembling stable fluorescently indexed block copolymer biomimetic membranes on silica microspheres, which enable multiplexed differential binding assays using flow cytometry. Overall, this study presents a high-throughput alternative to the screening of copolymer biomimetic

membranes against membrane-bound components using flow cytometry and it may ultimately prove to be a robust and versatile new platform.

5.6 Acknowledgements

The present work was done in collaboration with Matthew Rush (Center for Biomedical Engineering at The University of New Mexico and Center for Integrated Nanotechnologies | Los Alamos National Laboratory) and Stacy M. Copp, PhD (Center for Integrated Nanotechnologies | Los Alamos National Laboratory).

5.7 References

1. Kulshrestha AS, Mahapatro A. Polymers for Biomedical Applications. In: *ACS Symposium Series, Ebooks*. Vol. 977. American Chemical Society; 2008:1-7. doi:10.1021/bk-2008-0977.ch001.
2. Ulery BD, Nair LS, Laurencin CT. Biomedical applications of biodegradable polymers. *J Polym Sci Part B Polym Phys*. 2011;49(12):832-864. doi:10.1002/polb.22259.
3. Capperauld I. Suture materials: A review. *Clin Mater*. 1989;4(1):3-12. doi:10.1016/0267-6605(89)90021-8.
4. Kasser MJ. Regulation of UHMWPE biomaterials in total hip arthroplasty. *J Biomed Mater Res Part B Appl Biomater*. 2012;101(3):400-406. doi:10.1002/jbm.b.32809.
5. Kannan RY, Salacinski HJ, Butler PE, Hamilton G, Seifalian AM. Current status of prosthetic bypass grafts: A review. *J Biomed Mater Res Part B Appl Biomater*. 2005;74B(1):570-581. doi:10.1002/jbm.b.30247.
6. Maitz MF. Applications of synthetic polymers in clinical medicine. *Biosurface and Biotribology*. 2015;1(3):161-176. doi:10.1016/J.BSBT.2015.08.002.
7. Wang XP, Chen TN, Yang ZX. Modeling and simulation of drug delivery from a new type of biodegradable polymer micro-device. *Sensors Actuators, A Phys*. 2007;133(2 SPEC. ISS.):363-367. doi:10.1016/j.sna.2006.06.016.
8. Adams ML, Lavasanifar A, Kwon GS. MINIREVIEW Amphiphilic Block Copolymers for Drug Delivery. *Pharm Assoc J Pharm Sci*. 2003;92:1343-1355.
9. Langer R, Tirrell DA. Designing materials for biology and medicine. *Nature*. 2004;428(6982):487-492. doi:10.1038/nature02388.
10. Blanz A, Armes SP, Ryan AJ. Self-Assembled Block Copolymer Aggregates: From Micelles to Vesicles and their Biological Applications. *Macromol Rapid Commun*. 2009;30(4-5):267-277. doi:10.1002/marc.200800713.
11. Discher DE, Ortiz V, Srinivas G, et al. Emerging applications of polymersomes in delivery: From molecular dynamics to shrinkage of tumors. *Prog Polym Sci*. 2007;32(8-9):838-857. doi:10.1016/j.progpolymsci.2007.05.011.
12. Liao J, Wang C, Wang Y, Luo F, Qian Z. Recent advances in formation, properties, and applications of polymersomes. *Curr Pharm Des*. 2012;18(23):3432-3441.
13. Anajafi T, Mallik S. Polymersome-based drug-delivery strategies for cancer therapeutics. *Ther Deliv*. 2015;6(4):521-534. doi:10.4155/tde.14.125.
14. Goertz MP, Marks LE, Montañó GA. Biomimetic Monolayer and Bilayer Membranes Made From Amphiphilic Block Copolymer Micelles. *ACS Nano*.

- 2012;6(2):1532-1540. doi:10.1021/nn204491q.
15. Kojima M, Hirai Y, Yabu H, Shimomura M. The Effects of Interfacial Tensions of Amphiphilic Copolymers on Honeycomb-Patterned Films. *Polym J*. 2009;41(8):667-671. doi:10.1295/polymj.PJ2009027.
 16. Bermudez H, Brannan AK, Hammer DA, Bates FS, Discher DE. Molecular Weight Dependence of Polymersome Membrane Structure, Elasticity, and Stability. *Macromolecules*. 2002;35(21):8203–8208. doi:10.1021/MA020669L.
 17. Discher DE, Eisenberg A. Polymer Vesicles. *Science (80-)*. 2002;297(5583):967-973. doi:10.1126/science.1074972.
 18. Lee JC-M, Santore M, Bates FS, Discher DE. From Membranes to Melts, Rouse to Reptation: Diffusion in Polymersome versus Lipid Bilayers. *Macromolecules*. 2001;35(2):323–326. doi:10.1021/MA0112063.
 19. Park JH, Sun Y, Goldman YE, Composto RJ. Amphiphilic Block Copolymer Films: Phase Transition, Stabilization, and Nanoscale Templates. *Macromolecules*. 2009;42(4):1017-1023. doi:10.1021/ma8023393.
 20. Collins AM, Timlin JA, Anthony SM, Montañó GA. Amphiphilic block copolymers as flexible membrane materials generating structural and functional mimics of green bacterial antenna complexes. *Nanoscale*. 2016;8(32):15056-15063. doi:10.1039/C6NR02497A.
 21. Jacobson K, Dietrich C. Looking at lipid rafts? *Trends Cell Biol*. 1999;9(3):87-91. doi:10.1016/S0962-8924(98)01495-0.
 22. Lim S, de Hoog H-P, Parikh A, Nallani M, Liedberg B. Hybrid, Nanoscale Phospholipid/Block Copolymer Vesicles. *Polymers (Basel)*. 2013;5(3):1102-1114. doi:10.3390/polym5031102.
 23. Fernandez Oropeza N, Zurek NA, Galvan-De La Cruz M, et al. Multiplexed Lipid Bilayers on Silica Microspheres for Analytical Screening Applications. *Anal Chem*. 2017;89(12):6440–6447. doi:10.1021/acs.analchem.7b00296.
 24. Fabry-Wood A, Fetrow ME, Brown CW, et al. A Microsphere-Supported Lipid Bilayer Platform for DNA Reactions on a Fluid Surface. *ACS Appl Mater Interfaces*. 2017;9(35):30185–30195. doi:10.1021/acsami.7b11046.
 25. Adams PG, Collins AM, Sahin T, et al. Diblock Copolymer Micelles and Supported Films with Noncovalently Incorporated Chromophores: A Modular Platform for Efficient Energy Transfer. *Nano Lett*. 2015;15(4):2422-2428. doi:10.1021/nl504814x.
 26. Heyse S, Vogel H, Sanger M, Sigrist H. Covalent attachment of functionalized lipid bilayers to planar waveguides for measuring protein binding to biomimetic membranes. *Protein Sci*. 1995;4(12):2532-2544. doi:10.1002/pro.5560041210.

27. Rao J, Zhang H, Gaan S, Salentinig S. Self-Assembly of Polystyrene-b-poly(2-vinylpyridine) Micelles: From Solutions to Silica Particles Surfaces. *Macromolecules*. 2016;49(16):5978-5984. doi:10.1021/acs.macromol.6b01074.
28. Lauer S, Goldstein B, Nolan RL, Nolan JP. Analysis of Cholera Toxin–Ganglioside Interactions by Flow Cytometry. *Biochemistry*. 2002;41(6):1742-1751. doi:10.1021/bi0112816.
29. Shi J, Yang T, Kataoka S, Zhang Y, Diaz AJ, Cremer PS. GM1 Clustering Inhibits Cholera Toxin Binding in Supported Phospholipid Membranes. *Am Chem Soc* . 2007;129(18):5954–5961. doi:10.1021/JA069375W.
30. Hammer DA, Robbins GP, Haun JB, et al. Leuko-polymersomes. *Faraday Discuss*. 2008;139:129-141. doi:10.1039/B717821B.
31. Ghoroghchian PP, Li G, Levine DH, et al. Bioresorbable Vesicles Formed through Spontaneous Self-Assembly of Amphiphilic Poly(ethylene oxide)-block-polycaprolactone. *Macromolecules*. 2006;39(5):1673-1675. doi:10.1021/ma0519009.

Chapter 6. **Summary and Future Directions**

Overall, the results of the present work demonstrate the viability of assembling stable biomimetic membranes on microspheres for flow-based screening applications, similar to those required for screening applications.

First, we built fluorescently indexed lipid membranes on silica microspheres that use different concentrations of fluorescently tagged lipids and potentially different compositions to enable multiplexed differential binding assays using flow cytometry. More specifically, we demonstrated this multiplexed approach by measuring specific affinity of two well-characterized protein-membrane systems. In that work we successfully assessed the preferential binding of fluorescently labeled proteins to microsphere-supported-membranes containing different amounts of ligand targets. The present work reports the development of a small multiplex, but with the potential of being expanded. Furthermore, this study provides a stepping stone towards the development of a flow-based, multiplexable and high-throughput screening assays involving membrane-associated components. For instance, collaborators of ours have reported the successful use of multiplexable microsphere-supported lipid bilayers in the screening of DNAzyme reactions by implementing DNA nanotechnologies on a fluid lipid surface.

Second, we used fluorescently-tagged lipid membranes on silica microspheres to screen the membrane disruption effects of surfactants and toxins using flow cytometry, with results corroborated using microscopy. We developed and tested a membrane disruption assay where we relied on the loss of fluorescence of the fluorescently-tagged lipid membranes supported on microspheres in the presence of the surfactant or toxin to

determine the perturbation, disruption or elimination of the membranes. The results obtained are consistent with previously reported data from similar studies done on planar-supported membranes. Moreover, we explored the option of backfilling or repairing the disrupted membranes supported on microspheres with a secondary set of liposomes, as previously done by other groups on planar-supported membranes. The present work on membrane disruption assays has the potential of being a platform that will allow us to test membrane-disrupting agents, proteins, toxins, lipases and antimicrobial peptides. Studies can be performed against different membrane compositions, and also to investigate the effect of varying environmental factors like pH, ionic strength, and buffers.

Third, we built and characterized multiplexed fluorescently indexed membranes on silica microspheres using block copolymers as a synthetic alternative to lipids. The properties of block copolymer membranes like permeability and lateral diffusivity, can be tuned by varying the block copolymer molecular weight. Furthermore, we demonstrated the ability of microsphere-supported block copolymer biomimetic membranes with different compositions to enable multiplexed differential binding assays using flow cytometry. The present work presents a promising alternative to lipids in the development of biomimetic membranes supported on microspheres for flow-based studies of membrane-bound components, one that may ultimately prove to be a robust and versatile new platform.

Future directions

Fluorescently-indexed biomimetic membranes on silica microspheres have proven to be an effective platform for the high-throughput screening of the interactions of membranes

with membrane-bound and membrane-associated components. However, most of the work presented here tested proof-of-principle assays as a way of assessing the efficacy of our platform. Future experiments should use our newly developed fluorescently-indexed biomimetic membranes on silica microspheres to explore more complex and innovative approaches in areas such as protease assay development, drug screening and antimicrobial peptide screening.

Although effective, the multiplexed sets of microsphere-supported membranes presented here are small sets (of 3 to 5 components). Future expansion of these sets to much larger multiplexed sets would provide an important improvement for screening applications. This long-term goal can be achieved by following two different paths. First, one could explore by fluorescently-indexing the silica microspheres, instead of the membranes. Provided that the labeling does not alter the silica's ability to support membranes, this would present itself as a more stable and robust platform. Alternatively, one could assemble biomimetic membranes on commercially available highly multiplexed polymer microspheres. However, this approach will likely require extensive modification of the surface of the polymer beads to support model membranes. In either approach, the successful achievement of this goal would provide an ideal platform to investigate membrane protection assays, and biomolecular interactions with membranes or membrane-supported molecules.

Appendix I. Additional work

Appendix I. 1 Introduction

Appendix I presents additional work done in the course of this overall study, but which is still in progress or presented some challenges that have not yet been overcome. First, we investigated the development and use of membranes supported on naturally buoyant microspheres such as functionalized polystyrene. Polystyrene microspheres are widely commercially available in different sizes and with different fluorescent tags which increases the multiplexing opportunities. To overcome the hydrophobic nature of polystyrene, we worked with different functionalized polystyrene beads (carboxylated or biotinylated). Unfortunately, that did not result in reproducible or reliable membrane structures supported on the beads. Therefore, we also attempted to modify the bead polystyrene surface via UV or ozone exposure, an approach that was not successful either.

In spite of our inability to fully characterize the lipid structure built on the polystyrene microsphere's surface, we attempted to run a lipid protection assay. This assay relies on the quenching effect of propidium iodide (PI) on FITC. FITC was coated on the surface of the bead using BSA-FITC, and we investigated the ability of PI to diffuse across the membrane. We were able to obtain some positive results; however, they were not fully reproducible.

The material presented in chapter 5 also inspired some work exploring the interaction of differently structured polymers such as chitosan and poly-L-lysine (fluorescently tagged) with varying lipid composition and charge on the microsphere-supported

membrane structures. The results were not conclusive, as we observe very high non-specific binding of the polymers to any membrane composition or charge, as well as to the bare silica microspheres.

Appendix I. 2 ADDITIONAL WORK FOR CHAPTER 4 – DETECTION OF MEMBRANE DISRUPTION ON MICROSPHERE SUPPORTED-BIOMIMMETIC MEMBRANES

In addition to the work presented in chapter 4 and chapter 5, there is a different set of experiments that were inconclusive

Appendix I. 2.1 Membrane disruption assay using the surfactants SDS and Triton X-100.

Introduction. Based on the background and motivations reported on chapter 4, we explored and tested this set of experiments as our first attempt at studying the interaction between surfactants or toxins and biomimetic membranes supported on microspheres. After careful consideration, we later moved to the use of different surfactants.

Materials. The lipids 1,2-dioleoyl- sn-glycero- 3-phosphoethanolamine-N- (7-nitro- 2-1,3-benzoxadiazol-4- yl (NBD-DOPE), and 1-palmitoyl-2- oleoyl-sn- glycero-3-phosphocholine (POPC) were purchased from Avanti Polar Lipids in lyophilized form. As solvent for lipids, we used chloroform that contains 1%-5% of ethanol as a stabilizer, purchased from EMD Millipore. All the experiments were performed using phosphate-buffered saline (PBS) as the main buffer, and bovine serum albumin (BSA) as a blocking and passivating agent; both were purchased from Sigma Aldrich. The sodium dodecyl sulfate (SDS) was purchased from Bio Rad at 10% (w/v), and the Triton X-100 was purchased from OmniPur via Sigma Aldrich. The non-porous silica microspheres (3.14 μm) suspended in deionized water with 0.02% sodium azide were purchased from Spherotech. Finally, the samples were screened using a BD Accuri C6 flow cytometer.

Methods. The membrane disruption assay was performed following the same protocol reported in chapter 4. Briefly, fluorescently-tagged membranes (DOPC + 0.2% mol NBD-DOPE) were assembled on silica microspheres and were exposed to increasing concentrations of Triton X-100 (0.0024 – 0.24 mM) and increasing concentrations of SDS (0.08 – 8 mM) for about 15 minutes. The loss of fluorescence in the samples presented to the surfactants was calculated and analyzed as an indication of membrane disruption.

Results and Discussions. SDS has a c.m.c. of ~ 8-8.5mM and Triton X-100 has a c.m.c. ~ 0.22 -0.24 mM. The surfactant's concentration ranges were chosen to include values way below the c.m.c and one value around the c.m.c. Figure AI-1A shows the median fluorescence intensity in the FL-1 channel (NBD detection channel) in the absence and

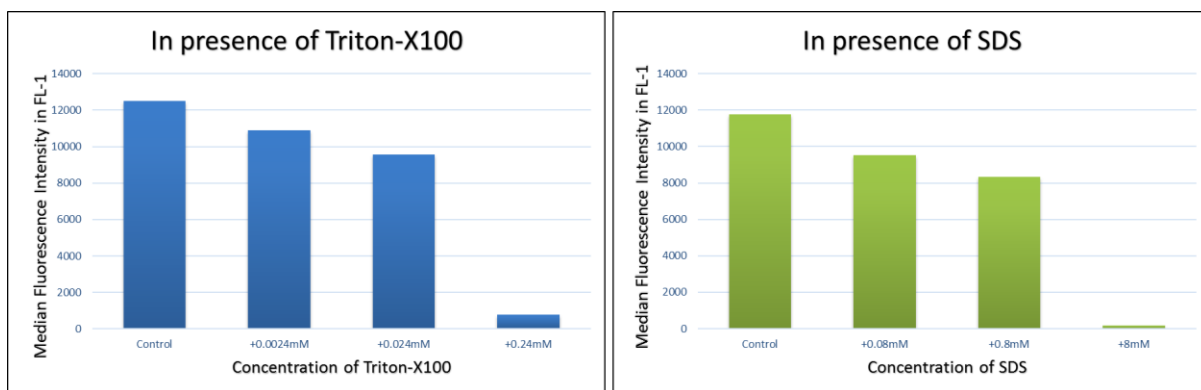


Figure AI-1. Silica microsphere-supported POPC + 0.2% mol NBD-DOPE membranes' median fluorescence intensity in the FL-1 channel (NBD detection channel) in: **A)** the absence and increasing presence (0.0024, 0.024, and 0.24 mM) of Triton X-100. **B)** the absence and increasing presence (0.08, 0.8, and 8 mM) of SDS.

increasing presence of Triton X-100. The data shows that even in the presence of 0.0024 mM of Triton X-100 (a hundredth of the c.m.c. value) there is some loss of fluorescence indicating some level of membrane disruption, while in the presence of 0.24 mM Triton X-100 (about the c.m.c. value) the fluorescence value drops close to the background level indicating a complete destruction of the membrane. Figure AI-1B show the median

fluorescence intensity in the FL-1 channel (NBD detection channel) in the absence and increasing presence of SDS. Similar to the Triton X-100 case, the data in Figure AI-1B shows that even in the presence of 0.08 mM of SDS (a hundredth of the c.m.c. value) there is some loss of fluorescence indicating some level of membrane disruption, while in the presence of 8 mM Triton X-100 (about the c.m.c. value) the fluorescence value drops close to the background level indicating a complete destruction of the membrane.

Conclusions. The data in Figure AI-1 indicates that both Triton X-100 and SDS are harsh surfactants, which even at small concentrations can cause serious disruptions on the membrane. Moreover, the high viscosity of Triton X-100 makes it a difficult chemical to work with. Hence, we concluded that other surfactants (like LDAO) would be better candidates to show the gradual disrupting effect on microsphere-supported biomimetic membranes.

Appendix I. 2.2 Lipid protection assays

Appendix I. 2.2.1 Preliminary results

Introduction. As useful as it has proven to be, silica is a good but not optimal material for flow cytometric and high-throughput analysis. A significant limitation is that silica's high density compared to water makes silica microspheres precipitate in several seconds, thus requiring the need for constant mixing or shaking of the samples. As an alternative, we are working on the introduction of a second multiplexable platform built on naturally buoyant carboxylated-polystyrene microspheres. Polystyrene microspheres are widely commercially available in different sizes and with different fluorescent tags which increases the multiplexing opportunities. Membranes supported on polystyrene have not been extensively studied and they will require characterization to assess the quality and uniformity of the membrane bilayer, information obtained through membrane disruption studies. Hence, we will concurrently test both the silica and functionalized polystyrene microspheres for their potential use as platforms for membrane disruption assays. Thus, success in this aim will yield technology for important membrane disruption screening and also help demonstrate new material constructs that may lead to improved general flow cytometry studies using model membranes on naturally buoyant microspheres.

Materials. The lipid 1-palmitoyl-2-oleoyl-sn-glycero-3-phosphocholine (POPC) was purchased from Avanti Polar Lipids in lyophilized form. As solvent for lipids, we used chloroform that contains 1%-5% of ethanol as a stabilizer, purchased from EMD Millipore. All the experiments were performed using phosphate-buffered saline (PBS) as the main buffer, bovine serum albumin (BSA) as a blocking agent, BSA-FITC a passivating agent,

and propidium iodide (PI) as a FITC quencher. All of these materials were purchased from Sigma Aldrich. The non-porous silica microspheres (3.14 μm) and the carboxylated-polystyrene microspheres (5 μm) both suspended in deionized water with 0.02% sodium azide were purchased from Spherotech. Finally, the samples were screened using a BD Accuri C6 flow cytometer.

Methods. As a first step, the microspheres' (either silica or carboxylated-polystyrene) surface was passivated with 0.4mg/ml Bovine serum albumin tagged with Fluorescein

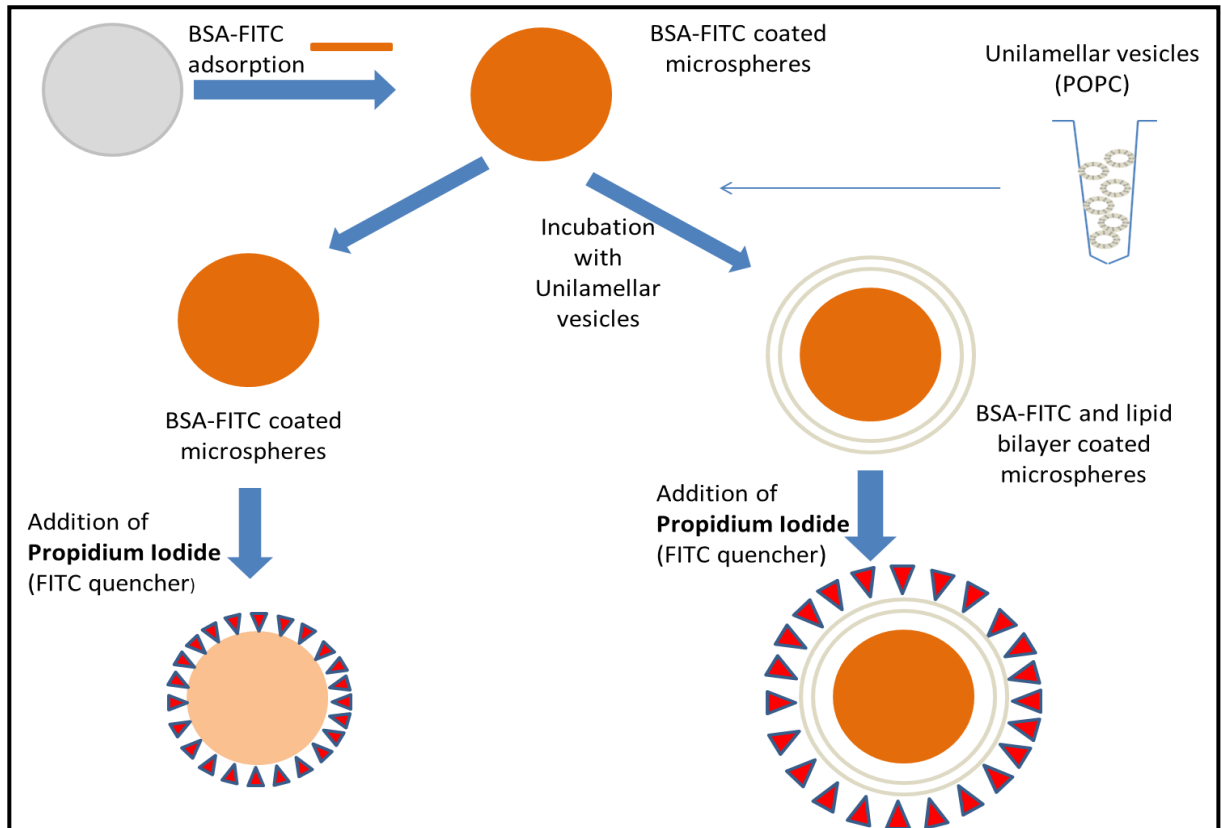
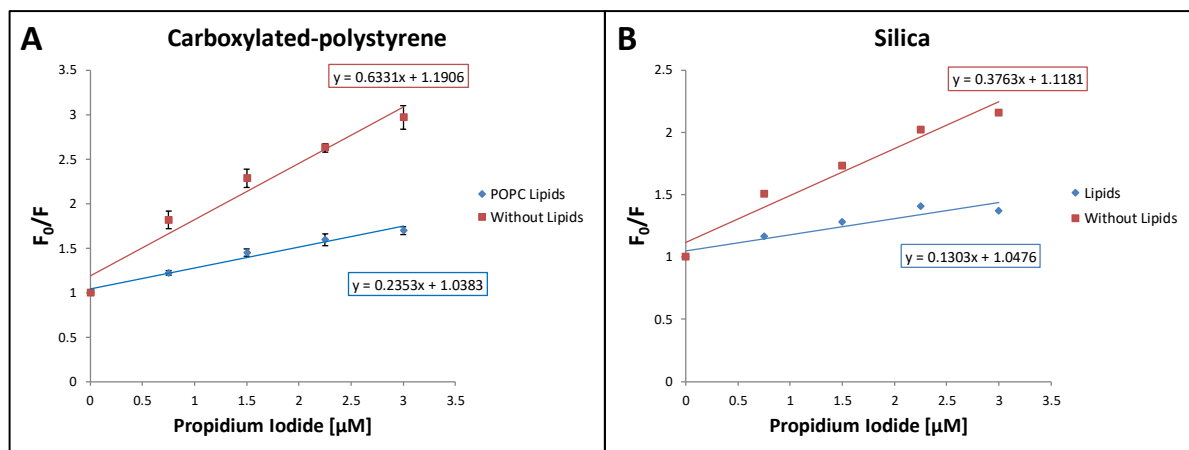


Figure AI-2. Schematic of the lipid protection assay on membrane supported on microspheres.

isothiocyanate (BSA-FITC) overnight at 4 °C. The next day, the sample with the passivated beads was rinsed twice by centrifugation at 10,000 rpm for 45 seconds removing the supernatant, and replacing the buffer. Then, the sample was split into 2 equal parts; one of

the parts will serve as control and the other will later be liposome-coated. Following the same procedure described in chapters 3 and 4. The second set (liposome-coated) was incubated with liposomes (1 mM lipid concentration of 100% POPC), later incubated with BSA as a blocking step and then rinsed. The control group was incubated with PBS buffer, BSA as blocking step and later rinsed. Both sets were kept treated under the same rotation and temperature conditions. Finally, both sets were split into aliquots of equal volume and incubated with increasing concentrations of propidium iodide (PI), which is a FITC quencher (Figure AI-2 shows a schematic of the process). After a 30-minute incubation at room temperature the samples were analyzed in the flow cytometer to obtain the loss of fluorescence in both sets, to later compare them to one another.

Results and Discussions. Figure AI-3 shows the results of the experiment in the form of Stern-Volmer plots. These show the relative fluorescence F_0/F (F_0 fluorescence intensity without quencher and F is the fluorescence intensity with quencher) with respect to the



F_0 = sample in the absence of quencher
 F = sample in the presence of quencher

Figure AI-3. Stern-Volmer plots (fluorescence intensity without quencher over fluorescence intensity with quencher) vs. concentration of quencher in solution. **A)** In carboxylated-polystyrene microspheres. **B)** In silica microspheres.

concentration of the quencher present in solution.¹ Figure AI-3A shows the results of the

lipid protection assay performed in carboxylated-polystyrene microspheres done in triplicate; the error bars represent plus/minus one standard deviation. Figure AI-3B shows the results of the lipid protection assay performed in silica microspheres. In both cases we can observe there is more quenching in the absence of lipids membranes (red lines) versus in the microspheres bearing membranes (blue lines). Consequently, given the PI is not permeable to the lipid membrane we can conclude that there is a continuous membrane structure supported on BSA-FITC coated microspheres.

Conclusion (Part 1). Although encouraging at first, unfortunately the results were not reliably reproducible. This could have been due to poor or non-uniform BSA-FITC passivation of the silica microspheres or by the formation of non-uniform or irregular lipid structures (neither bilayers or monolayers) on the carboxylated-polystyrene microspheres. We explored these possibilities by running the following experiments.

Appendix I. 2.2.2 BSA-FITC and fluorescein passivation of silica microspheres

The formation of lipid bilayer on silica surfaces via spontaneous fusion of lipid vesicles onto the silica surface has been widely reported, previously,² and in the present work (chapter 3 and chapter 4). However, the membrane disruption assay as described here, relies on the uniform coating of the bead by a fluorescent component before the assembly of the biomimetic membrane on the surface. Here, we tested the effectiveness of the silica bead passivation process with BSA-FITC and with fluorescein.

Briefly, silica microspheres in PBS buffer at pH 7.35 were incubated with ~0.5mg/ml BSA-FITC (Figure AI-4A) or with ~0.5mg/ml Fluorescein (Figure AI-4B) at different temperatures overnight. The samples were screened using a flow cytometer, before and after some washing and rinsing cycles.

Figure AI-4A shows the bar graphs showing the median fluorescence intensity in FL-1 of all the samples after passivation with BSA-FITC in the hot room at 37 °C (blue bars),

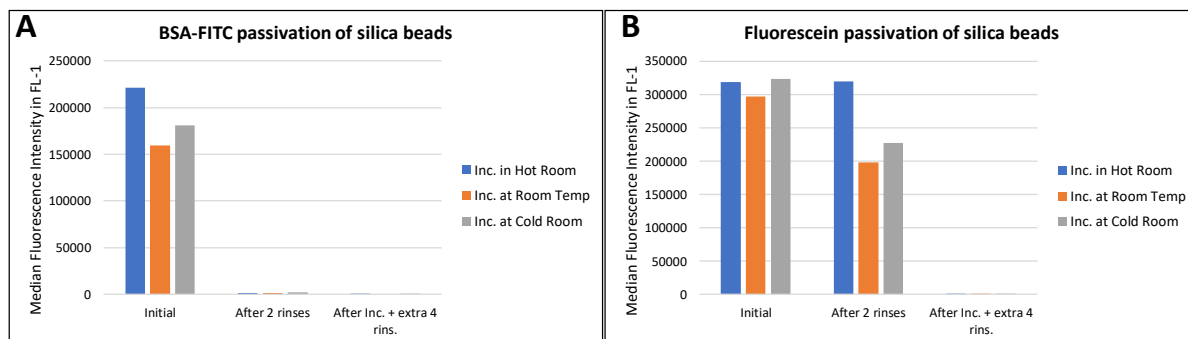


Figure AI-5. Passivation of silica microspheres at different temperatures before rinsing, after 2 rinses and after 4 extra rinses. The data shows the median fluorescence intensity in the FL-1 channel. **A)** BSA-FITC as a passivating agent. **B)** Fluorescein as a passivating agent.

at room temperature (orange bars), and in the cold room at 4°C (gray bars). The samples were analyzed right after incubation, after a couple of rinse steps and after four additional rinse cycles. The data indicates that under the three different incubation temperatures the

beads have a high initial fluorescence, but after only a couple of rinse steps, the fluorescence levels drop to only a couple thousand. Finally, after the 4 additional rinse cycles, the fluorescence drops close to background level.

Figure AI-4B shows the bar graphs showing the median fluorescence intensity in FL-1 of all the samples after passivation with fluorescein in the hot room at 37 °C (blue bars), at room temperature (orange bars), and in the cold room at 4°C (gray bars). The samples were analyzed right after incubation, after a couple of rinse steps and after four additional rinse cycles. The data indicates that under the three different incubation temperatures the beads have a high initial fluorescence, and unlike the BSA-FITC case, the fluorescence levels decreases only minimally right after a couple of rinses. However, after the 4 additional rinse cycles, the fluorescence drops to very low values.

Conclusion (Part 2). Silica has a small negative charge and so does BSA; hence, the BSA passivation of silica has proven to be difficult as shown in Figure AI-4. Although fluorescein adsorbed onto the surface seems more resistant to a couple of rinses, having the sample undergo further washing steps, as required by the reported protocols, removes the fluorescein from the bead's surface. Therefore, it is necessary to find a different fluorescent compound that is compatible with silica, preferably slightly positively charged and hydrophilic, which at the same time would not alter the properties of silica as a great lipid membrane support. Even if stable and uniform passivation is achieved, the surface of the coated bead should be screened for possible modifications that would prevent the assembly of biomimetic membranes. The success in this aim would provide the opportunity of producing indexed highly-multiplexed sets of non-porous silica microspheres, similar to the commercially available polystyrene ones. This would provide a new and innovative

platform to explore the interaction of biomimetic membranes with different biocomponents.

Appendix I. 2.2.3 BSA-passivated carboxylated-polystyrene coated with fluorescently-tagged (99.8%mol POPC + 0.2%mol NBD-DOPE) lipids

Briefly, we incubated the carboxylated-polystyrene with BSA instead of BSA-FITC and then incubated with 99.8%mol POPC + 0.2%mol NBD-DOPE liposomes instead of 100%mol POPC. Later, the fluorescence level of the sample was screened with a flow cytometer at times 0, 15, 30 and 60 minutes. The purpose of this test was to compare the fluorescence levels of the lipid structures on the carboxylated-polystyrene beads (5 μ m) to the fluorescence levels of the lipid structures on the silica beads (7.9 μ m), where we know that lipid structure formed is a bilayer.

Figure AI-5A shows the median fluorescence intensity in FL-1 channel (NBD-detection channel) of the samples with POPC + 0.2% mole NBD-DOPE lipids supported on the carboxylated-polystyrene microspheres at times 0, 15, 30 and 60 minutes. The fluorescence level stabilizes after 15 minutes to ~ 3,000 to 4,000. These values are very low compared to the fluorescence observed on the silica beads (Figure AI-5B) and even accounting for the difference in the beads' sizes, we can conclude that the structures formed

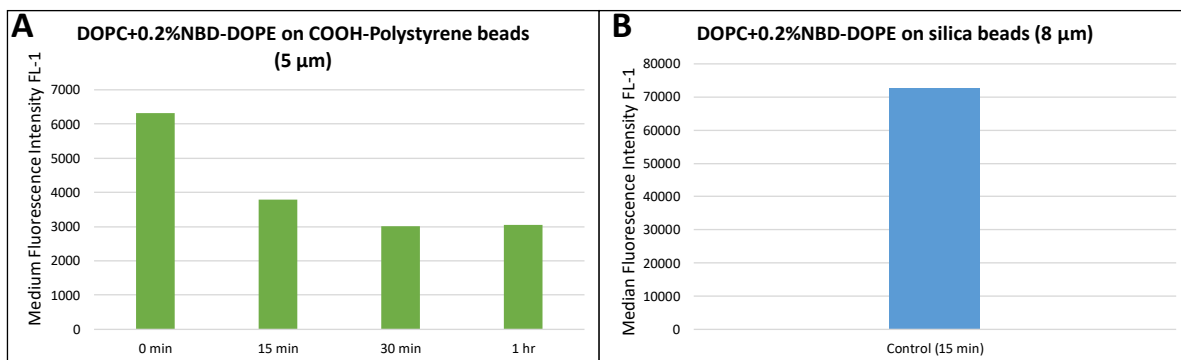


Figure AI-5. Assembly of lipid structures (DOPC + 0.2%mol NBD-DOPE) on **A**) BSA-passivated carboxylated-polystyrene microspheres (5 μ m), and **B**) non-porous silica (8 μ m) microspheres.

on the carboxylated-polystyrene beads are neither bilayers, nor monolayers.

Conclusion (Part 3). Polystyrene is a highly hydrophobic material, therefore not an ideal support for lipid bilayer membranes. To mitigate this problem, we chose functionalized (carboxylated) polystyrene microspheres. The carboxyl groups on the surface of the beads should make it less hydrophobic. Moreover, we passivated the surface of the beads with BSA in the hopes of helping reduce the hydrophobicity of the polystyrene. Unfortunately, the data observed on Figure AI-5 indicates otherwise. Hence, different approaches should be explored to form biomimetic membranes on polystyrene microspheres. For instance, an option would be to test different functional groups on polystyrene beads and at higher concentrations. In addition, the possibility of covalently binding the lipids to functionalized polystyrene beads should be researched and explored.

Acknowledgments. The work done on lipid protection assay was done in collaboration with Dr. Nesia A. Zurek and Mirella Galvan-De La Cruz.

Appendix I. 2.3 Surface modification of polystyrene microspheres

Introduction. As stated in the conclusion (part 3) of the last section, there is a need to further modify the surface of functionalized polystyrene microspheres to achieve a more hydrophilic surface. In order to achieve it, we treated the surface of the polystyrene beads with UV-ozone exposure,^{3,4} and with O₂ plasma,^{5,6} as both methods are generally used to functionalize polystyrene surfaces.

Materials. The silica microspheres (3.14 μm), the plain polystyrene microspheres (5 μm) and the carboxylated-polystyrene microspheres (5 μm) were purchased from Sphertotech. Pieces of Fisherbrand Plastic Petri Dishes were used as control. The samples were treated using the UVO-Cleaner by Jelight Company, Inc. Model No 144AX or a Harrick Plasma Cleaner PDC-32G. The flow cytometric data was obtained using either the BD Accuri C6 flow cytometer or the ThermoFisher Scientific Attune NxT.

Methods. In both sets of experiments, small pieces of a petri dish were first treated, and the surface modification was determined by a qualitative change in the water contact angle. If the treatment process resulted in a better wetting ability of polystyrene, then the sample treatment was applied to the microspheres, which were later coated with fluorescently-tagged liposomes to test their ability to support biomimetic membranes by measuring the fluorescence intensity using a flow cytometer.

Results and Discussions.

- UV-ozone treatment of polystyrene samples.

First, a piece of petri dish polystyrene served as a control (Figure AI-6A), a second piece was directly exposed to UV-ozone for 30 minutes (Figure AI-6B), and a third one was

submerged in DI water and exposed to UV-ozone for 30 minutes (Figure AI- 6C). Figure

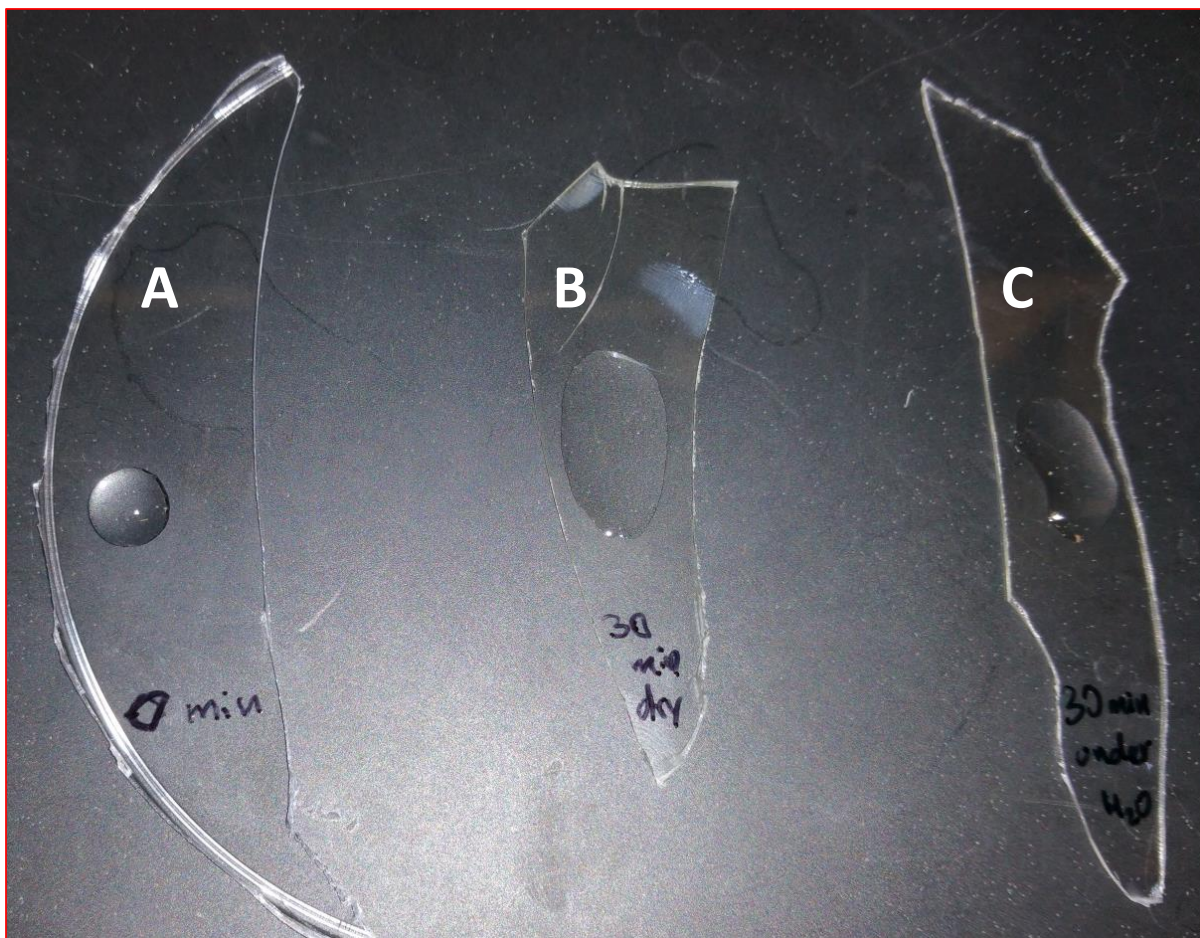


Figure AI-6. Modification of polystyrene surface via UV-ozone. **A)** Control (0 minutes of exposure). **B)** Direct exposure (30 minutes). **C)** Under-water exposure (30 minutes).

AI-6 shows the three different pieces as a support of 100 μl of water. Figure AI-6A shows the control, and as expected the observed contact angle is very high, due to the high hydrophobicity of the untreated polystyrene. Figures AI-6B and AI-6C show that the UV treatment of the sample (either directly or under water) reduces the water contact angle significantly.

The microspheres come already suspended in a solution, so to expose the beads directly becomes challenging as the beads need to be dried before treatment and resuspended after

treatment. Therefore, we decided to place the beads submerged on DI water on a watch glass and expose it to UV-ozone for 0, 2, 5, 10 and 15 minutes. After the treatment, the beads were re-suspended in PBS buffer, and then analyzed in the flow cytometer. Figure AI-7A shows the fluorescence intensity in FL-1 (Laser 488, Filter 533/30nm band pass) after treatment. Unfortunately, the data clearly indicates that the exposure to UV is making the beads fluorescent and it is detectable in the channel that we primarily used to detect the presence of fluorescent membranes. Figure AI-7B shows the fluorescence levels in FL-1 as a function of the time of exposure has a quadratic nature. Hence, until we are able to

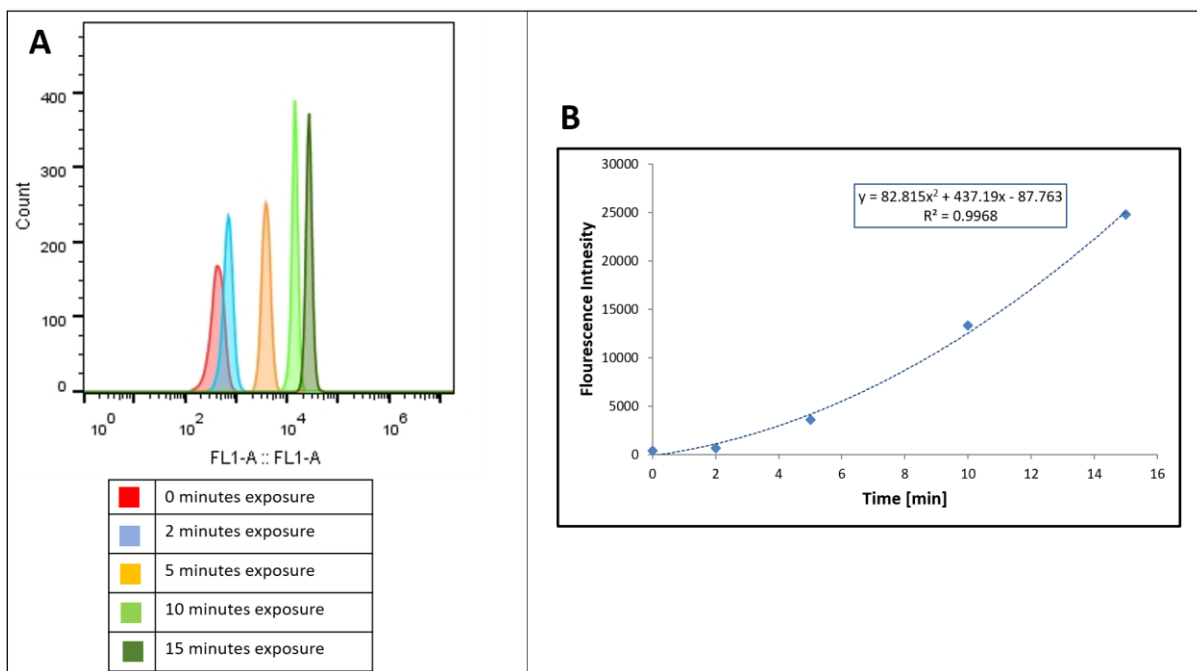
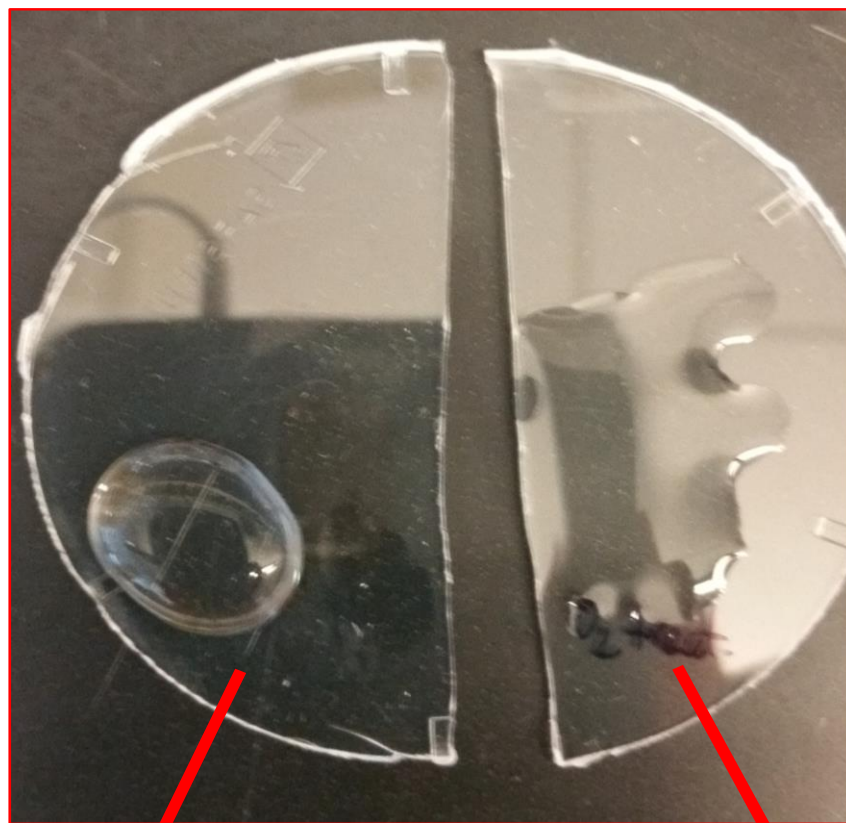


Figure AI-7. **A)** Fluorescence of UV treated beads at different times: 0 minutes (red), 2 minutes (blue), 5 minutes (orange), 10 minutes (light green) and 15 minutes (dark green). **B)** Fluorescence intensity as a function of time of UV exposure.

better understand the aspects of this chemistry process that make the beads fluorescent as function of UV time exposure, another surface modification method should be pursued.

- O₂ plasma treatment of polystyrene and carboxylated-polystyrene samples.

First, a piece of petri dish polystyrene served as a control, and a second piece was



Untreated

O₂ plasma treated

Figure AI-1. Modification of polystyrene surface via O₂ plasma treatment. Exposure time ~1 minute.

directly exposed to O₂ plasma for 1 minute. Figure AI-8 shows the two different pieces as a support of 100 μ l of water. In the control, and as expected, the observed contact angle is very high, due to the high hydrophobicity of the untreated polystyrene. Figures AI-8 also shows that the O₂ plasma treatment of the sample reduces the water contact angle significantly.

The plain polystyrene and carboxylated-polystyrene beads in storage solution were

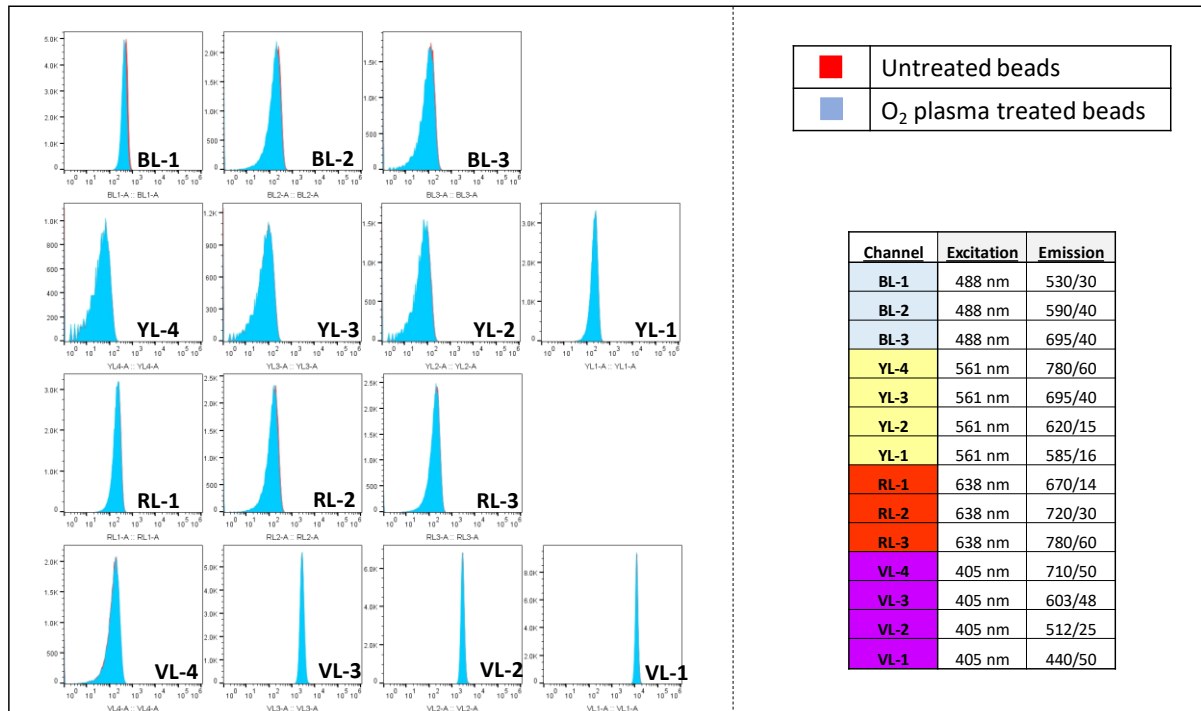


Figure AI-9. Median fluorescence intensity of carboxylated-polystyrene microspheres (5 μm) in all the detection channels of the Attune NxT flow cytometer. Untreated beads or control (red), O₂ plasma treated beads (light blue).

placed on a watch glass and exposed to O₂ plasma for 1 minute. Given the results from the surface treatment with UV-ozone, we decided to evaluate the fluorescence of beads before and after treatment in all the detection channels available on the Attune NxT. Figure AI-9 shows the fluorescence levels of the untreated carboxylated-polystyrene beads (red histograms) and treated carboxylated-polystyrene beads (light blue histograms), and no major difference in fluorescence can be observed in any of the detection channels. Similar results were obtained using plain polystyrene microspheres (Figure AI-Extra-1, located at the end of this Appendix). Hence, the next step was to try to assemble membrane structures on the treated beads' surfaces. We attempted to assemble lipid membranes with 99.8%mol DOPC + 0.2%mol NBD-DOPC liposomes on silica beads (for control) and on the O₂ plasma treated polystyrene (plain and carboxylated) microspheres by following the

protocol reported on chapters 3 and 4, except for the final rinsing steps to minimize sample to sample variability.

Figure AI-10 shows the fluorescence intensity in the BL-1 channel (NBD detection channel) of the different samples tested. Figure AI-10A shows the fluorescence of bare silica beads (red) and of the lipid-coated silica beads (light blue), which shows a very narrow distribution with high fluorescence, both indicative of the formation of uniform complete membranes on the beads.

Figure AI-10B shows the fluorescence of plain polystyrene beads (red), the O₂ plasma

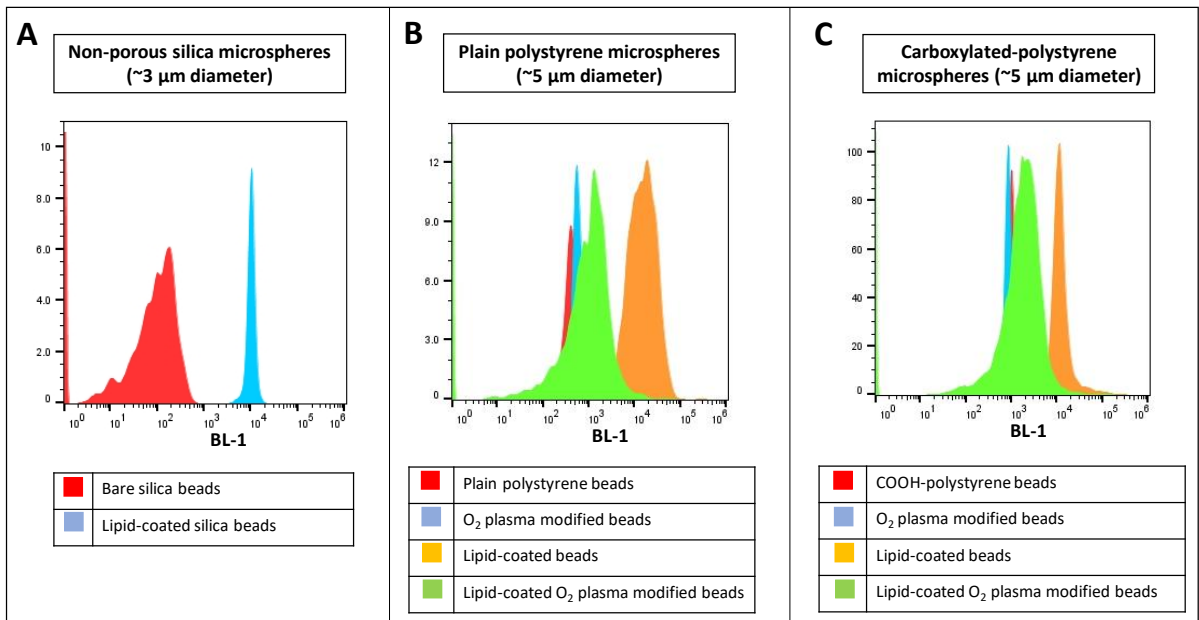


Figure AI-10. Fluorescence levels in the BL-1 channel (Excitation 488 nm; Emission 533/30 nm) of bare, modified, lipid-coated bare beads or lipid-coated modified beads. **A)** In non-porous silica microspheres (3 μm). **B)** In plain polystyrene microspheres (5 μm). **C)** In carboxylated-polystyrene microspheres (5 μm).

treated plain polystyrene beads (light blue), the lipid-coated plain polystyrene beads (orange), and the lipid-coated- O₂ plasma treated plain polystyrene beads (green). Contrary to intuition, the fluorescence levels observed in the untreated beads is higher than the one observed on the treated ones, but in both cases the fluorescence distribution is very broad.

These two observations might be explained by the possible formation of aggregates of liposomes on the beads' surface instead of a biomimetic membrane, especially considering that we omitted the final rinsing steps to remove the excess liposomes. Figure AI-10C shows the fluorescence of carboxylate-polystyrene beads (red), the O₂ plasma treated carboxylate-polystyrene beads (light blue), the lipid-coated carboxylate-polystyrene beads (orange), and the lipid-coated- O₂ plasma treated carboxylate-polystyrene beads (green). The obtained results are very similar to those observed in Figure AI-10B, and the possible explanations remain the same.

The inability of the plasma treated (plain and carboxylated polystyrene) beads to support membrane bilayers can be due the fact that the O₂ plasma treatment can reduce the contact angle to ~ 35°, as reported by Guruventket, et al.,⁶ which is not a low enough angle compared to the contact angle on silica surfaces of ~20° or less.⁷ Another possibility is that surface modification of the beads was not uniform, a difficulty hard to overcome given the small and colloidal nature of the samples.

Conclusion. The successful modification of the surface of polystyrene microspheres could represent an important stepping stone towards the development of a multiplexable, naturally-buoyant and high-throughput compatible platform to present biomimetic membranes against other biomolecules. Nevertheless, the surface modification methods explored in this section have proven not to be effective or still require some re-designing in the protocol to optimize the results. Therefore, some alternative ways of modifying the surface of polystyrene microspheres should be pursued.

**Appendix I.3 ADDITIONAL WORK FOR CHAPTER 5 – DETECTION OF
MEMBRANE-POLYMER INTERACTIONS ON MICROSPHERE
SUPPORTED-BIOMIMMETIC MEMBRANES**

**Appendix I.3.1 Chitosan interaction with microsphere-supported membranes with
different lipid compositions.**

Introduction. The aim of chapter 5 is to perform flow cytometry studies of polymer-membrane interactions on multiplexed microspheres. The interaction of polymers with lipid membranes and cell membranes is of key importance for the development of novel medical devices, drug delivery mechanisms, and the discovery of antimicrobials and antimicrobial surfaces.⁸ Polymers are used for various biomedical purposes such as drug delivery, as biosensors, and for surgical sutures and implants.⁹ The polymer-membrane interaction seems to be dictated by the membrane composition and charge and the polymer's charge and structure.¹⁰ Among the polymers that have been reported to interact with different lipid composition is chitosan, which is an extensively studied cationic polymer with non-toxicity, antibacterial activity, antioxidant activity, and high biocompatibility.^{11,12} Chitosan is used in different areas such as cosmetics and foods,¹³ but most importantly it has a variety of pharmaceutical and biomedical applications. For instance, chitosan is used as a drug delivery agent,^{14,15} in tissue engineering,^{16,17} and in gene delivery.^{12,18} Chitosan's adhesion to different substrates as a function of pH and contact time has been characterized.^{19,20} Furthermore, chitosan has been reported to interact with anionic lipids, such as DPPG.^{21,22} Moreover, chitosan has the advantage of being

widely commercially available at a low cost. Hence, we decided to screen the preferential binding of fluorescently-tagged chitosan to microsphere-supported membranes with different lipid composition and charge (non-ionic, cationic, and anionic lipids). Fluorescently-labeled chitosan is commercially available for high prices; therefore, we chose to do the fluorescent tagging ourselves.

Materials. The lipids 1-palmitoyl-2-oleoyl-sn-glycero-3-phosphocholine (POPC), 1,2-dipalmitoyl-sn-glycero-3-phospho-(1'-rac-glycerol) (DPPG), 1,2-dioleoyl-3-trimethylammonium-propane (DOTAP), and 1,2-dioleoyl-sn-glycero-3-phosphoethanolamine-N-(7-nitro-2-1,3-benzoxadiazol-4-yl) (NBD-DOPE) were purchased from Avanti Polar Lipids in lyophilized form. As solvent for lipids, we used chloroform that contains 1%-5% of ethanol as a stabilizer, purchased from EMD Millipore. The phosphate-buffered saline (PBS), the bovine serum albumin (BSA), the dehydrated methanol, and the low molecular weight chitosan (50-190 kDa) were purchased from Sigma Aldrich. The acetic acid and the sodium hydroxide were purchased from EMD Millipore. The assays were performed in PBS pH 4.5 – 5.5. The non-porous silica microspheres (7.9 μm) were purchased from Spherotech. The chitosan fluorescent tagging measurements were performed with the Perkin Elmer Lambda 35 UV/VIS Spectrometer, and the assay measurements were performed with the Accuri C6 flow cytometer.

Methods.

Fluorescent tagging of chitosan. First, chitosan was covalently modified by linking the isothiocyanate group of FITC to the primary amine group of the d-glucosamine residue in chitosan, following the protocol reported by Qaqish et al.,²³ and by Yuqing et al.²⁴ Briefly,

0.2 g of chitosan was dissolved in 20 ml of 0.1M acetic acid, followed by the additions of 20 ml of dehydrated methanol to the solution. Then, 20 ml of FITC solution (1mg/ml FITC in methanol) were added to achieve a d-glucosamine: FITC residue ratio of ~ 1:50. The reaction was allowed to proceed for 3 h in the dark at room temperature. Afterwards, the FITC-labeled chitosan was precipitated in 0.1 M sodium hydroxide solution. The precipitate was extensively washed with deionized distilled water and separated by centrifuge until there is complete absence of free FITC fluorescence signal in the washing medium. The last washing step needs to be with acetic acid instead of water, since chitosan is soluble in acetic acid and not in water. The resulting stock and dilutions should be kept in the dark at ~ 4 °C. Finally, the FITC labeling efficiency was determined by measuring the absorbance intensity of FITC-chitosan solution against standard solutions of FITC using UV-Vis spectrometer.

Screening of preferential binding of chitosan-FITC to different membrane compositions and charges. Second, we assembled different sets of biomimetic membranes on silica microspheres following the protocol reported in chapters 3 and 4, including the BSA passivation and rinsing steps. The tested membranes compositions were: 100%mol POPC, 90%mol POPC+10%mol DOTAP, and 90%mol POPC+10%mol DPPG. Each set of samples was incubated with increasing amounts chitosan-FITC (0, 0.2, 2, 20 μ M) for ~30 minutes and immediately analyzed on the flow cytometer.

Disruption effects of chitosan on differently-charged fluorescently tagged membranes. Third, the potential disruption effect of chitosan on the membranes was tested by first assembling membranes with the following compositions: 99.8%mol POPC+0.2%mol NBD-DOPE, 89.8%mol POPC+0.2%mol NBD-DOPE+10%mol DOTAP, and 89.8%mol

POPC+0.2%mol NBD-DOPE+10%mol DPPG. Then, each set of samples was incubated with increasing amounts chitosan (0, 0.2, 2, 20 μM) for ~30 minutes and immediately analyzed on the flow cytometer.

Results and Discussions.

Fluorescent tagging of chitosan. Figure AI-Extra-2 shows **A**) the schematic illustration of the chemical synthesis of FITC-labeled chitosan, **B**) a picture of the last centrifuge step in the fluorescent-tagging process, where it can be observed that the precipitate has a yellow/orange color indicative of the presence of FITC and the supernatant is clear and FITC-free. **C**) pictures of a 10X and a 100X dilution of chitosan-FITC in PBS buffer.

Figure AI-Extra-3 shows that 2.5 μM FITC in PBS has an absorbance of 0.165 at 494nm, it also shows that 100X dilution of chitosan-FITC in PBS has an absorbance of 0.130 at 497nm. Based on this information and using Beer-Lambert Law, we can calculate the initial concentration FITC in the chitosan-FITC solution.

$$A = \varepsilon cL . \quad \longrightarrow \quad A_F = \varepsilon C_F L \quad \text{and} \quad A_{CFD} = \varepsilon C_{CFD} L$$

where, A_F and C_F are the absorbance and the concentration (2.5 μM) of FITC in PBS, respectively; and A_{CFD} and C_{CFD} are the absorbance and the concentration of the 100X diluted chitosan-FITC in PBS, respectively.

$$\varepsilon L = \frac{A_F}{C_F} = \frac{A_{CFD}}{C_{CFD}} \quad \rightarrow \quad C_{CFD} = \frac{A_{CFD} * C_F}{A_F} = \frac{0.130 * 2.5\mu\text{M}}{0.165} \quad \rightarrow \quad C_{CFD} \approx 2\mu\text{M}$$

Therefore, the concentration of the original solution of chitosan-FITC dissolved in acetic acid has a concentration of approximately 0.2mM of FITC.

Assuming we did not lose any chitosan in the washing process, we started with 0.2 g of low molecular chitosan in 50 ml of solution. The molecular weight of the chitosan subunit is ~ 178 g/mole. Then,

$$\frac{0.2g \text{ chitosan}}{50ml \text{ sol.}} * \frac{1 \text{ mole chitosan}}{178 \text{ g chitosan}} * \frac{1000ml \text{ sol.}}{1L \text{ sol.}} \approx 0.02M = 20mM$$

$$\frac{\text{chitosan}}{\text{FITC}} = \frac{20mM}{0.2mM} = \frac{100}{1}$$

Then, the chitosan/FITC ratio is 100:1.

Screening of preferential binding of chitosan-FITC to different membrane compositions and charges. Figure AI-11 shows the 10% scatter plot of side scatter versus FL-1 (FITC detection channel on the Accuri C6) of the BSA-passivated silica microspheres and the

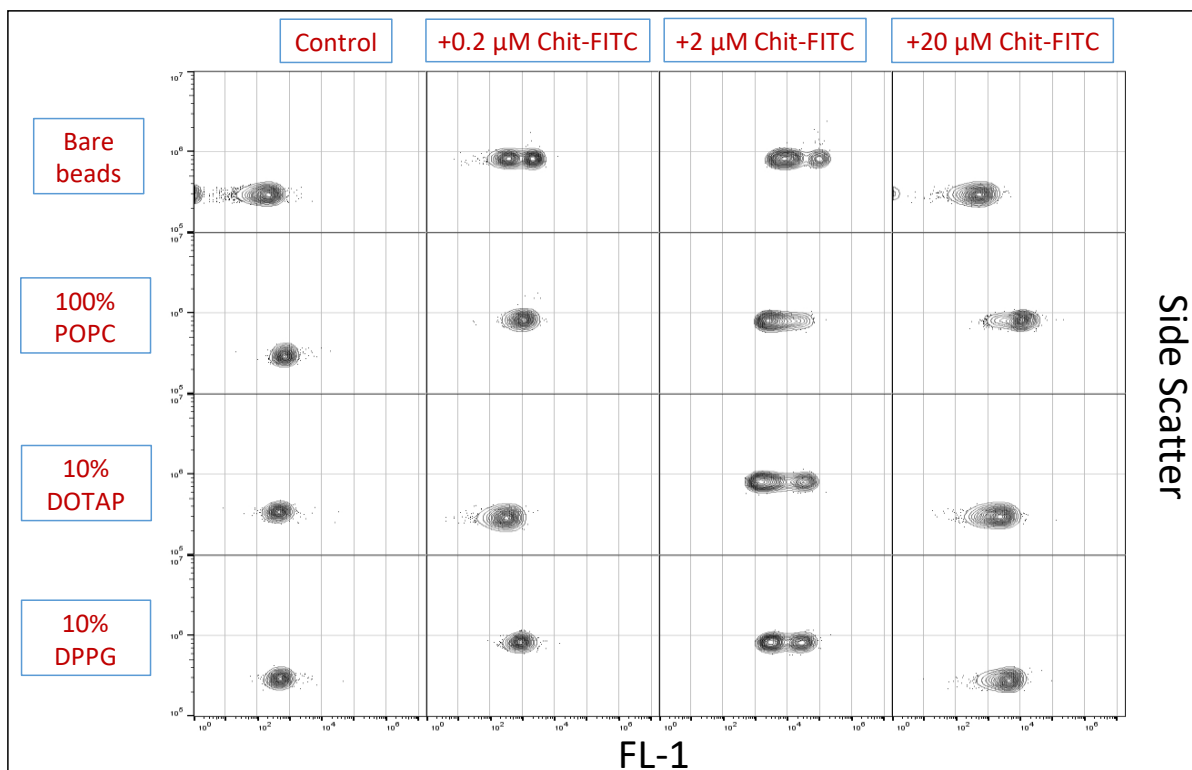


Figure AI-11. Scatter plots (side scatter vs. FL-1) showing three sets of silica microsphere-supported membranes: 100%mol POPC (non-ionic), 90%mol POPC+10%mol DOTAP (cationic), and 90%mol POPC+10%mol DPPG (anionic) in the presence of increasing concentration of chitosan-FITC (0.2, 2, 20 μ M).

differently-charged membranes supported on silica beads in the presence of increasing concentration of chitosan-FITC.

The BSA-passivated silica microspheres show a double population of in the presence of 0.2 and 2 μM chitosan-FITC both with higher fluorescence than the background. This can be due to the poor BSA passivation of silica, or it could be due to the low concentration (below of the saturation point) of FITC. However, the BSA-passivated silica microspheres in the presence of 20 μM chitosan-FITC shows very low fluorescence, which can be indication of saturation of FITC on the beads resulting on self-quenching. Moreover, these results show very high non-specific binding of the chitosan-FITC to the silica beads. In the presence of 0.2 μM chitosan-FITC, the non-ionic membranes (100% POPC) and the anionic membranes (POPC+10%mol DPPG) show a more significant increase in the FL-1 fluorescence compared to the increase observed on the cationic membranes (POPC+10%mol DOTAP). This can be due to the electrostatic interaction between the cationic chitosan and the cationic membranes. In the presence of 2 μM chitosan-FITC, the non-ionic membranes present less dispersed population compared to the anionic and cationic membranes where double populations can be observed. The lower population fluorescence is comparable to the one observed in the non-ionic membranes, whereas the higher population fluorescence in the anionic lipids shows a higher concentration of beads and a better-defined distribution. In the presence of 20 μM chitosan-FITC all the membranes show a single population with a broad distribution in the FL-1 channel. The non-ionic membranes show a higher fluorescence level, in the FL-1 channel, compared to the anionic and cationic membranes, which show fluorescence levels comparable to one another.

Disruption effects of chitosan on differently-charged fluorescently tagged membranes.

Figure AI-12 shows the 10% scatter plot of side scatter versus FL-1 (NBD detection channel on the Accuri C6) of the BSA-passivated silica microspheres and the differently-charged NBD-labeled membranes supported on silica beads in the presence of increasing concentration of chitosan.

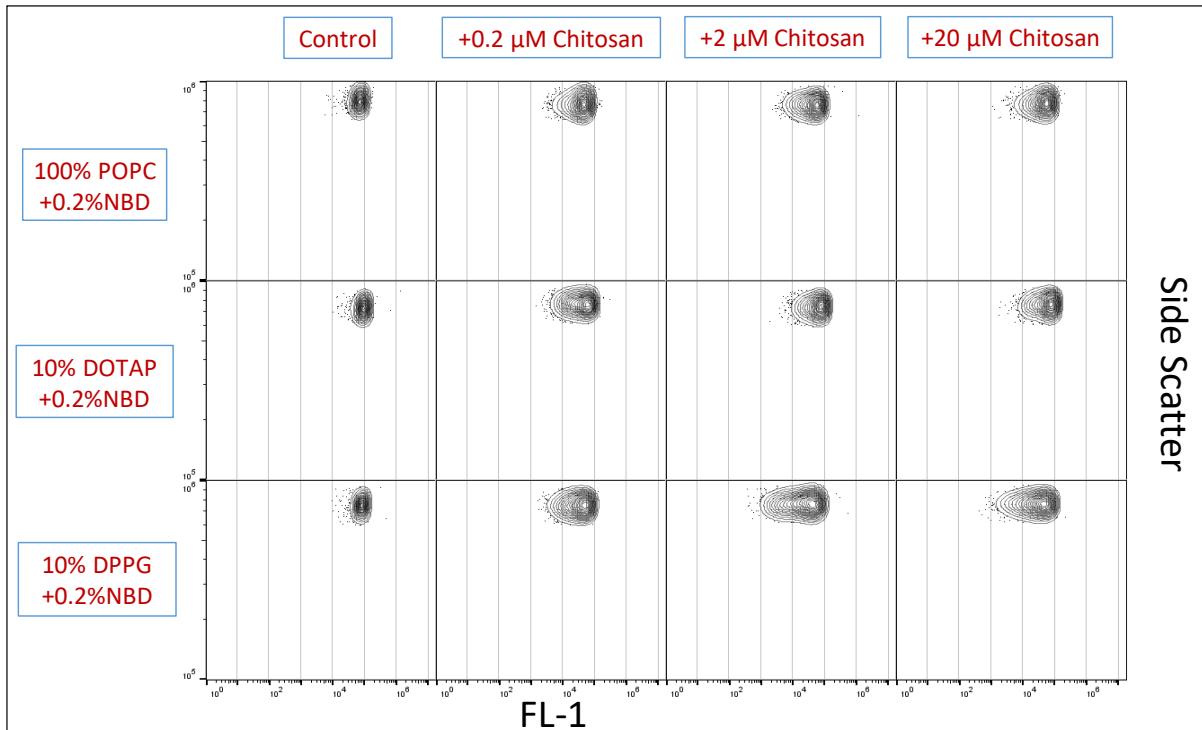


Figure AI-12. Scatter plots (side scatter vs. FL-1) showing three sets of silica microsphere-supported fluorescently-tagged membranes: POPC+0.2%mol NBD-DOPE (non-ionic), POPC+2%mol NBD-DOPE+10%mol DOTAP (cationic), and POPC+2%mol NBD-DOPE+10%mol DPPG (anionic) in the presence of increasing concentration of chitosan (0.2, 2, 20 μ M).

The initial FL-1 fluorescence level is the same for all three sets of samples: non-ionic membranes (POPC + 0.2%mol NBD-DOPE), cationic membranes (POPC+ 0.2%mol NBD-DOPE+ 10%mol DOTAP), and anionic membranes (POPC+ 0.2%mol NBD-DOPE+ 10%mol DPPG). The three sets of membranes show that in the presence of either 0.2, 2, or 20 μ M chitosan, the fluorescence FL-1 level remains the same as the one observed

initially, and the distributions remain tight for the non-ionic and cationic membranes, whereas on the anionic membranes the samples show a slightly broader distribution, but the median fluorescence remain the same. These data indicate that chitosan does not act as a disrupting agent on the biomimetic membranes.

Conclusion. Chitosan is a polymer of great interest as it serves many biomedical purposes. However, the data obtained here shows that it has a very high non-specific binding to silica and to different membrane compositions. Another problem is the fact that chitosan is soluble in acidic solutions and it aggregates in PBS pH 7.4, while FITC as a fluorescent tag for chitosan requires to work in a small pH range close the physiological range, as FITC has pH-dependent absorption.²⁵ Also, BSA (what we use for blocking) is positively charged under acidic conditions,²⁶ which can also be electrostatically interacting with the chitosan in solutions. Hence, the protocol for the study of the interaction of chitosan with differently-charged membrane presented on silica microspheres needs to be further refined. If the new approaches prove to be effective, a broader range of different compositions membranes could be screened against chitosan. However, for the time purposes, choosing a different biologically relevant polymer is a better alternative.

Appendix I. 3.2 Poly-L-lysine (PLL) interaction with bead-supported membranes with different lipid compositions.

Introduction. The need for the study of the interaction between polymers and membranes was discussed in chapter 5 and the previous section of this chapter (Chitosan interaction with microsphere-supported membranes with different lipid compositions). Poly-L-lysine is a cationic polymer used in food, and with several biomedical applications,²⁷ including tissue culture,²⁸ drug delivery,²⁹ as a gene carrier,³⁰ and as a lipase inhibitor,³¹ among many others. The interaction of poly-L-lysine and charged lipid membranes has been studied. For instance, it has been reported that Poly-L-lysine differentially interacts with anionic/zwitterionic and neat zwitterionic bilayer membranes supported on planar cleaved mica.³² It has also been reported that poly-L-lysine can pass through anionic lipid bilayers.³³ Hence, we decided to screen the preferential binding of low molecular weight fluorescently-tagged poly-L-lysine to microsphere-supported membranes with differently charged lipids.

Materials. The lipids 1-palmitoyl-2-oleoyl-sn-glycero-3-phosphocholine (POPC), 1,2-dipalmitoyl-sn-glycero-3-phospho-(1'-rac-glycerol) (DPPG), 1,2-dioleoyl-3-trimethylammonium-propane (DOTAP), and 1,2-dioleoyl-sn-glycero-3-phosphoethanolamine-N-(7-nitro-2,1,3-benzoxadiazol-4-yl) (NBD-DOPE) were purchased from Avanti Polar Lipids in lyophilized form. As solvent for lipids, we used chloroform that contains 1%-5% of ethanol as a stabilizer, purchased from EMD Millipore. The phosphate-buffered saline (PBS), the bovine serum albumin (BSA), the poly-L-lysine (PLL) and poly-L-lysine hydrobromide-FITC Labeled (PLL-FITC) were purchased in

powder form from Sigma Aldrich. The assays were performed in PBS pH 7.4. The non-porous silica microspheres (7.9 μm) were purchased from Spherotech. The assay measurements were performed with the Accuri C6 flow cytometer.

Methods.

Screening of preferential binding of PLL-FITC to different membrane compositions and charges. We assembled different sets of biomimetic membranes on silica microspheres following the protocol reported in chapters 3 and 4, including the BSA passivation and rinsing steps. The tested membranes compositions were: 100 mol% POPC, 90 mol% POPC+10 mol% DOTAP, and 90 mol% POPC+10 mol% DPPG. Each set of samples was incubated with increasing amounts PLL-FITC (0, 0.02, 0.2, 2 μM) for ~10 minutes and immediately analyzed on the flow cytometer.

Disruption effects of PLL on differently-charged fluorescently tagged membranes. The potential disruption effect of PLL on the membranes was tested by first assembling membranes with the following compositions: 99.8%mol POPC+0.2%mol NBD-DOPE, 89.8%mol POPC+0.2%mol NBD-DOPE+10%mol DOTAP, and 89.8%mol POPC+0.2%mol NBD-DOPE+10%mol DPPG. Then, each set of samples was incubated with increasing amounts PLL (0, 0.02, 0.2, 2 μM) for ~10 minutes and immediately analyzed on the flow cytometer.

Results and Discussions.

Screening of preferential binding of PLL-FITC to different membrane compositions and charges. FigureAI-13 shows the 10% scatter plot of side scatter versus FL-1 (FITC detection channel on the Accuri C6) of the BSA-passivated silica microspheres and the

differently-charged membranes supported on silica beads in the presence of increasing concentration of PLL-FITC.

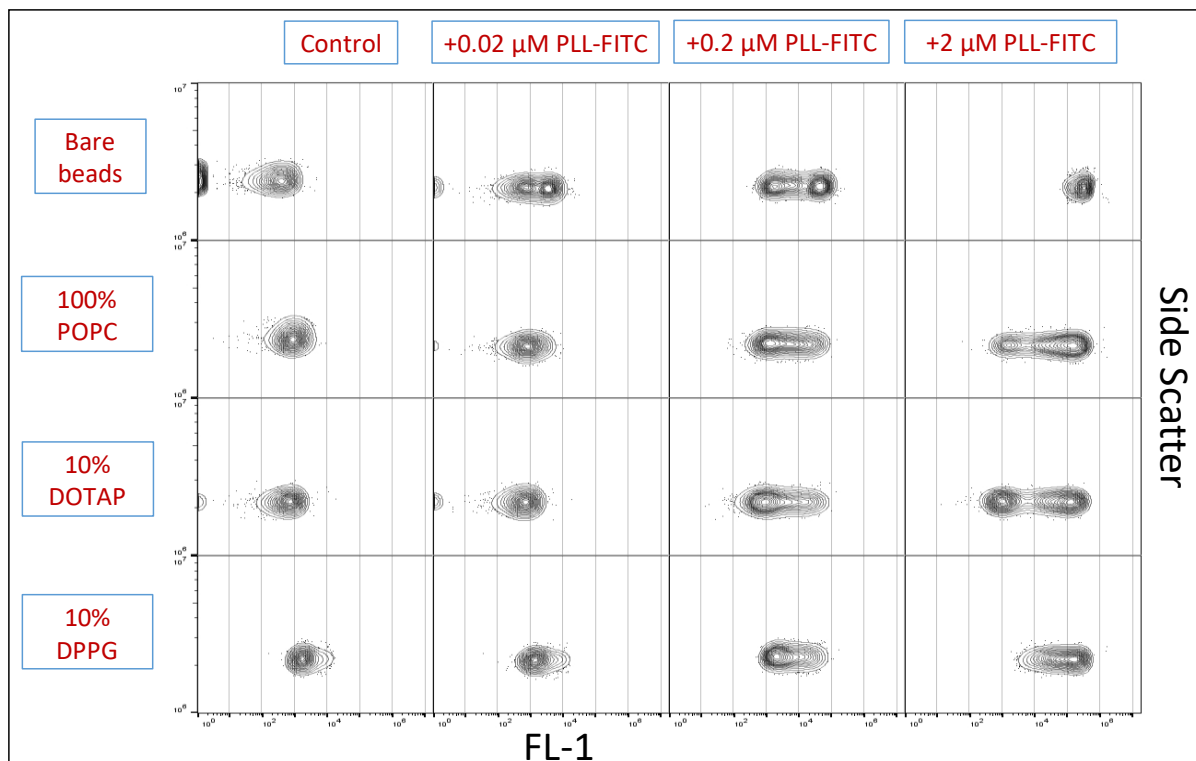


Figure AI-13. Scatter plots (side scatter vs. FL-1) showing three sets of silica microsphere-supported membranes: 100%mol POPC (non-ionic), 90%mol POPC+10%mol DOTAP (cationic), and 90%mol POPC+10%mol DPPG (anionic) in the presence of increasing concentration of PLL-FITC (0.02, 0.2, 2 μ M).

Similar to the chitosan case, the BSA-passivated silica beads show a double population of in the presence of 0.02 and 0.2 μ M PLL-FITC, both with higher fluorescence than the background. Meanwhile, the presence of 2 μ M PLL-FITC presents a single narrow population with high fluorescence in FL-1, showing saturation of PLL-FITC and high non-specific binding to silica. In the presence of 0.02 μ M PLL-FITC, the three sets of membranes: non-ionic (100% POPC), cationic (POPC+ 10%mol DOTAP), and anionic (POPC+10%mol DPPG) show no increase in the FL-1 channel, indicating very low to no-interaction of that concentration of PLL-FITC with the membranes. In the presence of 0.2

μM PLL-FITC the three sets of membranes show higher fluorescence in FL-1, and very broad population distributions that resulted in similar median fluorescence intensities. This indicates non-specific binding of PLL or FITC to the differently-charged membranes. Finally, in the presence of 2 μM PLL-FITC the non-ionic membranes show what seems to be a very broad single population, with the highest concentration of bead at the higher fluorescence level, showing high non-specific binding. The cationic membranes show a clear double population where the lower fluorescence level corresponds to the background level and the higher fluorescence level is similar to the one observed on the non-ionic membranes. Finally, the anionic membranes show a single population with a not-so broad distribution with high FL-1 fluorescence level, which can be indicative of electrostatic interaction of DPPG with PLL.

Disruption effects of PLL on differently-charged fluorescently tagged membranes. Figure AI-14 shows the 10% scatter plot of side scatter versus FL-1 (NBD detection channel on the Accuri C6) of the BSA-passivated silica microspheres and the differently-charged NBD-labeled membranes supported on silica beads in the presence of increasing concentration of PLL.

The initial FL-1 fluorescence level is the same for all three sets of samples: non-ionic membranes (POPC + 0.2%mol NBD-DOPE), cationic membranes (POPC+ 0.2%mol NBD-DOPE+ 10%mol DOTAP), and anionic membranes (POPC+ 0.2%mol NBD-DOPE+ 10%mol DPPG). The three sets of membranes show that in the presence of either 0.02, 0.2, or 2 μM PLL, the fluorescence FL-1 level remains the same as the one observed in the control samples. Moreover, the distributions of the three sets of membranes remain

tight. These data indicate that chitosan does not act as a disrupting agent on the biomimetic membranes.

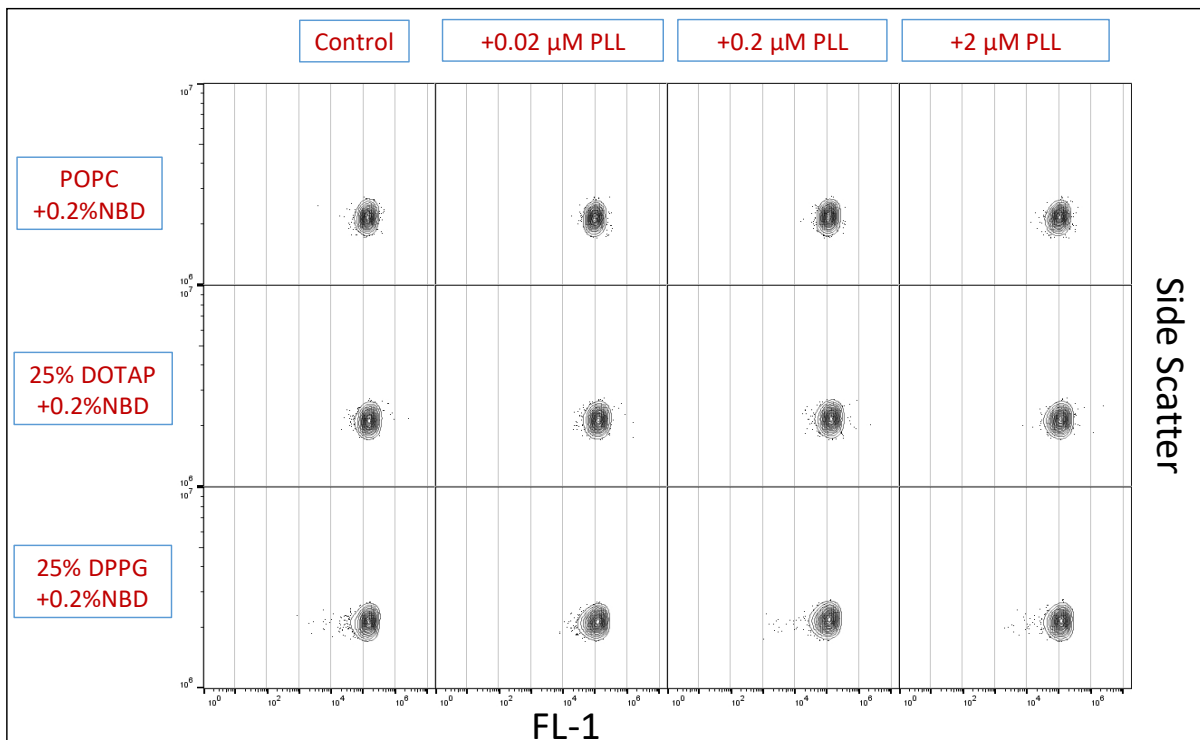


Figure AI-14. Scatter plots (side scatter vs. FL-1) showing three sets of silica microsphere-supported fluorescently-tagged membranes: POPC+0.2%mol NBD-DOPE (non-ionic), POPC+2%mol NBD-DOPE+10%mol DOTAP (cationic), and POPC+2%mol NBD-DOPE+10%mol DPPG (anionic) in the presence of increasing concentration of PLL (0.02, 0.2, 2 μM).

Conclusion. The double populations in the presence of certain concentrations of PLL-FITC remain a setback and something that needs to be further explored for better understanding. In addition, membranes with higher concentrations of DOTAP and DPPG should be screened against PLL-FITC in an attempt to test the possible electrostatic interactions. Moreover, different fluorescent dyes could be used as tag for PLL; dyes that are known to have little to no interaction with lipid membranes. Finally, an alternative non-ionic blocking agent could be used instead of BSA to mitigate non-specific interactions.

Appendix I. 4 REFERENCES

1. Keizer J. Nonlinear fluorescence quenching and the origin of positive curvature in Stern-Volmer plots. *J Am Chem Soc.* 1983;105(6):1494-1498. doi:10.1021/ja00344a013.
2. Tero R, Takizawa M, Li Y-J, Yamazaki M, Urisu T. Lipid Membrane Formation by Vesicle Fusion on Silicon Dioxide Surfaces Modified with Alkyl Self-Assembled Monolayer Islands. *Langmuir.* 2004;20(18):7526–7531. doi:10.1021/LA0400306.
3. Huang W, Fan H, Zhuang X, Yu J. Effect of UV/ozone treatment on polystyrene dielectric and its application on organic field-effect transistors. *Nanoscale Res Lett.* 2014;9(1):479. doi:10.1186/1556-276X-9-479.
4. Yusilawati AN, Maizirwan M, Hamzah MS, Ng KH, Wong CS. Surface Modification of Polystyrene Beads by Ultraviolet/Ozone Treatment and its Effect on Gelatin Coating. *Am J Appl Sci.* 2010;7(6):724-731.
5. Beaulieu I, Geissler M, Mauzeroll J. Oxygen Plasma Treatment of Polystyrene and Zeonor: Substrates for Adhesion of Patterned Cells. *Langmuir.* 2009;25(12):7169-7176. doi:10.1021/la9001972.
6. Guruvenket S, Rao GM, Komath M, Raichur AM. Plasma surface modification of polystyrene and polyethylene. *Appl Surf Sci.* 2004;236:278–284. doi:10.1016/j.apsusc.2004.04.033.
7. Jung J-W, Wan J. Supercritical CO₂ and Ionic Strength Effects on Wettability of Silica Surfaces: Equilibrium Contact Angle Measurements. *Energy Fuels.* 2012;26(9):6053–6059. doi:10.1021/EF300913T.
8. Kahveci Z, Martínez-Tomé M, Esquembre R, Mallavia R, Mateo C. Selective Interaction of a Cationic Polyfluorene with Model Lipid Membranes: Anionic versus Zwitterionic Lipids. *Materials (Basel).* 2014;7(3):2120-2140. doi:10.3390/ma7032120.
9. Langer R, Tirrell DA. Designing materials for biology and medicine. *Nature.* 2004;428(6982):487-492. doi:10.1038/nature02388.
10. Sasaki DY, Zawada N, Gilmore SF, et al. Lipid membrane domains for the selective adsorption and surface patterning of conjugated polyelectrolytes. *Langmuir.* 2013;29(17):5214-5221. doi:10.1021/la400454c.
11. Samal SK, Dash M, Van Vlierberghe S, et al. Cationic polymers and their therapeutic potential. *Chem Soc Rev.* 2012;41(21):7147-7194. doi:10.1039/c2cs35094g.
12. Richardson SC, Kolbe H V, Duncan R. Potential of low molecular mass chitosan as a DNA delivery system: biocompatibility, body distribution and ability to complex and protect DNA. *Int J Pharm.* 1999;178(2):231-243.

13. Rinaudo M. Chitin and chitosan: Properties and applications. *Prog Polym Sci.* 2006;31(7):603-632. doi:10.1016/j.progpolymsci.2006.06.001.
14. Lien C-F, Molnár E, Toman P, et al. In vitro assessment of alkylglyceryl-functionalized chitosan nanoparticles as permeating vectors for the blood-brain barrier. *Biomacromolecules.* 2012;13(4):1067-1073. doi:10.1021/bm201790s.
15. Bilensoy E, Sarisozen C, Esendağlı G, et al. Intravesical cationic nanoparticles of chitosan and polycaprolactone for the delivery of Mitomycin C to bladder tumors. *Int J Pharm.* 2009;371(1-2):170-176. doi:10.1016/j.ijpharm.2008.12.015.
16. Shi W, Nie D, Jin G, et al. BDNF blended chitosan scaffolds for human umbilical cord MSC transplants in traumatic brain injury therapy. *Biomaterials.* 2012;33(11):3119-3126. doi:10.1016/j.biomaterials.2012.01.009.
17. Wang Y, Shi R, Gong P, et al. Bioelectric effect of a chitosan bioelectret membrane on bone regeneration in rabbit cranial defects. *J Bioact Compat Polym.* 2012;27(2):122-132. doi:10.1177/0883911512436773.
18. Nimesh S, Thibault MM, Lavertu M, Buschmann MD. Enhanced gene delivery mediated by low molecular weight chitosan/DNA complexes: effect of pH and serum. *Mol Biotechnol.* 2010;46(2):182-196. doi:10.1007/s12033-010-9286-1.
19. Lim C, Lee DW, Israelachvili JN, Jho Y, Hwang DS. Contact time- and pH-dependent adhesion and cohesion of low molecular weight chitosan coated surfaces. *Carbohydr Polym.* 2015;117:887-894. doi:10.1016/j.carbpol.2014.10.033.
20. Lee DW, Lim C, Israelachvili JN, Hwang DS. Strong adhesion and cohesion of chitosan in aqueous solutions. *Langmuir.* 2013;29(46):14222-14229. doi:10.1021/la403124u.
21. Henriksen I, Våagen SR, Sande SA, Smistad G, Karlsen J. Interactions between liposomes and chitosan II: Effect of selected parameters on aggregation and leakage. *Int J Pharm.* 1997;146(2):193-203. doi:10.1016/S0378-5173(96)04801-6.
22. Mady MM, Darwish MM, Khalil S, Khalil WM. Biophysical studies on chitosan-coated liposomes. *Eur Biophys J.* 2009;38(8):1127-1133. doi:10.1007/s00249-009-0524-z.
23. Qaqish R, Amiji M. Synthesis of a fluorescent chitosan derivative and its application for the study of chitosan–mucin interactions. *Carbohydr Polym.* 1999;38(2):99-107. doi:10.1016/S0144-8617(98)00109-X.
24. Ge Y, Zhang Y, He S, Nie F, Teng G, Gu N. Fluorescence Modified Chitosan-Coated Magnetic Nanoparticles for High-Efficient Cellular Imaging. *Nanoscale Res Lett.* 2009;4(4):287-295. doi:10.1007/s11671-008-9239-9.
25. Hayward R, Saliba KJ, Kirk K. The pH of the digestive vacuole of *Plasmodium falciparum* is not associated with chloroquine resistance. *J Cell Sci.* 2006;119(Pt

- 6):1016-1025. doi:10.1242/jcs.02795.
26. Phan HTM, Bartelt-Hunt S, Rodenhausen KB, Schubert M, Bartz JC. Investigation of Bovine Serum Albumin (BSA) Attachment onto Self-Assembled Monolayers (SAMs) Using Combinatorial Quartz Crystal Microbalance with Dissipation (QCM-D) and Spectroscopic Ellipsometry (SE). Hinderberger D, ed. *PLoS One*. 2015;10(10):e0141282. doi:10.1371/journal.pone.0141282.
 27. Shukla SC, Singh A, Pandey AK, Mishra A. Review on production and medical applications of ϵ -polylysine. *Biochem Eng J*. 2012;65:70-81. doi:10.1016/J.BEJ.2012.04.001.
 28. Yavin E, Yavin Z. Attachment and culture of dissociated cells from rat embryo cerebral hemispheres on polylysine-coated surface. *J Cell Biol*. 1974;62(2):540-546.
 29. Shen WC, Ryser HJ. Poly(L-lysine) has different membrane transport and drug-carrier properties when complexed with heparin. *Proc Natl Acad Sci U S A*. 1981;78(12):7589-7593.
 30. Chiou HC, Tangco M V, Levine SM, et al. Enhanced resistance to nuclease degradation of nucleic acids complexed to asialoglycoprotein-polylysine carriers. *Nucleic Acids Res*. 1994;22(24):5439-5446.
 31. Tsujita T, Takaichi H, Takaku T, Sawai T, Yoshida N, Hiraki J. Inhibition of lipase activities by basic polysaccharide. *J Lipid Res*. 2007;48(2):358-365. doi:10.1194/jlr.M600258-JLR200.
 32. Spurlin TA, Gewirth AA. Poly-L-Lysine-Induced Morphology Changes in Mixed Anionic/Zwitterionic and Neat Zwitterionic-Supported Phospholipid Bilayers. *Biophys J*. 2006;91(8):2919-2927. doi:10.1529/biophysj.106.082479.
 33. Menger FM, Seredyuk VA, Kitaeva M V., Yaroslavov AA, Melik-Nubarov NS. Migration of Poly-l-lysine through a Lipid Bilayer. *J Am Chem Soc*. 2003;125(10):2846–2847. doi:10.1021/JA021337Z.

Appendix I. 5 EXTRA FIGURES

Appendix I, Figure AI-Extra-1. Plain polystyrene beads after O₂ plasma treatment.

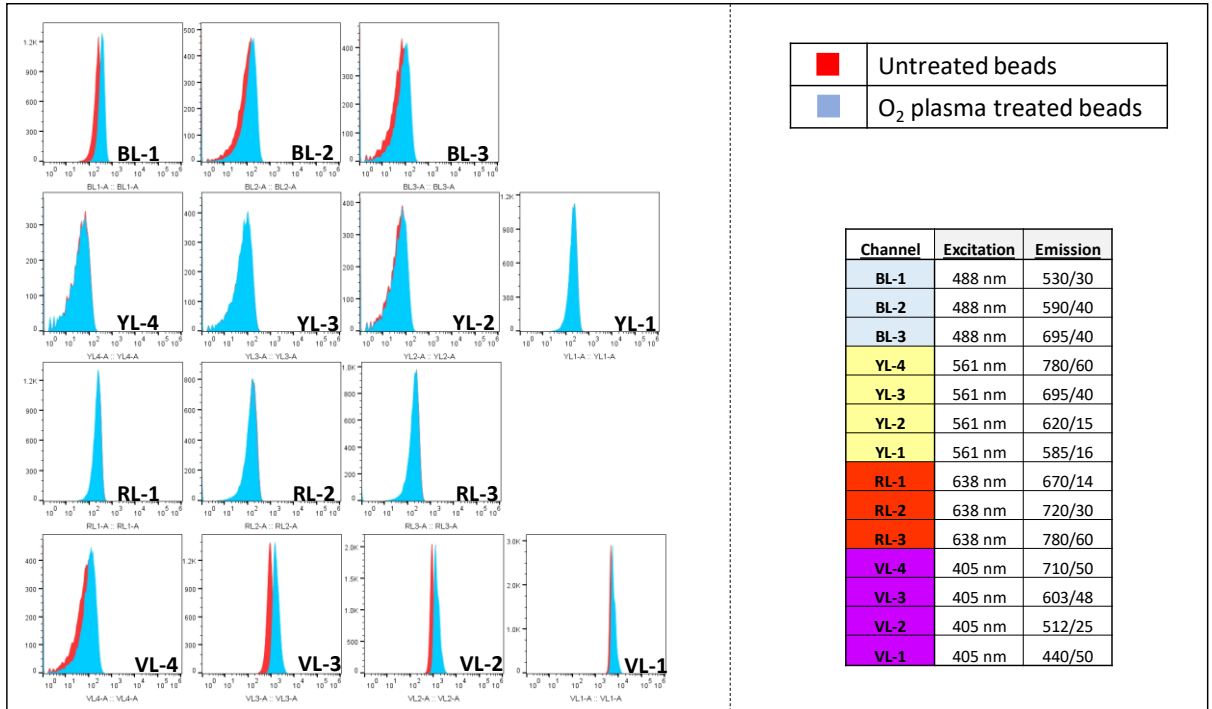


Figure AI-Extra-1. Median fluorescence intensity of plain-polystyrene microspheres (5 μm) in all the detection channels of the Attune NxT flow cytometer. Untreated beads or control (red), O₂ plasma treated beads (light blue).

Appendix I, Figure AI-Extra-2. FITC-labeling of chitosan.

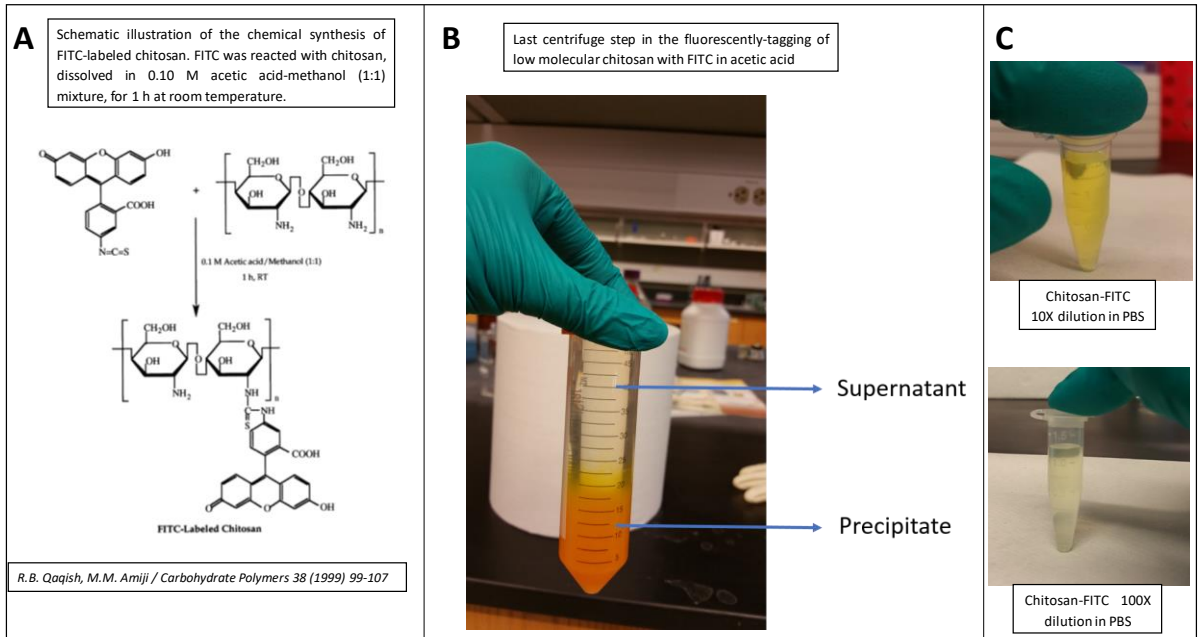


Figure AI-Extra-2. Fluorescein labeling of chitosan. **A)** Schematic illustration of the chemical synthesis of FITC-labeled chitosan. **B)** Last centrifuge step in the fluorescently-tagging of low molecular chitosan with FITC in acetic acid. **C)** 10X and 100X dilution of chitosan-FITC in PBS buffer.

Appendix I, Figure AI-Extra-3. Absorbance of chitosan-FITC and FITC in PBS.

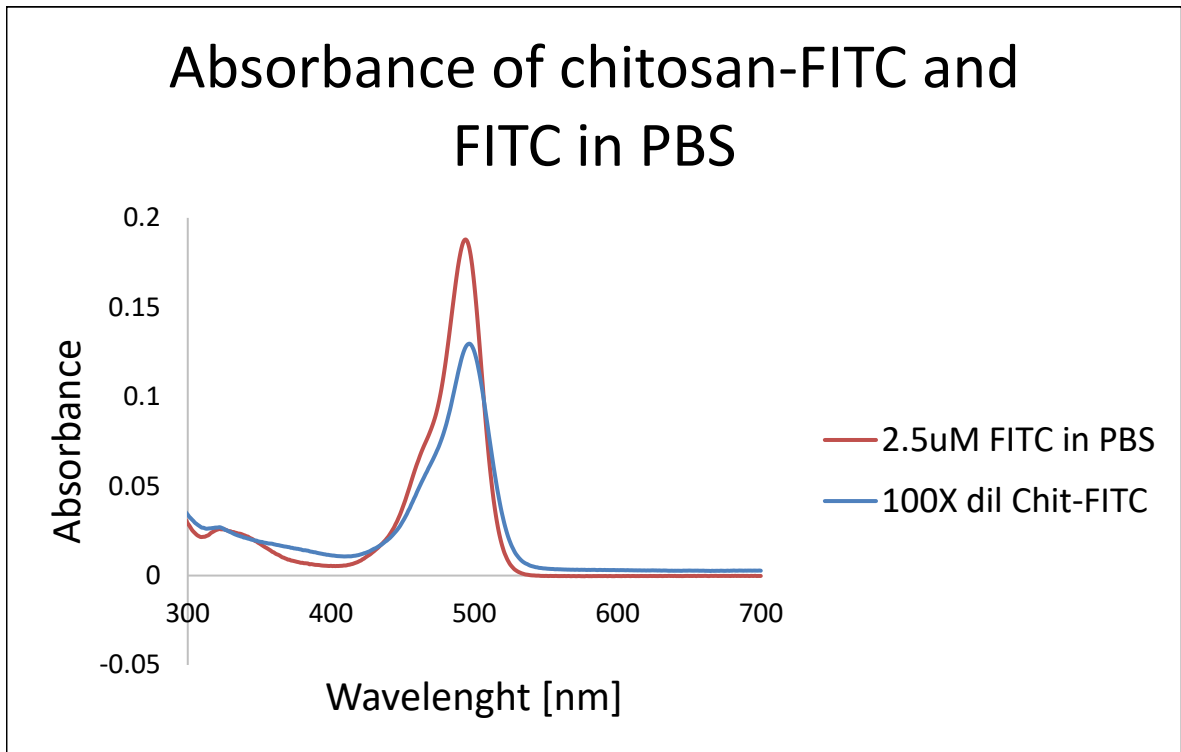


Figure AI-Extra-3. Absorbance of 2.5 μM FITC in PBS and 100X dilution of chitosan-FITC in PBS.

Appendix II.
Extra Figures for Chapters 3, 4 and 5.

Appendix II 3

Figure A3.1: Time stability of individual and multiplex sets. The stability of the multiplexed sample over time is shown by comparison of individual and multiplexed samples.

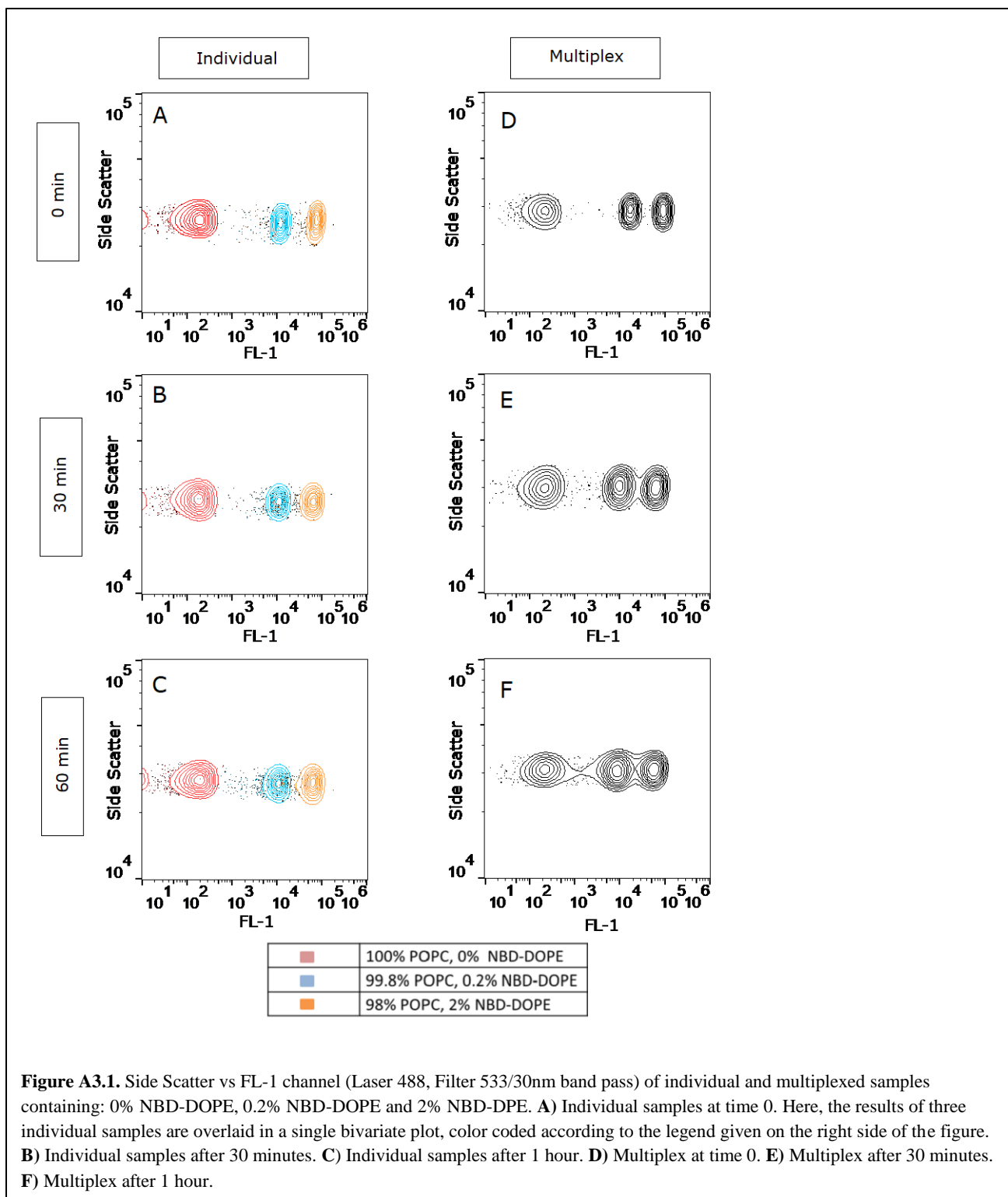


Figure A3.2: Cholera toxin B subunit-Alexa 647 does not have specific interactions with the NBD-DOPE multiplex label. Bivariate plots of Cholera Toxin B subunit and NBD-DOPE indicate that no concentration-dependent interaction occurs between CTxB and the labeled lipid used for multiplexing.

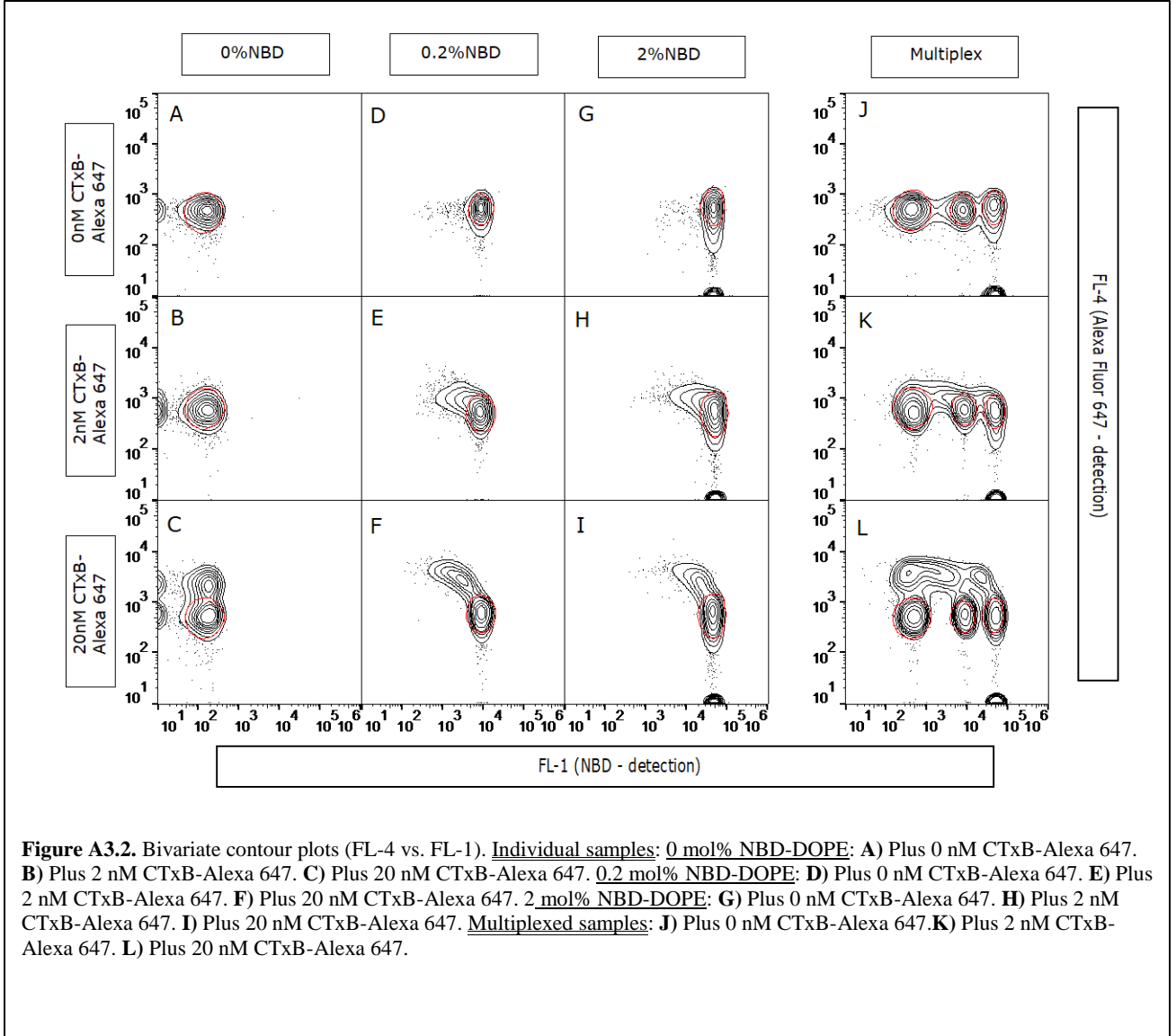


Figure A3.3: Compensation details for biotin-streptavidin assays. Details of the compensation matrix applied to the biotin-streptavidin assay are presented.

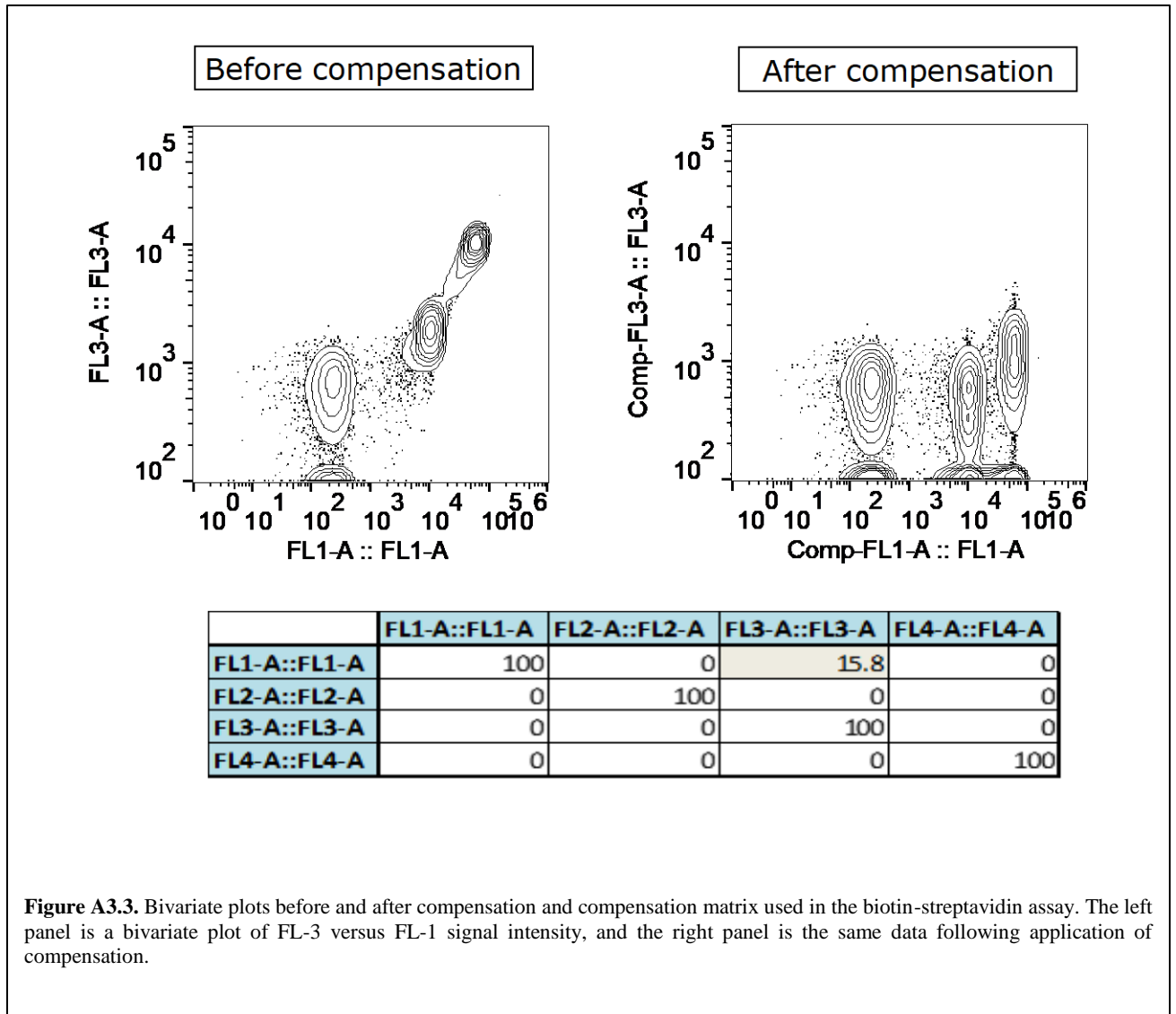


Figure A3.3. Bivariate plots before and after compensation and compensation matrix used in the biotin-streptavidin assay. The left panel is a bivariate plot of FL-3 versus FL-1 signal intensity, and the right panel is the same data following application of compensation.

Figure A3.4: Interaction of Biotin-DOPE and Streptavidin-PE/Cy5 in the individual sample and multiplex approaches. Bivariate plots of streptavidin-biotin assay are shown for individual and multiplex samples.

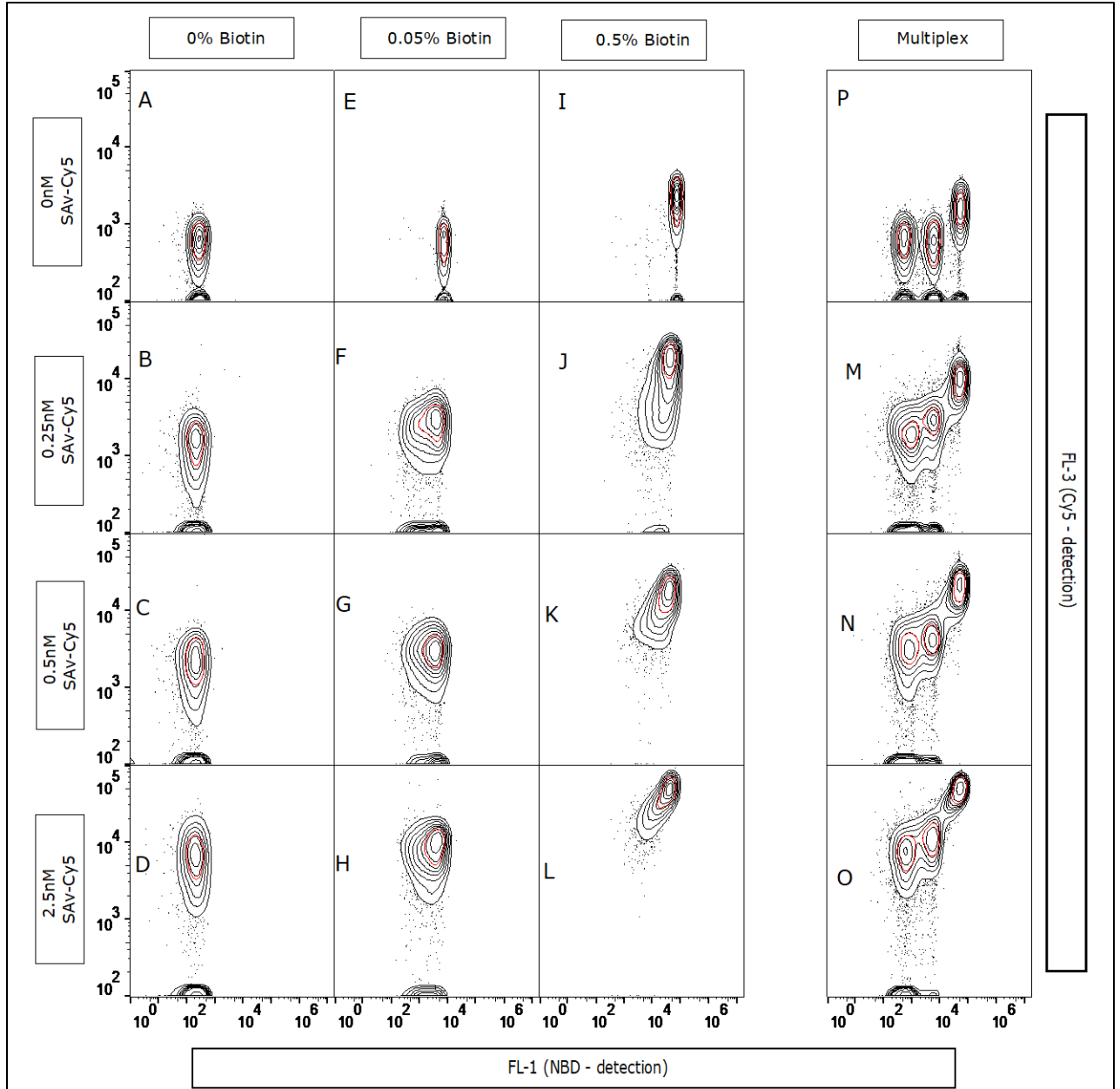


Figure A3.4. Bivariate contour plots (compensated FL-3 vs. FL-1). Individual samples: 0 mol% Biotin: **A)** Plus 0 nM SAV-Cy5. **B)** Plus 0.05 nM SAV-Cy5. **C)** Plus 0.25 nM SAV-Cy5. **D)** Plus 0.5 nM SAV-Cy5. 0.05 mol% Biotin: **E)** Plus 2.5 nM SAV-Cy5. **F)** Plus 0 nM SAV-Cy5. **G)** Plus 0.05 nM SAV-Cy5. **H)** Plus 0.25 nM SAV-Cy5. **I)** Plus 0.5 nM SAV-Cy5. **J)** Plus 2.5 nM SAV-Cy5. 0.5 mol% Biotin: **K)** Plus 0 nM SAV-Cy5. **L)** Plus 0.05 nM SAV-Cy5. **M)** Plus 0.25 nM SAV-Cy5. **N)** Plus 0.5 nM SAV-Cy5. **O)** Plus 2.5 nM SAV-Cy5. Multiplexed samples: **P)** Plus 0 nM SAV-Cy5. **Q)** Plus 0.05 nM SAV-Cy5. **R)** Plus 0.25 nM SAV-Cy5. **S)** Plus 0.5 nM SAV-Cy5. **T)** Plus 2.5 nM SAV-Cy5.

Figure A3.5: Streptavidin-PE/Cy5 does not have specific interactions with the NBD-DOPE multiplex label. Bivariate plots of Streptavidin-PE/Cy5 and NBD-DOPE indicate that no concentration-dependent interaction occurs between streptavidin and the labeled lipid used for multiplexing.

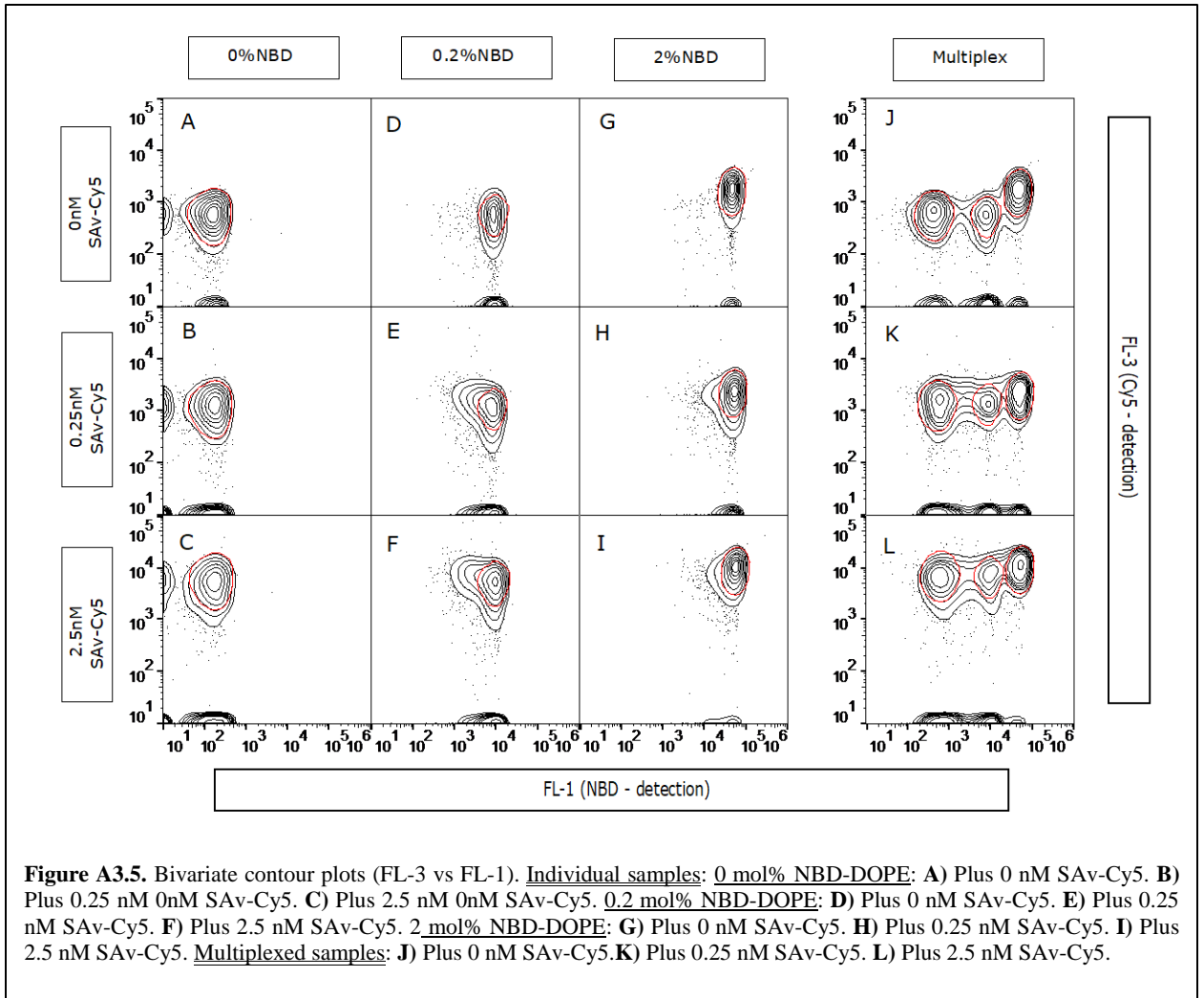


Figure A3.5. Bivariate contour plots (FL-3 vs FL-1). Individual samples: 0 mol% NBD-DOPE: **A)** Plus 0 nM SA v-Cy5. **B)** Plus 0.25 nM SA v-Cy5. **C)** Plus 2.5 nM SA v-Cy5. 0.2 mol% NBD-DOPE: **D)** Plus 0 nM SA v-Cy5. **E)** Plus 0.25 nM SA v-Cy5. **F)** Plus 2.5 nM SA v-Cy5. 2 mol% NBD-DOPE: **G)** Plus 0 nM SA v-Cy5. **H)** Plus 0.25 nM SA v-Cy5. **I)** Plus 2.5 nM SA v-Cy5. Multiplexed samples: **J)** Plus 0 nM SA v-Cy5. **K)** Plus 0.25 nM SA v-Cy5. **L)** Plus 2.5 nM SA v-Cy5.

Figure A3.6: Compensation details for cross reactivity assays. Details of the compensation matrix as applied in the cross-reactivity assay are presented.

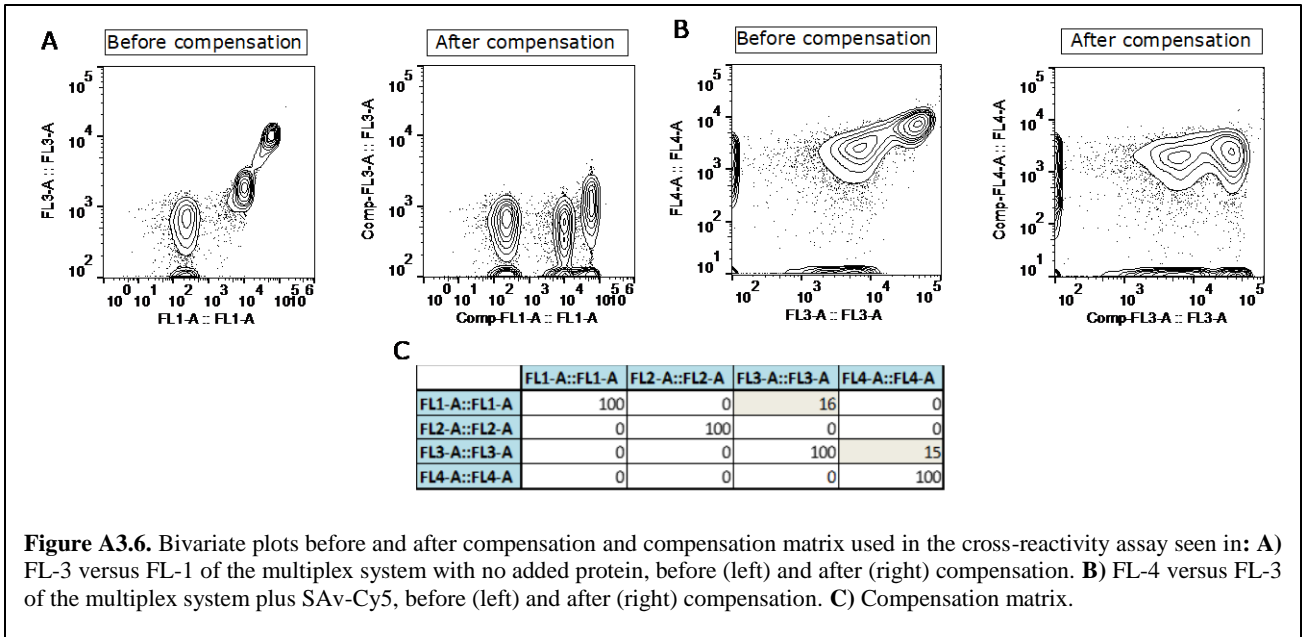
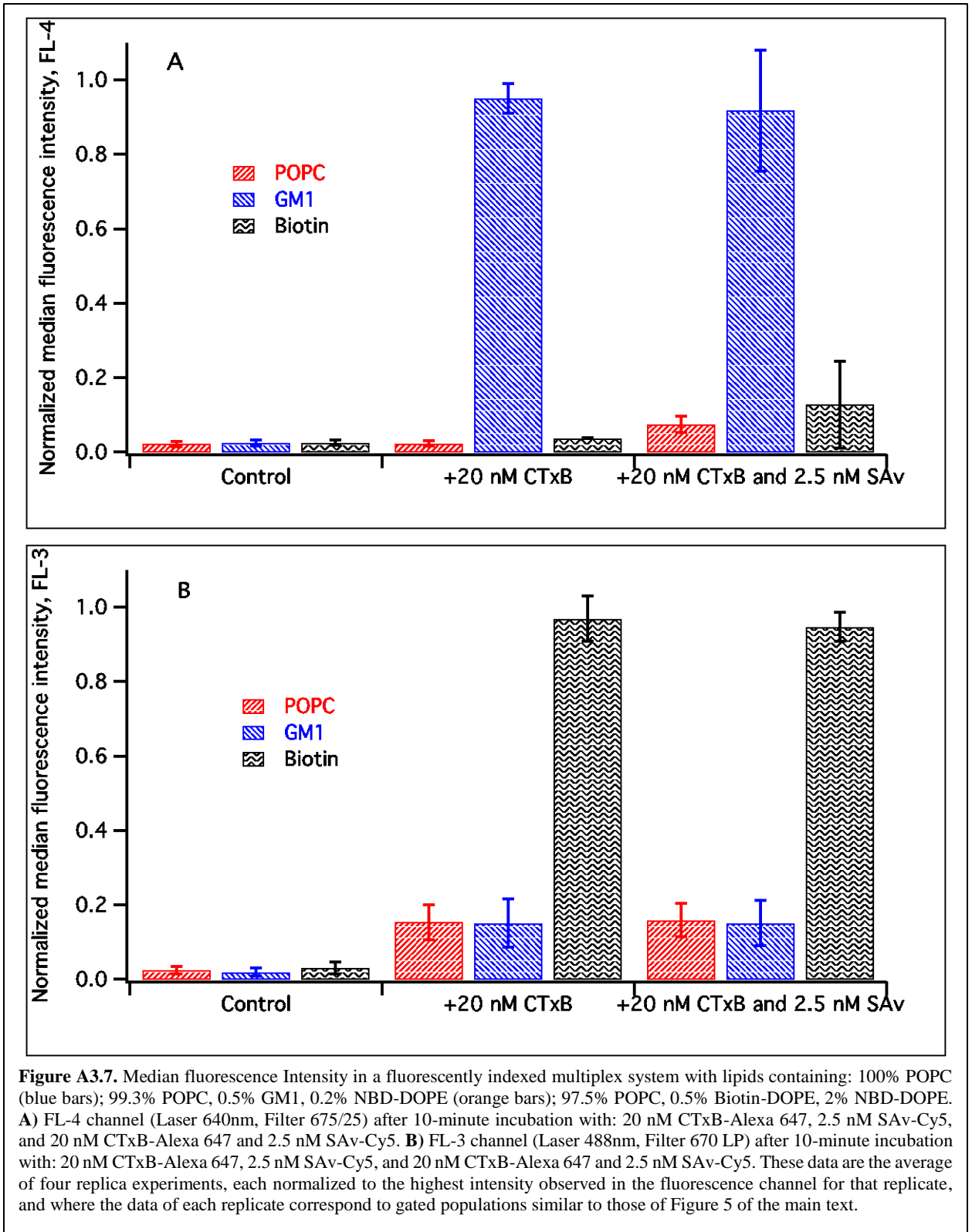


Figure A3.6. Bivariate plots before and after compensation and compensation matrix used in the cross-reactivity assay seen in: **A**) FL-3 versus FL-1 of the multiplex system with no added protein, before (left) and after (right) compensation. **B**) FL-4 versus FL-3 of the multiplex system plus SA_v-Cy5, before (left) and after (right) compensation. **C**) Compensation matrix.

Figure A3.7: Cross-reactivity median fluorescence intensities – Median fluorescence intensities in FL-4 and FL-3 in cross-reactivity assay are presented.



Appendix II 4

Figure A4.1: Fluorescent membranes supported on planar glass after LDAO treatment.

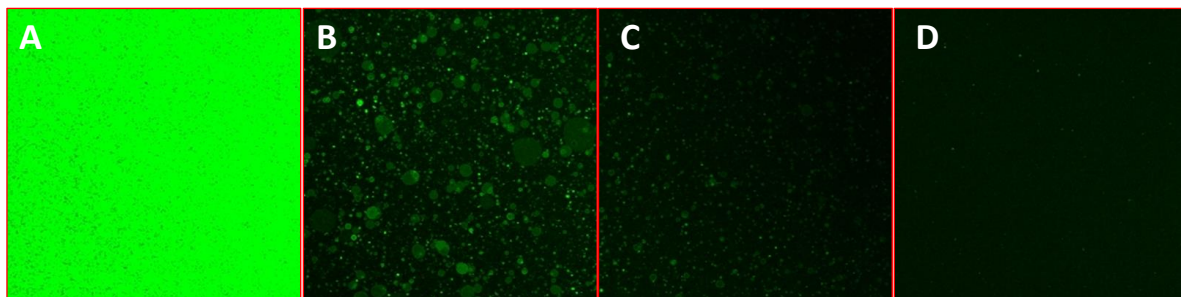


Figure A4.1. Fluorescent microscopy images (40X magnification, zoom 2.0) of lipid membranes (99.8%mol DOPC+0.2%mol NBD-DOPE) supported on planar glass and incubated with 1.5 mM LDAO. **A)** Control (0 mM LDAO) at time 0 minutes. **B)** After 25 minutes. **C)** After 30 minutes. **D)** After 45 minutes.

Figure A4.2: LDAO effect on different membrane compositions. Fluorescently-tagged membranes supported on microspheres after treatment with LDAO

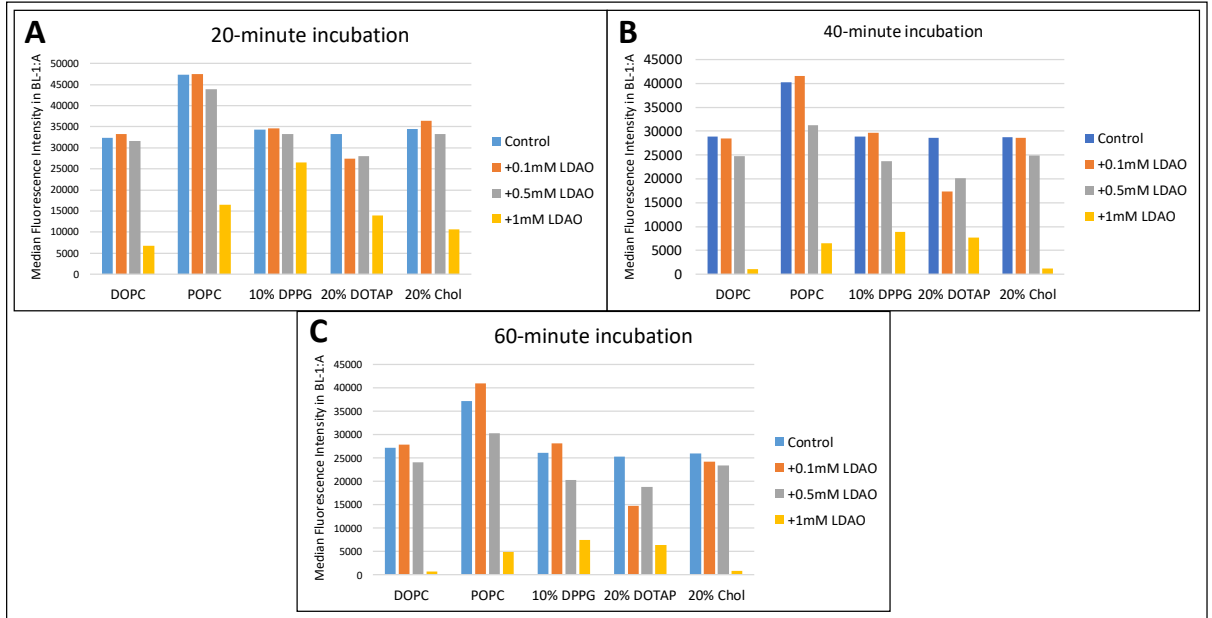
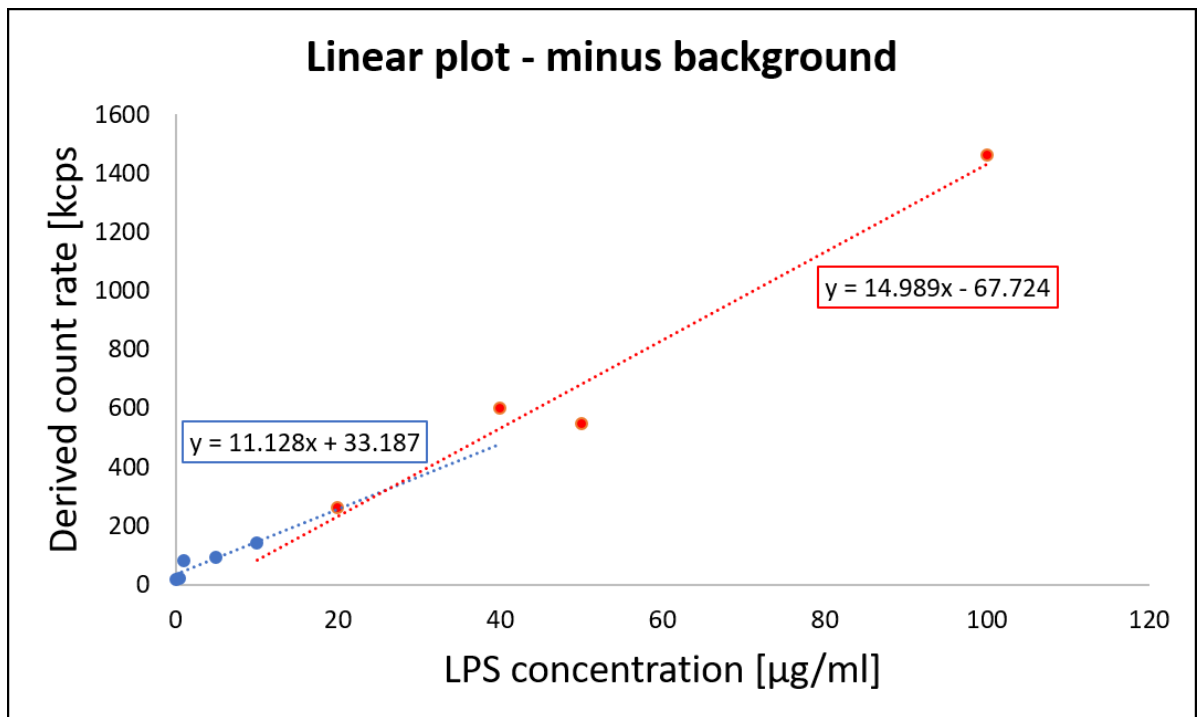


Figure A4.2. Median fluorescence intensity in the BL-1 channel (NBD detection channel) of silica microsphere-supported membranes tagged with 0.2%mol NBD-DOPE and different membrane compositions in the presence of 0 mM LDAO (blue bars), 0.1 mM LDAO (red bars), 0.5 mM LDAO (gray bars), and 1 mM LDAO (yellow bars). **A)** After a 20-minute incubation. **B)** After a 40-minute incubation. **C)** After a 60-minute incubation.

Figure A4.3. Derived count rate as a function of LPS concentration.



LPS c.m.c. \approx 26 $\mu\text{g/ml}$

Figure A4.3. Determination of LPS critical micelle concentration.

Figure A4.4: Fluorescent membranes supported on planar glass after LPS treatment.

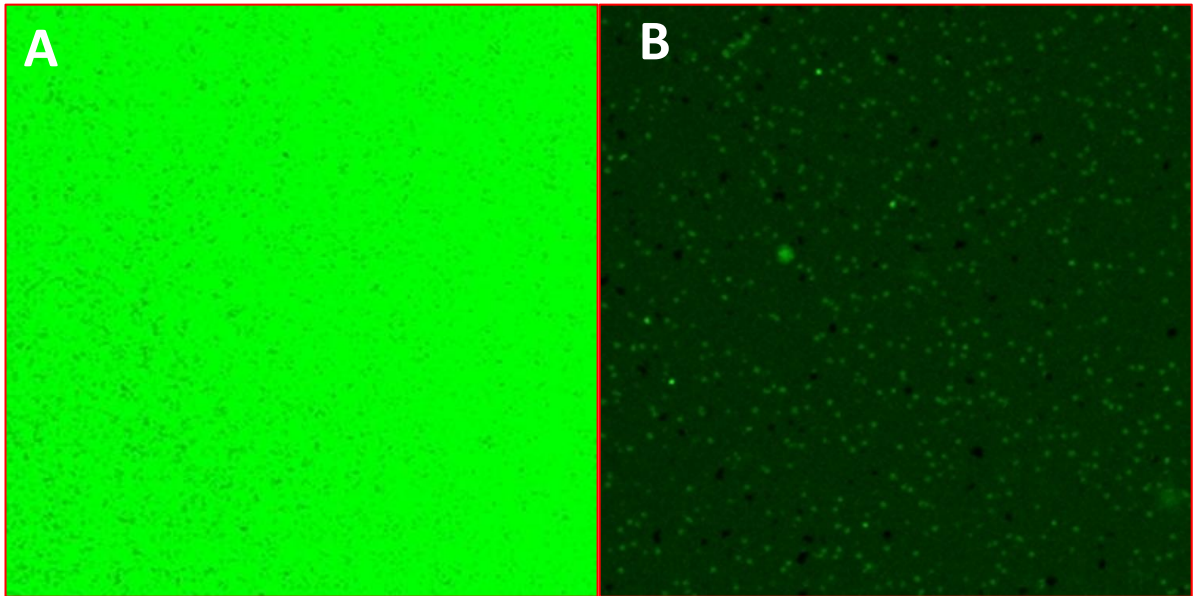


Figure A4.4. Fluorescent microscopy images (40X magnification, zoom 2.0) of lipid membranes (99.8%mol DOPC+0.2%mol NBD-DOPE) supported on planar glass. **A)** Control (0 µg/ml LPS) at time 0 minutes. **B)** After a 30-minute incubation with 500 µg/ml of LPS.

Figure A4.5: LPS effect on different membrane compositions. Fluorescently-tagged membranes supported on microspheres after treatment with LPS

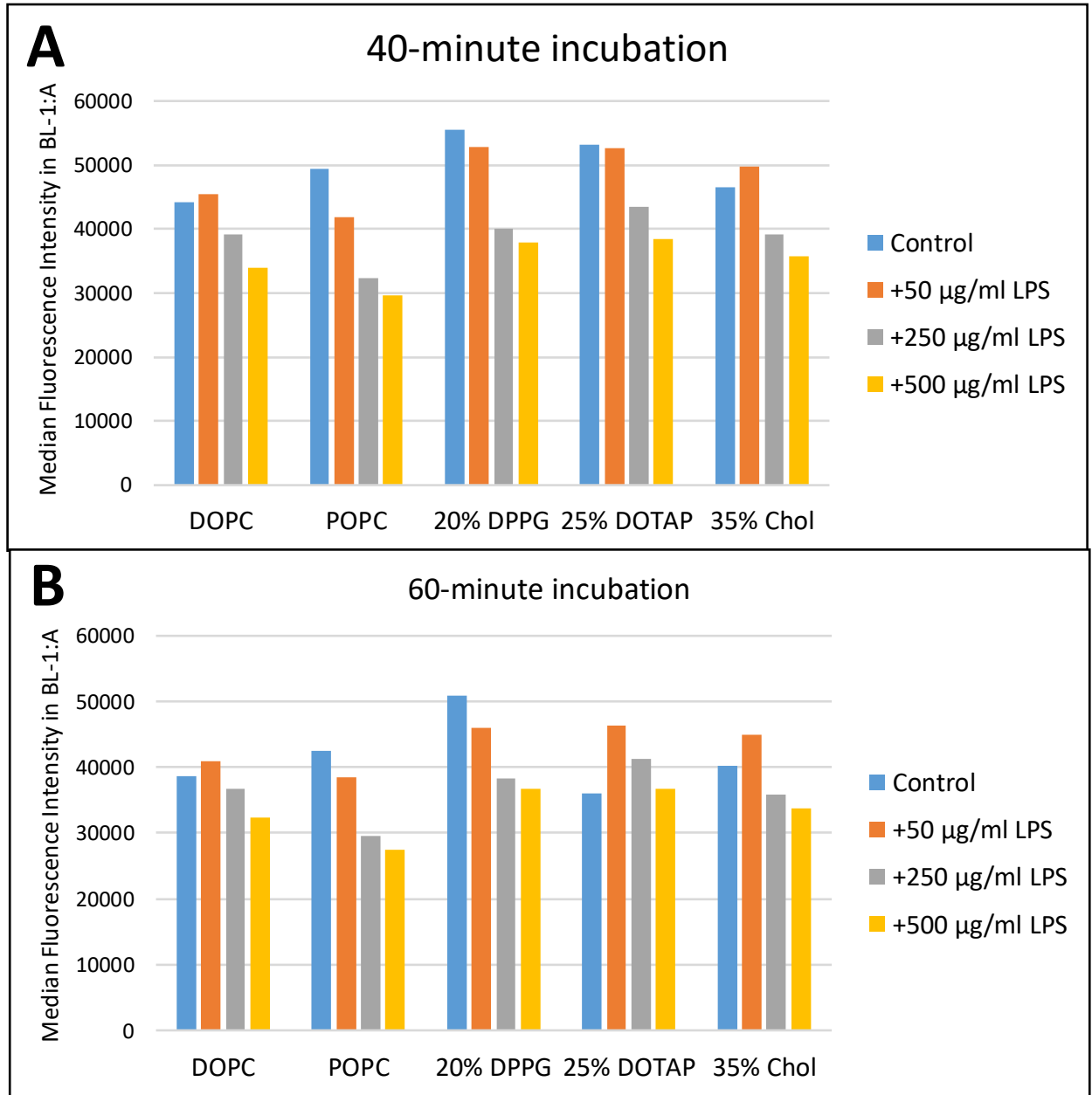
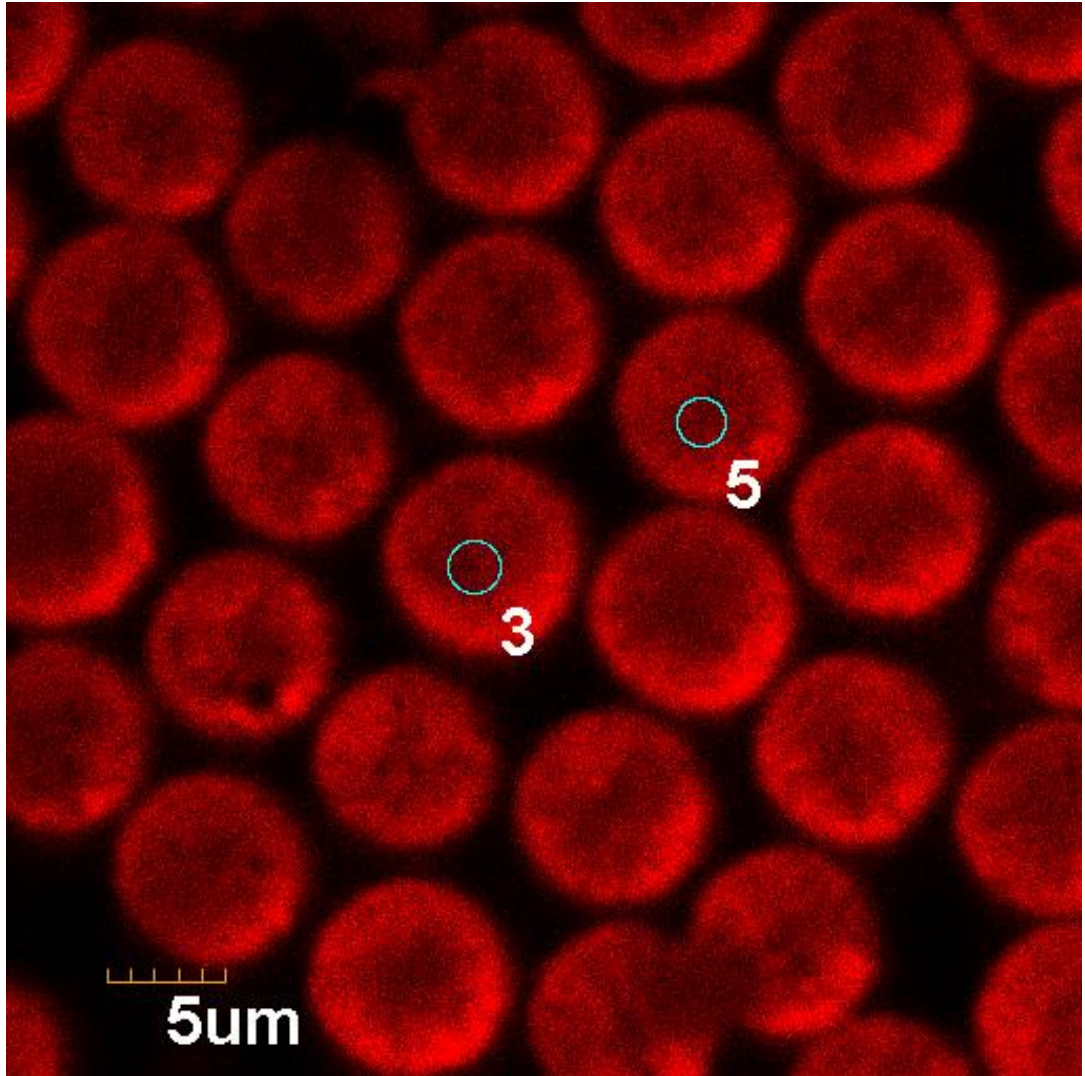


Figure A4.5. Median fluorescence intensity in the BL-1 channel (NBD detection channel) of silica microsphere-supported membranes tagged with 0.2%mol NBD-DOPE and different membrane compositions in the presence of 0 mM LPS (blue bars), 50 µg/ml LPS (red bars), 250 µg/ml LPS (gray bars), and 500 µg/ml LPS (yellow bars). **A**) After a 40-minute incubation. **B**) After a 60-minute incubation.

Appendix II 5

Movie A5.1: Fluorescence recovery after photobleaching.



Movie A5.1. Preview image of the movie showing fluorescence recovery after photobleaching (FRAP) in biomimetic membranes (1 mM pEO-b-pBD + 0% mol GM1 + 1% mol Texas-Red-DHPE) supported on silica microspheres.

Figure A5.1: Data of the fluorescence recovery after photobleaching.

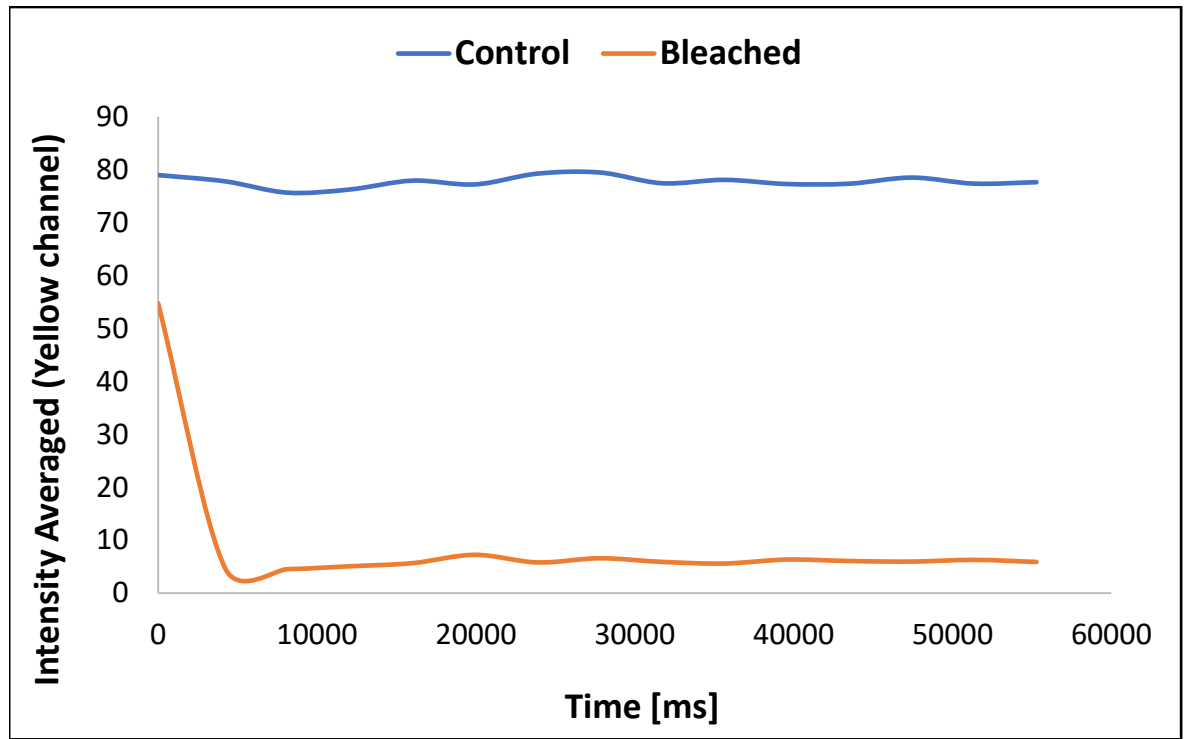


Figure A5.1. Analysis of the fluorescence recovery after photobleaching (FRAP) in biomimetic membranes (1 mM pEO-b-pBD + 0%mol GM1 +1%mol Texas-Red-DHPE) supported on silica microspheres.

Figure A5.2: Time stability of polymer membranes supported on silica beads.

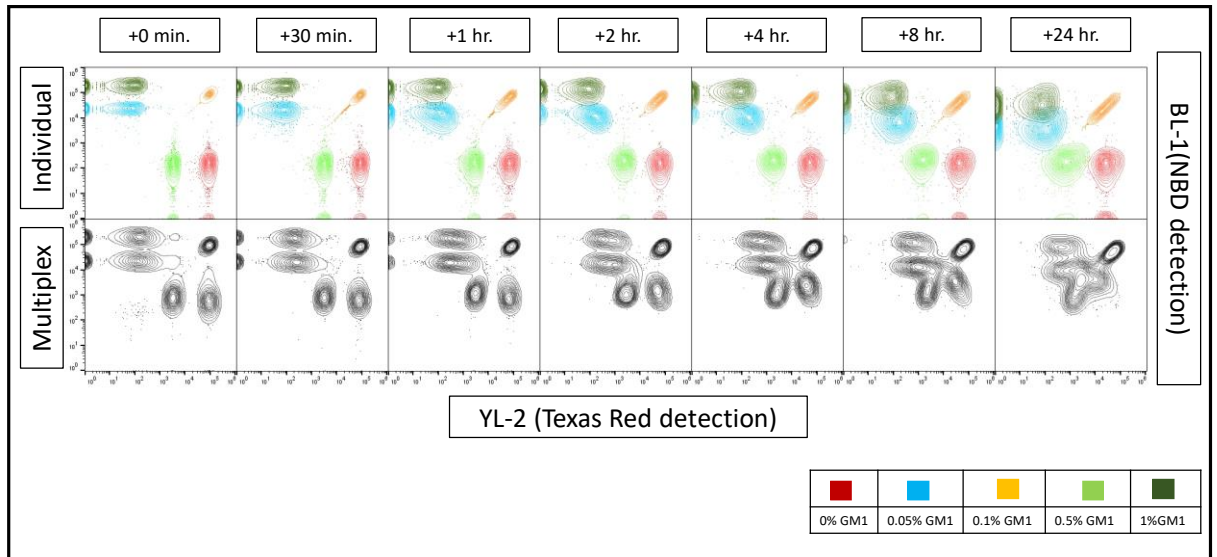


Figure A5.2. Time stability (at 0, 0.5, 1, 2, 4, 8 and 24 hours) of individual and multiplex of microsphere supported containing 1mM pBD-pEO, 0% GM1, 1%mol Texas Red-DHPE (red); 1mM pBD-pEO, 0.05% GM1, 0.2%mol NBD-DOPE (light blue); 1mM pBD-pEO, 0.1% GM1, 2%mol NBD-DOPE, 1%mol Texas Red-DHPE (yellow); 1mM pBD-pEO, 0.5% GM1, 0.01% Texas Red-DHPE (light green); and 1mM pBD-pEO, 1% GM1, 2%mol NBD-DOPE (dark green).

Figure A5.3: Samples before and after compensation.

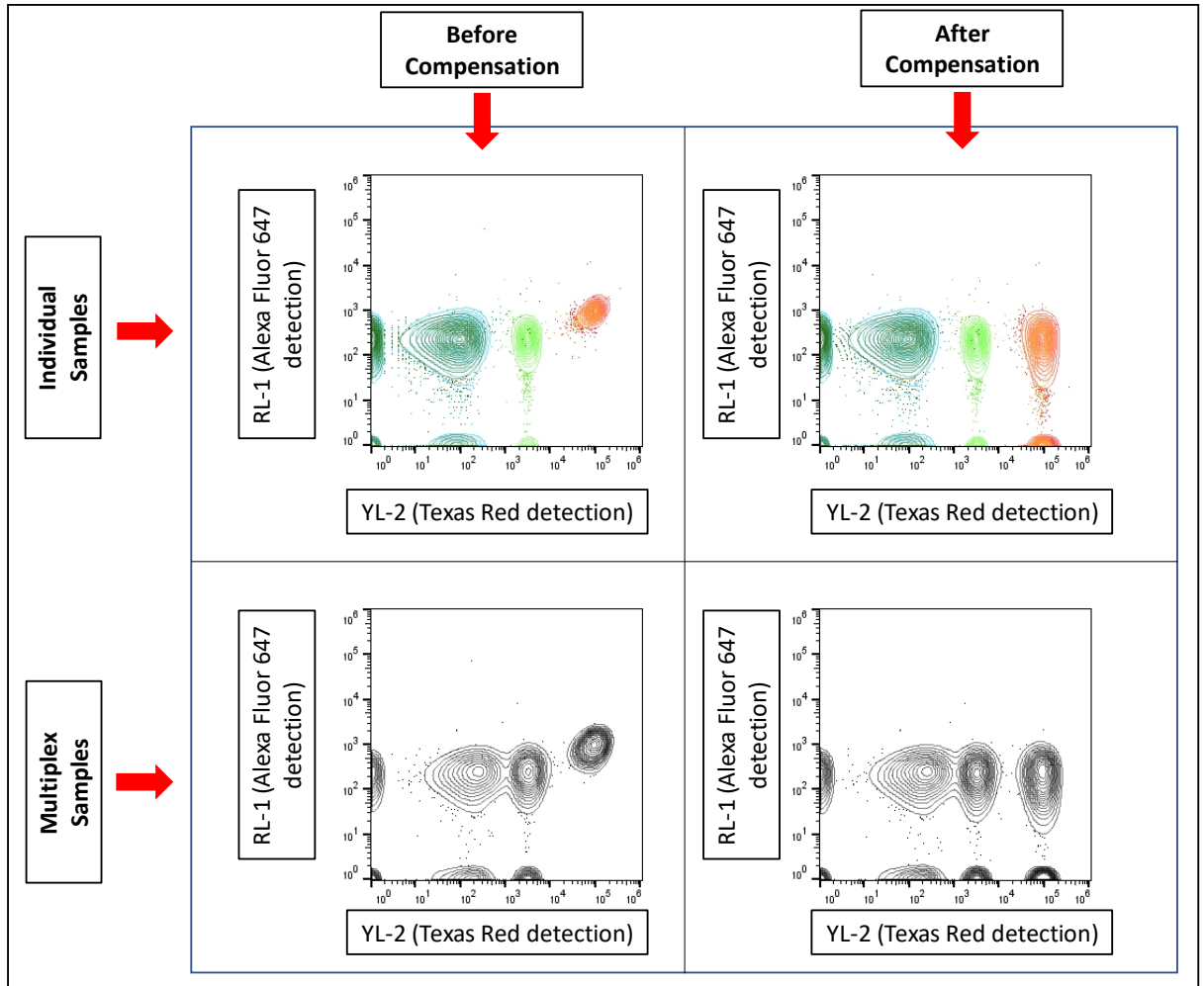


Figure A5.3. Individual and multiplex samples before and after compensation in the RL-1 channel (Excitation 638 nm; Emission 670/14 nm) and the YL-2 channels (Excitation 561 nm; Emission 620/15 nm).

Figure A5.4: Compensation matrix.

	BL1-A::BL1-A	YL2-A::YL2-A	RL1-A::RL1-A
BL1-A::BL1-A	100	0	0
YL2-A::YL2-A	0	100	0.9
RL1-A::RL1-A	0.001	1	100

Figure A5.4. Compensation matrix.